Measurement, Assessment, Analysis and Improvement of Transition Zones in Railway Track

Wang, Haoyu

DOI
10.4233/uuid:73830b2c-deb1-4da9-b19c-5e848c5cfa4d

Publication date
2018

Document Version
Final published version

Citation (APA)
Wang, H. (2018). *Measurement, Assessment, Analysis and Improvement of Transition Zones in Railway Track*. [Dissertation (TU Delft), Delft University of Technology]. https://doi.org/10.4233/uuid:73830b2c-deb1-4da9-b19c-5e848c5cfa4d

Important note
To cite this publication, please use the final published version (if applicable).
Please check the document version above.

Measurement, Assessment, Analysis and Improvement of Transition Zones in Railway Track

Haoyu WANG

Measurement, Assessment, Analysis and Improvement of Transition Zones in Railway Track

Dissertation

for the purpose of obtaining the degree of doctor
at Delft University of Technology
by the authority of the Rector Magnificus, Prof.dr.ir. T.H.J.J. van der Hagen,
chair of the Board for Doctorates
to be defended publicly on
Monday 04, March 2019 at 10:00 o'clock
by

Haoyu WANG

Master of Engineering in Railway Engineering, Beijing Jiaotong University, China

born in Shenyang, China

This dissertation has been approved by the promotors.

Composition of the doctoral committee:

Rector Magnificus,	Chairperson
Prof.dr.ir. R.P.J.B. Dollevoet,	Delft University of Technology, promotor
Dr.ir. V.L. Markine,	Delft University of Technology, copromotor

Independent members:

Prof.dr.ir. J.G. Rots,	Delft University of Technology
Prof.dr. E. Kassa,	Norwegian University of Science and Technology, Norway
Dr. G. Jing,	Beijing Jiaotong University, China
Dr. J. Varandas,	New University of Lisbon, Portugal
Prof. dr. R.M.P. Goverde,	Delft University of Technology, reserve member
Ir. T. Sysling,	ProRail B.V.

This research was funded by *China scholarship Council*, *Delft University of Technology*, and *European Commission (Horizon 2020, RISEN Project)*; and partly supported by *Roadscanners*, *ProRail*, and *Movares*.

Keywords: Transition zone, Measurement, Finite element method, Degradation, Prediction, Countermeasure

Printed by: Gildeprint - Enschede

Cover by: Haoyu Wang based on Starry Night painted by Vincent van Gogh

ISBN: 978-94-6323-539-6

An electronic version of this dissertation is available at

http://repository.tudelft.nl/.

To my beloved families

Summary

Transition zones in railway tracks are locations with considerable changes in the vertical stiffness of the track support, which can be found near bridges, culverts and tunnels. In such locations, the stiffness variation and the differential settlement of tracks (uneven settlement of the track on the embankment and of the engineering structure) result in amplification of the dynamic track forces. This amplification speeds up the degradation of ballast and subgrade, ultimately resulting in deterioration of the vertical track geometry, which can lead to deterioration of the passenger's comfort, failure of the track components, and in extreme cases to train derailment. Therefore, the track maintenance in transition zones requires substantial effort, up to eight times more effort than on open tracks (i.e. ballast tracks without any special elements).

Although the poor performance of the track in transition zones is frequently reported, the transition zones have not been paid enough attention. First of all, there is no specific experimental method for assessment of the track condition in transition zones. Therefore, the transition zones are usually treated as open tracks during inspections. Secondly, the effect of the differential settlement (one of the factors causing the transition zone problem) on the track degradation has not been sufficiently studied as compared to the effects of the stiffness variation. Also, due to the insufficient knowledge on the track behaviour in transition zones, the track settlement in transition zones cannot be predicted precisely. As a result, the maintenance is performed in a reactive way. Finally, although many countermeasures have been proposed for transition zones, the tools for assessment of their performance (especially on a long term) are still lacking, which causes difficulties for track designers when selecting the countermeasures. Clearly, the knowledge on the measurement, dynamic behaviour, degradation, and assessment of the track in transition zones should be improved.

This study intended to give answers to the following questions: (1) How to assess the condition of the tracks in transition zones? using which tool? (2) Which factor contributes more to the track degradation in transition zones, the uneven settlement or the stiffness variation? (3) How to predict the track settlement in transition zones on a long term? (4) How to assess the performance of the countermeasures for transition zones?

In attempt to answer these questions, an integrated methodology combing an innovative experimental method and numerical model for analysis of the dynamic behaviour and degradation of railway tracks in transition zones has been developed. The methodology consists of the following three parts:

- An advanced measurement technique based on the DIC (Digital Image Correlation) method that is used to measure the absolute dynamic displacements of rails/sleepers due to the passing trains. The advantage of this technique is that the vertical track displacements are measured simultaneously at **multiple points**, allowing obtaining the dynamic profile of the track section. Also, **no track possession** is required during the measurement. The measurement technique provides a basis for assessment of the **track condition** in the transition zones.
- A novel model for analysis of the dynamic responses in transition zones that uses the explicit Finite Element (FE) method. The track model accounts for both the vertical stiffness variation

and the **differential track settlement** in transition zones. The **nonlinear contact** elements are used to model the sleeper-ballast interface**,** which allows the **sleeper-ballast** interaction to more realistically be described as compared to the existing models.

- A novel procedure to predict the **long-term** track behaviour (settlement) in transition zones, which is based on the developed FE model of the transition zones and an empirical settlement model of ballast (developed by Y. Sato). Using this procedure, the track settlement in transition zones due to multiple passages of trains can be predicted, which can provide a basis for **planning track maintenance** in transition zones.

To demonstrate the developed methodology, it was used in a number of applications in this study such as:

- Assessment of the track condition in various transition zones,
- Numerical analysis of the track behaviour and of the factors influencing initiation and propagation of the track settlement in transition zones,
- Assessment of the performance of various countermeasures for transition zones.

Some additional studies on the effect of the moisture condition on track performance in transition zones and on the feasibility of using satellite radar for structural health monitoring of transition zones have been performed as well. The main conclusions of these studies can be summarised as follow:

- The numerical and experimental results confirmed the higher degradation of the track near engineering structures in transition zones as compared to the open track observed in situ.
- The track degradation and the length of the settlement affected zone in the Embankment-Bridge (EB) and the Bridge-Embankment (BE) transitions, which is defined by the train moving direction, are different. That was confirmed by the measurement and numerical results, and by field observations. This phenomenon was explained using the numerical model, namely that the initial location of the track settlement in the EB transition is primarily defined by the pitch motion of the bogies, while in the BE transition it is affected by the 'gliding' and 'bouncing' motion of the vehicle. The settlement affected zone in the BE transition is longer (depending on the velocity, approx. 2 times for 140 km/h) than the EB transition.
- The track condition in transition zones was successfully assessed using the measurement method. The condition assessment results have good correlation with maintenance history, and satellite data of the considered transition zones.
- The performance of various countermeasures for transition zones was successfully assessed using the developed methodology. The numerical results have shown that the sleepers with modified dimensions (preventive countermeasure) and the adjustable fasteners (corrective countermeasure) can significantly improve the track performance, 51% reduction in ballast stress and 93% reduction in the wheel-rail contact force respectively.

Using the integrated methodology, the research questions have been answered. The proposed methodology provides suitable tools for measurement, assessment, analysis and improvement of the tracks in transition zones. The methodology can be further applied to the design and optimisation of the track in transition zones.

Samenvatting

Overgangszones in spoorweggen zijn locaties met aanzienlijke veranderingen in de verticale stijfheid van de spoorondersteuning, die zich in de buurt van bruggen, duikers en tunnels bevinden. Op dergelijke locaties resulteren de stijfheidsvariatie en de differentiële zetting van sporen (ongelijkmatige zetting van het spoor op de baanlichaam en van de civiele constructies) in versterking van de dynamische spoorkrachten. Deze versterking versnelt de degradatie van ballast en ondergrond, wat uiteindelijk resulteert in verslechtering van de verticale spoorgeometrie. Dit kan leiden tot verslechtering van het comfort van de passagier, uitval van de spooronderdelen en in extreme gevallen tot ontsporing. Daarom vereist het spooronderhoud in overgangszones aanzienlijke inspanningen, tot acht keer meer inspanning dan op het standaard spoor (ballastsporen zonder speciale elementen).

Hoewel de slechte prestaties van de sporen in overgangszones vaak worden gemeld, is er nog niet genoeg aandacht aan de overgangszones gegeven. Allereerst is er geen specifieke experimentele methode voor het beoordelen van spoorconditie in overgangszones. Daarom worden de overgangszones gewoonlijk tijdens inspecties behandeld als het standaard spoor. Ten tweede is het effect van de differentiële zetting op de spoordegradatie niet voldoende bestudeerd in vergelijking met de effecten van de stijfheidsvariatie. Ook kan de spoorzetting in overgangszones, vanwege onvoldoende kennis over het spoorgedrag in overgangszones, niet nauwkeurig worden voorspeld. Als gevolg hiervan wordt het spooronderhoud op een reactieve manier uitgevoerd. Ten slotte ontbreken de instrumenten voor het beoordelen van hun prestaties (vooral op lange termijn), wat de trackontwerpers moeilijkheden bezorgt bij het selecteren van de tegenmaatregelen, hoewel er veel tegenmaatregelen zijn voorgesteld voor overgangszones. Het is duidelijk dat de kennis over het meten, het dynamische gedrag, de degradatie en het beoordelen van het spoor in overgangszones moet worden verbeterd.

Het doel van dit onderzoek was om antwoorden te geven op de volgende vragen: (1) Hoe moet de conditie van de sporen in overgangszones worden beoordeeld? Met welk instrument? (2) Welke factor draagt meer bij aan de spoordegradatie in overgangszones, de differentiële zetting of de stijfheidsvariatie? (3) Hoe kan de spoorzetting in overgangszones op lange termijn worden voorspeld? (4) Hoe kunnen de prestaties van de tegenmaatregelen voor overgangszones worden beoordeeld?

In een poging om deze vragen te beantwoorden, een geïntegreerde methodologie is ontwikkeld, die een innovatieve experimentele methode en een numeriek model combineert voor de analyse van het dynamische gedrag en de degradatie van het spoor in overgangszones. De methodologie bestaat uit de volgende drie delen:

- Een geavanceerde meettechniek gebaseerd op de DIC-methode (Digital Image Correlation) die wordt gebruikt om de absolute dynamische verplaatsingen van sporen / dwarsliggers als gevolg van de passerende treinen te meten. Het voordeel van deze techniek is dat de verticale spoorverplaatsingen gelijktijdig op **meerdere punten** worden gemeten, waardoor het dynamische profiel van het spoor kan worden verkregen. Ook is tijdens de meting **geen buitendienststelling**. De meettechniek biedt een basis voor het beoordelen van **de spoorconditie** in de overgangszones.

- Een nieuw model voor analyse van de dynamische reacties in overgangszones met de expliciete Eindige Elementen Methode (FEM). Het model is verantwoordelijk voor zowel de verticale stijfheidsvariatie als de **differentiële zetting** in overgangszones. N**iet-lineaire contactelementen** worden gebruikt om de dwarsligger-ballastinterface te modelleren, waardoor de **dwarsligger-ballastinteractie** realistischer kan worden beschreven in vergelijking met de bestaande modellen.
- Een nieuwe procedure om het gedrag van het spoor op de **lange termijn** (zetting) in overgangszones te voorspellen, die op het ontwikkelde FE-model van de overgangszones en een empirisch zetting model van ballast (ontwikkeld door Y. Sato) is gebaseerd. Met behulp van deze procedure kan de spoorzetting in overgangszones als gevolg van meerdere passages van treinen worden voorspeld, wat een basis kan bieden voor **het plannen van spooronderhoud** in overgangszones.

Om de ontwikkelde methodologie te demonstreren, werd deze in een aantal toepassingen in deze studie gebruikt, zoals:

- Beoordeling van de spoorconditie in verschillende overgangszones,
- Numerieke analyse van het spoorgedrag en van de factoren die de initiatie en verspreiding van de spoorzetting in overgangszones beïnvloeden,
- Beoordeling van de prestaties van verschillende tegenmaatregelen voor overgangszones.

Enkele aanvullende studies over het effect van de vochtgehalte op de spoorprestaties in overgangszones en over de haalbaarheid van het gebruik van satellietradar voor Stuctural Health Monitoring van overgangszones zijn ook uitgevoerd. De belangrijkste conclusies van deze studies kunnen als volgt worden samengevat:

- De numerieke en experimentele resultaten bevestigden de hogere degradatie van het spoor in overgangszones nabij civiele constructies in vergelijking met het standaard spoor dat in situ werd waargenomen.
- De spoordegradatie en de lengte van de zettingzone in de Baanlichaam-Brug en de Brug-Baanlichaam overgangen, gedefinieerd door de bewegingsrichting van de trein, zijn verschillend. Dat werd bevestigd door de metingen en het numerieke model en door veldwaarnemingen. Dit fenomeen werd verklaard aan de hand van het numerieke model, namelijk dat de initiële locatie van de spoor zetting in de Baanlichaam-Brug overgang in de eerste plaats wordt bepaald door de 'stamp' (Pitch in Engels)-beweging van de draaistellen, terwijl deze in de Brug-Baanlichaam overgang wordt beïnvloed door het 'glijd'- en 'stuiter'-beweging van het voertuig. De zettingzone in de Brug-Baanlichaam overgang is langer (afhankelijk van de snelheid, ongeveer 2 keer voor 140 km/u) dan de Baanlichaam-Brug overgang.
- De spoorconditie in overgangszones werd succesvol beoordeeld met behulp van de meetmethode. De resultaten van de conditiebepaling hebben een goede correlatie met onderhoudsgeschiedenis en satellietgegevens van de beschouwde overgangszones.
- De uitvoering van verschillende tegenmaatregelen voor overgangszones werd succesvol beoordeeld aan de hand van de ontwikkelde methodologie. De numerieke resultaten hebben aangetoond dat de dwarsliggers met gewijzigde afmetingen (preventieve tegenmaatregel) en de verstelbare bevestigingsmiddelen (corrigerende tegenmaatregel) de prestaties van het

spoor aanzienlijk kunnen verbeteren, respectievelijk 51% vermindering van de ballastspanning en 93% vermindering van de contactkracht in het Wiel-Railcontact.

Met behulp van de geïntegreerde methodologie zijn de onderzoeksvragen beantwoord. De voorgestelde methodologie biedt geschikte hulpmiddelen voor het meten, beoordelen, analyseren en verbeteren van het spoor in overgangszones. De methodologie kan verder worden toegepast op het ontwerp en de optimalisatie van het spoor in overgangszones.

Contents

Thesis contents

The material presented in this dissertation is based on the following papers:

PAPER A

Haoyu Wang and Valeri Markine. Methodology for the Comprehensive Analysis of Railway Transition Zones. Computers and Geotechnics, 99 (2018), pp.64-79. doi: 10.1016/j.compgeo.2018.03.001.

PAPER B

Haoyu Wang, Valeri Markine, Xiangming Liu, 2017. Experimental analysis of railway track settlement in transition zones. Proceedings of the Institution of Mechanical Engineers, Part F: Journal of Rail and Rapid Transit, p.0954409717748789. doi:10.1177/0954409717748789.

PAPER C

Haoyu Wang and Valeri Markine. Finite element analysis of the dynamic behaviour of track transition zones during train passing processes. Under review.

PAPER D

Haoyu Wang and Valeri Markine. Modelling of the long-term behaviour of transition zones: Prediction of track settlement. Engineering Structures, 156 (2018), pp.294-304. doi:10.1016/j.engstruct.2017.11.038.

PAPER E

Haoyu Wang and Valeri Markine. Corrective countermeasure for track transition zones: adjustable fastener. Engineering Structures 169 (2018): 1-14. doi: 10.1016/j.engstruct.2018.05.004.

PAPER F

Haoyu Wang, Mika Silvast, Valeri Markine and Bruce Wiljanen. Analysis of the Dynamic Wheel Loads in Railway Transition Zones Considering the Moisture Condition of the Ballast and Subballast. Applied Sciences, 7(12), p.1208. doi:10.3390/app7121208.

PAPER G

Haoyu Wang, Ling Chang, Valeri Markine, Structural Health Monitoring of Railway Transition Zones Using Satellite Radar Data. Sensors 2018, 18(2), 413. doi:10.3390/s18020413.

Part I

EXTENDED SUMMARY

PI

Chapter 1. Railway track in transition zones

In this chapter, the transition zones in railway tracks are introduced, together with the summary of the current problems related to the transition zones and the literature review of the recent studies on the transition zones. The research motivation, questions, and method, as well as the dissertation outline are presented here.

1.1 Background

Transition zones in railway tracks are the locations with considerable changes in the vertical support, which are typically located near engineering structures, such as bridges, culverts, tunnels and level crossings.

A typical transition zone is shown in Figure 1a, where the definitions used in this study are indicated. The track longitudinal level measured in this location by the inspection coach (Eurailscout UFM120) is shown in Figure 1b, where two large irregularities in the track geometry appear before and after the bridge can be seen. The degradation process of the transition zone is schematically shown in Figure 1c. The ballast track in transition zones can be divided into two sections: the settlement affected zone that is close to the bridge, and the open track. Depending on the moving direction of trains, the Embankment-Bridge (EB) transition and the Bridge-Embankment (BE) transition can be recognized.

As a result of degraded track longitudinal level, the following problems are often observed in transition zones:

- Damage of the track components: rail surface defects, broken fasteners, cracks in concrete sleepers, breakage of ballast particles, and voids between sleepers and ballast (also known as hanging sleepers) [1-13];
- Deterioration of the track geometry, i.e. extra settlement appearing on tracks and forming a 'dip' [11, 14-16];
- Deterioration of the passenger's comfort [17].

The track deterioration process in transition zones is accelerated with the increase of the operational velocities of the passing trains, leading to a tremendous increase of the maintenance efforts on correction of the track geometry in transition zones [11]. Transition zones require more maintenance like tamping and adding ballast (ballast blowing) as compared to the open tracks [5, 16]. For instance, in the Netherlands, the maintenance activities on the track in transition zones are performed up to 4-8 times more often than on open tracks [9, 18]. In the US $200 million is spent on maintenance of the track in transition zones annually, while in Europe about €97 million is spent on similar maintenance activities [19, 20]. Obviously, there is a need to improve the track performance in transition zones.

PI

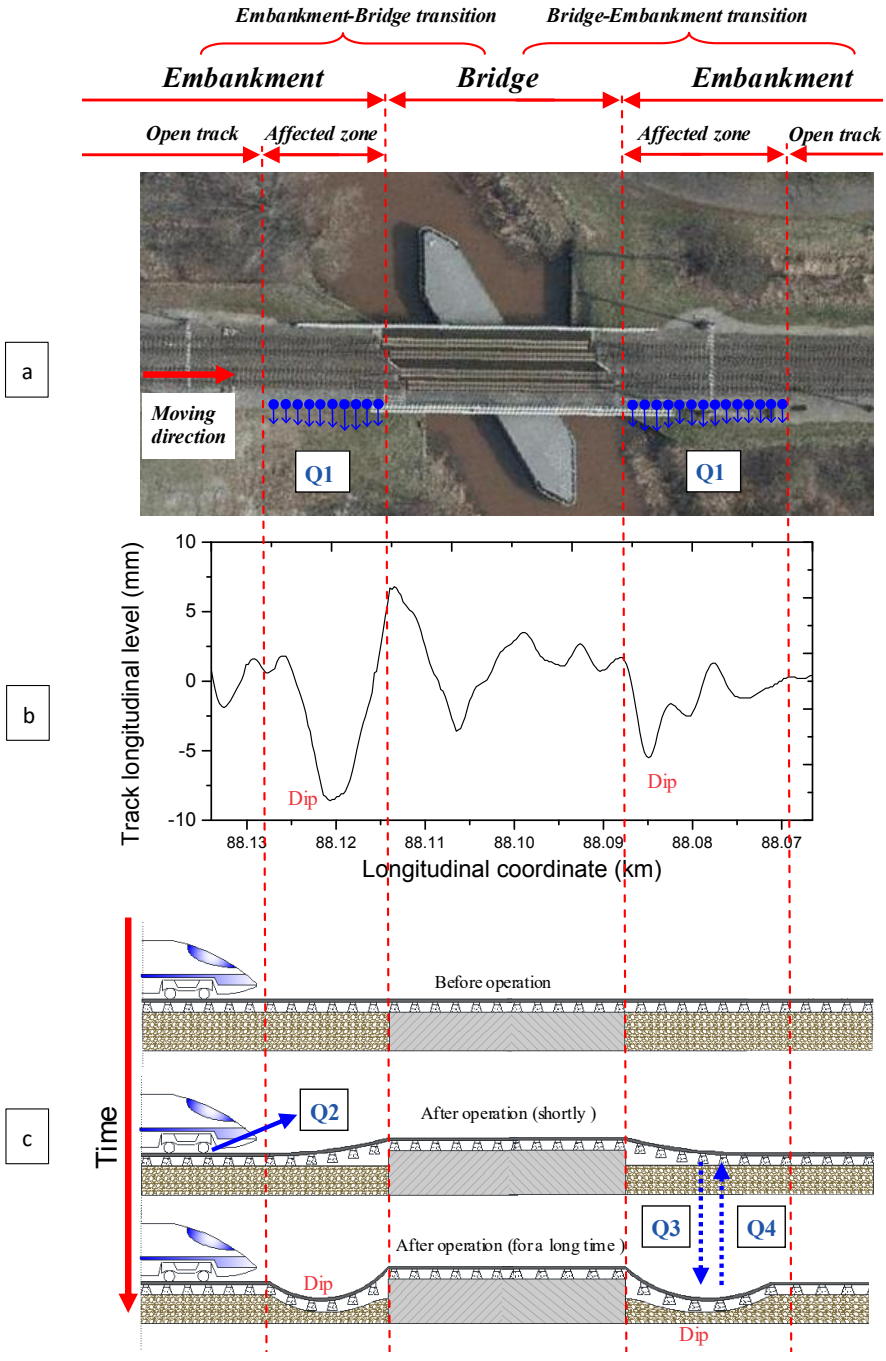

Figure 1. Introduction of transition zone: (a) Top view; (b) Track longitudinal level measured by the inspection coach; (c) Schematic diagram of track degradation in transition zones.

Based on literature review [11], there are three major factors causing the track degradation in transition zones, that are the differential settlement, the stiffness variation and the geotechnical/construction/maintenance issue.

In transition zones, the differential settlement always appears due to the difference of the material properties between the ballast track and the engineering structure. The engineering structure often composed of concrete or steel material, is supported by stiff layers (e.g., bridge piers are supported by firm soil or bedrock) and, therefore, has almost no settlement. On the contrary, the ballast track has larger settlement, which is mainly caused by the compaction of the ballast and soil layers and the breakage and pulverisation of ballast particles [8]. The permanent settlement of ballast in open tracks after construction or maintenance (tamping) can be divided into two stages according to the deformation mechanism of ballast [15, 21-23] (see Figure 2). Stage 1 is the rapid compaction and abrasion process that happens shortly after construction or tamping [15, 21]. In this stage, the main deformation mechanism is the volumetric compaction of the ballast particles. Stage 2 is the normal settlement process happening until the end of a maintenance interval, wherein the main deformation mechanism is the frictional sliding of particles [21, 24-27]. The settlement growth for ballast tracks is nonlinear in Stage 1, while it is almost linear in Stage 2 [21, 22]. The differential settlement can also be considered as a geometrical irregularity, which plays a major role in the degradation process of the track in transition zones [17, 28-32].

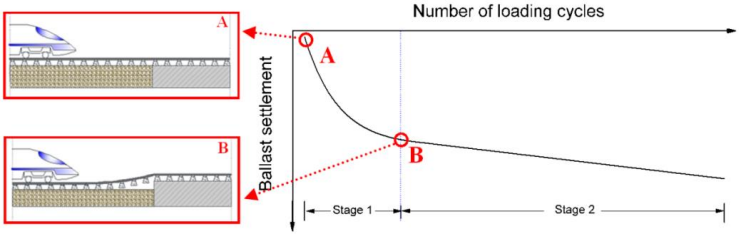

Figure 2. Schematic permanent settlement curve of ballast as function of loading cycles.

Besides the differential settlement, there is also the abrupt change in the vertical stiffness of the track [6, 13, 33-36] in transition zones. Since the vertical track stiffness determines the rail deflection during train passages, the stiffness variation leads to the changes in the vertical acceleration of moving trains and then results in the changes of the vertical wheel forces (about 9% increase calculated in [34]), the rail vertical accelerations [6], and the ballast stresses. The influence of the differential settlement becomes larger with the increase of the train velocities [6].

In addition, there are the geotechnical, construction and maintenance issues that affect the performance of transition zones, such as the poor quality of used materials, inadequate compaction and consolidation of the fill and embankment, poor drainage conditions [7, 11].

1.2 Research questions, and methods

PI

Although the causes of transition zone problems are known as mentioned earlier, there is still a discussion on which factor is more important. Most of the existing studies focus on stiffness variation, while the differential settlement has been less considered. In addition, there is no specific experimental method for assessment of the track performance in transition zones. Currently, the transition zones are treated as open tracks. Also, due to the insufficient knowledge on the track behaviour in transition zones, the track settlement in transition zones cannot be predicted precisely. As a result, the maintenance is performed in a reactive way. Lastly, although many countermeasures have been proposed for transition zones, there is no tool for assessment of the performance of the countermeasures, which causes difficulties for track designers when selecting countermeasures. Clearly, the knowledge on the measurement, dynamic behaviour, degradation, and improvement of the track in transition zones should be improved. Therefore, the research questions of this dissertation are as follow:

Q1: How to assess the condition of the tracks in transition zones? Using which tool?
Q2: Which factor contributes more to the track degradation in transition zones, the uneven settlement or the stiffness variation?
Q3: How to predict the track settlement in transition zones on a long term?
Q4: How to assess the performance of the countermeasures for transition zones?

The four research questions are inter-related. Q1 is proposed because there is no specific experimental method for performance assessment of the tracks in transition zones. Currently, the transition zones are treated as open tracks. However, due to the difference in the degradation mechanism, it is necessary to develop a specific measurement method for transition zones. The focus location of Q1 is indicated in Figure 1a.

If Q1 is answered, the track quality in transition zones can be assessed, which can provide more information for analysis of the primary cause of track problems in transition zones (Q2). Q2 is indicated in Figure 1c, where both the stiffness variation and the differential settlement appear in the transition zone. With better understanding of the degradation mechanism (answered by Q2), the settlement of the track in transition zones can be predicted more precisely (Q3). It is important since the studies on the long-term behaviour of transition zones are relatively rare and currently their maintenance is performed in a reactive way when some of the performance indicators exceed their limits, which is expensive and inefficient. Q3 is indicated by the dotted line pointing from the track geometry after operation shortly to the degraded track geometry after operation for a long time in Figure 1c. Finally, based on Q2 and Q3, the design improvement (countermeasures) of transition zones can be better assessed (Q4). The corrective countermeasures, which can quickly eliminate the void under sleepers when the differential settlement appears in transition zones and which have never been considered in the existing research, can be analysed. Q4 is indicated by the dotted line pointing at the opposite direction of Q3 in Figure 1c.

To answer the research questions, an integrated numerical and experimental methodology for analysis of the dynamic behaviour and degradation mechanism of the track in

transition zones is developed. The integrated methodology developed in this study consists of the following parts:

- An advanced measurement technique which uses DIC (Digital Image Correlation)-device to measure the dynamic displacements of rails at multiple points along the track in transition zones
  --This measurement technique is capable of assessing the track condition of transition zones, which is based on the idea in [4, 37, 38] but using advanced equipment (the DIC-device) and demonstrated in [38, 39]. It can measure the rail displacements at multiple points of transition zones during trains passing. The measured displacements can describe a detailed dynamic profile of the tracks in transition zones, based on which the track condition in transition zones can be assessed. It requires no track possession during the measurements.

- A novel model for analysis of the dynamic responses in transition zones using explicit Finite Element (FE) method, which accounts for both the stiffness variation and the differential settlement
  --The novelty of the model is it can model the realistic settlement curve of rails, the hanging sleepers, and therefore it can be better study the causes of the track degradation in transition zones. This model has been developed by the author since 2012.

- A novel iterative procedure to predict the track settlement in transition zones which combines the FE model of transition zones and an empirical settlement model of ballast
  --The procedure can study the long-term behaviour of transition zones. The empirical settlement model considers the two-stage settlement characteristics of ballast (see Figure 2) and the nonlinear relationship between ballast stress and ballast settlement [40]. The iterative procedure consists the following steps: (1) simulation of the vehicle-track and sleeper-ballast interaction during a train passing the transition zone, using the 3D FE model, to obtain the stresses in ballast; (2) calculation of the track settlement for a given number of loading cycles based on the ballast stresses, using the empirical settlement model; (3) adjusting the FE transition zone model based on the calculated settlement under each sleeper for the step (1) in the next iteration.

Each part of the integrated methodology can be used separately. When combining together, the integrated methodology can provide a comprehensive analysis for the tracks in transition zones. The applications are as follow:

- This advanced measurement technique has been used for analysis the track condition in three transition zones. The settlement affected zone has been detected and the hanging sleepers have been detected. Besides, the condition of the tracks in the transition zones has been assessed. The results have also been used to validate the numerical results and experimental results of the satellite system and inspection coaches.

PI

- The developed FE model has been used to study the effect of the differential settlement and stiffness variation on the track degradation in transition zones. The dynamic responses including wheel loads, ballast stress, rail stress, and car body acceleration are analysed.
- Another application of the methodology is the assessment of design modifications (countermeasures). Both a preventive and a corrective countermeasure used in the transition zones are analysed using the FE model. Besides, the effect of the moisture condition on the dynamic responses of the track in transition zones has been studied using the model.
- The predict procedure has been used to predict the relative the track settlement in the transition zone. Also, the settlement pattern is analysed. The sensitive parameters of the procedure are studied and the advice on maintenance for designers and maintenance staff are provided.

1.3 Dissertation outline

The outline of the dissertation is shown in Figure 3.

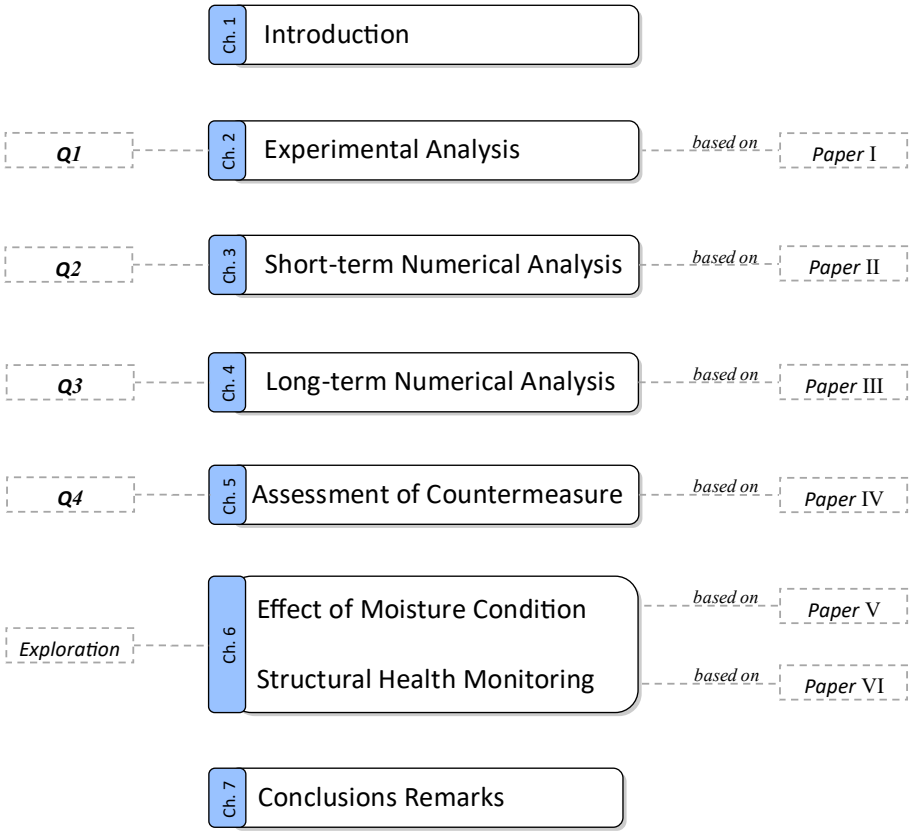

Figure 3. Outline of the dissertation.

The measurement method and the experimental analysis of the transition zone are presented in Chapter 2, which answers **Q1**. The FE model of the transition zone is introduced in Chapter 3 and then compared with the measured results. Using the model, the short-term dynamic behaviour of the transition zone is studied and the effect of the two factors is compared, which answers **Q2**. In Chapter 4, the settlement prediction procedure is described and the long-term behaviour of the transition zone is discussed, which provides the answer to **Q3**. The FE model of the transition zone is used as an assessment tool for countermeasures. Two countermeasures are assessed as examples in Chapter 5, which answers **Q4**. In addition, the effect of the moisture condition and the structural health monitoring of transition zones are explored in Chapter 6. The Ground Penetration Radar is used to study the moisture condition of ballast and subballast in transition zones. The satellite radar (InSAR) is used to monitor the structural health of a transition zone. At last, conclusions are given in Chapter 7.

PI

Chapter 2. Experimental Analysis

*An advanced measurement method for transition zones is proposed to answer **Q1** (see Figure 1a). After that, the experimental analysis using the method to assess the performance of transition zones is presented. The measurement technique employs a contactless mobile device for measuring displacements at multiple locations in transition zones. Three transition zones under various condition are measured. The dynamic profile of the track is analysed. The output of the experimental analysis will be used as the input for the short-term numerical analysis. This chapter is based on **[Part II: Paper I]**.*

2.1 Introduction to DIC

The proposed measurement method for transition zones is using the DIC (Digital Image Correlation) technique, which is an optical method using tracking and image registration techniques for accurate measurements in images. A reference image is captured before displacement and a series of pictures are taken subsequently during the movement. The images are analysed using a numerical matching technique to identify the most similar patterns in the subsequent images, which is based on the assumptions that the pattern is approximately constant between successive images and that the local textural information is unique. The matching algorithm compares the image subsets in the reference image with the image subsets in the current image [41]. Matching criteria are available such as in [42] and [43]. The method combines the continuous recording of horizontal and vertical displacements with no contact with the measuring targets, excluding any interference between the measured surface and the measuring device [44-46]. It often consists of high-resolution digital cameras which record the displacement of targets, and post-processors which analyse the changes in the images.

The device used in this study is shown in Figure 4, which includes a high-speed camera, software, and targets. In the normal monitoring condition, the accuracy of 0.1 mm can be obtained and the maximum measurement frequency is up to 400 Hz. Since the device has never been used in railway engineering, it has been tested in the laboratory prior to the field measurement to find the optimal operating parameters.

Figure 4. Setting of DIC-device: high-speed camera, software and targets on rails and sleepers.

In the laboratory tests, the DIC-based device was used to measure the motion of the actuator of a hydraulic press machine, which is the periodic vertical motion with the frequency of 0.1 Hz and the peak-peak amplitude of 10 mm. The tested operating parameters are shown in Figure 5. The details of the tests can be found in ***[Part II: Paper I]***.

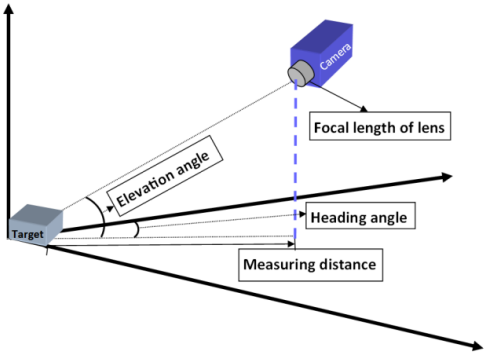

Figure 5: Illustration of operating parameters of DIC measurement.

After tests, the optimal operating parameters are proposed in Table 1. The elevation angle is a sensitive parameter, which is recommended to be smaller than 10° when the distance is 7.5 m and the height difference between the camera and the rail is 1.3 m.

Table 1 Recommended operating parameters.

Parameter	Suggest value
Elevation angle (°)	<10
Heading angle (°)	<30
Measuring distance (m)	7.5
Focal length (mm)	50

2.2 Field Measurements set-up

To demonstrate the measurement technique, the experimental analysis was applied to three transition zones were assessed using the DIC-based device, namely Transition A, B and C as shown in Figure 6. It should be noted Transition B is the one shown in Figure 1a. In Transition A and B, the embedded rail system is used on the bridges, while the ballast track with concrete sleepers is used on the embankment, as shown in Figure 6a and c respectively. According to the experience of maintenance staff, Transition A was in poor condition while Transition B in healthy condition. Therefore, larger dynamic displacements were expected in the affected zone than in the open track (referred as the affected zone) in Transition A. In Transition C, the ballast was used above the bridge and the performance was also poor, as shown in Figure 6e.

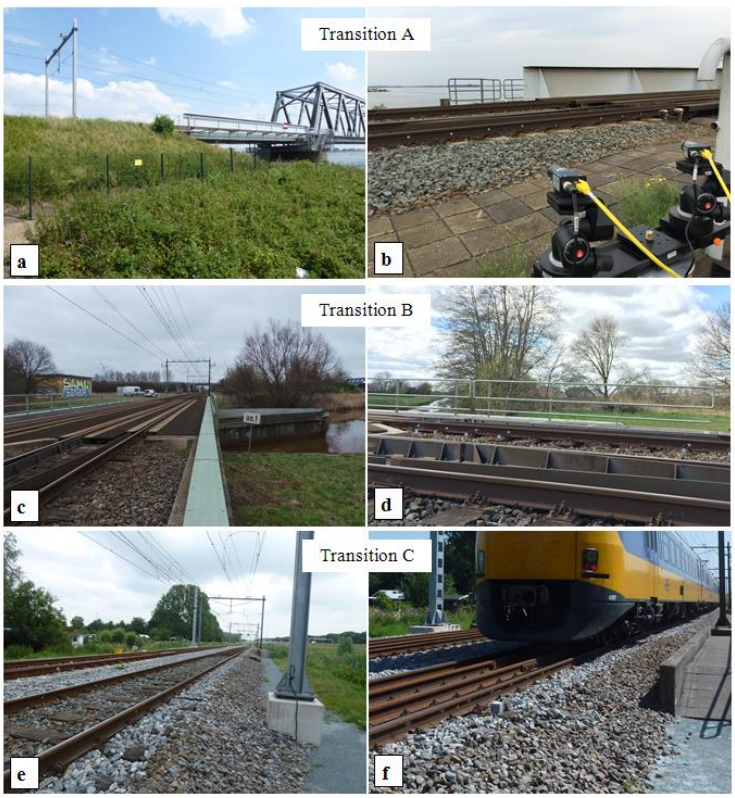

Figure 6. Photos of Transition A, B and C: overall photos (left) and partial photos of the targets on the rail (Right).

The measurement locations in the three transition zones is given in Figure 7 (based on Figure 1a). The first sleeper was located at 0.3 m from the abutment of the bridge and the sleeper spacing was 0.6 m. The measured locations are indicated by the red circles. During the measurement of Transition A, two synchronised cameras were used. One camera focused the track close to the bridge, from 0 m to 2.4 m; the other focused the track further, from 4.2 m to 6

PI

m. The rail displacement in open track (at 60.3 m) was measured separately since it was too far from the bridge. In total, 7 train passages were measured in the affected zone and 11 train passages were measured in the open track. The measuring frequency was 78 Hz. Similarly, measuring frequency in Transition B was 78 Hz. The rail displacements in the EB and BE transition were measured separately. 42 train passages were measured in the EB transition and were measured in the BE transition. In the measurement of Transition C, the measuring frequency was 31 Hz and 4 train passages were recorded. For convenience, the measured points on the rail are numbered from the bridge, wherein the negative sign is used to indicate the EB transition, while the positive the BE transition.

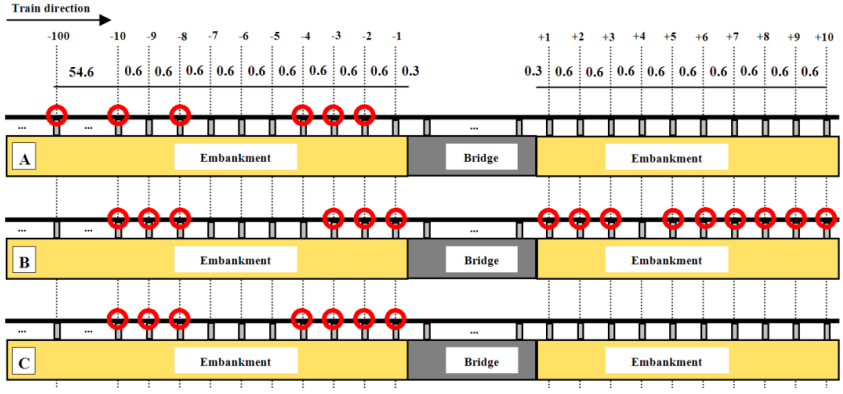

Figure 7. Schematic plan of measurements.

Using the measurement data in Transition A, the length of the affected zone is analysed. The rail displacements measured in the open track are compared with the rail displacements closer to the bridge. In addition, comparing with the measurement results of the EB transitions in Transition A, B and C, the relationship between the dynamic profile and the performance is studied. Moreover, since the displacements are measured on both sides (the EB and BE transitions) of Transition B, the dynamic profiles on different sides can be analysed.

2.3 Measurement results

2.3.1 Length of the affected zone

The measured examples of the displacements of the Rail-2, Rail-3, Rail-8 and Rail-100 (the open track) in Transition A are shown in Figure 8.

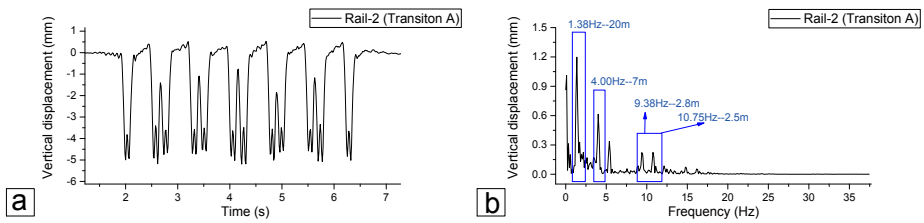

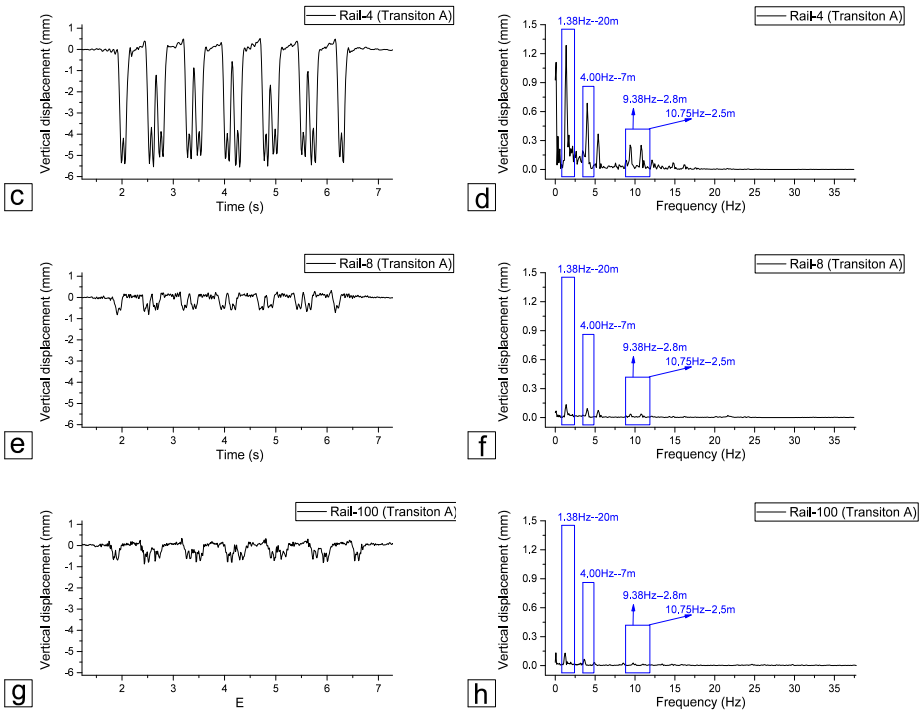

Figure 8. Rail vertical displacements at four locations of Transition A in time domain (a), (c), (e) and (g); in frequency domain (b), (d), (f) and (h).

As it can be seen from Figure 8, the peaks in the time history curves correspond to the passage of each wheel set. In the frequency domain, the peaks are matched very well with the frequencies due to the distances between the wheels of the train. Taking the displacement of Rail-2 (Figure 8b) for example, when the velocity of the trains is around 100 km/h, the 1st characteristic frequency is 1.38 Hz that corresponds to the bogie distance of 20 m; the 2nd characteristic frequency is 4.00 Hz that corresponds to the distance between two bogies of the neighbouring vehicles of 7 m; the characteristic frequencies of 9.38 Hz and 10.75 Hz correspond to the wheel distance in the bogies of 2.8 m and 2.5 m respectively. These characteristic frequencies can also be found in the measurements in other locations (Figure 8d, f and h). This shows that the results measured by the DIC-based device are correct.

The maximal displacements in all passages at multiple locations of Transition A are collected. Then, the average of the maximal displacements is calculated for each location, as shown in Figure 9, which can be considered as the dynamic profile of Transition A. It can be seen that the affected zone is most likely located within Rail-8 (4.5 m from the bridge), because the displacements at Rail-8 are similar to the ones at the open track (Rail-100), and much smaller than the displacements at Rail-2 and Rail-3. Since the condition of Transition A was considered as poor, the track settlement in the affected zone is naturally larger than in the transition zone of good condition. Therefore, 4.5 m can be considered as the upper limit for the length of the affected

PI

zone for this type of EB transition. Note that since the length of the affected zone depends on its engineering structure, the local subgrade property, and the train direction (e.g. EB and BE), it is only valid for the similar EB transitions. To validate this assumption and to study the affected zone, the rail displacements were also measured in another two transition zones.

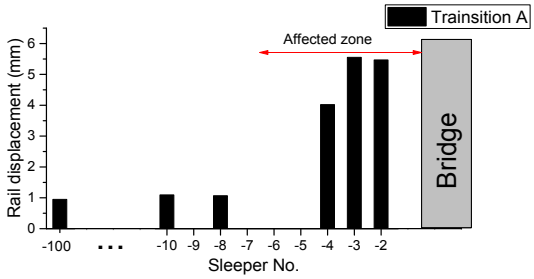

Figure 9. Dynamic profile of Transition A.

2.3.2 Dynamic profiles of transitions in various conditions

The example of the rail displacements measured at Rail-3 and Rail-8 in Transition A, B and C are shown in Figure 10.

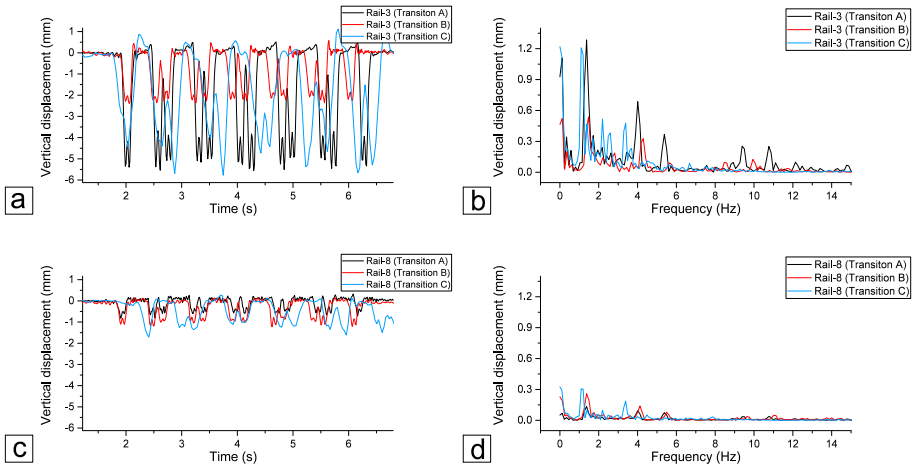

Figure 10. Rail vertical displacement at Rail-3 and Rail-8 in all transitions.

Comparing the results obtained in Transition B and Transition A and C, it can be seen that the rail displacements at Rail-8 are similar, which are 1.06 m, 0.63 mm and 1.06 mm respectively. It is logical, since the rail displacements at Rail-8 are close to the displacements in the open tracks, and the open tracks in the three transition zones are similar. However, the rail displacements at Rail-3 are considerably different, which are 5.27 mm, 2.27 mm and 4.86 mm in Transition A, B, and C, respectively. This means that the void under the hanging sleepers under Rail-3 in Transition A and C is larger than in Transition B. Based on the measurement results, the track in Transition A and C are in worse condition than in Transition B, which is in agreement with the track condition

known from the experience of maintenance staff. Based on the measurement results the dynamic profiles of Transition A, B and C were obtained, which are compared in Figure 11.

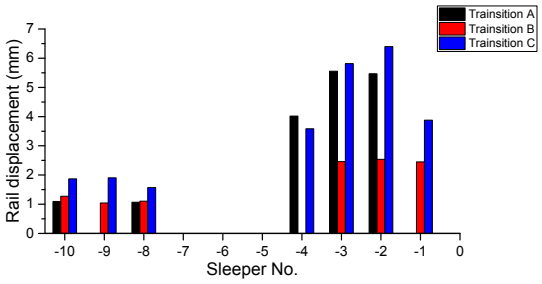

Figure 11. Comparison of vertical rail displacements in affected zone of two transitions.

By comparing the rail displacements at the close location from the bridge (Rail-2, Rail-3, and Rail-4) to that at the distant location (Rail-8, Rail-9, and Rail-10), the rail displacements are sharply increased in the affected zones (within Rail-8) in all three transition zones, as seen from Figure 11. The larger rail displacements confirm the 'dip' often reported in the transition zones (e.g., in [7]). The high displacements of rail indicate that the sleepers are in poor supporting condition, which leads to a significant redistribution of the wheel load [1, 32].

The rail displacements in Rail-2, Rail-3, and Rail-4 of Transition A were bigger than in Transition B, while the rail displacements in Rail-8, Rail-9, and Rail-10 were very close. It matches very well the experience of maintenance staff of these transitions that Transition A is in poor condition and Transition B is in good condition. Therefore, the ratio between the average of the rail displacements close to the bridge and that further from the bridge has a good correlation with the condition of the transition zones, which can be used as a Track Transition Quality Index (TTQI).

$$TTQI = \frac{\frac{1}{3}(Rail_{-2}+Rail_{-3}+Rail_{-4})}{\frac{1}{3}(Rail_{-8}+Rail_{-9}+Rail_{-10})}, \quad (1)$$

The calculated TTQIs of all three transition zones are shown in Table 2. The higher value indicates the worse condition of the transition zone. Therefore, by measuring the ratio of a transition zone, it is possible to know in which condition the transition is.

Table 2. Calculation of the measurements from the transition zones

Transition	Condition	$\frac{1}{3}(Rail_{-2}+Rail_{-3}+Rail_{-4})$ (mm)	$\frac{1}{3}(Rail_{-8}+Rail_{-9}+Rail_{-10})$ (mm)	Ratio (TTQI)
A	Poor	5.51	1.08	5.1
B	Good	2.48	1.14	2.2
C	Poor	5.36	1.78	3.0

Since currently there is no special detection method or evaluation standard for transition zones and maintenance scheme of transition zones are determined mostly by experience, this method has a potential to assess the condition and to determine maintenance scheme for certain

types of transition zones. However, it should be noted that all ratios obtained here are for the EB transition with similar structure (no special countermeasure is used).

PI

2.3.3 Dynamic profiles of two sides of transition bridge

The maximal displacements of rails at various locations in Transition B are summarized in Figure 12 where the average values are indicated by dots.

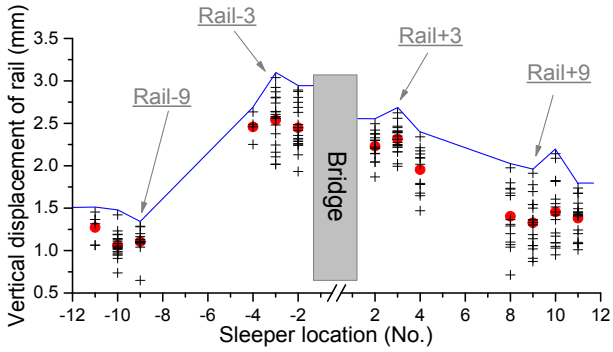

Figure 12. Summary of maximal rail displacements measured in Transition B. Average values are indicated by dots. Maximum are indicated by blue lines.

The measurement results show that rail displacements are significantly increased in both EB and BE transitions. As it can be seen from Figure 12, the maximal displacements near the bridge are larger in the EB transition than in the BE transition (compare the displacements 3.25 mm and 2.75 mm at Rail-3 and Rail+3 respectively). The affected zone is on the other hand is longer in the BE transition than in the EB transition zone (compare the displacements 2.25 mm and 1.5 mm at Rail+10 and Rail-10 respectively). Rail-10 is already open track while Rail+10 is still affected zone. The longer affected zone in the BE transition is related to the vertical bouncing motion of the vehicle that will be explained using the numerical model in Chapter 3.

To explain the dynamic behaviour of the transition zone with the differential settlement, the short-term numerical analysis is performed in the next Chapter.

2.4 Conclusions

This chapter answers **Q1** (How to assess the condition of the tracks in transition zones? using which tool?).

- A measurement method that can capture the detailed dynamic profile of the tracks in transition zones is proposed. The advantage of the method is that it can measure the dynamic displacements of rails at multiple points without track possession.

- The measurement method is used to assess the track condition in three transition zones. The results of the measurements match very well with the experience of maintenance staff, which demonstrates the capability of the method.

- Experimental analysis is performed according to the measurement results. The length of the affected zone in transition zones is determined. It is found that the dynamic profiles of the two sides of the bridge are different. The dynamic profile of the tracks can reflect the condition of the EB transition, based on which a Track Transition Quality Index is proposed for the assessment of the quality of transition zones.

Based on the accurate dynamic profile of the transition zones, the dynamic behaviour of transition zones can be better analysed. The measurement results will be used as an input to answer **Q2** in Chapter 3. It should be noted the measurements were conducted on the Dutch railway lines (max operational velocity is 140-160 km/h, the foundation is relatively soft, wheels are in good condition). For other circumstances, the experimental results could be different. The detailed experimental analysis can be found in ***[Part II: Paper I]***.

PI

Chapter 3. Numerical analysis: short-term behaviour

*In order to answer **Q2** (see Figure 1c), a novel model for analysis of the dynamic responses in transition zones (modelled according to the transition zone in Figure 1) is developed, which uses contact elements to describe the sleepers-ballast interface and the pre-loading features. As a result, the more realistic settlement curve of the rails and the dynamic responses of the sleepers can be obtained. The numerical analysis of the short-term behaviour of the track in the transition zone is studied using the FE model. This is the second part of the developed methodology. The measured rail displacements from the experimental analysis (Transition B) are used to tune the differential settlement value used in the FE model. The dynamic responses (wheel loads, ballast stress, rail stress, and car body acceleration) are obtained using the FE model to study the degradation mechanism of the track in the transition zone. Also, the parametric studies of the differential settlement value and the velocity are conducted. This chapter is based on **[Part II: Paper II].***

3.1 Finite Element model of transition zones

The FE model is developed according to the typical transition zone (see Figure 1a), which consists of two ballast tracks on embankments and a slab track on a bridge, as shown in Figure 13. The ballast tracks are both 48 m long and the bridge is 24 m long. The 'bridge' in the model is symbolical and not analysed since the purpose is to study the effect of the transition zone rather than the bridge itself. Using the transition zone model, two types of transition (the EB and the BE transition) can be analysed in one run. Since the left end of the model is set as 0 m, the EB transition locates at 48 m, and the BE transition locates at 72 m. The total length of the model is 120 m.

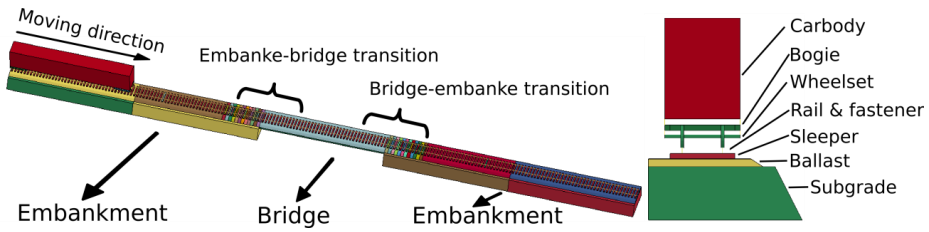

Figure 13. FE model of the transition zone.

The components of ballast tracks are rails, fasteners, sleepers, ballast and subgrade. The rails are modelled by Hughes-Liu beam elements with 2*2 Gauss quadrature integration [47]. The cross-sectional and mass properties of the UIC54 rails are used and the element length of rail is 75 mm. Spring-damper elements between rails and sleepers are used to simulate fasteners. In the vertical direction, these springs have nonlinear properties so that in compression they have the

stiffness of rail pads; while in tension, the stiffness is much higher to simulate the clamping effect of fasteners. The material properties of spring-damper elements are collected in Table 3. Note that the parameters of the numerical model are determined by the suggestions in [10, 48-52] and tuned by field measurement results.

Table 3. Material properties of spring-damping elements

	Horizontal	Vertical	Longitudinal
Stiffness (N/m)	1.5E6	1.20E8 (compression) 1.20E11 (tension)	1.5E6
Damping (N*s/m)	5.00E4	5.00E4	5.00E4

Sleepers, ballast, and subgrade are modelled by three-dimensional elastic bodies which are composed of the selective reduced integrated hexahedral solid elements [47]. The selective reduced integration is one-order lower than full integration which assumes that pressure is constant throughout the element to avoid pressure locking during nearly incompressible flow [47]. Since the main concern in this model is the behaviour of ballast, small elements are used to model sleepers and ballast, which are 75 mm. On the contrary, the element length of the subgrade is 0.3 m. The thickness of the ballast and subgrade layers is 0.3 m and 2 m, respectively. The bridge is simplified as a two-layer structure, with a concrete slab and a support layer. The rails on the bridge are direct fastened to the concrete slab. In the current study, the elements used for the sleepers, ballast, subgrade as well as the bridge have linear isotropic elastic material properties, which are presented in Table 4.

Table 4. Material properties of solid elements

	Sleeper	Ballast	Concrete slab	Support layer	Subgrade
Elastic Modulus (Pa)	3.65E10	1.2E8	3.50E10	3.30E10	1.80E8
Poisson's ratio	0.167	0.25	0.167	0.25	0.25
Suggested by	[50]	[50]	[51]	[52]	[10]

The vehicle is a passenger train, which is modelled as a mass-spring system. It consists of a car body, two bogies and four wheel sets connected by the primary and secondary suspensions, which are modelled using rigid bodies and spring-damper elements. The parameters of the vehicle are based on [53] and adapted to a Dutch passenger train [5, 54]. Contact between wheel and rail is modelled using the Hertzian spring with the stiffness:

$$k_H = \sqrt[3]{\frac{3E^2Q\sqrt{R_{wheel}R_{railprof}}}{2(1-v^2)^2}}, \tag{2}$$

where E is the modulus of elasticity of the wheel and rail; v is the Poisson's ratio; Q is the static vertical wheel load; R_{wheel} is the radius of the wheel; $R_{railprof}$ is the radius of the railhead [55, 56].

The connection between sleepers and ballast is modelled by contact elements in order to accurately present the spatial movement of sleepers and consequent ballast stresses. The contact

elements employ the penalty method, which places normal interface springs between all penetrating nodes and the contact surface, as shown in Figure 14.

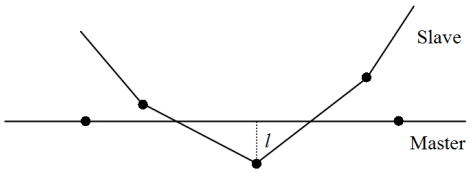

Figure 14. Schematic diagram of the penalty contact method.

According to the method, the search for penetrations between the bottom surface of sleepers and the top surface of ballast is made for every time step during the calculation. In the case that no penetration happens, no force is added. When the penetration between contact surfaces is found, a force proportional to the penetration depth is applied to resist and ultimately eliminate the penetration [47]. If slave node n_s penetrates through master segment s_i, the interface force vector f_s can be expressed as:

$$f_s = -lk_i n_i, \qquad if\ l < 0\ , \tag{3}$$

where l is the penetration; k_i is the stiffness factor for master segment s_i; n_i is normal to the master segment at the contact point. The stiffness factor k_i is:

$$k_i = \frac{f_{si} K_i A_i^2}{V_i}, \tag{4}$$

where f_{si} is a scale factor for the interface stiffness; K_i is the bulk modulus; A_i is the face area of the element that contains s_i; V_i is volume [47].

The simulation procedure consists of two phases. In the beginning, only the gravity is applied to the model to reach the equilibrium state. After equilibrium state has been achieved, the velocity is applied to vehicle components so that the train moves from the left end to the right end. During the passage, the train first moves across the EB transition and then the BE transition.

3.2 Sleeper-ballast interaction

As discussed above, it is of importance to simulate the differential settlement. According to field measurements and laboratory tests [1, 21, 22, 24, 25, 57], the ballast track is rapidly compacted after construction or maintenance (see Figure 2). The ballast track on the embankment is assumed to have an even settlement while the bridge is unsettled. A downwards displacement is applied to the ballast and subgrade layers in the ballast tracks on both sides of the bridge, while the vertical geometry of the bridge remains unchanged. The value of differential settlement used in the model is determined by tuning according to the field measurement results of Transition B in Chapter 2. The value 4 mm is obtained and used here. Other values of the differential settlement are discussed in Chapter 3.2. It should be noted that the value highly depends on the track and traffic

PI

condition. For other transition zones, it could be different and the field measurement is therefore necessary. The effects of the differential settlement and train velocity are discussed in Chapter 3.4.

Because the sleepers are clamped to rails by fasteners, voids under the sleepers will occur at the beginning of the simulation as a result of the differential settlement. After the stabilisation phase, the sleepers near the bridge are hanged due to the bending resistance of rails. Figure 15 shows the vertical coordinates of the sleepers and ballast in the BE transition in the equilibrium state; and the time history of the vertical coordinate of a hanging sleeper (Sleeper+2) during the vehicle passing. The numbering system similar to the field measurements is used here.

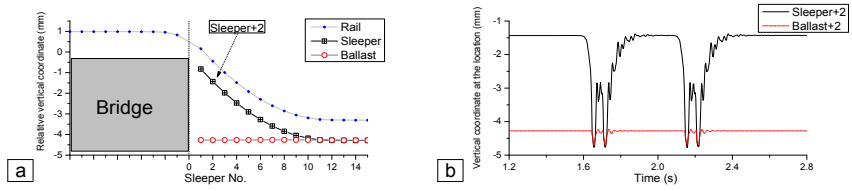

Figure 15. Vertical coordinates of rail, sleepers and ballast at BE transition due to 4 mm settlement of ballast (a); Time history of vertical coordinate of Sleeper+2 during vehicle passing (b).

3.3 Model validation

The maximum of the vertical displacements of the rail during the train passing is calculated using the FE model, as shown in Figure 16. The simulation results are compared with the measurement results of Transition B presented in Chapter 2.3, where the black dots and crosses correspond to the simulation and measurement results, respectively. The value of differential settlement used in the model is 4 mm. The velocity of the moving vehicle is adjusted according to the measurement.

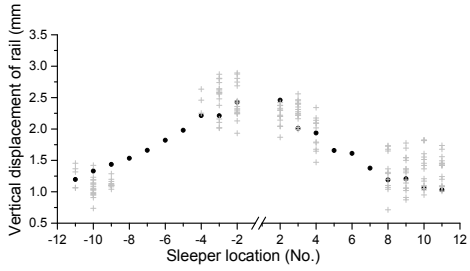

Figure 16. Comparison between measurements and simulation: black dots - simulation and cross - measurement results.

From Figure 16, it can be seen that the measured and simulated displacements follow the same pattern, i.e. they increase near the bridge and decrease as the distance from the bridge grows. Also, the magnitude of the measured and simulated displacements is very close, which means that settlement assumed in the numerical model is close to the actual settlement of the measured transition zone. A detailed comparison between the measurement and simulation

results is given in Figure 17. In the frequency domain, the results are filtered using a low-pass filter with the cutting frequency of 35 Hz. More validation can be found in ***[Part II: Paper II]I***.

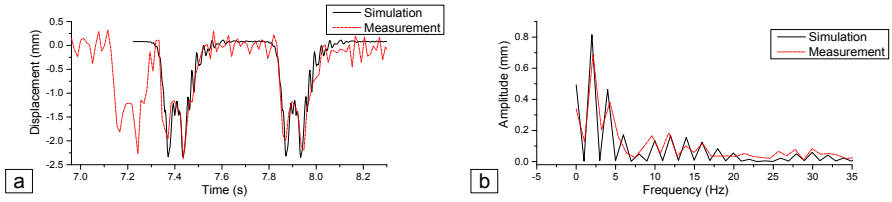

Figure 17. Detailed comparisons of measurement and simulation results in the time domain (a), in the frequency domain (b).

Figure 16 and Figure 17 show that the simulation results have a good correlation with the measurement data both in the time and frequency domain. Therefore, it can be concluded that the model can accurately describe the dynamic behaviour of the transition zone and can be used in the further study.

3.4 Simulation results

Using the FE model, the dynamic wheel forces during the train passing the transition zone (at the velocity of 144 km/h) are shown in Figure 18 where the wheel forces on the bridge are in the shaded area since they are out of the scope of this study. In order to compare the effect of the differential settlement, a transition zone without the differential settlement (stiffness variation only) is used as a reference. Note that the stiffness variation is considered in both cases, while the differential settlement is only considered in one case. For convenience, the two cases are referred to as *No settlement case* (stiffness variation only) and *Settlement case*. In addition, the maximal wheel forces on the embankment are collected in Table 5 as well as the increase percentages w. r. t. open tracks.

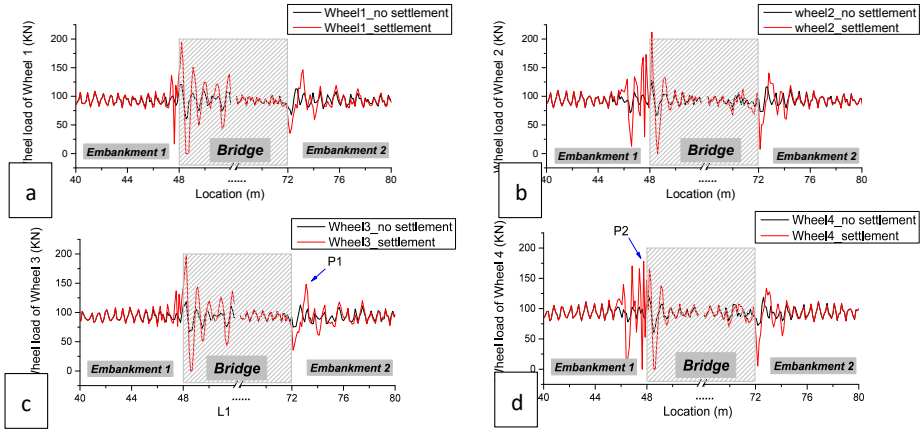

PI

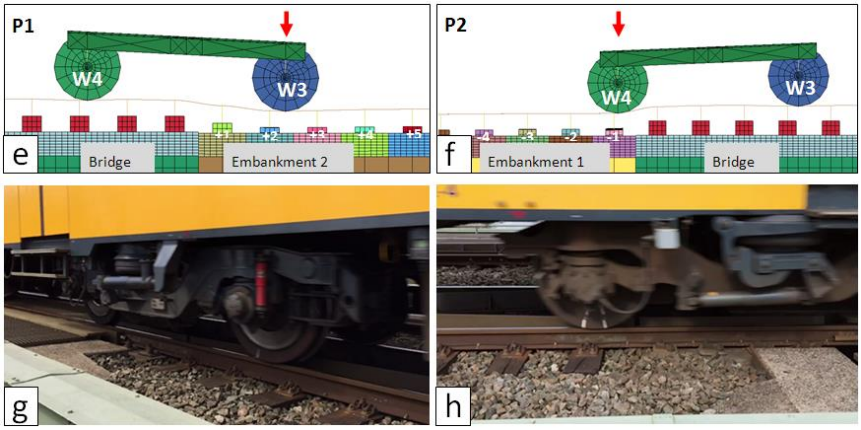

Figure 18. Calculated wheel loads of four wheel sets (a)-(d); the rear bogie at corresponding moment of P1 from the FE model (e) and from the field photo (g); the rear bogie at corresponding moment of P2 from the FE model (f) and from the field photo (h).

Table 5. Maximal wheel loads (kN)

		EB transition	BE transition
Far from the bridge (Open track)		93.1	93.1
No settlement	Wheel 1	93.1	113.2
	Wheel 2	93.1	117.0
	Wheel 3	93.1	112.8
	Wheel 4	93.1	**119.0**
Settlement	Wheel 1	136.4	146.3
	Wheel 2	172.8	140.8
	Wheel 3	136.9	**148.2**
	Wheel 4	**178.0**	133.3

3.4.1 Stiffness variation vs Stiffness variation&differential settlement

From Figure 18a-d and Table 5, it can be seen that although both stiffness variation and differential settlement increase the wheel loads, the increase caused by the settlement is significantly higher (91.2% compared to open tracks) than that the increase generated by the stiffness variation alone (27.8% compared to open tracks).

Also, the wheel forces of all wheels are significantly amplified in both transitions when the differential settlement is considered. The increase explains the extra degradation often observed in transition zones.

3.4.2 EB transition vs BE transition

It can also be seen that the behaviour of the EB transition is different from that of the BE transition. The amplification of the forces in EB transition is higher and closer to the bridge (above Sleeper-1, see Figure 18f), which can be found in Figure 18b and Figure 18d, e.g., the increases are

up to 85.6% and 91.2% in the case of differential settlement. On the contrary, the amplification of the forces in the BE transition appears further from the bridge (above the Sleeper+2 and Sleeper+3, see Figure 18e) with the lower increases (approximately 50%).

It confirms the theoretical analysis in [13]: when the wheel approaches the bridge, the wheel force is increased at the abutment due to the fast elevation; when the wheel leaves the bridge, the wheel drops off and impacts on the embankment at the location depending on the train speed. The higher the speed, the larger distance from the abutment the wheel drops at. After dropping at the embankment, wheels may bounce on the tracks on the embankment, which causes large fluctuation of wheel loads (see the BE transition in Figure 18a-d). This explains why the affected zone in the BE transition is longer than that in the EB transition (see measurement results in Figure 12).

3.4.3 Effect of vehicle

Moreover, the wheel forces of four wheels are different, which shows that using the vehicle model instead of moving loads is necessary for the study of transition zones. The front wheels (see Figure 18a for Wheel 1 and Figure 18c for Wheel 3) mainly cause an impact on the BE transition when the bogie is leaving the bridge, which correspond to Figure 18e and Figure 18g. The rear wheels (see Figure 18b for Wheel 2 and Figure 18d for Wheel 4) generate the highest force in the EB transition when the bogie is moving to the bridge, which correspond to Figure 18f and Figure 18h.

The pitch motion of the bogie can be clearly seen in Figure 18e and Figure 18f, which is due to the presence of differential settlement and also affected by the stiffness of suspensions. In the EB transition, the wheel loads are increased by the rapid change of the elevation and the load redistribution between wheels caused by the pitch motion of the bogie. The amplified zone in the EB transition is in particular determined by the geometrical properties of the bogie. In the BE transition, the wheels ‘glides’ from the bridge, ‘drops’ and later ‘bounces’ on the ballast track, which causes the increase of the wheel loads. The amplified zone in the BE transition is determined by the train velocity and the differential settlement. Similarly, the car body of the vehicle also rotated due to differential settlement, which can be proved by the variation of two bogies (see Table 5).

3.4.3 Ballast stress vs wheel load

The maximal stresses in the ballast layer due to passing trains at various locations are shown in Figure 19. The transition zone without the differential settlement is also used as a reference. The stresses are collected by the following methods. (1) The ballast elements under one sleeper are considered as a group (unit). (2) The stresses history curves of the ballast elements from a group during the train passage are collected and the average is calculated. (3) The maximum of the average stresses of a group (under a sleeper) is obtained. (4) The values under other sleepers in the transition zone are collected.

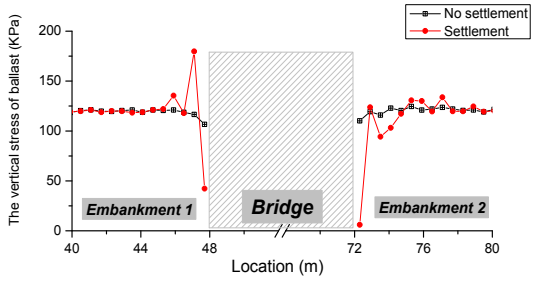

Figure 19. Average vertical stress in ballast.

Figure 19 shows ballast stresses are also significantly increased near the bridge in the transition zone with the differential settlement, but different on the two sides. In the transition zone without the differential settlement, the ballast stresses are only slightly increased in the BE transition. In the EB transition (with differential settlement), the ballast stresses are increased within a shorter zone (2.1 m) and with high amplification (179.8 kPa); while in the BE transition, the amplification appears until 5.1 m with a smaller value (133.7 kPa).

Ballast stresses (Figure 19) correlate mostly but not exactly to wheel loads (see Figure 18). For instance, the wheel force reaches the maximal at Sleeper-1 (0.3 m) in the EB transition. However, the highest ballast stress appears at Sleeper-2. One reason is that the sleepers are still hanging under the passing vehicle load. At this moment, the stress in rail increases, while the stress in ballast does not. In the BE transition, the highest wheel force is above Sleeper+2 and Sleeper+3; on the contrary, the ballast stress under Sleeper+3 is lower than others, while it reaches the maximum at Sleeper+9. It is also because the vehicle fluctuates heavily after it leaves the bridge. The reduction of the ballast stress under Sleeper+3 can be explained by wheels bouncing over the sleeper.

Therefore, even though the increased wheel force is the major resource for the amplification of ballast stress, the ballast stress is also caused by the supporting condition of sleepers and the spatial movement of sleepers.

3.5 Parametric study of the model

Two critical parameters of the transition zone model are discussed, which is the value of the differential settlement and the train velocity.

3.5.1 Effect of differential settlement

To study the differential settlement, three degradation processes of transition zones are considered, which are new (after construction), slightly degraded, and degraded. The values of the differential settlement in the three cases are 0 mm, 2 mm, and 4 mm, respectively. The wheel loads and ballast stresses are analysed and shown in Figure 20 and Figure 21 respectively. It should be noted that the rapid compaction of ballast tracks (Stage 1 in Figure 2) is somewhat inevitable due to the material property of ballast and the issues of construction and maintenance. The 0 mm case does not exist after the operation. It is only used as a reference to analyse the effect of the differential settlement on the dynamic responses. The train velocities are 144 km/h (as same as

the previous chapter).

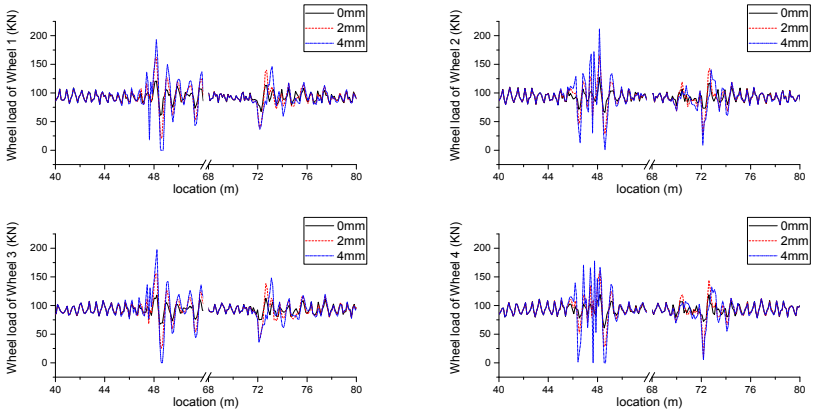

Figure 20. Comparison of the wheel loads among three differential settlement cases.

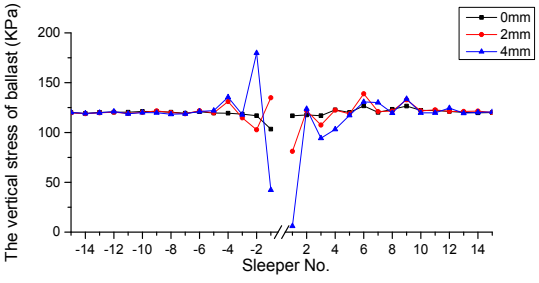

Figure 21. Comparison of the ballast stresses among three differential settlement cases.

As expected, both the wheel loads and ballast stress are increased as the differential settlement grows. In the case of the new transition zone (0 mm), the wheel loads are slightly increased (e.g., 113 kN at 72.7 m, increased by 23.7%). This confirms the findings in [6, 13, 33-36] that the stiffness variation leads to the increase of wheel loads. Comparing the slightly degraded transition zone (2 mm) to the degraded transition zone (4 mm), it can be found that the amplification of the wheel loads and ballast stress becomes higher as the differential settlement increases.

3.5.2 Effect of train velocity

The effect of the train velocity on the dynamic responses of transition zones is discussed. Three values of the train velocity are considered, which are low (72 km/h), medium (144 km/h) and high (288 km/h). The comparisons of the wheel loads and ballast stresses are shown in Figure 22 and Figure 23. It should be noted that the differential settlement is 4 mm in all the three cases (as same as Chapter 3.3).

PI

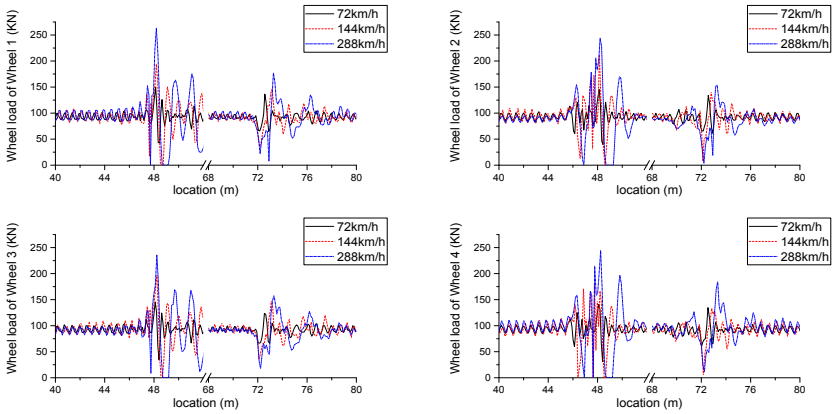

Figure 22. Comparison of the wheel loads among three velocity cases.

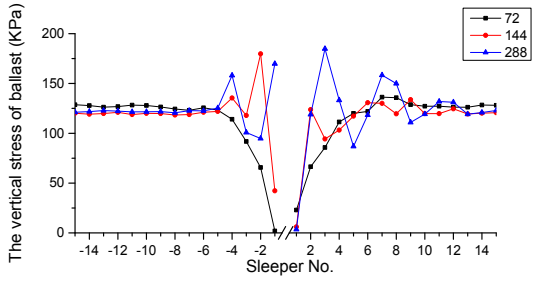

Figure 23. Comparison of the ballast stresses among three velocity cases.

As it can be seen from Figure 22, the wheel loads rise with the increase of the train velocity. For example, the amplification of the wheel load of Wheel 1 is 150 kN at 48.1 m in the case of the low velocity (72 km/h), and the amplification in the case of the high velocity (288 km/h) is 263 kN, which is increased by 75.3%. It is consistent with the finding in [6]. Figure 23 shows that the ballast stresses are barely increased when the trains move at the low velocity (72 km/h), and the ballast stresses are increased with the velocity. In the BE transition, both the amplitude and the length of the fluctuation of the ballast stress are increased. The reason is that when trains 'drop down' from the bridge to the embankment, the higher the velocity is, the further the trains land.

3.5 Conclusions

This chapter answers **Q2** (Which factor contributes more to the track degradation in transition zones, the uneven settlement or the stiffness variation?)

- The developed FE model of the transition zone, which considers the differential settlement and sleeper-ballast contact, is described. The differential settlement of the FE model is tuned according to the measurement results in the experimental analysis (Transition B). After that, dynamic rail displacements calculated by the FE model is compared with the measurement results to validate the model.

- The short-term numerical analysis of the transition zone using the FE model explains the degradation mechanism of transition zones and also confirms the findings of the experimental analysis.

- The increase caused by the differential settlement is significantly higher (up to 90%) than that the increase generated by the stiffness variation alone. Therefore, the differential settlement should always be taken into account when analysing or improving the track performance in transition zones.

- In the EB transition, the wheel loads are increased by the rapid change of the elevation and the load redistribution between wheels caused by the pitch motion of the bogie. The amplified zone in the EB transition is in particular determined by the geometrical properties of the bogie. In the BE transition, the wheels 'glides' from the bridge, 'drops' and later 'bounces' on the ballast track, which causes the increase of the wheel loads. The amplified zone in the BE transition is determined by the train velocity and the differential settlement.

With a better understanding of the causes of the track degradation in transition zones, the track settlement can be predicted more precisely (**Q3**). In addition, the FE model will be used as a part of the prediction procedure for transition zones in Chapter 4. The detailed analysis can be found in ***[Part II: Paper II]***.

PI

Chapter 4. Numerical analysis: long-term behaviour

*In order to answer **Q3** (see Figure 1c), a novel iterative procedure to predict the track settlement in transition zones is proposed in this chapter. After that, the long-term numerical analysis of the transition zone is presented using the method, which is the third part of the methodology. The settlement prediction procedure is introduced and the track settlement in the transition zone (see Figure 1a) after the 2-year operation is predicted. The settlement pattern is analysed and compared with the history of track longitudinal level measured by the inspection coach. This chapter is based on **[Part II: Paper III].***

4.1 Settlement prediction procedure

To predict the settlement in the transition zone, the developed FE model (presented in Chapter 3) is coupled with an empirical settlement model. As mentioned in Chapter 1, the ballast settlement can be divided into 2 stages (see Figure 2). The total settlement of the ballast at location i can be calculated as:

$$S_i = S_{Ii} + S_{IIi}\,, \tag{5}$$

where S_i is the total settlement of the ballast at location i; S_{Ii} and S_{IIi} are the settlement value of ballast generated at location i in Stage 1 and Stage 2, respectively. S_I depends on the traffic, construction, maintenance, and geotechnical conditions and therefore different in each case. In the current study, it is determined by using the experimental method presented in Chapter 2 and also used in the short-term numerical analysis (Chapter 3), which is 4 mm. S_{IIi} is a function of the loading cycles, which can be written:

$$S_{IIi} = k_i \times N, \tag{6}$$

where k_i is the settlement rate at location i and N is the number of loading cycles. The settlement rate k_i can be calculated by the widely used empirical settlement model for ballast tracks, which describes the relationship between the settlement growth and the sleeper-ballast contact pressure. The empirical settlement model was initially proposed in [40] and later developed in [22]. According to this model, the sleeper-ballast pressure is used as an input to calculate the settlement rate k_i of train operation as:

$$k_i = 4.365 \times 10^{-12} \times (0.68 \times p)^{5.276}, \tag{7}$$

where p is the sleeper-ballast pressure; 4.365×10^{-12}, and 5.276 are fitting coefficients; and 0.68 is the contact area of the sleeper in [m^2] (the nominal concrete sleeper length 2.570 m time the nominal sleeper width 0.265 m, as used in [58]). According to Equation (7), the settlement rate at location i (S_i) is shown in Figure 24.

PI

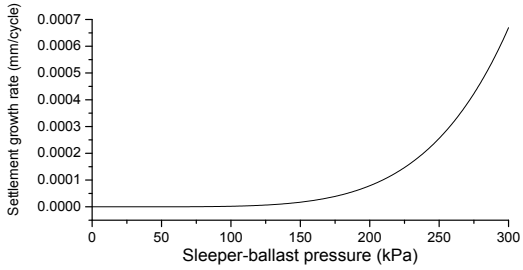

Figure 24. Relationship between settlement growth and sleeper-ballast pressure.

The iterative procedure for the settlement prediction in transition zones is presented in Figure 25. In the beginning, the existing ballast settlement due to rapid compaction S_I is applied and the ballast stress under each sleeper is calculated using the FE transition model (Step A to B). The settlement rate k_i is calculated according to Equation (7), which is Step B to C. Then, using Equation (6), the permanent settlement of ballast under each sleeper after N cycles of train operation S_{II} is calculated (Step C to D). The generated settlement (S_{II}) will be applied to the existing ballast settlement for the next iteration (Step D to A). It should be noted that the method predicts the absolute settlement, but since it is difficult to validate in the current stage, the predicted settlement can be better used relatively, e.g. for comparison of various track transition designs.

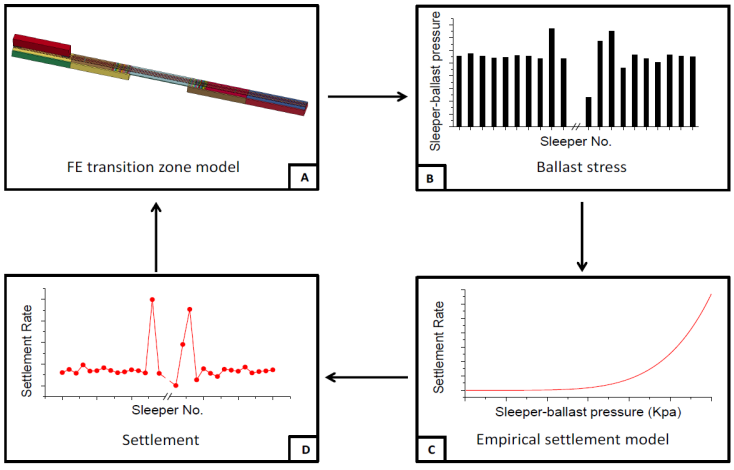

Figure 25. Iterative procedure to predict the settlement in the transition zone.

4.2 Prediction results

Using the prediction procedure, the 2-year track settlement in the transition zone model studied in Chapter 3.4 has been calculated. The results are shown in Figure 26, where the accumulated settlement curves after each run iteration are shown. The existing ballast settlement due to rapid compaction S_I is 4 mm as mentioned earlier. The number of loading cycles (N) in each cycle is

20,000, which is equivalent to 1.5 months of operation, assuming 5 vehicles in a train, 6 trains in an operational hour, and 15 operational hours in a day. Note that the number of loading cycles N can also be other values. A detailed parametric study can be found in ***[Part II: Paper III]***.

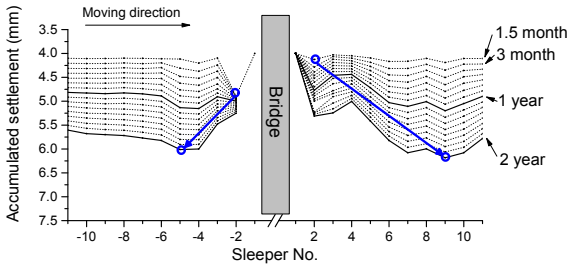

Figure 26. Predicted settlement after 2 years.

As it can be seen from Figure 26, the ballast settlement (dips) appears in the transition zone after a short time and accumulates over time in both transitions. In addition, the settlement expands in both transitions, which can be seen by the maximum of the settlement moves away from the bridge. The reason for that is that when the settlement appears in the ballast, the sleepers above the settlement ballast are hung. As the hanging process initiated, the stresses in the ballast under the hanging sleeper are reduced and the maximum stress in ballast is moved to the neighbouring sleeper. The high stress in the neighbouring sleeper leads to extra settlement, which results in the expansion of the settled zone. The finding is confirmed by field observations that the dips in transition zones gradually propagate farther from bridges. Figure 27 shows the measured track vertical geometry of a typical transition zone (shown in Figure 1) before and after 2 years of operation (without maintenance), where the propagation of dips can be seen, as indicated by arrows.

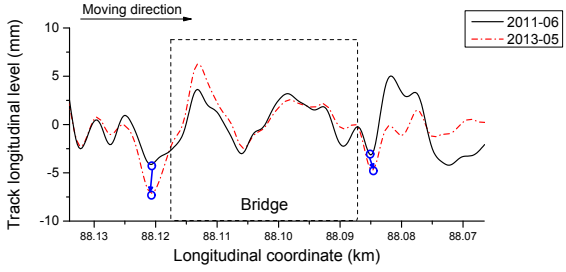

Figure 27. Measured track vertical geometry before and after 2 years of operation.

It can also be found in Figure 26 that the growth of the settlement is different in two transitions. In the embankment–bridge transition, the bottom of ballast settlement moves from Sleeper-2 (after 1.5 months) and Sleeper-5 (after 2 years). On the contrary, that in the BE transition moves from Sleeper+2 to Sleeper+9. As a result, the settlement in the EB transition is concentrated to the bridge, while that in the BE transition is dispersed away from the bridge. This is in agreement with the field observation (discussed in Chapter 2.3) and the short-term analysis

(discussed in Chapter 3.4). Since the growth of the settlement is different in the EB and the BE transition, the corresponding maintenance and mitigation should be considered separately.

PI

4.3 Conclusions

This chapter answers **Q3** (How to predict the track settlement in transition zones on a long term?).

- A novel prediction procedure for the track settlement in transition zones is introduced, which combines the developed FE model of transition zones (used in the short-term numerical analysis) and an empirical settlement model of ballast. In every iteration, the ballast stress calculated by the FE model is used as input for the empirical settlement model; after that, the newly generated ballast settlement is applied back to the FE model.

- The long-term numerical analysis of the transition zone is conducted using the prediction procedure, based on which the settlement and its growth in transition zones are analysed.

- The settlements (dips) appear in the transition zone after a short time. After that, the dips continuously grow and move away from the bridge as the number of loading cycles increasing. Since the stresses in the ballast under the hanging sleeper are reduced and the maximum stress in ballast is moved to the neighbouring sleeper, the settled zone is expanded from the bridge over time, which is confirmed by the history of the track geometry measurements.

- The settlement in the EB transition is concentrated to the bridge, while that in the BE transition is dispersed away from the bridge, which is in agreement with the field observation and the short-term analysis. Therefore, the maintenance in transition zones should be performed in different ways on two sides.

It should be noted that the method predicts the absolute settlement, but since it is difficult to validate in the current stage, the predicted settlement can be better used relatively. In order to improve the accuracy of the prediction procedure, more calibration of the method should be conducted in the future. The detailed analysis and parametric study of the method can be found in ***[Part II: Paper III]***.

Chapter 5. Assessment of countermeasures

*This chapter is to answer **Q4** (see Figure 1c), using the developed FE model of transition zones. A preventive countermeasure (modified sleepers) and a corrective countermeasure (adjustable fasteners) for the transition zone are assessed as examples. The countermeasures to analyse are introduced. After that, the effect of the countermeasures on the dynamic responses of the tracks in transition zones is analysed numerically, which can provide suggestions for designers or maintenance staff when selecting countermeasures. This is the application of the methodology. This chapter is based on **[Part II: Paper IV]**.*

5.1 Introduction to countermeasure

According to the settlement behaviour of ballast track (discussed in Chapter 1), The countermeasures for transition zones can be divided according to their application period, which is either the design stage (referred as preventive measures) or the operation stage (referred as corrective measures).

When designing a transition zone, the primary goal is to construct a zone with smooth changes from the embankment to the engineering structure [59]. The preventive countermeasures are applied to embankments or/and engineering structure, the intent of which is either to reinforce the ballast track [52, 60] or to decrease the stiffness of the track on the engineering structure [3, 61].

When the preventive countermeasures do not mitigate the track degradation efficiently, e.g. [4, 11], or no countermeasures are used, e.g. [1, 38], critical differential settlement may appear in a maintenance cycle. The differential settlement may result in the damage of track components and deterioration of the passenger's comfort. To mitigate the existing differential settlement, the corrective countermeasures are necessary. Besides, the hanging sleepers also appear in the vicinity of the engineering structure. However, due to the abutment or the transition structure, it is not always possible for tamping machines to perform track maintenance near engineering structures. In these situations, corrective countermeasures that can be performed manually or by small packing machines can be applied. The general principle of the corrective countermeasures is to fill the gaps between the sleepers and ballast to eliminate hanging sleepers.

5.2 Preventive countermeasure (modified sleepers)

Using modified (enlarged) sleepers in the ballast track can increase the contact area between sleepers and the ballast, and consequently reduce the ballast stress. Three modified sleeper designs for transition zones are analysed in a typical transition zone (as shown in Figure 1), which are wide sleepers, long sleepers, and long&wide sleepers. The dynamic responses of the transition zones using the three designs are compared with the transition zone without any countermeasure design (normal design). The velocity of the vehicle is 144 km/h, which is a typical operational

PI

velocity in the Netherlands. The modified sleepers are only used to replace the 12 sleepers close to the bridge from each side (i.e. 24 sleepers in total), because the amplification of the dynamic responses is mostly within this region as discussed in Chapter 3.4. The configuration of sleepers is shown in Figure 28.

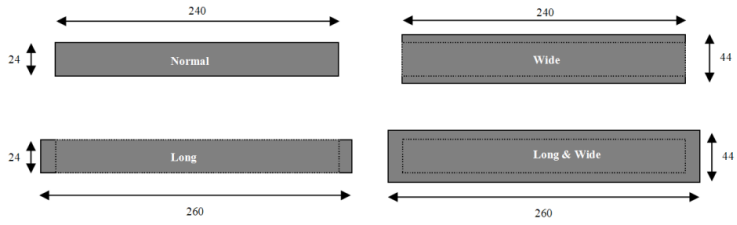

Figure 28. Shape of varied sleepers.

Since the permanent settlement of ballast is determined by the ballast stress, the maximum of ballast stress in the transition zone is used as criteria to assess the countermeasure, as shown in Figure 29.

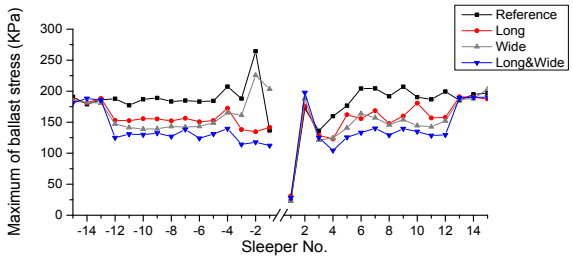

Figure 29. Maximum of the ballast stress of the preventive mitigation (modified sleeper).

As seen in Figure 29, using modified sleepers can significantly decrease the maximum of the ballast stress in most part of transition zones except Sleeper+2. The highest reduction can be found under Sleeper-2, where the maximum of ballast stress is reduced by 50.9%, 85.3% and 44.5% in the long sleeper, the wide sleeper and the long&wide sleeper designs compared with the reference design, respectively. However, the maximum of ballast stress under Sleeper+2 is not reduced by the modified sleepers, which is probably related to the high impact of the vehicle when it drops off from the bridge (discussed in Chapter 3). Alternatively, the under sleeper pad [3, 61] could be used in this specific location.

It can also be found that the wide sleeper design has better reduction effect near the bridge in the EB transition, compared to the long sleeper, while in the rest locations the effect is similar (compare 18.7% reduced by the long sleeper and 21.3% by the wide sleeper). The long&wide sleeper provides the best reduction which is 31.6% on average. Especially under Sleeper-2, the maximum of the ballast stress is 264.35 kPa in the normal transition and only 117.70 kPa in the long&wide sleeper transition.

From an economic point of view, the long sleeper is recommended, because it increases the material of sleepers only by 8.3% and yet reduces the maximum of the ballast stress by 18.7%. From the performance perspective, the long&wide sleeper is recommended since it provides the largest reduction of the maximal ballast stress.

5.3 Corrective countermeasure (adjustable fasteners)

One of the corrective countermeasures for transition zones considered here is the adjustable fastener, which intends to remove the gap under the hanging sleepers. The adjustable fastener consists of two adjustable plastic wedges, which can be inserted between sleepers and rails. The height of adjustable fasteners can be changed by adjusting the position of two wedges. It can remove the void under sleepers (if the sleepers are hung). When hanging sleepers appear, the height of the shims can be manually adjusted. As a result, the hanging sleepers can be restored to be fully supported by the ballast under. The operation for one side of a slab track (ten sleepers) required approximately fifteen minutes with three or four working staff.

The principle of using the adjustable fasteners is shown in Figure 30a and b. An example of the adjustable fastener used in track field is shown in Figure 30c [62]. The field measurement of using adjustable fasteners was performed in three typical transition zones. The test results show the adjustable fasteners are effective to mitigate the track degradation in the transition zones. More details can be found in ***[Part II: Paper IV]***.

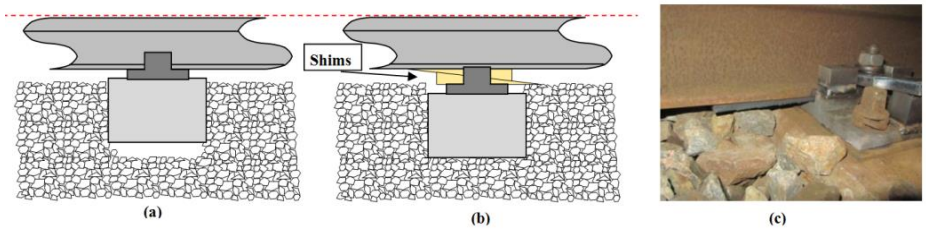

Figure 30. Schematic diagram of Adjustable fastener: (a) and (b) Working principle, (c) Examples of the adjustable fastener used in the track [62].

In order to model the transition zones with adjustable fasteners, the spring-damper elements of the transition model are extended, so that the gaps between the sleepers and ballast are eliminated, as shown in Figure 31. It should be noted that the stiffness and damping of adjustable fasteners are assumed to be the same as normal fasteners (normal rail pads) and constant at various adjusted height. The differential settlement is magnified in Figure 31. In the actual case, the differential settlement (4 mm) is much smaller compared to the size of a sleeper (240 mm in height).

PI

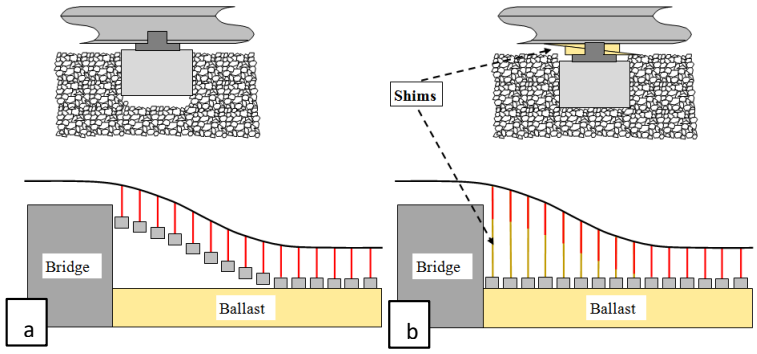

Figure 31. Schematic diagram of the simulation of the countermeasure: (a) Reference, (b) Using adjustable fasteners; Fasteners are indicated by the red lines.

Similar to the previous chapters, the maximum of the ballast stresses in the transition zone is used as criteria to assess the countermeasure. The maximum of the ballast stresses in the reference case and the adjustable fastener case is compared in Figure 32.

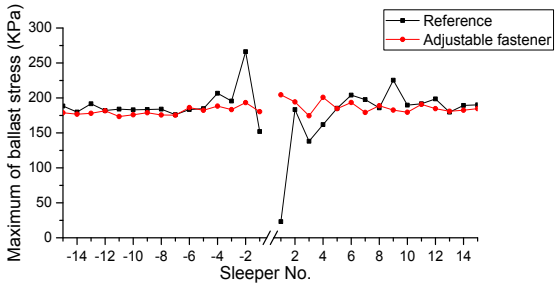

Figure 32. Maximum of the ballast stress of the corrective mitigation (adjustable fastener).

It can be seen in Figure 32 that the maximum of ballast stresses is similar at different locations after using the adjustable fasteners, in other words, the anomaly and fluctuation of ballast stresses are reduced. It indicates the ballast stresses are more evenly distributed along the track. This is especially visible at the location under Sleeper-2, where the maximum of ballast stress is reduced from 266 kPa to 193 kPa (reduced by 27.4%). Similar phenomena can be observed at Sleeper-4 and Sleeper+9 but with a small reduction. It should be noted that the maximum of ballast stress under Sleeper+3 and Sleeper+4 is increased to the normal level. This is also because the support conditions of these sleepers are restored after using the adjustable fasteners (from hanging to fully supported). It can be generalized that the stress anomaly in the transition zone disappears after eliminating the void by using the adjustable fasteners. Another example can be found in the BE transition, where the stress fluctuation is significantly diminished. For other dynamic responses, ***[Part II: Paper IV]***.

It can be found from the numerical results that the adjustable fasteners are effective to improve the stress state of ballast in the transition zone. However, it should be noted that adjusting the fasteners requires track possession.

5.4 Conclusions

This chapter answers **Q4** (How to assess the performance of the countermeasures for transition zones?).

- The developed FE model of transition zone can be used as an assessment tool for the countermeasures. Two countermeasures are assessed as examples, including a preventive countermeasure (modified sleepers) and a corrective countermeasure (adjustable fasteners).

- The effectiveness of the countermeasures is analysed by comparing the reduction of dynamic response after using the countermeasures. The numerical simulations have shown that the modified sleeper and adjustable fasteners can significantly improve the stress state of ballast in the transition zone and consequently mitigate the settlement development in transition zones.

It should be noted other countermeasures can also be studied using the model in the future. The results can used as a basis to provide guidance for the maintenance staff or designers when selecting countermeasures for transition zones. The adjustable fasteners have been tested in the field measurement, which can be found in ***[Part II: Paper IV]***.

PI

Chapter 6. Additional studies

Using the developed methodology, the effect of ballast moisture in transition zones and the use of satellite structural health monitoring for transition zones are explored in this chapter.

The moisture condition of the ballast is first measured using the Ground Penetration Radar (GPR) and compared to the track longitudinal level measured by the track inspection coaches. A strong connection is found between the high moisture condition and track degradation in the transition zones. The dynamic responses of the transition zones with high moisture condition are analysed numerically. This part is based on ***[Part II: Paper V].***

The feasibility of the satellite radar system (InSAR) for monitoring transition zones is explored. The settlement and its growth rate of the track in a transition zone are measured using the InSAR and analysed. In addition, the measurement results are cross-validated against the measurements obtained using the DIC device and an inspection coach. This part is based on ***[Part II: Paper VI].***

6.1 Effect of moisture condition

Moisture condition of the ballast may play an important role in the rapid degradation of tracks and consequently geometry irregularities. Excess water in substructures significantly reduces the resilience of tracks [63, 64] and increases track settlement [65-67]. The loss in resilient modulus and the increase of settlement have significant implications for transient vertical displacements and track performance.

This chapter presents an analysis of the moisture condition to explore the relationship between moisture and track condition in transition zones. One of the three transition zones is analysed as an example. Other measurement results can be found in ***[Part II: Paper V]***. The moisture condition in the transition zones is measured by the use of ground penetrating radar (GPR) [32, 33], which is compared to the track geometry measured by inspection coaches. The relationship between moisture condition and geometry irregularity is analysed. After that, transition zones in high moisture condition are numerically studied using the developed FE method (described in Chapter 3). The high moisture conditions are considered as a reduction of elastic modulus. The wheel loads of the transition zone in the high moisture case are compared with a reference case to analyse the effect of moisture conditions.

6.1.1 Introduction to GPR

GPR uses a radio wave source to transmit a pulse of electromagnetic energy into the inspected medium [68]. Its principle in railway measurements is shown in Figure 33. GPR is an effective and non-invasive tool for mapping railway structures and analysing subsurface conditions. The

PI

reflected energy, originating from the interfaces between materials of different dielectric properties, is received and recorded for analysis. GPR data consists of changes in reflection amplitude, changes in the arrival time of specific reflections, and signal attenuation [69, 70]. The method provides a continuous profile of the thickness and properties of railway structures, which can be used to analyse the quality of track substructures, such as the moisture susceptibility of ballast and subballast, fouling of ballast, layer deformation and mud pumping [71-73].

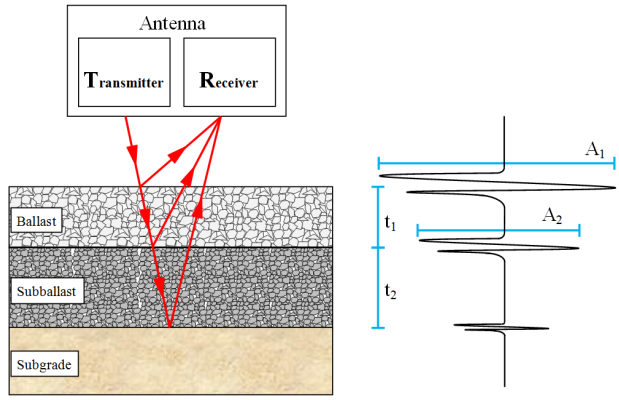

Figure 33. Measuring principle of GPR. A_1 stands for the amplitude of the reflection between the sleeper and ballast; A_2 stands for the amplitude of the reflection between the ballast and subballast; t_1 stands for the travel time in ballast; t_2 stands for the travel time in subballast.

GPR measurements for this case study were performed using a GSSI SIR-30 GPR system, manufactured by Geophysical Survey Systems Inc, including a 400 MHz antenna attached to a VR-Track Ltd Tka-8 maintenance engine, as illustrated in Figure 34.

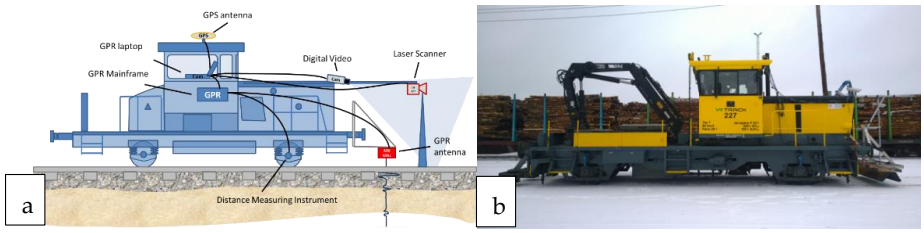

Figure 34. Railway engine with GPR system: (a) schematic diagram; (b) photograph.

The moisture condition of three bridge transition zones on a Finnish railway line was measured using GPR. To study the effect of the moisture condition, the longitudinal level (rail height) measured by track inspection coaches in a similar period using a 5 m-chord method was also collected.

6.1.2 Experiment analysis of transition zones

Measurement results of an open track section are shown in Figure 35 as a reference case. A photo of the track is shown in Figure 35a, the moisture profile in Figure 35b and longitudinal level (rail height) in Figure 35c. The vertical axis of the moisture profile (Figure 35b) indicates the depth

under rails in meters. Although the subballast layer ideally ends 1.2 m, it often settles deeper, especially in transition zones. As a result, the measurement results are collected down to 1.8 m. The ballast, subballast and subgrade are dry, as indicated by the red colour of the moisture profile. The irregularity of the longitudinal track level is less than 2 mm, which is relatively small.

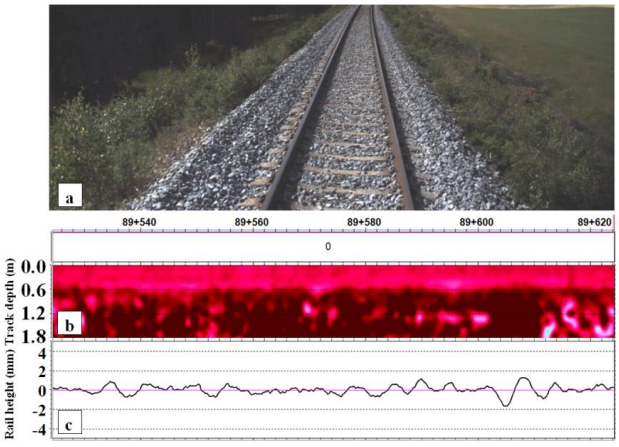

Figure 35. Measurement results of open track: (a) photograph of the track; (b) the moisture profile; (c) the longitudinal track level.

Measurement results from Transition Zone A are shown in Figure 36. This transition zone is composed of the embankment and a 41 m long concrete bridge. The photo of the bridge taken by the onboard video camera during the GPR measurements is shown in Figure 36a. The ballast is laid on the bridge, the depth of which is around 0.6 m beneath rails. GPR data from the concrete bridge is out of the focus of this study and therefore blocked out. Approach slabs are employed at both ends of the bridge. The slabs are made of concrete and laid diagonally from the ballast layer to the subballast layer.

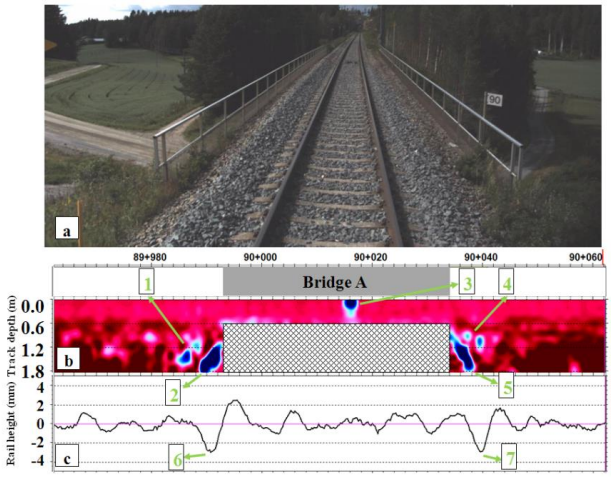

Figure 36. Measurement results of the transition zone.

PI

Moisture susceptibility increases before and after the bridge, as can be seen from Figure 36 (see the blue zones indicated by No. 1 and No. 4). The blue zones of No. 2 and No. 5 are caused by approach slabs, since the concrete has a similar expression as highly susceptible moisture areas after post-processing. Figure 36c shows that the irregularity of the track increases significantly before and after the bridge (indicated by No. 6 and No. 7), which reached 3.0 mm and 2.9 mm, respectively. These two irregularities indicate the appearance of differential track settlement, which agrees with dips found in other transition zones, such as in [7, 37, 38]. The transition zone has both increased moisture susceptibility and track irregularity based on the moisture profile and the track longitudinal level data on both ends of the bridge.

6.1.3 Numerical analysis of transition zones

Ballast in transition zones often has poor drainage conditions [7, 11, 16]. High moisture in the ballast leads to approximately 50% reduction in stiffness [63, 64]. Therefore, the model considers ballast with high moisture in the transition zone by reducing stiffness by 50%. In this case, ballast areas in the transition zones assumed to be affected by high moisture (50% stiffness reduction) are within an 8-sleeper distance from the bridge and are shown with blue colour in Figure 37. The ballast stays unchanged in the reference case.

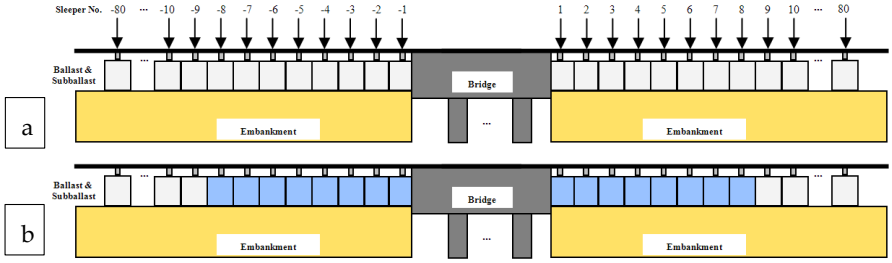

Figure 37. Simulation of the transition zone with high moisture: (a) the reference case; (b) the high moisture case.

The dynamic wheel loads of Wheel 1 are shown in Figure 38. The horizontal axis represents the distance along the transition zone model, where the bridge is located between 48 m and 72 m. Dynamic wheel loads on the bridge are not analysed here, and therefore their responses are covered by the shaded area. The dynamic wheel loads are zoomed before and after the bridge in Figure 38b and Figure 38c, respectively.

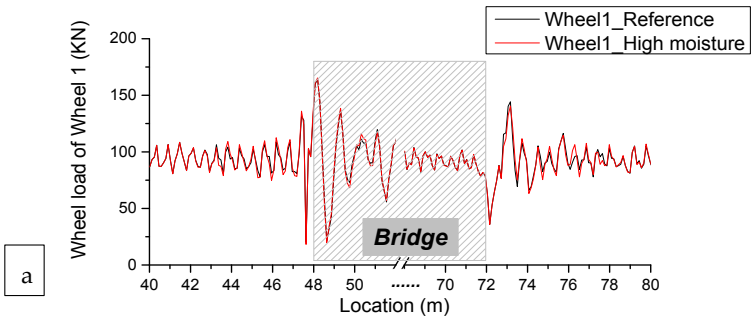

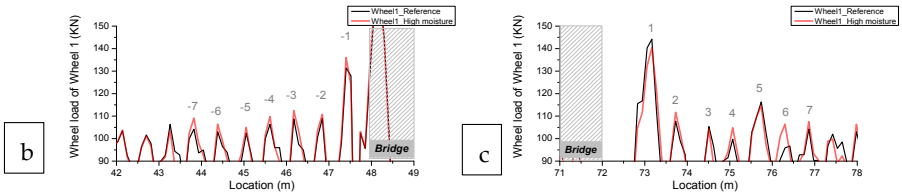

Figure 38. Dynamic wheel load of Wheel 1: (a) overview; (b) zoom-in of the EB side; (c) zoom-in of the BE side [unit: kN].

Comparing to the reference case, the dynamic wheel loads of Wheel 1 in the high moisture case are slightly increased at most locations before and after the bridge (43 m-48 m and 72 m-78 m), while they remain the same at further locations. This is reasonable since the stiffness of ballast is reduced only at these locations (8-sleeper distances, corresponding to 43.2 m-72 m and 72 m-76.8 m). Similarly, the slight increase is also found in the dynamic wheel loads of the other three wheels at most locations before and after the bridge. The average increase of the wheel load is 3%. For detailed statistics, please read ***[Part II: Paper V]***. It should be noted the dynamic wheel loads in the high moisture case are lower than that in the reference case at some individual peaks. This is caused by the dynamic vibration of the vehicle.

6.1.4 Conclusions

The effect of the moisture in transition zones is discussed, including the field measurements using GPR and the numerical analysis using the FE model (described in Chapter 3). The following conclusions are drawn from the results.

- The high moisture areas appear mostly before and after the bridges in transition zones. Track irregularities can also be found at the corresponding locations, which imply a strong connection between the high moisture conditions and track degradation.
- High moisture areas tend to be located at the bottom of the ballast layer, the bottom of the subballast layer, and above the abutments.
- The numerical study shows that the average of dynamic wheel load peaks for all wheels in the transition zone in the high moisture condition is slightly increased (ranging from 0.2% to 2.6%) compared to the reference condition. Since the high dynamic wheel loads will lead to fast track degradation, the simulation results confirm that the high moisture condition is one of the sources of the fast degradation often reported in transition zones.

6.2 Structural health monitoring

Without timely maintenance, the differential settlement may lead to the damage of track components and loss of passenger's comfort. To ensure the safety of railway operations and reduce the maintenance costs, it is necessary to consecutively monitor the structural health condition of transition zones in an economical manner and detect the changes at an early stage. However, using the current in-situ monitoring of transition zones is hard to achieve this goal, because most in situ techniques (e.g., inspection coaches) are labour-consuming and usually not

frequently performed (approximately twice a year in the Netherlands).

PI

Therefore, this chapter proposes a contactless system that uses satellite radar interferometric (Synthetic Aperture Radar Interferometry, referred to as InSAR) techniques [74-76] to complement the current in situ measurements. The InSAR measurements are obtained on a bi-/tri-weekly basis, and with high precision (at millimetre level) [77, 78], which can detect track degradation at a desirable frequency.

In this chapter, the InSAR measurement results are first discussed. Then the cross-validation is performed using the in-situ measurement from the inspection coach. Other validation can be found in ***[Part II: Paper VI]***.

6.2.1 Introduction of Satellite Radar Interferometry

InSAR uses two or more satellite radar measurements of the same area to extract ground deformation remotely and periodically, with millimeter-level precision. A SAR satellite operates using a side-looking geometry and illuminates a swath parallel to the satellite's nadir track by transmitting a series of radar pulses from a fixed antenna [79], see Figure 39a. The ground targets with a strong scattering reflection, e.g., rail bars, can be well observed using SAR satellites. When two (or more) SAR images, acquired at the same time from a different orbital track or acquired at the separated time but imaging the same area, are available, the temporal evolution of ground targets can be retrieved by the InSAR techniques. For instance, the two SAR images are called the master image and slave image; see Figure 39b. The slave image must be co-registered and resampled with regard to the geometry of the master image. The interferometric phase is derived from the pixel-by-pixel multiplication with the conjugate complex of a pixel, in the master and slave image. After that, the persistent scattered interferometric (PSI) processing is conducted, the temporal behaviour of the ground targets with strong reflection, high coherence, stable phase values over time, can be observed.

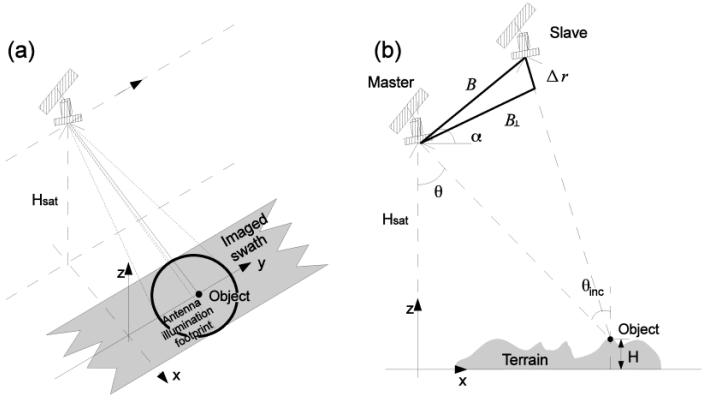

Figure 39. (a) SAR and (b) repeat-pass InSAR imaging geometry, adapted from [76].

It should be noted that all the satellite radar measurements are relative with regard to a reference epoch and reference point. By comparing the spatial coordinates of the unloaded tracks

to the reference point, the increase of the track settlement at various locations can be obtained. Moreover, the high growth rate of the settlement indicates the fast degradation of the track, which suggests the track condition is poor, and vice versa.

6.2.2 Measurement results

The track settlement measured by the TerraSAR-X satellites in the transition zone is shown in Figure 40b, along with the photograph of the transition zone (Figure 40a) and track alignment measured by the inspection coach (Figure 40c). The sampling resolution is indicated by the yellow square in Figure 40a, as well as the satellite flying direction and radar signal direction. Note that since the image resolution of the TerraSAR-X satellite is 3 m, the double tracks are considered as one. The satellite flying direction and radar signal direction are indicated as well. As SAR satellites can only observe the ground targets with a strong scattering reflection, the ground targets with a poor scattering reflection over this railway segment cannot be detected. Therefore, the spatial sampling is not always 3 m, and the distance between the adjacent SAR measurement points shown in Figure 40b varies.

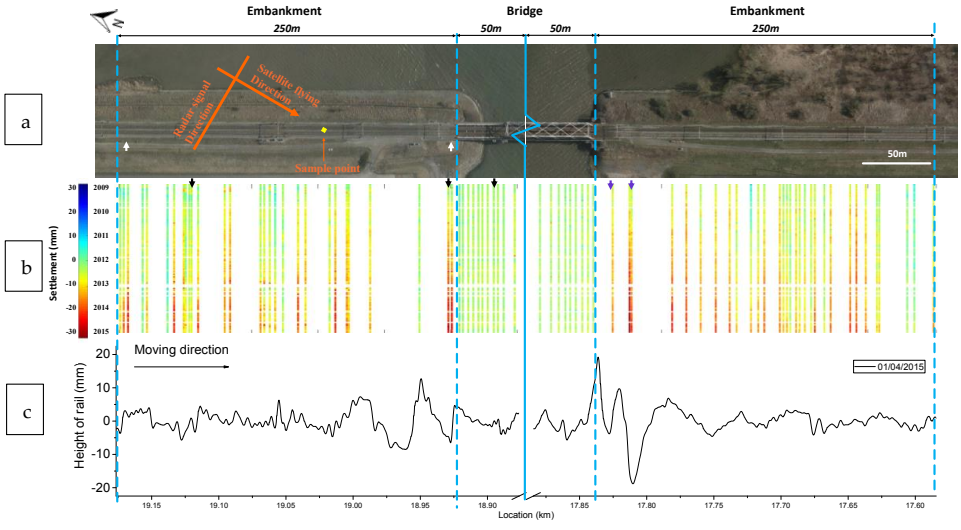

Figure 40. Measurement results of the transition zone: (a) Top-view photograph; (b) Settlement profile measured the satellite system; (c) Track longitudinal level measured by the inspection coach. The middle parts of the bridge are abbreviated. The yellow square indicates the sampling resolution (3 × 3 m). The satellite flying direction and radar signal direction are indicated.

As shown in Figure 40, the settlement on the embankment and the settlement on the bridge are so different that the bridge can be clearly distinguished from the embankment. The settlement of the track on the bridge is relatively stable with marginal fluctuations. On the contrary, the settlement of the track on the embankment increases over time. The increase of the settlement varies from different locations, i.e., the track settles more at the location close to the

bridge and less at the location far from the bridge, which is in agreement with the findings from other field measurements in [1, 11, 38].

PI

To study the track settlement in different regions of the transition zone, the InSAR measurements in three representative points of the transition zone are further analysed, including one point from the ballast track close to the bridge (affected zone), one point far from the bridge and one point the on the bridge (indicated by the black arrows in Figure 40). The settlement histories of points and their rate are shown in Figure 41. Figure 41 clearly shows that track close to the bridge settles much faster than that farther from the bridge, while the settlement on the bridge remains stable. This proves that InSAR can measure the settlement rate in transition zones in this case, which can provide insightful information to understand the degradation process of the transition zones. It should be noted that the feasibility and the quality of InSAR-based structural health monitoring over transition zones may differ in other cases, due to, e.g., the track orientation of a transition zone, satellite viewing geometry and satellite data availability. In addition, sufficient persistent scatters (PS)s are required in the transition zones in order to assess the condition. It can be insured either by increasing the resolution of the satellite or by installing an object (e.g., a pile) in the transition zones.

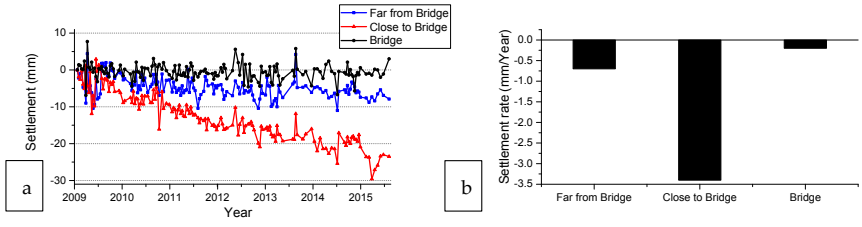

Figure 41. Settlement history of the typical points in the transition zones: (a) Settlement history curve; (b) Settlement rate.

As shown in Figure 40, the fluctuation of the track alignment is significantly amplified near the bridge. On the contrary, the track irregularities are much smaller on the bridge and the embankment farther from the bridge. The results of the inspection coach (see Figure 40c) correlate very well with the results of the InSAR since the locations with the large fluctuations of track alignment are mostly the locations with the large settlement. It is reasonable because the differential settlement leads to the poor supporting condition of rails and sleepers, which can be observed as track irregularities. It should be noted that the track irregularities are not only caused by the differential settlement, but also by rail defects. This is the reason for the small discrepancies between the settlement and the track alignment.

6.2.3 Conclusions

The feasibility of InSAR application on transition zones is studied. Measurements using the InSAR technique are performed in a transition zone. The results are cross-validated using the data from an inspection coach. The following conclusions are drawn from the results.

- The settlement on the embankment and bridge is significantly different in the studied transition zone. The embankment and the bridge of the transition zone can be clearly distinguished in the satellite data.
- The measurement results of the InSAR are compared with the results of the inspection coach. These measurements have a very good correlation. Therefore, the InSAR system is suggested to monitor the condition of the transition zones, which can provide track settlement at a high frequency (once per 11 days) and low cost.

PI

Chapter 7. Concluding remarks

7.1 Main conclusions

The dissertation presents a methodology for analysis of the dynamic behaviour of railway tracks in transition zones, which includes the experimental analysis, as well as the numerical short-term and long-term track behaviour analysis. The methodology was successfully demonstrated by applying it to the condition assessment of transition zones, study on track degradation mechanism in transition zones, long-term track settlement prediction in transition zones, and assessment of countermeasures in transition zones. The methodology is an effective tool for maintenance staff or track designers. In addition, the effect of the moisture condition in transition zones and the structural health monitoring for transition zones were explored. The research questions raised in this study were addressed and the results are summarised below.

Q1: *How to assess the condition of the tracks in transition zones? using which tool?*

Chapter 2 aims to address this research question by presenting an advanced measurement method specifically developed for transition zones. The novelty of the method is that it can measure the dynamic displacements of rails at multiple points in transition zones without track possession, which provides the dynamic profile of the track in transition zones. By analysing the dynamic profile, the condition of transition zones can be assessed. The method has been successfully applied to several transition zones and the following conclusions were drawn.

- The rail displacements near the bridge are considerably increased on both Embankment-Bridge (EB) and Bridge-Embankment (BE) transition. The rail displacements further from embankment are similar to those in the open tracks. The length of the affected zone in the EB transition is determined based on the measurements.
- The dynamic profile of the tracks can reflect the condition of the tracks in transition zones. The proposed Track Transition Quality Index was calculated for considered transitions and had good correlation with the observed condition of the transition zones.
- The measured track displacements in the EB and BE transitions were different. The affected zone in the EB transition was short and had higher value of the displacements, while the affected zone in BE transition was much longer but with smaller displacement amplification.

Q2: *Which factor contributes more to the track degradation in transition zones, the uneven settlement or the stiffness variation?*

In order to answer this question, a novel model for analysis of the dynamic responses in transition zones was developed (Chapter 3) to study the effect of the differential settlement on the track degradation in transition zones. The model includes several novel features as compared to the existing models, such as using the contact elements to describe the sleeper-ballast interaction. The numerical simulations showed that the increase caused by the differential

settlement is significantly higher (up to 90%) than that the increase generated by the stiffness variation alone. Therefore, the differential settlement should always be taken into account when analysing or improving the track performance in transition zones. Other important conclusions from the numerical study are as follows:

- The numerical simulations confirmed the in-situ observations that the dynamic behaviour and degradation mechanism in EB and BE transition zones are different. The wheel loads in EB transition are higher than in BE zone and occurred near the bridge, while the wheel loads in BE transition are lower (still higher than in open track) and were spread over a longer distance.
- In the EB transition, the wheel loads are increased by the rapid change of the elevation and the load redistribution between wheel sets caused by the pitch motion of the bogie. The affected zone in the EB transition is determined by the geometrical properties of the bogie. In BE transition, the increase of the wheel loads is caused by the 'gliding' and 'bouncing' motion of the vehicle. The affected zone in BE transition is determined by the train velocity and the differential settlement.
- Ballast stresses are significantly increased near the bridge in the transition zone due to the differential settlement. The increased ballast stresses usually correlate mostly but not exactly with the increased wheel loads, which shows the analysis of ballast stresses is necessary for study of the transition zones.

Q3: *How to predict the track settlement in transition zones on a long term?*

Chapter 4 aims to address this research question by presenting a novel settlement prediction procedure for transition zones. The method combines the developed FE model of transition zones and an empirical settlement model of ballast. The prediction procedure was applied in a transition zone, and the parameters of the method were discussed. The following conclusions were drawn:

- The settlements (dips) appear in the transition zone after a short time. After that, the dips continuously grow as the number of loading cycles increasing.
- Since the stresses in the ballast under the hanging sleeper are reduced and the maximum stress in ballast is moved to the neighbouring sleeper, the settled zone is expanded from the bridge over time, which is confirmed by the history of the track geometry measurements.
- The settlement in the EB transition is concentrated to the bridge, while that in the BE transition is spread over longer distance from the bridge, which is in agreement with the field observation and the short-term analysis.
- The method predicts the absolute settlement, but since it is difficult to validate, the predicted results can be better used relatively, e.g. for comparison of various designs.

- **Q4**: *How to assess the performance of the countermeasures for transition zones?*

Chapter 5 aims to address this research question. Using the developed FE model of transition zones, the performance of the countermeasures can be assessed. Several preventive

and corrective countermeasures were assessed. From the results of the numerical simulations, the following conclusions were drawn:

- The numerical simulations have shown that the sleepers with modified dimensions (preventive countermeasure) and adjustable fasteners (corrective countermeasure) can significantly improve the track performance (51% reduction in ballast stress when using modified sleepers, 93% reduction in wheel-rail contact force when using adjustable fasteners).
- The modified sleepers are effective to reduce the ballast stress in transition zones. Among all the designs, the long&wide sleeper is recommended from the performance point of view since it provides the largest reduction of the maximal ballast stress.
- Using the adjustable fasteners is effective to eliminate the anomaly and fluctuation of ballast stresses, achieving a better stress distribution in ballast in transition zones.

Some additional work was conducted. The moisture condition of the ballast was measured using the Group Penetrating Radar and the effect of the moisture condition on the dynamic responses of the track in transition zones was analysed numerically for the first time. Besides, the feasibility of the satellite radar system for monitoring transition zones was explored, wherein the settlement measured using the InSAR was analysed and cross-validated against the measurements obtained using the DIC device and the inspection coach. The main conclusions are:

- High moisture areas are most likely to appear before and after the bridges in transition zones. A strong correlation between the high moisture conditions and the track degradation has been found.
- The numerical analysis shows that the wheel forces are slightly increased (up to 2.6%) because of the high moisture.
- The measurement results of the satellite radar are compared with the results of in-situ monitoring systems and good correlations among them have been found.
- The embankment and the bridge in the transition zone can be clearly distinguished from the satellite data. The InSAR system can monitor the health condition of the transition zones at a high frequency (once per 11 days) to provide guidance (e.g., suspect locations) for the local inspection or maintenance.

7.2 Recommendations

Based on the experience of the author, the following recommendations are provided for coming researchers.

7.2.1 Recommendations for numerical studies of transition zones

The future work should be focused on the application and improvement of the integrated methodology, such as coupling the methodology with numerical optimisation methods. More transition zones should be measured using the proposed experimental analysis method so that the normal distribution of the differential settlement in transition zones can be discovered. The plastic

material property of ballast should be considered in the FE model. The prediction procedure of transition zones should be validated against field measurements. More mitigation analyses (especially the corrective countermeasures) should be conducted in order to understand the benefits and drawbacks of the countermeasures. In addition, the moisture condition should be considered when studying the dynamic responses of transition zones.

7.2.2 Recommendations for future research directions

As mentioned above, there are three major reasons for transition zone problems, which are the differential settlement, stiffness variation, and geotechnical/construction issues. The geotechnical/construction issues are barely discussed. This dissertation studies both the stiffness variation and differential settlement thoroughly, and explores one kind of geotechnical issues, which is the moisture condition. However, there are still many others, e.g., inadequate compaction of the fill in transition zones. In the author's opinion, the geotechnical/construction issues should be properly studied in the future.

References

1. Stark, T.D. and S.T. Wilk, *Root cause of differential movement at bridge transition zones.* Proceedings of the Institution of Mechanical Engineers, Part F: Journal of Rail and Rapid Transit, 2015.
2. Paixao, A., E. Fortunato, and R. Calcada, *Design and construction of backfills for railway track transition zones.* Proceedings of the Institution of Mechanical Engineers, Part F: Journal of Rail and Rapid Transit, 2013. **229**(1): p. 58-70.
3. Alves Ribeiro, C., et al., *Under sleeper pads in transition zones at railway underpasses: numerical modelling and experimental validation.* Structure and Infrastructure Engineering, 2014. **11**(11): p. 1432-1449.
4. Coelho, B., et al., *An assessment of transition zone performance.* Proceedings of the Institution of Mechanical Engineers, Part F: Journal of Rail and Rapid Transit, 2011. **225**(2): p. 129-139.
5. Zuada Coelho, B., *Dynamics of railway transition zones in soft soils (Doctoral dissertation)*. 2011.
6. Lei, X. and B. Zhang, *Influence of track stiffness distribution on vehicle and track interactions in track transition.* Proceedings of the Institution of Mechanical Engineers, Part F: Journal of Rail and Rapid Transit, 2010. **224**(6): p. 592-604.
7. Nicks, J.E., *The bump at the end of the railway bridge (Doctoral dissertation)*. 2009, Texas A&M University.
8. Gallage, C., B. Dareeju, and M. Dhanasekar, *State-of-the-art : track degradation at bridge transitions.* Proceedings of the 4th International Conference on Structural Engineering and Construction Management 2013, 2013.
9. Hölscher, P. and P. Meijers, *Literature study of knowledge and experience of transition zones*, in *Delft: report*. 2007.
10. Read, D. and D. Li, *Design of track transitions.* TCRP Research Results Digest 79, 2006.
11. Li, D. and D. Davis, *Transition of Railroad Bridge Approaches.* JOURNAL OF GEOTECHNICAL AND GEOENVIRONMENTAL ENGINEERING, 2005.
12. Thompson, D.R. and P.K. Woodward. *Track stiffness management using the XiTRACK GeoComposite*. in *Permanent Way Institution Journal and Report of Proceedings*. 2004.
13. Kerr, A.D. and B.E. Moroney, *Track transition problems and remedies.* PROC. OF THE AMERICAN RAILWAY ENGINEERING ASSOCIAT, 1993. **94**: p. 25.
14. (ERRI), E.R.R.I., *Bridge ends. Embankment Structure Transition. State of the Art Report.* 1999.
15. Selig, E.T. and J.M. Waters, *Track geotechnology and substructure management*. 1994: Thomas Telford.
16. Li, D., D. Otter, and G. Carr, *Railway bridge approaches under heavy axle load traffic: problems, causes, and remedies.* Proceedings of the Institution of Mechanical Engineers, Part F: Journal of Rail and Rapid Transit, 2010. **224**(5): p. 383-390.

17. Banimahd, M., et al., *Behaviour of train–track interaction in stiffness transitions.* Proceedings of the ICE - Transport, 2012. **165**(3): p. 205-214.
18. Varandas, J.N., P. Hölscher, and M.A.G. Silva, *Dynamic behaviour of railway tracks on transitions zones.* Computers & Structures, 2011. **89**(13-14): p. 1468-1479.
19. Sasaoka, C. and D. Davis, *Long term performance of track transition solutions in revenue service. Technology Digest TD-05-036, Transportation Technology Center.* Inc., Association of American Railroads, 2005.
20. Hyslip, J.P., D. Li, and C. McDaniel. *Railway bridge transition case study*. in *Bearing Capacity of Roads, Railways and Airfields. 8th International Conference (BCR2A'09)*. 2009.
21. Sato, Y., *Japanese Studies on Deterioration of Ballasted Track.* Vehicle System Dynamics, 1995. **24**(sup1): p. 197-208.
22. Dahlberg, T., *Some railroad settlement models—a critical review.* Proceedings of the Institution of Mechanical Engineers, Part F: Journal of Rail and Rapid Transit, 2001. **215**(4): p. 289-300.
23. Indraratna, B., et al., *Field assessment of the performance of a ballasted rail track with and without geosynthetics.* Journal of Geotechnical and Geoenvironmental Engineering, 2010. **136**(7): p. 907-917.
24. Suiker, A.S.J. and R. de Borst, *A numerical model for the cyclic deterioration of railway tracks.* International Journal for Numerical Methods in Engineering, 2003. **57**(4): p. 441-470.
25. Varandas, J.N., P. Hölscher, and M.A.G. Silva, *A Settlement Model for Ballast at Transition Zones.* Proceedings of the Tenth International Conference on Computational Structures Technology, 2010.
26. Lichtberger, B., *Track maintenance strategies for ballasted track – a selection.* Rail Engineering International Edition, 2001.
27. Iwnicki, S.D., S. Grassie, and W. Kik, *Track Settlement prediction using computer simulation tools.* Vehicle System Dynamics, 2000. **33**(Supply): p. 2-12.
28. Lei, X. and L. Mao, *Dynamic response analyses of vehicle and track coupled system on track transition of conventional high speed railway.* Journal of Sound and Vibration, 2004. **271**(3-5): p. 1133-1146.
29. Banimahd, M. and P.K. Woodward, *3-Dimensional Finite Element Modelling of Railway Transitions.* 9th International Conference on Railway Engineering, 2007.
30. Zhai, W.M. and H. True, *Vehicle-track dynamics on a ramp and on the bridge: simulation and measurement.* Vehicle System Dynamics, 1999. **33**(Supply): p. 11.
31. Plotkin, D. and D. Davis, *Bridge approaches and track stiffness*. 2008.
32. H. Wang, et al., *Analysis of the Dynamic Behaviour of a Railway Track in Transition Zones With Differential Settlement*, in *2015 Joint Rail Conference, San Jose, California, USA, March 2015*. 2015. p. 7.
33. Hunt, H., *Settlement of railway track near bridge abutments.* Proc ICE: Transport 1997, 1997. **123(1):**: p. 6.
34. Li, Z. and T. Wu, *Vehicle/track impact due to passing the transition between a floating slab and ballasted track*, in *Noise and Vibration Mitigation for Rail Transportation Systems*. 2008, Springer. p. 94-100.

35. Namura, A. and T. Suzuki, *Evaluation fo countermeasures against differential settlement at track transitions.* QR of RTRI, 2007. **48**(3).
36. Lundqvist, A., R. Larsson, and T. Dahlberg, *Influence of railway track stiffness variations on wheel/rail contact force.* Track for High-Speed Railways, Porto, Portugal, 2006.
37. Le Pen, L., et al., *The behaviour of railway level crossings: insights through field monitoring.* Transportation Geotechnics, 2014. **1**(4): p. 201-213.
38. Markine, V., H. Wang, and I. Shevtsov. *Experimental Analysis of the Dynamic Behaviour of a Railway Track in Transition Zones*. in *Proceedings of the Ninth International Conference on Engineering Computational Technology, P. Iványi and B.H.V. Topping, (Editors), Civil-Comp Press, Stirlingshire, United Kingdom, paper 3, 2014.* 2014.
39. Wang, H., et al., *Improvement of train-track interaction in transition zones via reduction of ballast damage*, in *The Dynamics of Vehicles on Roads and Tracks*. 2016, CRC Press. p. 1173-1184.
40. Sato, Y. *Optimization of track maintenance work on ballasted track*. in *Proceedings of the World Congress on Railway Research (WCRR'97), B*. 1997.
41. Bhandari, A.R., W. Powrie, and R.M. Harkness, *A digital image-based deformation measurement system for triaxial tests.* Geotechnical Testing Journal, 2012. **35**(2): p. 209-226.
42. Giachetti, A., *Matching techniques to compute image motion.* Image and Vision Computing, 2000. **18**(3): p. 247-260.
43. Tong, W., *An evaluation of digital image correlation criteria for strain mapping applications.* Strain, 2005. **41**(4): p. 167-175.
44. Koltsida, I., A. Tomor, and C. Booth, *The use of digital image correlation technique for monitoring masonry arch bridges*, in *ARCH 13*. 2013: Split, Croatia.
45. McCormick, N. and J. Lord, *Digital image correlation for structural measurements.* Proceedings of the Institution of Civil Engineers, 2012. **165**(4): p. 185.
46. Sutton, M., et al., *Determination of displacements using an improved digital correlation method.* Image and vision computing, 1983. **1**(3): p. 133-139.
47. Hallquist, J.O., *LS-DYNA theory manual.* Livermore software Technology corporation, 2006. **3**: p. 25-31.
48. Bezin, Y., et al., *An investigation of sleeper voids using a flexible track model integrated with railway multi-body dynamics.* Proceedings of the Institution of Mechanical Engineers, Part F: Journal of Rail and Rapid Transit, 2009. **223**(6): p. 597-607.
49. Zhai, W.M., K.Y. Wang, and J.H. Lin, *Modelling and experiment of railway ballast vibrations.* Journal of Sound and Vibration, 2004. **270**(4-5): p. 673-683.
50. Paixao, A., E. Fortunato, and R. Calcada, *A numerical study on the influence of backfill settlements in the train/track interaction at transition zones to railway bridges.* Proceedings of the Institution of Mechanical Engineers, Part F: Journal of Rail and Rapid Transit, 2015.
51. Shi, J., et al., *Measurements and simulation of the dynamic responses of a bridge-embankment transition zone below a heavy haul railway line.* Proceedings of the Institution of Mechanical Engineers, Part F: Journal of Rail and Rapid Transit, 2012. **227**(3): p. 254-268.

PI

52. Shan, Y., B. Albers, and S.A. Savidis, *Influence of different transition zones on the dynamic response of track–subgrade systems.* Computers and Geotechnics, 2012. **48**: p. 21-28.
53. Iwnick, S., *Manchester Benchmarks for Rail Vehicle Simulation.* Vehicle System Dynamics, 1998. **30**(3-4): p. 295-313.
54. Wan, C., V.L. Markine, and I.Y. Shevtsov, *Improvement of vehicle–turnout interaction by optimising the shape of crossing nose.* Vehicle System Dynamics, 2014. **52**(11): p. 1517-1540.
55. Knothe, K. and S. Grassie, *Modelling of railway track and vehicle/track interaction at high frequencies.* Vehicle system dynamics, 1993. **22**(3-4): p. 209-262.
56. Esveld, C., *Modern railway track*. Vol. 385. 2001: MRT-productions Zaltbommel, The Netherlands.
57. Guerin, N., et al., *Experimental identification of a ballast settlement law.* CANADIAN GEOTECHNICAL JOURNAL, 1999. **36**(3): p. 523-532.
58. Li, X., J.C.O. Nielsen, and B.A. Pålsson, *Simulation of track settlement in railway turnouts.* Vehicle System Dynamics, 2014. **52**(IAVSD Proceeding Supplement): p. 19.
59. Sañudo, R., et al., *Track transitions in railways: A review.* Construction and Building Materials, 2016. **112**: p. 140-157.
60. Kaewunruen, S. *Dynamic responses of railway bridge ends: A systems performance improvement by application of ballast glue/bond*.
61. Insa, R., et al., *Analysis of the influence of under sleeper pads on the railway vehicle/track dynamic interaction in transition zones.* Proceedings of the Institution of Mechanical Engineers, Part F: Journal of Rail and Rapid Transit, 2011. **226**(4): p. 409-420.
62. BAM and Movares. *Pictures from ShimLift*. 2017; Available from: http://www.baminfra.nl/nieuws/shimlift-betere-spoorligging-en-efficienter-onderhoud.
63. Lekarp, F., U. Isacsson, and A. Dawson, *State of the art. I: Resilient response of unbound aggregates.* Journal of transportation engineering, 2000. **126**(1): p. 66-75.
64. Stark, T.D., et al. *Evaluating Fouled Ballast Using Seismic Surface Waves*. in *2016 Joint Rail Conference*. 2016. American Society of Mechanical Engineers.
65. Indraratna, B., et al., *Compression and degradation of railway ballast under one-dimensional loading.* Australian Geomechanics, 1997. **32**(December): p. 48-61.
66. Indraratna, B., et al., *Geotechnical properties of ballast and the role of geosynthetics.* Institution of Civil Engineers. Proceedings. Ground... 2006.
67. Han, X. and E.T. Selig. *Effects of fouling on ballast settlement*.
68. Daniels, D.J., *Ground penetrating radar*. 2005: Wiley Online Library.
69. Silvast, M., et al., *An inspection of railway ballast quality using ground penetrating radar in Finland.* Proceedings of the Institution of Mechanical Engineers, Part F: Journal of Rail and Rapid Transit, 2010. **224**(5): p. 345-351.
70. Saarenketo, T., *Electrical properties of road materials and subgrade soils and the use of ground penetrating radar in traffic infrastructure surveys*. 2006, University of Oulu.
71. Silvast, M., et al., *Identifying frost-susceptible areas on Finnish railways using the ground penetrating radar technique.* Proceedings of the Institution of Mechanical Engineers, Part F: Journal of Rail and Rapid Transit, 2013. **227**(1): p. 3-9.

72. Saarenketo, T., M. Silvast, and J. Noukka. *Using GPR on railways to identify frost susceptible areas*. in *Proceedings of the international conference and exhibition railway engineering 2003*. 2003. London, UK.

73. Hugenschmidt, J., *Railway track inspection using GPR.* Journal of Applied Geophysics, 2000. **43**(2): p. 147-155.

74. Chang, L., R. Dollevoet, and R.F. Hanssen, *Railway infrastructure monitoring using satellite radar data.* International Journal of Railway Technology, 2014. **3**(2): p. 1-13.

75. Chang, L., *Monitoring civil infrastructure using satellite radar interferometry*. 2015, TU Delft, Delft University of Technology.

76. Bamler, R. and P. Hartl, *Synthetic aperture radar interferometry.* Inverse problems, 1998. **14**(4): p. R1.

77. Ferretti, A., C. Prati, and F. Rocca, *Permanent scatterers in SAR interferometry.* IEEE Transactions on geoscience and remote sensing, 2001. **39**(1): p. 8-20.

78. Ferretti, A., et al., *Submillimeter accuracy of InSAR time series: Experimental validation.* IEEE Transactions on Geoscience and Remote Sensing, 2007. **45**(5): p. 1142-1153.

79. Elachi, C. and J.J. Van Zyl, *Introduction to the physics and techniques of remote sensing*. Vol. 28. 2006: John Wiley & Sons.

Part II:

APPENDED PAPERS

PII

Paper I

Experimental analysis of railway track settlement in transition zones

Haoyu Wang, Valeri Markine, Xiangming Liu[1]

[1]Delft University of Technology, Delft, the Netherlands

Published by Proceedings of the Institution of Mechanical Engineers, Part F: Journal of Rail and Rapid Transit p.0954409717748789.

Abstract

Transition zones in railway tracks are the locations with considerable changes in the vertical support structures. Due to the differential stiffness and settlement in the open track and the engineering structure resulting in the dynamic amplification of the wheel forces, the track settlement is usually observed in the approaching zones. The settlement in transition zones is detrimental to the track components and passenger comfort.

This paper presents the results of the experimental analysis performed in three transition zones which were in various conditions. The dynamic displacements of rails due to a passing train were measured at multiple points (dynamic profile) in the approaching zones. The device employed is a contactless mobile device for measuring displacements, which is based on the Digital Image Correlation (DIC) technique. Because the operational parameters of the DIC-based devices are important for measurement accuracy, prior to the in situ measurements, this device was tested in a laboratory to study the influence of the operational parameters, including the elevation/heading angles, the focal length of the cameras and the measuring distance.

After determining the optimal operational parameters for the railway field, the multiple-point measurements were performed in the transition zones. The length of the approaching zone was studied first. Also, the dynamic profiles of the embankment-bridge and bridge-embankment transitions were analysed. Finally, by comparing the multiple-point displacements in the approaching zones in different conditions, it was found that the dynamic profile of the rail displacements has a good correlation with the track condition in the transition zone. The results are presented and discussed.

Keywords

Railway, Transition zone, Measurement, Digital Image Correlation.

1 Introduction

Transition zones in railway track network are locations with considerable change in the supporting structures. Typically, they are located near engineering structures, such as bridges, culverts and tunnels. A typical track transition zone is shown in Figure 1.1, wherein an embankment is connected with a culvert.

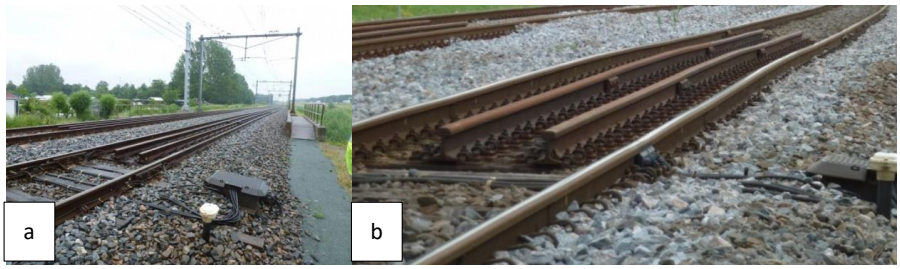

Figure 1.1. A typical track transition zone: (a) global view; (b) close-up view.

In such locations, the vertical stiffness of the track support abruptly changes, resulting in amplification of the dynamic forces acting on the track, which ultimately leads to accelerated deterioration of the vertical track geometry [1-3]. In addition, since the engineering structures always settle much slower than the embankment, the differential settlement between the engineering structure (e.g., bridge) and open track always occurs. Such initial settlement contributes significantly to the amplification of the wheel forces and ultimately to the deterioration of the track geometry in the transition zone [4, 5]. Therefore, maintenance of the track geometry in the transition zones requires substantial efforts. For example, in the Netherlands, the track maintenance in the transition zones is performed up to 4-8 times more often than on the open track [6, 7]. In the US $200 million is spent annually to maintain the transition zones, while in Europe about €97 million is spent [8, 9].

The ballast track in the transition zones can be divided into two parts (Figure 1.2): the open track that is relatively far from the engineering structure and therefore unaffected by the presence of the engineering structure; and the approaching zone which is located close to the engineering structure and suffers from the settlement [2-5, 10, 11]. The settlement in the approaching zone, showed as a dip in Figure 1.2b, typically appears shortly after installation/renewal of the track. This phenomenon has been confirmed by a survey of the performance of track transition zones, which revealed that 51% of the studied transition zones had experienced such a settlement [3]. The dip also appears in the transition zone between the embankment and the level crossing [12].

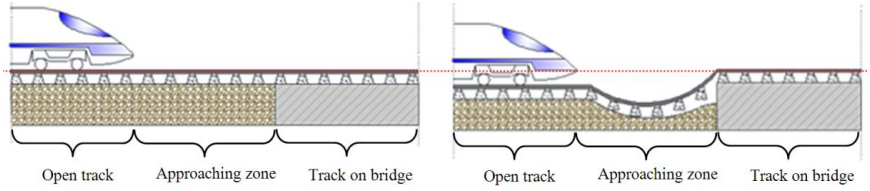

Figure 1.2. Schematic diagram of differential settlement in transition zone: (a) immediately after construction or maintenance (no settlement); (b) after a few month of operation.

Theoretically, such a significant irregularity in the track geometry may trigger considerable wheel-rail interaction forces, which may result in damage to the track components, affect the

passenger comfort, and even lead to a train derailment. Ultimately, it may raise the need for additional maintenance and increase the life cycle costs. However, the length of the approaching zone and the magnitude of the settlement (the profile of the settlement) usually are not clearly defined. Therefore, the maintenance of the track in the transition zone is difficult to plan and to perform timely.

The field measurements and analysis of the transition zone behaviour are somewhat lacking or even scarce [2]. In [13] it was stated that the track degradation in the transition zones is far from being solved because the mechanism of applied countermeasures is not entirely understood. In [14] it was also pointed out that despite the efforts undertaken to minimise the track transition zone problems, the transition zones continue to exhibit poor performance and a considerable amount of maintenance effort was still spent at these locations. Similarly, such track transition zones experiencing severe settlements have been observed by the authors during this study.

In some studies the measurements in the transition zones performed at one point in the approaching zone that are later compared with one point measured in the open track and one point measured on the bridge, such as in [2, 5, 10]. In this way, the location and the amplitude of the dynamic profile of the dip (Figure 1.2b) are not clear. A better method is to measure the displacement of sleepers at multiple locations simultaneously in the approaching zone, such as in [12, 15].

Similar to the idea of multiple-point measurements in [12, 15], this paper presents the results of the experimental study performed on 3 transition zones. The dynamic displacements of the rails in this study are measured simultaneously at multiple points (up to 8 points, with a minimal spacing of 0.6m) in the approaching zone so that the dynamic profile of the track displacements can be obtained. The measurement device used in this study is a contactless mobile device for measuring displacements based on the Digital Image Correlation (DIC) principle. The measuring method was first presented in April, 2014 [16] and later in [17]. By studying the dynamic responses in the transition zones, the following aspects are discussed in this paper:

(1) The length of the approaching zone (that is affected by the settlement);
(2) The dynamic profiles of the rail displacement in the embankment-bridge and the bridge-embankment transitions;
(3) The dynamic profiles of the transition zones in various conditions.

A brief overview of the measurement techniques used in transition zones is given in Section 2. Since the operational parameters of the DIC-based devices are important for measurement accuracy and the device used here had not been applied for railway measurements, it was tested in the laboratory first. The sensitivity of the operational parameters, including the measuring angle, the distance and the focal length of the lens, was analysed in Section 3. After that, the measurements of the dynamic displacement at multiple points on the rails in the approaching zones were performed and the dynamic behaviour of the track was analysed as presented in Section 4 and discussed in Section 5. Finally, the findings and conclusions are summarised in Section 6.

2 Measurement techniques in transition zones

The vertical rail displacements in the transition zones discussed in the literature can be divided into two categories, namely the permanent displacements and the transient ones. The permanent displacement, also named settlement, is the absolute static rail displacement referring to the

original position without loading, while the transient displacement is the relative rail displacement during train passage w.r.t. to the unloaded position. When the contact between sleepers and ballast is in good condition, such as in the open track, the transient displacement of the rail should remain constant, while the permanent displacement may grow slowly. However, in the approaching zones, the contact status between sleepers and ballast is often poor, which is presented by a void in ballast under sleepers and also called hanging sleeper [18, 19]. Due to the void, the hanging sleepers can move with less constraint during trains passing. The stress in ballast adjacent to the hanging sleeper is increased and later leads to the track degradation [5]. Therefore, the transient displacements of the track can indicate the track degradation. Usually, the higher the transient displacements in the transition are, the worse the condition of the transition zone is. The number of the experimental studies of transition zones is rather limited as compared to the studies of other sections of track. An overview of the experimental studies and the measurement techniques used therein available in the literature is given below.

In [10], the plain transition zones (the transition zone without countermeasures) was studied, wherein the permanent settlement of the track was measured using the *optical level*. It was found that the settlement in the open tracks was larger than the settlement on the bridges, but smaller than those in the approaching zones. Later, in [8] the track geometry data of two transition zones were studied. The data was obtained by automated track geometry *measurement vehicles* for a period of 3 years. It was also reported that the rail at the bridge approaching zone settled after tamping and resulted in a dip in the track reoccurring near the bridge and the reason for the settlement was that the tamping maintenance process loses effectiveness near to the fixed structure. A recent measurement was conducted in [5], who used *LVDTs* (linear variable differential transformers) to measure the permanent settlement and transient displacements in the two transition zones. It was found that the permanent settlements in the approaching zone were much bigger than those in the open track only after a half-year of operation.

A transition zone using approaching slab has been experimentally studied in [2, 15], wherein the transition zone used a 4m reinforced concrete slab on each side of the culvert. The concrete slab was laid under the ballast layer with one end hinged at the culvert and the other end free in the embankment. *Geophone* was used to measure both the permanent and the transient sleeper displacement during train passages. It was also found that the biggest transient displacements of the sleepers were in the approaching zones, while the displacements on the culvert were the smallest.

As for the high speed tracks, a laser-based monitoring system, *Position Sensitive Detector* (PSD), was used to measure the transient displacements of rails in a transition zone in the Portuguese high-speed railway (220km/h) [20]. Later, *LVDTs* and *PSDs* were used to measure the transient displacements of rails in a transition zone in the Spanish high-speed railway (220km/h). Since the transition zones were well constructed with the reinforce backfill, no differential settlements were found in the approaching zones [21, 22]. However, since the design and maintenance of the transition zones in the high-speed tracks are different from those in the normal-speed tracks, these two studies are not considered here.

In the transition zone between the embankment and the level crossing, *Geophones, DIC-based devices* were used to measure the transient displacement of multiple sleepers in the approaching zone [12]. A dip (dynamic profile) was found, located from 2.52m to 7.83m and centred at 5.15m.

All the available measurement results in track transition zones are summarised in Table 1.1.

Table 1.1. Summary of measurement results in track transition zones.

Measured displacements	Vertical displacement sleepers/ track (mm)			Countermeasures	Measuring equipment	Reference
	Open track	Approaching zone	Bridge			
Permanent	29.2	35.3	16.2	- (Plain)	Optical level	[10]
	45.4	47.3	19.1	HMA (Hot Mix Asphalt)		
	35.6	40.2	18.3	Cement		
	39.4	43.4	15.8	Geocell		
	24.9	16.4	0.3	Concrete approaching slab	Geophone, high-speed camera	[2, 15]
	2.0	3.6	-	-(Plain)	LVDT	[5]
	0.5	7.2	-	-(Plain)		
Transient	1.2	6.8	0.8	Concrete approaching slab	Geophone, high-speed camera	[2, 15]
	0.8	11.2	0.3			[2, 15]
	0.4	1.7	-	-(Plain)	LVDT	[5]
	0.8	5.2	-	-	Geophone, DIC	[12]+
	0.6	0.5	0.4	Backfill	PSD	[20]*
	0.8	0.5	0.5	Backfill	LVDT, PSD	[21, 22]*

+The measurements for the transition zone of a level crossing instead of a bridge

* The measurements are for the high speed lines, while the rest are for normal speed lines.

Based on this review (Table 1.1) the following conclusions can be made:

(1) The displacements in the approaching zones are the largest, while the displacements on the bridge are the smallest ones, in both permanent and transient measurements performed on the normal-speed tracks.

(2) The field measurements in transition zones in railway track are relatively insufficient in number. Also, the measurements did not cover transitions in different conditions.

(3) The behaviour of transition zones is complex and difficult to predict. Also, this behaviour depends on the design of the transition zones, i.e. with or without various countermeasures. Even for the transition zones of the same type, the behaviour may vary, depending on the geotechnical conditions and train operation. For example, in [3] the half of the studied transition zones suffered from severe settlements, while the other half not. Therefore it is necessary to propose an assessment method, which can easily evaluate the quality of transition zones.

(4) Some countermeasures did not improve the performance of transition zones. For example, there was no reduction of the permanent settlement in the transition zones achieved by HMA, cement and geocell as compared to the transition zone without countermeasures (e.g. in [10]). Using the approach slab has an even negative effect on the settlement reduction in transition zones [2].

(5) In most mentioned measurements, only one point was measured in each zone, i.e. open track, the approaching zone and the bridge. However, using only one point is difficult to capture the location with the largest displacement. Also, the length of the affected approaching zone is not

known. In [15], 5 sleepers in the approaching zone were measured. However, due to rotation of the approaching slab, the dynamic profile was different from that of the plain transition zones. Also in the measurement of the transition zone of the level crossing [12], 7 sleepers in the approaching zone were measured. Due to the structural difference of the level crossing, the dynamic profile was also different. Although the transition structures are different, the method that measures at multiple points of the approaching zone was successfully proved to provide more insights of the track behaviour than the one-point measurement.

The paper presents the detailed experimental study of three transition zones in various conditions. The dynamic profiles of transition zones were measured simultaneously in several points instead of one point, using a DIC-based device. The results of the field measurements using the DIC-based devices in railway are described in the following section.

3 DIC-based measurement devices

In this section, the measurement device used here, which is based on the Digital Image Correlation (DIC), is presented. The DIC-based devices have been widely used in civil engineering, which are mainly to measure the plastic deformation of concrete bridges [23, 24], or the strain of material [25-27]. However, a relatively small number of papers reported that DIC-based devices were used in the railway field, where the displacements at higher frequency are generated. The applications of the DIC-based devices in railway field are reviewed first. After that, several sensitive operational parameters of the DIC-based device were tested, since it has never been used for railway purposes before.

3.1 Application of DIC-based devices in railways

DIC is an optical method, which uses tracking and image registration techniques for accurate measurements in images. A reference image is captured before displacement and a series of pictures are taken subsequently during the movement. The images are analysed using a numerical matching technique to identify the most similar patterns in the subsequent images, which is based on the assumptions that the pattern is approximately constant between successive images and that the local textural information is unique. The matching algorithm compares the image subsets in the reference image with the image subsets in the current image [28]. Matching criteria are available such as in [29] and [30]. The method combines continuous recording of horizontal and vertical displacements with no contact with the measuring targets, excluding any interference between the measured surface and the measuring device [24, 26, 31]. It often consists of high-resolution digital cameras which record the displacement of targets, and post-processors which analyse the changes in the images.

In [32], a DIC-based device was successfully employed to measure the complex dynamic deflection histories of sleepers at three locations during train passages, which was validated by Geophones. Accurate measurement results were achieved up to 100km/h of the train speed by using a 30 fps camera. However, the authors pointed out that only one sleeper or location could be monitored at a time. The similar comparison between the DIC-based device and Geophones can also be found in [33, 34]. In addition, the ground vibration has small influence to the camera at a distance of 6m from the rail [32]. A recent study discussed the ground vibration could be found in [35].

The measured train speed was raised to 180km/h in [36], using a camera up to 500fps, in the measurements of railway bridges. The measurement results were validated by LVDTs and the

obtained precision was below 0.1mm for the distance of 15m.The displacements of rail were measured by a DIC-based device in [37]. By using 4 synchronised cameras, multiple locations along the track were measured. The cameras were 100fps and they were positioned at the distance of 10 m. The rail strains measured by DIC-based devices were compared to Finite element simulation results, and a good correlation is achieved again [38].

In [12], the displacements of sleepers along the transition zone between the embankment and a level crossing were measured using DIC devices. The train speed was around 112km/h. The measurement results at multiple locations had a good correlation with Geophones. In most cases the measurement results of DIC have better quality than those of Geophones.

Compared to the traditional measurement methods used in railway fields, such as LVDT and Geophones, the DIC-based devices have some advantages [32, 33, 37]. The major advantage of the DIC-based devices is that they can perform measurements from a distance. Therefore, the measurements can be performed in a safe zone of a railway track, for example, staying at a distance further than 3.25m from the track. The zone within 3.25m is a dangerous zone according to the Dutch railway safety regulations. In addition, the installation of DIC-based devices is less time-consuming. The traditional contact measuring equipment requires at least one maintenance window (track possession) to be installed on the track (e.g. attaching sensors to the rails) and another window to be removed. However, most of the installation work of the DIC-based devices, including setting cameras and computers, can be conducted outside of the track that does not require the possession time. Moreover, the DIC-based devices can obtain the measurement data off-line, i.e. the recorded videos can be processed later in the office. Besides, DIC-based devices can measure the absolute displacements instead of the relative displacement.

Since the possession time of tracks is expensive and the access to the track is increasingly difficult, the DIC-based devices have become very attractive in the monitoring of railway tracks. In this study, a DIC-based device is applied to measure the rail displacements at multi-points in the transition zones. Because the operational parameters of the DIC-based devices, which may be limited in the railway field operation, are important to accuracy, the device was tested in the laboratory to study the sensitivity of the key parameters. The main limitations of the DIC-based devices in practical operation are as follows:

(1) The elevation and heading angle of cameras to targets should be small enough. Ideally, the cameras should be perpendicular to the displacement plane of the measured targets. However, in most cases, cameras have to face the measured targets with the elevation or/and heading angle, due to the constraint of the track field. For example, the two inner rails of a double track railway are always blocked by the outer rails.

(2) There is a conflict between the field of view and the resolution of cameras. A larger field of view and a higher resolution of the camera are both desirable, but cannot be achieved at the same time. On the one hand a larger field of view can cover more sleepers; on the other hand, the larger field of view reduces the resolution of the camera, which affects the measurement accuracy. To study the relationship between the measurement accuracy and operational parameters, a series of experiments were performed in the railway laboratory of Delft University of Technology, the Netherlands.

3.2 Laboratory tests of the operational parameters

The operational parameters to test are the elevation and heading angle, the measuring distance, and the focal length. The DIC-based device used here consists of cameras (up to 400fps), lenses of various focal lengths, and the processing system, as shown in Figure 1.3. The system is called Video Gauge System (VGS) and provided by Imetrum.

Figure 1.3. Components of the DIC-based device: (a) a high speed camera; (b) processing system; (c) a tripod; (d) targets.

In the laboratory tests, the DIC-based device was used to measure the motion of the actuator of a hydraulic press machine, which is the periodic vertical motion with the frequency of 0.1Hz and the peak-peak amplitude of 10mm. The tested operational parameters are shown in Figure 1.4. The tested values of the operational parameters of the device are shown in Table 1.2. The reference combination of the parameters is 0° elevation angle, 0° heading angle, 7.5m measuring distance, and 75mm lens (the values in bold in Table 1.2). During the test, the values of only one parameter were changed, while the others parameters have the reference values. The results of the testing were in details presented in [17]. The influence of the operational parameters on the measurement accuracy is shown in Figure 1.5.

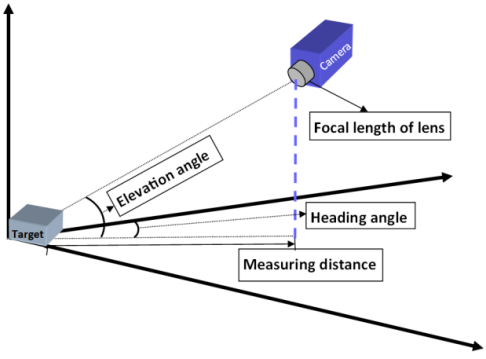

Figure 1.4. Illustration of the operational parameters.

Table 1.2 Tested value of the operational parameters.

Parameters	Values
Elevation angle (°)	**0**, 2.5, 5, 7.5, 10
Heading angle (°)	**0**, 5, 15, 30, 45
Measuring distance (m)	2.5, 5.0, **7.5**
Focal length of lens (mm)	16, 25, 50, **75**

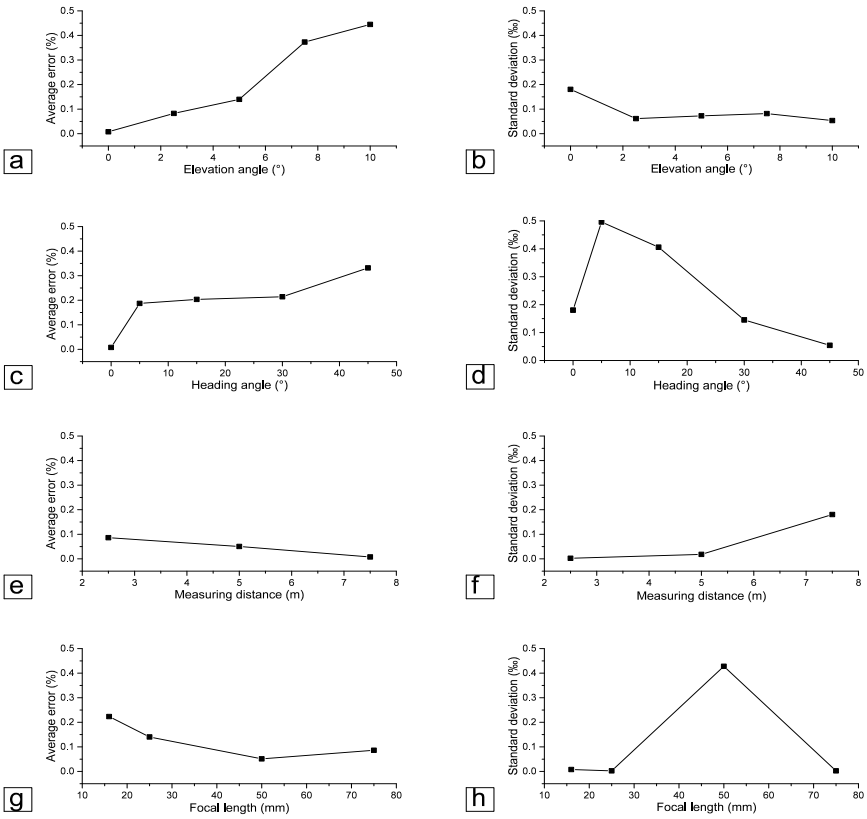

Figure 1.5. Effect of elevation angle: Average Error (a) and Standard Deviation (b); Effect of heading angle: Average Error (c) and Standard Deviation (d); Effect of measuring distances: Average Error (e) and Standard Deviation (f); Effect of focal length: Average Error (g) and Standard Deviation (h).

From Figure 1.5, it can be seen that the average error and the standard deviation in all the tests are less than 5% and 5‰ respectively. This confirms the feasibility of the DIC-based device for railway engineering applications, as in [32, 33, 36, 38].

Although both the elevation and the heading angles can generate the average error, the average error is more sensitive to the elevation angle rather than the heading angle. As it can be seen from Figure 1.5a and Figure 1.5b, the average error reaches 4.5% when the elevation angle is 10°, while the average error is only 3.3% when the heading angle is already 45°. This is logical since the target is moving in the vertical direction. Even though the angles are inevitable due to the field restrictions, the heading angle should be constrained to 30° and the elevation angle should be constrained to 10°, regarding the accuracy of measurements.

On the contrary to the angles, the average error introduced by the measuring distance is relatively small, as shown in Figure 1.5e. To increase the field of view (to measure as many sleepers as possible) while not reducing the accuracy, a long measuring distance, for instance 7.5m,

is recommended. Measuring on a long distance has a clear advantage, since the effect on the ground vibrations due to the passing trains will be reduced. The measuring distance of 7.5m is also beyond the so-called “dangerous zone” in the Netherlands, wherein the human presence is not allowed if the track is in operation. The focal length of 50mm for the reference distance (7.5m) generates the smallest average error (Figure 1.5) and it is therefore recommended.

Finally, the proposed operational parameters are listed in Table 1.3. Note, that the elevation angle is smaller than 10°, when the distance is 7.5m and the height difference between the camera and the rail is 1.3m.

Table 1.3 Suggestion of the operational parameters.

Parameter	Suggest value
Elevation angle (°)	<10
Heading angle (°)	<30
Measuring distance (m)	7.5
Focal length (mm)	50

With a better understanding of the measuring device, the field measurements in the transition zones were conducted, which are presented in the following section.

4 Field measurements in transition zones

The measurements of the transition zones using the DIC-based device were analysed in this section. The purposes of the measurements are:

(1) to determine the length of the approaching zone in transition zones;

(2) to explore the difference of the dynamic profiles of the embankment-bridge and bridge-embankment transitions;

(3) to study the relationship between the dynamic profile and the health condition of transition zones.

4.1 Field introduction

Three transition zones were measured using the DIC-based device, which are named Transition A, B and C as shown in Figure 1.6. In Transition A and B, the embedded rail system are used on the bridges, while the ballast track with concrete sleepers are used on the embankment, as shown in Figure 1.6a and c respectively. According to the maintenance history, Transition A was in poor condition while Transition B in healthy condition. Therefore, larger dynamic displacements were expected in the approaching zone than in the open track in Transition A. In Transition C, the ballast was used above the bridge and the performance was also in poor condition, as shown in Figure 1.6e.

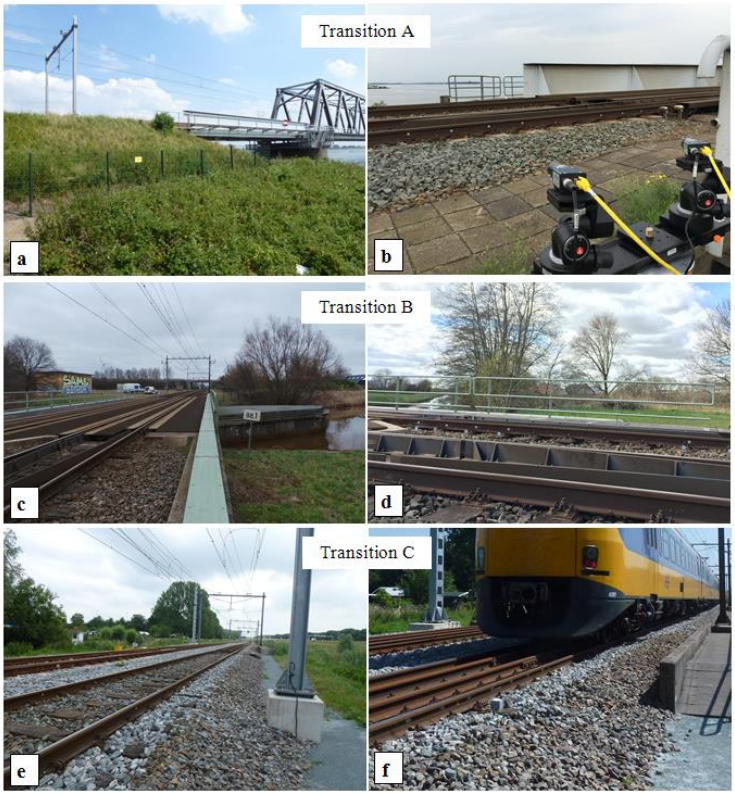

Figure 1.6. Photos of Transition A, B and C: overall photos (left) and partial photos of the targets on the rail (Right).

The layout of the measurements in the three transition zones is given in Figure 1.7. The first sleeper was located at 0.3m from the abutment of the bridge and the sleeper spacing was 0.6m. The measured locations are indicated by the red circles. During the measurement of Transition A, two synchronised cameras were used. One measured the track close to the bridge, from 0m to 2.4m; the other measured the track further, from 4.2m to 6m. The rail at 60.3m was measured apart since it is too far from the bridge. In total, 7 train passages were measured in the approaching zone and 11 train passages were measured in the open track. The measuring frequency was 78Hz. Similarly, measuring frequency in Transition B was 78Hz. The embankment-bridge and bridge-embankment transition were measured separately. 42 train passages were measured in the embankment-bridge transition and were measured in the bridge-embankment transition. In the measurement of Transition C, the measuring frequency was 31Hz and 4 train passages were recorded.

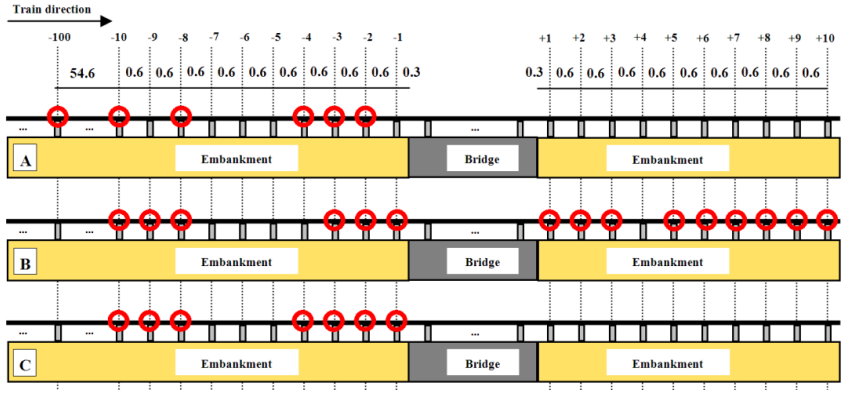

Figure 1.7. Schematic plan of measurements.

The passing trains are the Dutch passenger trains. Their geometrical parameters of the train are shown in Figure 1.8 [2]. Their velocities are between 80km/h and 140km/h, while the axle loads (empty train) are around 16t. During the measurement, the velocities were around 100km/h. The setting of the DIC-based device was the same as proposed in Table 1.4.

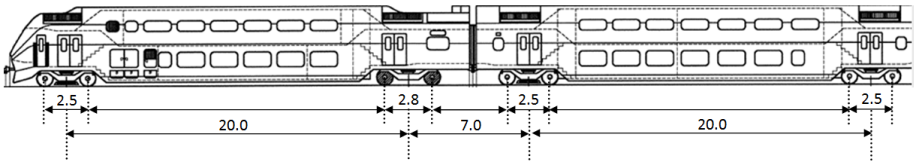

Figure 1.8. Vehicle configuration.

Using the measurement data in Transition A, the length of the approaching zone is analysed. The rail displacements measured in the open track (at 60.3m from the bridge) are compared with the rail displacements closer to the bridge. Since the performance of Transition A was in poor condition, larger dynamic displacements are expected in the approaching zone than in the open track. Moreover, using the measurement results in Transition B, the dynamic profiles of the embankment-bridge and bridge-embankment transitions are analysed. In addition, comparing with the measurement results of the embankment-bridge transitions in Transition A, B and C, the relationship between the dynamic profile and the performance is studied.

4.2 Length of approaching zone

The measured examples of the displacements of the rail at -1.5m, -4.5m and -60.3m (the open track) in Transition A are shown in Figure 1.9. Note that the number of the distance is calculated from the end of the abutment. For convenience, the negative sign is used to indicate the left side of the bridge (the embankment-bridge transition) while the positive the right side (the bridge-embankment transition).

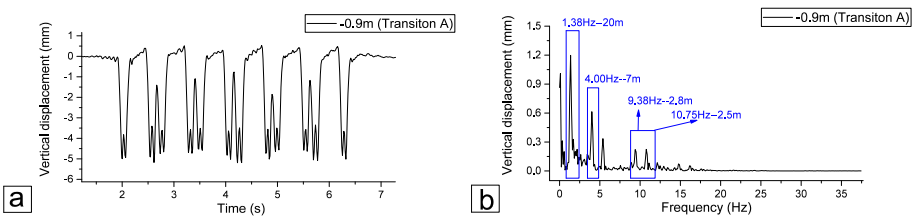

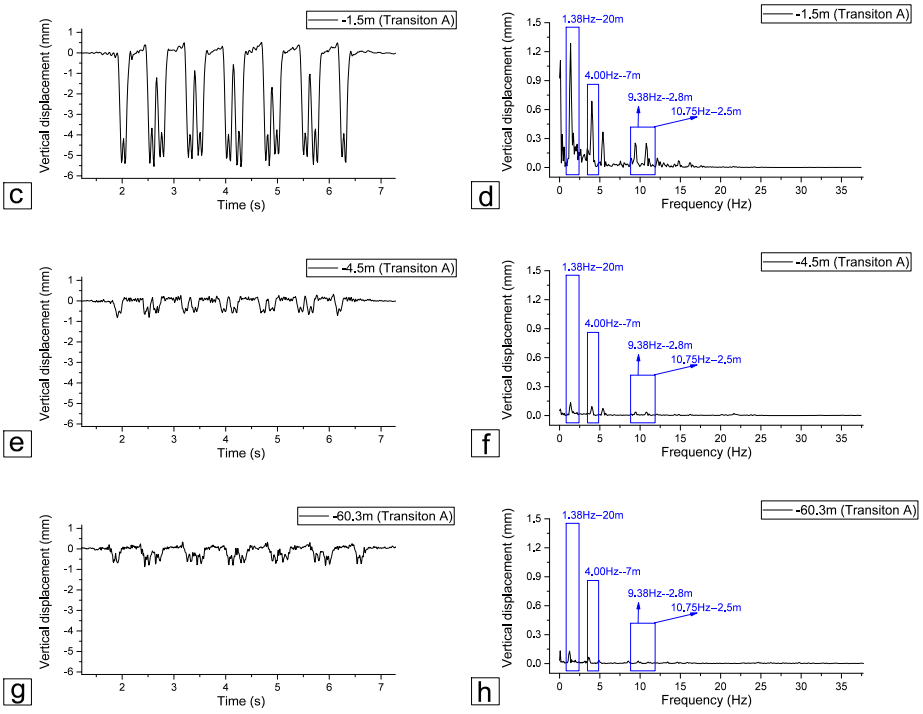

Figure 1.9. Rail vertical displacements at four locations of Transition A in the time domain (a), (c), (e) and (g); in the frequency domain (b), (d), (f) and (h).

As it can be seen from Figure 1.9, the peaks in the time history curves correspond to the passage of each wheelset. In the frequency domain, the peaks are matched very well with the frequencies due to the characteristic length of the train. Taking the displacement of Rail -0.9m (Figure 1.9b) for example, when the velocity of the trains is around 100km/h, the 1st characteristic frequency is 1.38Hz that corresponds to the bogie distance of 20m (Figure 1.8); the 2nd characteristic frequency is 4.00Hz that corresponds to the distance between two bogies of the neighboring vehicles of 7m; the characteristic frequencies of 9.38Hz and 10.75Hz correspond to the wheel distance in the bogies of 2.8m and 2.5m respectively. These characteristic frequencies can also be found in the measurements in other locations (Figures 13d, f and h). This shows that the results measured by the DIC-based device are correct.

Comparing the displacements measured in the three locations (Figure 1.9), it can be concluded that the approaching zone in this transition is within 4.5m from the abutment of the bridge, since the displacements at -4.5m (Figure 1.9e) are similar to the ones at the open track (Figure 1.9g), and much smaller than the displacements at -0.9m and -1.5m (Figure 1.9a and c).

In the measurements shown in Figure 1.9, the maximal displacements at 60.3m, 4.5m, 1.5m and 0.9m are 0.88mm, 0.82mm, 5.19mm and 5.55mm respectively. In the same way, the maximal displacements in other passages were collected. The average values of the maximal displacements of at multiple locations can be considered as the dynamic profile of Transition A as shown in Figure 1.10.

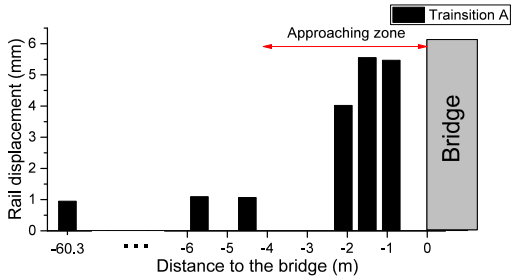

Figure 1.10. Statistics of the vertical rail displacements at all measured points of Transition A.

From Figure 1.10, it can be seen that the approaching zone is most likely located within 4.5m from the bridge. Since the condition of the Transition A was considered as poor, the track settlement in the approaching zone is naturally larger than in transition zone of good condition. Therefore, 4.5m can be considered as the upper limit for the length of the approaching zone for this type of transition zone. Note that since the length of the approaching zone depends on its engineering structure and the local subgrade property, it is only valid for similar transition zones. To validate this assumption and to study the approaching zone, the rail displacements were also measured in another two approaching zones. The results of these measurements are discussed in the next section.

4.3 Dynamic profiles of the embankment-bridge and bridge-embankment transitions

The measured examples of the rail displacements in both the embankment-bridge the bridge-embankment transitions in Transition B are shown in Figure 1.11. The rail displacements measured at the symmetric locations of the bridge are compared.

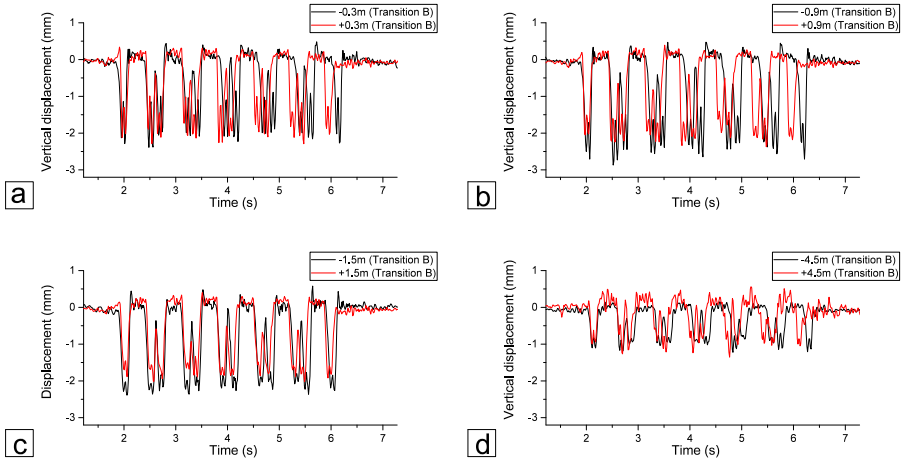

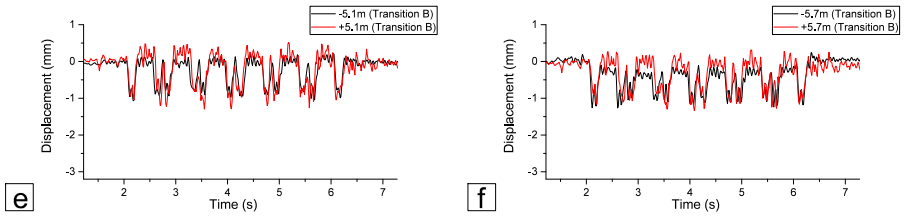

Figure 1.11. Rail vertical displacements in the embankment-bridge and the bridge-embankment transitions of Transition B.

As it can be seen from Figure 1.11, the peaks at the symmetric locations the embankment-bridge and the bridge-embankment transition zones are generally similar, except that at ±0.9m and ±1.5m the rail displacements on embankment-bridge are larger. The largest difference is around 30%, which can be found in Figure 1.11b, where the maximal displacement at -0.9m is 2.69mm while that at +0.9m is 2.37mm. It is in agreement with the theoretical analysis in [1] numerical simulation in [4], wherein the dynamic behaviour of the train in two types of the transition zones are different. It is a remarkable fact that Transition B is in healthy condition. For transition zones in poor condition, the simulation may be different.

Figure 1.12 also shows that the rail displacements at the close locations (±0.3m, ±0.9m and ±1.5m) are much larger than those at the relative distant locations (±4.5m, ±5.1m and ±5.7m), which is in agreement with Transition A. The dynamic profile of Transition B is described in Figure 1.12.

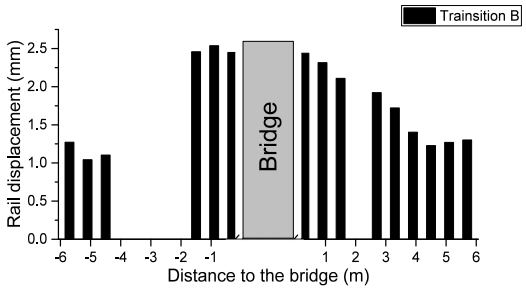

Figure 1.12. Statistics of the vertical rail displacements at all measured points of Transition B.

As seen from Figure 1.12, the dynamic profiles of the two types of transitions are both increased close to the bridge. The rail displacement in the embankment-bridge transition gradually decreases from 0.3m to 4.5m. Differently, the largest rail displacement in the bridge-embankment transition zones appears at 0.9m instead of the 0.3m (the closed one). This is discussed later.

4.4 Dynamic profiles of transitions in various conditions

The example of the rail displacements measured at -1.5m and -4.5m in Transition A, B and C are shown in Figure 1.13. The maximal displacements corresponding to the passing bogies are listed in Table 1.4.

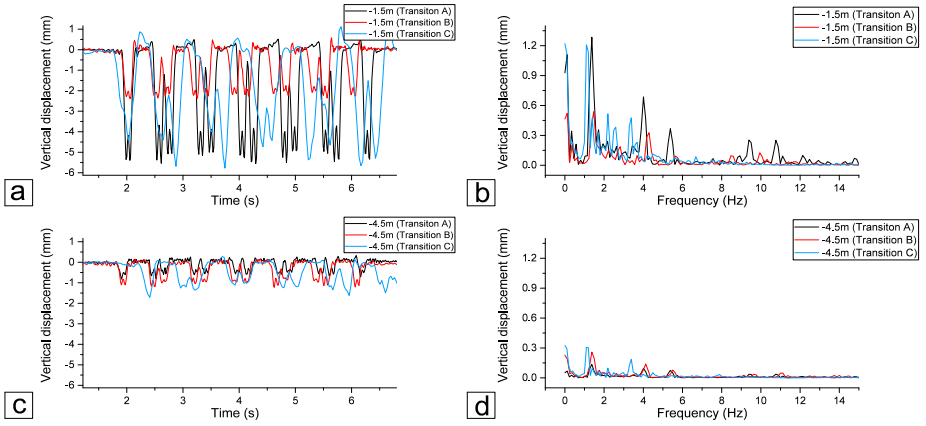

Figure 1.13. Rail vertical displacement of Transition B at -1.5m and -4.5m compared with Transition A.

Table 1.4. Peaks (mm) corresponding to bogies in Figure 1.13.

Bogie No.	Transition A		Transition B		Transition C	
	-1.5m	-4.5m	-1.5m	-4.5m	-1.5m	-4.5m
1	5.39	0.82	2.39	1.11	4.45	1.71
2	5.54	0.80	2.36	1.19	4.40	1.26
3	5.08	0.60	2.27	1.01	5.69	1.36
4	5.16	0.61	2.36	1.04	4.02	1.11
5	5.00	0.56	2.27	0.96	5.77	1.03
6	5.27	0.57	2.20	0.96	4.73	1.24
7	5.55	0.59	2.26	1.02	4.43	1.20
8	5.51	0.59	2.14	1.22	5.37	1.34
9	4.94	0.49	2.23	0.86	4.65	1.62
10	5.05	0.56	2.08	0.96	5.65	1.49
11	5.45	0.66	2.36	1.14	5.29	1.15
12	5.34	0.72	2.26	1.21	3.84	1.08
Average	5.27	0.63	2.27	1.06	4.86	1.30
Standard deviation	0.21	0.10	0.09	0.11	0.64	0.21

Comparing the results obtained in Transition B and Transition A and C, it can be seen that the rail displacements at -4.5mm are similar as shown in Figure 1.13c, which are 1.06m, 0.63mm and 1.06mm respectively (Table 1.4). It is reasonable, since the rail displacements at -4.5m are close to the displacements in the open tracks, and the open tracks in the three transition zones are similar. The rail displacements at -1.5m in Transition A, B and C are considerably different, which are 5.27mm, 2.27mm and 4.86mm respectively (Table 1.4). This means that the void at -1.5m in Transition A and C is larger than in Transition B. Hanging sleepers are expected in such locations. Therefore, the track in Transition A and C are in worse condition than in Transition B, which is in agreement with the health condition known from the maintenance history. Based on the measurement results the dynamic profiles of the Transition A, B and C were obtained, which are compared in Figure 1.14.

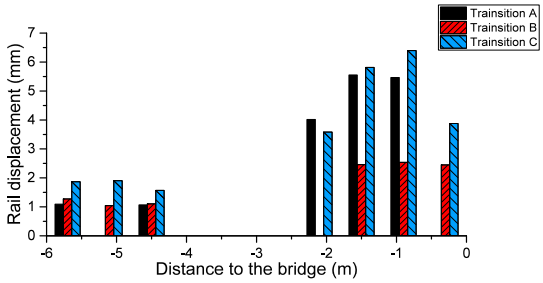

Figure 1.14. Comparison of vertical rail displacements in the approaching zone of two transitions.

As it can be seen from Figure 1.14, the rail displacements are sharply increased in the approaching zones (0.0-4.5m) in all transition zones, by comparing the rail displacements in 0.3m-1.5m and 4.5m-5.7m zones. The larger rail displacements confirm the "dip" often reported in the transition zones (e.g. in [3]). The high displacements of rail indicate that the sleepers are in poor supporting condition, which leads to a significant redistribution of the wheel load [4, 5].

The increase of the rail displacements near the abutment (0.3m-1.5m) in these transitions can be explained by dynamic behaviour when the bogie moves from the embankment to the bridge. At the moment, one wheel of the bogie is on the embankment and the other on the bridge, more loads distribute to the wheel on the embankment due to its low position. As a result, the wheel-rail interaction force is increased in the zone corresponding to the wheel distance in a bogie (2.5m/2.8m). Following this hypothesis, the force of the rear wheel reaches the maximum when bogie is half on the embankment and half on the bridge (1.25m/1.4m). This hypothesis is in agreement with the results of the numerical simulations of transition zones, where the higher ballast stresses were also observed on the distance depending on the wheel distance in a bogie [4]. It also explains the reason that the highest rail displacement appears at -0.9m or -1.5m instead of -0.3m, which is different from the bridge-embankment transition in Transition B (see Section 4.3).

5 Discussion

From the measurement results presented above, it can be observed that the rail displacements in 0.3m-1.5m of Transition A were bigger than in Transition B, while the rail displacements in 4.5m-5.7m were very close. It matches very well the maintenance history of these transitions (Transition A in poor condition and Transition B in good condition). It has been found the ratio of the average of the rail displacements in 0.3m-1.5m over those in 4.5m-5.7m has a correlation to the performance of the transition zones. The physical meaning of the ratio is how many times larger the rail displacement in the approaching zone than in the open track. The calculations are shown in Table 1.5, where $Rail_{0.3-1.5m}$ is the average of the rail displacement at 0.3-1.5m; and $Rail_{4.5-5.7m}$ is the average of the rail displacement at 4.5-5.7m. The distance is calculated from the bridge and only on the embankment-bridge transition, as shown in Figure 1.7.

Table 1.5. Calculation of the measurements from the transition zones

Transition	Condition	$Rail_{0.3-1.5m}$ (mm)	$Rail_{4.5-5.7m}$ (mm)	Ratio
A	Poor	5.51	1.08	5.1
B	Good	2.48	1.14	2.2
C	Poor	5.36	1.78	3.0

As seen from Table 1.5, the ratio correlates very well to the condition of the transition zones, wherein 2.2 is for the healthy condition and 5.1 for the poor condition. According to [1, 5, 39], the settlement in the transition zone is a self-perpetuating system. The differential settlement leads to redistribution of wheel load, which in turns initiates larger differential settlement. Assuming the ratio is 1 for a perfect transition zone, when no settlement exists in the approaching zone and $Rail_{0.3-1.5m}$ and $Rail_{4.5-5.7m}$ are same. As the transition is in use, the ratio increases. The higher value indicates the worse condition of the transition zone, while the lower value the healthier. Therefore, the ratio can reflect the degradation of a transition zone. By measuring the ratio of a transition zone, it is possible to know in which condition the transition is. For Transition C, both high $Rail_{0.3-1.5m}$ and $Rail_{4.5-5.7m}$ lead to a relative lower ratio, compared to Transition A. It indicates the open track is in poor condition as well as the approaching zone.

Since currently there is no special detection method or KPIs for transition zones and maintenance scheme of transition zones are determined mostly by experience, this method has a potential to assess the condition and to determine maintenance scheme for certain types of transition zones. However, it should be noted that the ratio obtained here are for the transition zones without countermeasures with Dutch passenger trains running at normal operational velocity (80km/h-140km/h). These values may be affected by the transition zone type, configuration and velocity of trains. Before using the ratio as a KPI for transition zones, numerous measurements of transition zones should be conducted.

6 Conclusion

This paper presents results of the experimental study performed on three transition zones in various conditions. The dynamic displacements of rails were measured at multiple points in the approaching zone. The measurement device employed is a contactless mobile device for measuring displacements, which is based on the DIC technique. Using this method, the dynamic profile of the track (the dynamic displacement of rail along the track) in the approaching zones (instead of a single point measurement) can be obtained. The health condition in the transition zones can be assessed, and therefore the maintenance schemes can be better determined.

Because the operational parameters of the DIC-based devices are important to accuracy, the measurement device was tested in the laboratory to determine the optimal range of its operational parameter. It has been found that elevation angle of the cameras is the most sensitive parameter and a set of the operational parameter is proposed for the field measurement.

After the determining the working ranges of the operational parameters, the measurements were performed on three transition zones. The length of the approaching zone (4.5m) was determined based on the measurements performed at the different distances from the bridge. The rail displacements are considerably increased in the approaching zone, while the rail displacements are similar to those in the open track, beyond the approaching zone.

It has also been found that the dynamic profiles of the embankment-bridge and the bridge-embankment transition are both increased close to the bridge. However, the rail displacement in the embankment-bridge transition gradually decreases, while the highest rail displacement in the bridge-embankment transition appears at 0.9m or 1.5m to the bridge. A possible explanation is that more loads distribute to the wheel on the embankment when the bogie moves from the embankment to the bridge.

Another finding is that the dynamic profiles of the transition zone in various conditions are significantly different. The ratio between the rail displacements in 0.3m-1.5m and 4.5m-5.7m is calculated to study the degradation in the approaching zones. The results show that the ratio has good correlation with the health condition of the measured transition zones.

PII-I

Reference

1. Kerr AD and Moroney BE. Track transition problems and remedies. PROC of the American railway engineering association. 1993; 94: 25.

2. Zuada Coelho B. Dynamics of railway transition zones in soft soils (Doctoral dissertation). 2011.

3. Nicks JE. The bump at the end of the railway bridge (Doctoral dissertation). Texas A&M University, 2009.

4. H. Wang, V. L. Markine, Shevtsov IY and Dollevoet R. Analysis of the Dynamic Behaviour of a Railway Track in Transition Zones With Differential Settlement. 2015 Joint Rail Conference, San Jose, California, USA, March 2015. 2015, p. 7.

5. Stark TD and Wilk ST. Root cause of differential movement at bridge transition zones. Proceedings of the Institution of Mechanical Engineers, Part F: Journal of Rail and Rapid Transit. 2015.

6. Hölscher P and Meijers P. Literature study of knowledge and experience of transition zones. Delft: report. 2007.

7. Varandas JN, Hölscher P and Silva MAG. Dynamic behaviour of railway tracks on transitions zones. Computers & Structures. 2011; 89: 1468-79.

8. Hyslip JP, Li D and McDaniel C. Railway bridge transition case study. Bearing Capacity of Roads, Railways and Airfields 8th International Conference (BCR2A'09). 2009.

9. Sasaoka C and Davis D. Long term performance of track transition solutions in revenue service. Technology Digest TD-05-036, Transportation Technology Center. Inc, Association of American Railroads. 2005.

10. Li D and Davis D. Transition of railroad bridge approaches. Journal of Geotechnical and Geoenvironmental Engineering. 2005.

11. Plotkin D and Davis D. Bridge approaches and track stiffness. Final Report, DOT/FRA/ORD-08-01, Federal Railroad Administration. 2008.

12. Le Pen L, Watson G, Powrie W, Yeo G, Weston P and Roberts C. The behaviour of railway level crossings: insights through field monitoring. Transportation Geotechnics. 2014; 1: 201-13.

13. Gallage C, Dareeju B and Dhanasekar M. State-of-the-art : track degradation at bridge transitions. Proceedings of the 4th International Conference on Structural Engineering and Construction Management 2013. 2013.

14. Paixao A, Fortunato E and Calcada R. Design and construction of backfills for railway track transition zones. Proceedings of the Institution of Mechanical Engineers, Part F: Journal of Rail and Rapid Transit. 2013; 229: 58-70.

15. Coelho B, Hölscher P, Priest J, Powrie W and Barends F. An assessment of transition zone performance. Proceedings of the Institution of Mechanical Engineers, Part F: Journal of Rail and Rapid Transit. 2011; 225: 129-39.

16. Wang H, Markine V and Shevtsov I. The Analysis of Degradation Mechanism in Track Transition Zones using 3D Finite Element Model. Proceedings of the Second International Conference on Railway Technology: Research, Development and Maintenance, J Pombo,(Editor), Civil-Comp Press, Stirlingshire, United Kingdom, paper 227, 2014 doi: 104203/ccp. 2014.

17. Markine V, Wang H and Shevtsov I. Experimental Analysis of the Dynamic Behaviour of a Railway Track in Transition Zones. Proceedings of the Ninth International Conference on

Engineering Computational Technology, P Iványi and BHV Topping, (Editors), Civil-Comp Press, Stirlingshire, United Kingdom, paper 3, 2014 2014.

18. Bezin Y, Iwnicki SD, Evans G, Shahzad F, de Vries E and Cavalletti M. An investigation of sleeper voids using a flexible track model integrated with railway multi-body dynamics. Proceedings of the Institution of Mechanical Engineers, Part F: Journal of Rail and Rapid Transit. 2009; 223: 597-607.

19. Lundqvist A and Dahlberg T. Load impact on railway track due to unsupported sleepers. Proceedings of the Institution of Mechanical Engineers, Part F: Journal of Rail and Rapid Transit. 2005; 219: 67-77.

20. Pinto N, Ribeiro CA, Gabriel J and Calcada R. Dynamic monitoring of railway track displacement using an optical system. Proceedings of the Institution of Mechanical Engineers, Part F: Journal of Rail and Rapid Transit. 2013; 229: 280-90.

21. Paixão A, Fortunato E and Calçada R. Transition zones to railway bridges: Track measurements and numerical modelling. Engineering Structures. 2014; 80: 435-43.

22. Paixão A, Alves Ribeiro C, Pinto N, Fortunato E and Calçada R. On the use of under sleeper pads in transition zones at railway underpasses: experimental field testing. Structure and Infrastructure Engineering. 2014; 11: 112-28.

23. Macdonald J, Dagless E, Thomas B and Taylor C. Dynamic measurements of the second Severn crossing. Proceedings of the Institution of Civil Engineers Transport. Institution of Civil Engineers, 1997, p. 241-8.

24. Koltsida I, Tomor A and Booth C. The use of digital image correlation technique for monitoring masonry arch bridges. ARCH 13. Split, Croatia2013.

25. White D, Take W and Bolton M. Soil deformation measurement using particle image velocimetry (PIV) and photogrammetry. Geotechnique. 2003; 53: 619-32.

26. McCormick N and Lord J. Digital image correlation for structural measurements. Proceedings of the Institution of Civil Engineers. 2012; 165: 185.

27. Murray C, Hoag A, Hoult NA and Take WA. Field monitoring of a bridge using digital image correlation. Proceedings of the Institution of Civil Engineers-Bridge Engineering. Thomas Telford Ltd, 2014, p. 3-12.

28. Bhandari AR, Powrie W and Harkness RM. A digital image-based deformation measurement system for triaxial tests. Geotechnical Testing Journal. 2012; 35: 209-26.

29. Giachetti A. Matching techniques to compute image motion. Image and Vision Computing. 2000; 18: 247-60.

30. Tong W. An evaluation of digital image correlation criteria for strain mapping applications. Strain. 2005; 41: 167-75.

31. Sutton M, Wolters W, Peters W, Ranson W and McNeill S. Determination of displacements using an improved digital correlation method. Image and vision computing. 1983; 1: 133-9.

32. Bowness D, Lock A, Powrie W, Priest J and Richards D. Monitoring the dynamic displacements of railway track. Proceedings of the Institution of Mechanical Engineers, Part F: Journal of Rail and Rapid Transit. 2007; 221: 13-22.

33. Priest J, Powrie W, Yang L, Grabe P and Clayton C. Measurements of transient ground movements below a ballasted railway line. Géotechnique. 2010; 60: 667-77.

34. Priest JA and Powrie W. Determination of dynamic track modulus from measurement of track velocity during train passage. Journal of Geotechnical and Geoenvironmental Engineering. 2009; 135: 1732-40.

35. Wheeler LN, Take WA and Hoult NA. Measurement of rail deflection on soft subgrades using DIC. Proceedings of the Institution of Civil Engineers-Geotechnical Engineering. 2016; 169: 383-98.

36. Ribeiro D, Calçada R, Ferreira J and Martins T. Non-contact measurement of the dynamic displacement of railway bridges using an advanced video-based system. Engineering Structures. 2014; 75: 164-80.

37. Murray CA, Take WA and Hoult NA. Measurement of vertical and longitudinal rail displacements using digital image correlation. Canadian Geotechnical Journal. 2014; 52: 141-55.

38. Iryani L, Setiawan H, Dirgantara T and Putra IS. Development of a Railway Track Displacement Monitoring by Using Digital Image Correlation Technique. Applied Mechanics and Materials. Trans Tech Publ, 2014, p. 683-7.

39. Dahlberg T. Railway Track Stiffness Variations-Consequences and Countermeasures. International Journal of Civil Engineering. 2010; 8.

Paper II

Finite element analysis of the dynamic behaviour of track transition zones during train passing processes

Haoyu Wang, Valeri Markine[1]

[1]Delft University of Technology, Delft, the Netherlands

Under review

Abstract

Transition zones in railway tracks are the locations with considerable changes in rail supporting structures. Typically, they are located near engineering structures, such as bridges, culverts and tunnels. In such locations, the vertical stiffness of the track support varies, resulting in amplification of the dynamic forces acting on the track, which ultimately leads to the deterioration of vertical track geometry. Also, the differential settlement between embankment and bridges also aggravates the track degradation in transition zones, which significantly increases the maintenance efforts.

In order to better explain the fast degradation of the track in transition zones and to analyse the effect of stiffness variation and differential settlement on the degradation rate, a dynamic 3-D (explicit) finite element (FE) model has been developed. The model studies the transition zones after a few months of operation when the differential settlement appears due to the rapid compaction of ballast tracks. Moreover, the model uses contact elements to model the interface between sleepers and ballast so that the behaviour of hanging sleepers can be better studied. Also, using the pre-loading features in the explicit FE analysis, a more realistic settlement curve of rails and the hanging distance of sleepers can be obtained. Using this model, the analysis of ballast stresses and vehicle dynamics during trains passing can be performed.

The dynamic behaviour of transition zones with and without settlement was studied. The results show that the effect of the differential settlement on the dynamic responses and ultimately on track degradation is much larger than the effect of the stiffness variation alone (no settlement). The effects of the other factors, such as hanging sleepers and the vehicle are analysed as well.

Keyword

Transition zone, Railway, Finite element method, Dynamic behaviour, Hanging sleeper.

1 Introduction

Transition zones in railway tracks are the locations with considerable variation in the vertical stiffness of supporting structures. Typically, they are located near engineering structures, such as bridges, culverts, tunnels and level crossings. Two examples of transition zones are shown in Figure 2.1.

Figure 2.1. Track transition zones.

Having major problems with the track geometry, track transition zones require more maintenance (e.g. tamping and adding ballast) as compared to open tracks [1, 2] For instance, in the Netherlands, the maintenance activities on the tracks in transition zones are performed 4-8 times more often than those on open tracks [3, 4]. In the US, $200 million is spent annually on maintenance of the tracks in transition zones, while in Europe about €97 million is spent on the similar maintenance activities [5, 6]. Based on literature studies and field observations, the problems in transition zones include:

(1) Damage to track components: rail surface defects, broken fasteners, cracks in concrete sleepers, breakage of ballast particles, and voids between sleepers and ballast (also known as hanging sleepers) [2, 4, 7-17].

(2) Deterioration of the track geometry: extra settlement appearing on tracks and forming a “dip“ [18]. (It might be caused by the breakage of the track component, ballast pollution, ballast penetration into subgrade, and poor drainage [1, 15, 19].)

(3) Loss of the passenger’s comfort [20].

The damage to track components leads to the deterioration of track geometry, while track irregularities result in the increase of the wheel-rail contact forces and the sleeper-ballast contact forces acting on track structures, which forms a self-perpetuating system [14, 17, 20-23]. As a result, the tracks in transition zones deteriorate at an accelerated rate as compared to open tracks [17]. An example of the transition zone with large irregularities is shown in Figure 2.2. The transition zone in the figure is a bridge transition zone, and the bridge locates under the auxiliary rails.

Figure 2.2. Track settlement in the transition zone.

One reason for the track degradation in transition zones is the large abrupt change in vertical track stiffness and the consequent increase of dynamic wheel loads [13, 15, 17]. Since the rail deflection due to passing trains is determined by the vertical stiffness of tracks, the change of track stiffness results in a rapid elevation of wheels, which increases the acceleration of wheels. According to Newton's law, wheel forces will be increased, which leads to track degradation. The effect caused by the stiffness variation has been studied, e.g. in [12, 22, 24-26].

Another reason for the track degradation in transition zones is the differential settlement. After construction or maintenance (tamping), ballast tracks experience a period of rapid compaction [19, 27-30] which is to some extent inevitable [31]. On the contrary, the tracks on engineering structures (e.g. bridges) are barely settled, which generates the differential settlement in transition zones. The field measurement results can be found in [9, 15]. Similar to the stiffness variation, the differential settlement also leads to the rapid elevation of wheels and hence amplifies of wheel forces. Considering the elevation caused by the differential settlement could be much higher than that caused by the stiffness variation, the effect of the differential settlement on the track degradation in transition zones could be larger [20, 32-34]. It is therefore important to model the differential settlement in transition zones accurately.

A common method (e.g. in [13, 22, 32, 33]) to model the differential settlement in transition zones is: (1) decreasing the vertical level of the tracks on the embankment; (2) connecting the tracks on the embankment and the tracks on engineering structures, using a straight line. An exception can be found in [35], where a parabola was used to connect the lower and the higher tracks. However, the real settlement curve of the rails in transition zones is resulted by the weight of sleepers and the bending stiffness of rails, which is more complex than a straight line or a parabola.

Moreover, when the differential settlement appears in transition zones, some sleepers are not entirely supported by ballast. As a result, the sleepers may be pushed down by train loads and cause high dynamic impacts on ballast [34]. Since ballast settlement is proportional to ballast stress [27], it is necessary to model the interaction between sleepers and ballast accurately so that ballast stress can be studied in detail. However, in the most existing models for transition zones, sleepers and ballast are not separable, e.g. in [13, 16, 20, 21, 35-42], or ballast is modelled by spring elements, e.g. in [3, 20, 22, 25, 32, 43, 44].

A transition zone model focusing on the differential settlement and consequent sleeper-ballast interaction has been developed by the rail section of TU Delft. It was proposed in [45] and further

developed in [46] and [47]. The model studies the transition zones after a few months of operation, when the differential settlement appears due to the rapid compaction of ballast tracks. Moreover, the interfaces between sleepers and ballast are modelled using contact elements. As a result, a more accurate settlement curve of rail can be obtained and the effect of hanging sleepers can be analysed more accurately. (More details about the modelling of the ballast-sleeper interface and the hanging sleepers can be found in Section 2.4). The transition zone model is coupled with a whole vehicle model, following [3, 22, 24, 25, 32, 43, 44], which makes it possible to study the effect of vehicle dynamics.

The main goals of the study can be formulated as follows:

1) To develop the FE model of transition zones. The highlights of the model are:
   - More realistic settlement curve of rails
   - More accurate simulation of hanging sleepers (e.g. the hanging distance before train passing and the motion during train passing);
   - Detailed analysis of ballast stress;
   - More accurate analysis of vehicle dynamics during the train passing the transition zone;
   - Combination of the soft-hard (embankment-bridge) and the hard-soft (bridge-embankment) transitions in one model.

2) To analyse the dynamic behaviour of track components in the transition zone with differential stiffness and settlement (w.r.t. the transition zone with differential stiffness only);

3) To compare the effects of the soft-hard transition (the embankment-bridge transition) and the hard-soft transition (the bridge-embankment transition);

The numerical model and its main features are described in Section 2. Model validation against field measurement results is presented in Section 3. The dynamic behaviour of the transition zones with and without differential settlement is analysed in Section 4. Finally, some conclusions based on the results of numerical simulations are drawn in Section 5.

2 Numerical model of track transitions

2.1 Track model

The developed FE model of the transition zone consists of three main parts, namely two ballast tracks on embankment and a slab track on a bridge, as shown in Figure 2.3. In the model, the 'bridge' is symbolical and not analysed, because the purpose of the paper is to study the effect of the transition zone rather than the bridge itself. The bridge is simplified to reduce calculation costs. Using the transition zone model, two types of transition (the embankment-bridge and the bridge-embankment transition) can be analysed in one run. It should be noted that the bridge can affect the response on the bridge-embankment transition. The ballast tracks are both 48m long, and the bridge section is 24m long. Since the left end of the model is set as 0m, the embankment-bridge transition is at 48m, and the bridge-embankment transition is at 72m. The total length of the model is 120m. The length of the vehicle is 23m, which is shorter than the bridge. It guarantees that the whole vehicle can be on the bridge.

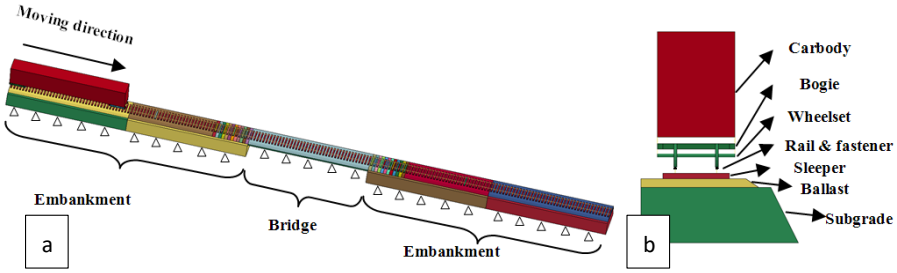

Figure 2.3. FE model of track transition zones: (a) full view, (b) cross-section of ballast track.

The loads are added to the model in two steps in order to reduce the dynamic instability. The gravity forces are first applied to the complete system formed by the vehicle, the track superstructure, the ballast and the subgrade. After certain balance time (as the vibrations due to the gravity forces damped out), the velocity is applied on the vehicle. In this study, the vertical acceleration of the carbody is used to determine the balance time, which is shown in Figure 2.4. It can be seen that the vibrations are damped out after 0.4s.

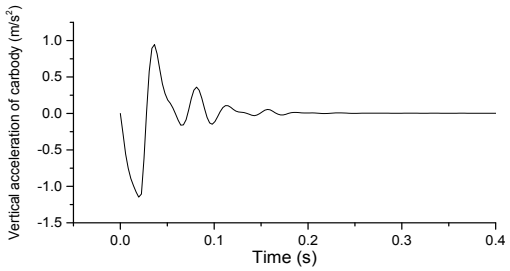

Figure 2.4. Vertical acceleration of the carbody in the first step.

It should be noted that the time to reach the equilibrium highly depends on the value of the differential settlement and the material property of the track (e.g. soft/stiff soil). It is 0.4s in this case, which may differ in other cases.

2.2 Track components

The components of the ballast track model are rails, fasteners, sleepers, ballast and subgrade. The rails are modelled by Hughes-Liu beam elements [48], whereas the cross-sectional and mass properties of the UIC54 rail are used. The length of rail elements is 75mm.

The fasteners connecting rails and sleepers are modelled using the spring-damper elements. In the vertical direction, these springs have bilinear properties. Therefore, the springs can model rail pads in compression, while the springs can model the clamping effect of fasteners in tension. The stiffness of springs is shown in Table 2.1.

Table 2.1. Properties of spring elements.

	Horizontal	Vertical	Longitudinal
Stiffness (N/m)	1.5E6	1.20E8 (Compression) 1.20E11 (Tension)	1.5E6
Damping (N*s/m)	5.00E4	5.00E4	5.00E4

The sleepers are modelled as 3D elastic bodies using solid elements so that the spatial movement of sleepers can be studied [49]. In addition, the ballast stresses caused by the spatial movement of sleepers can be better analysed. Despite the fact that the ballast can be more

accurately modelled using the discrete element method, it is not feasible to model the ballast as particles in the large-scale study (e.g. transition zones). Many studies (e.g. [24, 37, 50, 51]) have proved that some behaviour of ballast and hanging sleepers can be modelled accurately using simplified methods (e.g. solid elements). Following [34, 37], the ballast in this model is modelled by solid elements. The element length of 75mm is used for the sleepers and the ballast (there are eight elements within 1 sleeper space), while 0.3m is used for the subgrade. The thickness of ballast and subgrade layers is 0.3m and 2m, respectively.

The bridge is modelled as a concrete slab. The rails on the bridge are directly fastened to the concrete slab using spring-damper elements. The connection area between the ballast track (the track on the embankment) and the track on the bridge is shown in Figure 2.5.

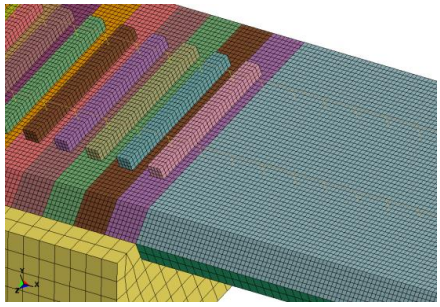

Figure 2.5. Part of the FE model with mesh details.

In the current study, the elements used for the sleepers, the ballast, the subgrade as well as the bridge have the linear isotropic elastic material properties, which are collected in Table 2.2.

Table 2.2. Material properties of solid elements.

	Sleeper	Ballast	Concrete slab	Support layer	Subgrade
Elastic Modulus (Pa)	3.65E10	1.2E8	3.50E10	3.30E8	1.80E8
Poisson ratio	0.167	0.25	0.167	0.25	0.25

At the junctions of the ballast tracks and the bridge, surface-surface contact elements are used so that ballast at the interface with the bridge can move vertically with friction. However, the longitudinal movement of ballast is constrained by the bridge. The silent boundary conditions are applied on both ends of the model to reduce the wave reflection effect [34]. The bottom of the embankment (subgrade layer) and the bridge (concrete layer) are fixed.

2.3 Vehicle model

The Vehicle model is idealized as a multibody system consisting of one carbody, two bogies and four wheelsets. The primary and secondary suspensions are modelled by spring-damper elements. The parameters of the vehicle are based on [52] and adapted to a Dutch passenger train [2, 53], as given in Table 2.3.

Table 2.3. Vehicle parameters.

Parameter	Value
Axle load (kN)	186.3
Distance between wheels (m)	2.5
Distance between axles (m)	20.0
Length of train body (m)	23.0
Primary suspension stiffness (N/m)	4.25E5
Primary suspension damping (N*s/m)	1.00E6
Secondary suspension stiffness (N/m)	4.68E5

Secondary suspension damping (N*s/m)	6.50E4
Secondary suspension Bending stiffness (Nm/rad)	1.05E4

The wheel-rail interaction model is designed as a penalty function with the purpose to ensure that the train nodes follow the line of the track. It does not attempt to account for the shape of the rail profile. To calculated the interaction force, a linear force-deflection relationship is assumed in compression, while no tensile force is generated [54]. The stiffness is derived from Hertz's theory, as shown in Equation (1) [55].

$$k_H = \sqrt[3]{\frac{3E^2Q\sqrt{R_{wheel}R_{railprof}}}{2(1-\nu^2)^2}}, \quad (1),$$

where: E is the modulus of elasticity of the wheel and rail; ν is the Poisson's ratio; Q is the static vertical wheel load; R_{wheel} is the radius of the wheel; $R_{railprof}$ is the radius of the railhead. In the study, the contact stiffness is 1.2E9 N/m, following [56, 57] Nonlinear Hertzian spring is not used due to the limitation of computational power.

PII-II

2.4 Sleepers-ballast interface

Many studies (e.g. [2, 9, 15]) confirmed the existence of hanging sleepers in transition zones. The presence of voids under these sleepers was proven to be strongly deleterious to the sleepers and adjacent ballast [49, 57-59]. The dynamic behaviour of a railway sleeper highly depends on its support condition [60-63]. Even a very small gap between a sleeper and ballast leads to an increase in the interaction force as wheels approach the sleeper [64]. Therefore, it is essential to model the contact between sleepers and ballast appropriately.

In order to accurately model the spatial movement of sleepers and consequent ballast stresses, the contact elements are applied between sleepers and ballast. According to the penalty method employed in the contact elements, the search for penetrations between the bottom surface of sleepers and the top surface of ballast is made every time step during the calculation. When the penetration between contact surfaces is found, a force proportional to the penetration depth is applied to resist and ultimately eliminate the penetration. This force is obtained by placing the normal interface springs between all penetrating nodes at contact surfaces [48]. The contact stiffness is determined by the minimum of the slave and master stiffness, which is the stiffness of the ballast in this case. The displacement of sleepers and ballast as well as the stresses of ballast due to a passing vehicle are discussed in Section 2.5 and Section 4.2 respectively.

2.5 Modelling of settlement

Due to the contact elements, it is possible for sleepers to be separated from ballast. It provides the possibility to simulate the hanging sleepers and differential settlement in transition zones.

As mentioned in Section 1, it is assumed that the rapid compaction of ballast tracks is completed so that there is a differential settlement in the transition zone. It is achieved by applying a downwards displacement only to the ballast and subgrade layers in the ballast tracks on the both sides of the bridge, while the bridge remains unchanged. It is remarkable to note that the value of the differential settlement is important, but difficult to measure precisely in reality. For instance, the void under sleepers measured in [65] had an error of 3mm. The value of the differential settlement used in this paper is selected from the values which are frequently reported in the field measurements in transition zones [3, 4, 9], which are ranged from 2mm to 10mm. Then the value is tuned by the field measurement of a transition zone (discussed in Section 3.2). As a result, 4mm is used as the differential settlement in the model. It should be noted that 4mm is a

relatively small value since the measured transition zone was in good condition. It is better to use this value when studying the transition zones at the early stage of degradation.

It should also be noted that this study focuses on the simple type of transition structure wherein the tracks on the embankment and the tracks on the bridge are connected without any countermeasures. The reason for that was to eliminate the effects of countermeasures. In addition, the non-countermeasure transitions are widely used in the Netherlands and the US [9, 66].

Because sleepers are clamped to rails by fasteners (as described in Section 2.2), voids under sleepers occur after applying differential settlement and gravity forces. After the stabilization phase, the sleepers near the bridge are hanging due to the bending resistance of rails. Figure 2.6 shows the vertical coordinates of the sleepers and the ballast at the bridge-embankment transition after the model has reached the equilibrium state. For convenience, the sleepers are numbered starting from the one closest to the bridge and have the positive sign on the bridge-embankment transition (see Figure 2.6) and the negative sign on the embankment-bridge transition (depending on the moving direction of the train). For example, the train passes Sleeper-10 to Sleeper-1 when it approaches the bridge, and later the train passes Sleeper+1 to Sleeper+10 when it leaves the bridge. Since the sleeper space is 0.6m, the distance from the bridge to each sleeper can easily be calculated. It should be noted that the coordinates of rails, sleepers and ballast at the equilibrium state can be obtained depending on the value of the different settlement. The capability to simulate the settlement curve of rails is one of the advantages of the model.

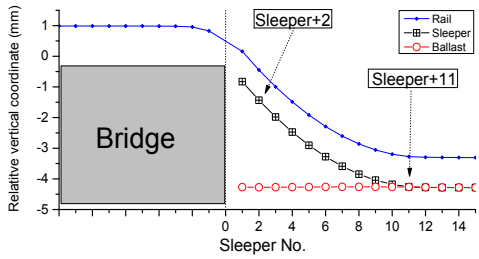

Figure 2.6. Vertical coordinates of rail, sleepers and ballast at the bridge-embankment transition due to 4 mm settlement.

From Figure 2.6 it can be seen that the first 10 sleepers close to the bridge are hanging as a result of the 4mm settlement. After Sleeper+11, the sleepers are fully supported by the ballast. It can also be seen that the hanging distance of Sleeper+1 is the highest and the hanging distances of other sleepers gradually reduce as the distance from the bridge increases. From Figure 2.6, it can clearly be seen that the settlement curve of the rail near the bridge is nonlinear, which is neither a straight line nor a parabola. The hanging values of the sleepers are presented as the difference between the vertical coordinates of the sleepers and ballast. The same situation is observed on the other side of the bridge (i.e. the embankment-bridge transition).

In the second phase of the simulation, the vehicle moves over the transition zone. Figure 2.7 shows the time history of the vertical coordinates of two sleepers (and the corresponding ballast elements) located close and far from the bridge (i.e. Sleeper+2 and Sleeper+11).

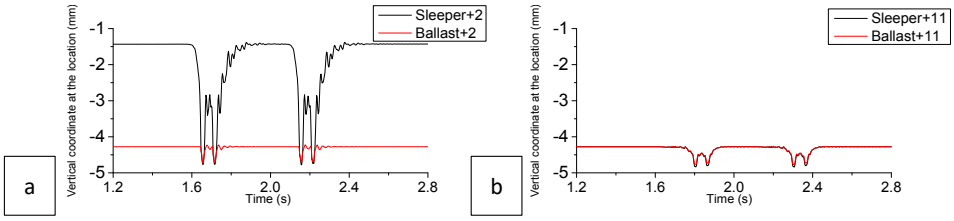

Figure 2.7. Time history of vertical coordinate due to the passing vehicle: Sleeper +2 (a) and Sleeper+11 (b).

It can be seen from Figure 2.7 that Sleeper+2 was hanging before the train came (1.6s). When the train moved above the sleeper during 1.6s to 2.4s, Sleeper+2 was pushed down and touched ballast, which also generated the displacements of ballast. After 2.4s, Sleeper+2 returned to its original hanging state, while Sleeper+12 was constantly rested on ballast. The significant distinction of the dynamic displacements of these two sleepers is a result of the differential settlement in the transition zone and may lead to the increase of wheel-rail contact forces and the stresses in ballast, which is discussed in Section 4. This also highlights the advantage of the transition zone model.

The mass-weighted nodal damping is applied globally to the nodes of the model. The track random irregularity is not considered at the current stage, but it can be easily included in future studies. The model is solved using the commercial software LS-DYNA. The study of the various mesh sizes was performed prior to this study; however, it is not included due to the limited space. Since the main focus of this study is on the sleeper-ballast connection, the mesh size of the ballast is relatively small. The time-step is 1.3E-5s, and the calculation takes around 10 hours using an 8-core (I7) workstation with High Parallel Computing (HPC).

3 Model validation

The validation of model includes three parts. First, the train/track model is validated, where a section of the open track of the model (6m from the bridge, suggested by [37]) is compared with the field and simulation results of open tracks from [37, 67, 68]. After that, the transition zone model with the settlement is verified using the filed measurement performed by the authors of this paper. At last, the carbody acceleration during the train passing the transition zone is compared with the filed measurement results performed by the authors of this paper. The parameters of the track model are same as Table 2.1 and Table 2.2.

3.1 Verification of the train/track model

The train/track model is compared with the result of a field measurement [67] and the similar FE simulations in [37] and [68]. The field measurement was performed in a heavy haul line in South Africa, where the velocity of the train was 47.5km/h and the axle load was 255kN. The FE results in [68] were calculated using a 2D model in ABAQUS explicit software, where the same velocity and axle load were applied. A more recent FE result in [37] was calculated using ABAQUS explicit software, wherein a similar 3D train/track model was developed. The train moved at 71 km/h and the axle load was 250kN.

Table 2.4. Comparison of the calculation results and the field measurement results from [67] and the simulation results from [68] and [37].

Components	Field measurement from [67]	2D FE Simulation from [68]	3D FE simulation from [37]	Simulation in this paper
Vertical acceleration of sleeper (g)	3-11	-	10	3.9
Stress at the bottom of the ballast layer (kPa)	100	112	104	81.6

In Table 2.4, the dynamic responses of sleeper and ballast are in reasonable agreement. The results in this paper are slightly different from the others, which is mainly due to the variation of axle load (186kN vs 255kN) and the difference in the vehicle configuration and velocity.

3.2 Verification of the displacements of the transition zone model

In this section, the results calculated using the transition zone model are compared with the measurement results. The velocity of the vehicle in the model is adapted for the measurement, which is 100km/h. The measurement device is DIC (Digital Image Correlation)-based device, which is named Video Gauge System (VGS). The VGS is a contactless mobile device for measuring displacements of selected targets as shown in Figure 2.8.

Figure 2.8. DIC-based device: (a) high speed camera, (b) operational system, and (c) targets on rails or sleepers.

The main parts of the DIC-based device are the video cameras and the post-processing software which recognizes and measures the target displacements. This technology allows monitoring non-contact multi-point measurements of strain, rotation and displacement. In the normal monitoring condition, the accuracy of 0.1mm can be achieved and the maximum measurement frequency is up to 400Hz. More details could be found in [69, 70].

The vertical displacement of the rail in the transition zone was measured at different locations during train passages, as shown in Figure 2.9. The transition zone includes two ballast tracks and an embedded track on the bridge, which is similar to the numerical model. The sleepers are numbered the same way as in the numerical model (see Section 2.5) according to the train direction. The rail targets are located above the sleepers, and therefore they have the numbering of the sleepers, as shown in Figure 2.9. It should be noted that the guardrails are usually used in tracks near bridges. However, since the guardrails do not continue on bridges, their effect on the performance of transition zones is negligible.

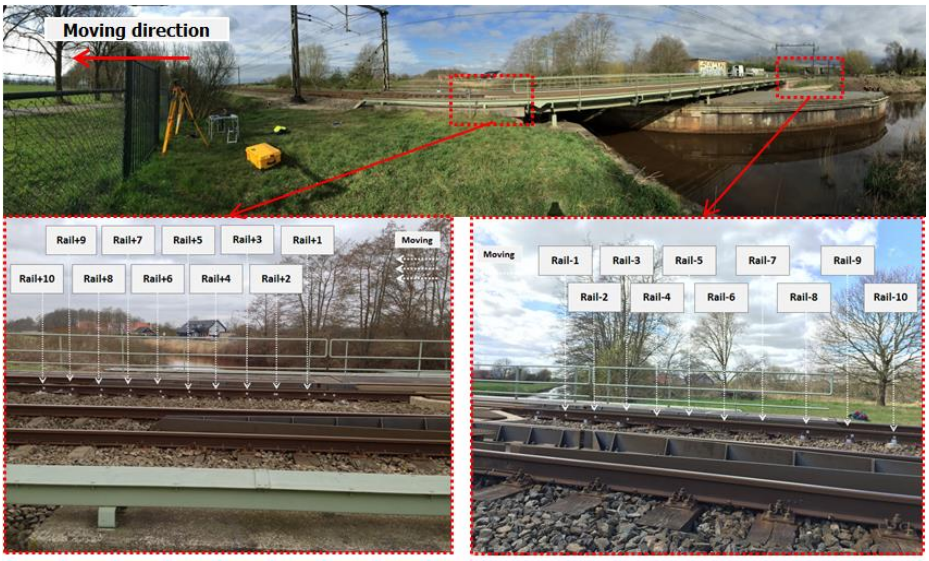

Figure 2.9. Measurement setup.

The maximum of the vertical displacements of rails during train passages was collected and compared with the simulation results as shown in Figure 2.10, wherein the black dots and crosses correspond to the simulation and measurement results respectively. The passing trains were the same as the one used in the model (see Table 2.3). The differential settlement used in the model was 4mm. From Figure 2.10, it can be seen that the measured and simulated displacements follow the same pattern, i.e. they increase near the bridge and decrease as the distance from the bridge increases. Also, the magnitude of the measured and simulated displacements is very close, which means that settlement assumed in the numerical model is close to the actual settlement of the measured transition zone. Therefore, the numerical model is capable of describing the major behaviour of the transition zone.

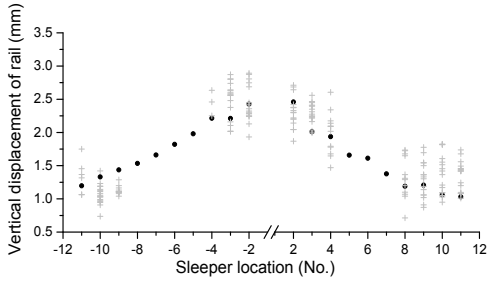

Figure 2.10. Comparison between measurements and simulation: black dots - simulation and cross - measurement results.

The detailed comparison between the measured and simulation results is given in Figure 2.11. The monitoring points of rail above the 2nd sleepers (i.e. Rail-2 and Rail+2) and the 11th sleepers (i.e. Rail-11 and Rail+11) on both sides of the bridge are selected, since the rail sections above the 2nd sleeper have large displacements, while the rail sections above the 11th sleeper have small displacements. In Figure 2.11, the rail displacements are compared in the time and frequency domains, while the letters *S* and *M* indicate the simulation and measurement results respectively.

In the time domain, the peaks in the curves of rail displacements correspond to the wheelsets of vehicles, where two closer peaks are from one bogie. Because only one vehicle is modelled in the simulation, the peaks in the simulation results are less than those in the measurement results. In the frequency domain, the results are filtered using a low-pass filter with the cutting frequency of 35Hz.

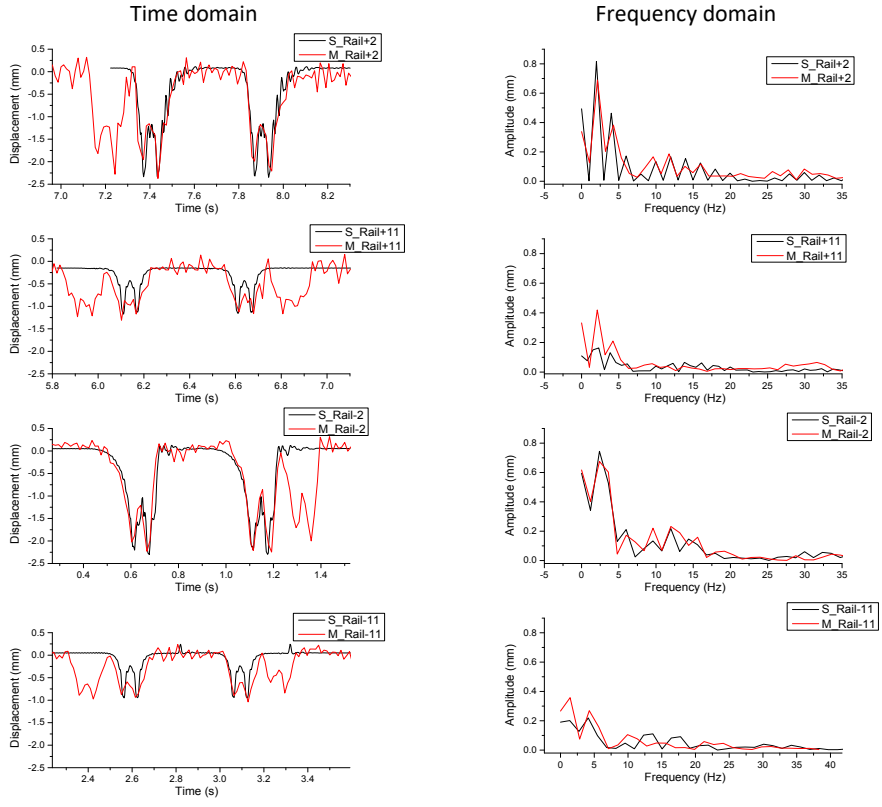

Figure 2.11. Detailed comparisons of measurement and simulation results in the time domain and in the frequency domain.

Both Figure 2.10 and Figure 2.11 show that the simulation results are in a good correlation with the measurement data both in the time and the frequency domains. It can be concluded that the model is able to describe the dynamic behaviour of transition zones.

3.3 Verification of the carbody acceleration of the transition zone model

The calculated carbody acceleration is compared with the results of field measurement, as shown in Figure 2.12. The accelerometer was installed at the window near the front bogie of the vehicle in the measurement. The node at the similar location is selected from the vehicle model. Again, a reasonable agreement can be found. The simulation result is more stable than the measurement results except in the transition zones. It is because the track irregularity is not considered in the model.

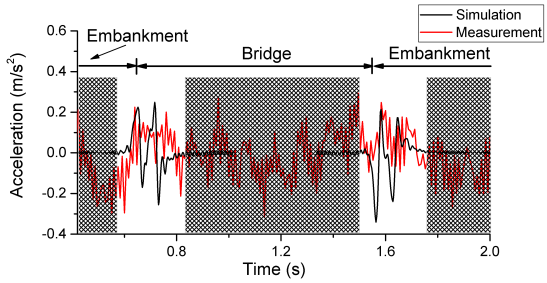

Figure 2.12. Comparison between the calculated carbody acceleration and the measured carbody acceleration.

All the comparisons show that the numerical model can provide reasonable results. Therefore, the model is used further in this study. It should be noted that since this study focuses on the dynamic responses of sleepers and ballast, the validation of the model is conducted in the low-frequency range rather than the high-frequency range (e.g. wheel-rail interaction).

4 Case study: the dynamic behaviour transition zones.

In this section, the transition zones with and without differential settlement are analysed using the proposed FE model. It should be noted that the transition zone with settlement refers to the transition zone considering both differential stiffness and settlement, while the transition zone without settlement refers to the transition zone considering only the differential stiffness. The differential settlement is set to 4mm as previously discussed and the dynamic responses due to the moving vehicle, such as wheel forces, rail stresses, and carbody acceleration, are obtained and analysed. Extra attention in the analysis is given to the stress distribution in ballast. The velocity of the vehicle is 144km/h, which is a typical operational velocity in the Dutch railway system.

4.1 Wheel forces

Figure 2.13 shows the wheel forces corresponding to four wheelsets passing the transition zones with and without the differential settlement. The horizontal axle represents the distance along the transition zone model. The bridge is located between 48m and 72m. The wheel loads on the bridge are not considered in this study and therefore these responses are covered by the shaded area in Figure 2.13. The maximal wheel forces of four wheelsets and their amplifications w.r.t. the average wheel forces far from the bridges are collected in Table 2.5.

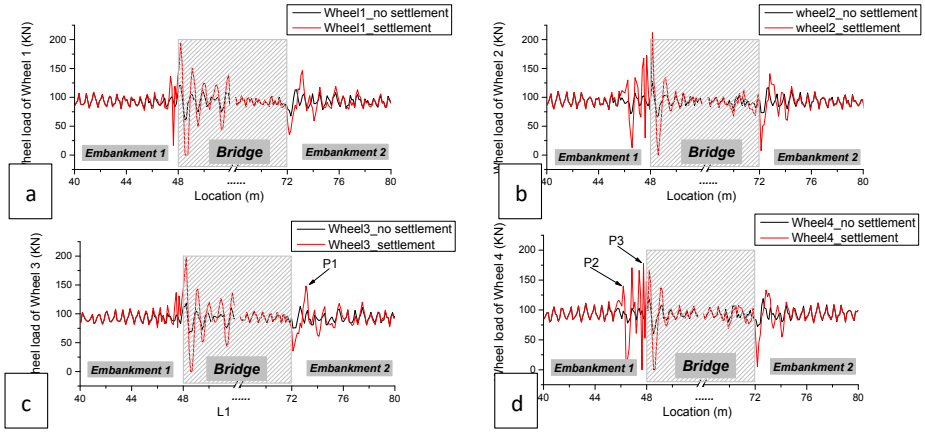

Figure 2.13. Wheel load of four wheelsets, simulations with and without settlement: (a) Wheel 1, (b) Wheel 2, (c) Wheel 3, and (d) Wheel 4.

Table 2.5. Calculation results of wheel loads.

	Wheelset No.	1	2	3	4
Embankment-bridge transition	Max wheel load, no settlement (KN)	93.1	93.1	93.1	93.1
	Increase (w.r.t. tangent track)	*0%*	*0%*	*0%*	*0%*
	Max wheel load, settlement (KN)	136.4	172.8	136.9	**178.0**
	Increase (w.r.t. tangent track)	*46.5%*	*85.6%*	*47.0%*	***91.2%***
Bridge-embankment transition	Max wheel loads, no settlement (KN)	113.2	117	112.8	**119**
	Increase (w.r.t. tangent track)	*21.6%*	*25.7%*	*21.2%*	***27.8%***
	Max wheel loads, settlement (KN)	146.3	140.8	**148.2**	133.3
	Increase (w.r.t. tangent track)	*57.1%*	51.2%	**59.1%**	43.1%

From Figure 2.13 the increase of the wheel forces before and after the bridge can clearly be seen. Also, from Figure 2.13 and Table 2.5 it can be seen that the amplification of the wheel forces in the case of the differential stiffness and settlement is much higher than that of the differential stiffness alone. It means that the effect of settlement is very important and should be taken into account when analysing and improving the transition zone performance.

Moreover, from these results, it can be seen that the amplification of the forces is the highest (91.2%) in the case of embankment-bridge transition and caused by the 4th wheelset (P3 in Figure 2.13d). In the bridge-embankment transition, the forces are also increased (59.1%) and caused by the 3rd wheelset (P1 in Figure 2.13c). However, in the case of the differential stiffness alone, the wheel forces are only increased in the bridge-embankment transition. These results show that the dynamic responses of the embankment-bridge and bridge-embankment transitions should be analysed separately.

In order to better understand the effect of the vehicle dynamics on the increase of the wheel forces in the transition zone, the bogie position at three moments is shown in Figure 2.14. It should be noted that the vertical displacements are magnified 50 times to show the rotation of the bogies clearly. In addition, a large deformation of the rail can be observed as well as the sleepers "sinking" to the ballast.

These moments corresponding to the highest wheel loads P1-P3 are shown in Figure 2.13. The P1 is the highest wheel load in the bridge-embankment transition that occurs when the rear bogie is half on the bridge and half on the embankment. The location of this force defined by the length of the bogie is between Sleeper+2 and Sleeper+3. This location correlates very well with the settlement location observed in the bridge-embankment transition (see the measurement results in Section 3.2).

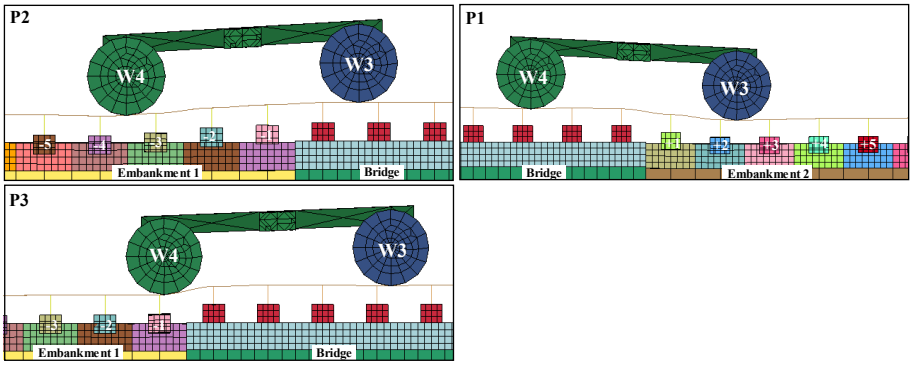

Figure 2.14. Motion of the front bogie corresponding to 3 highest forces (P1-P3) in Figure 2.13c,d.

When considering the embankment-bridge transition, the maximal wheel force (Table 2.5) is caused by the 4th wheelset of the rear bogie (the force P3 in Figure 2.13d). As it can be seen from Figure 2.14, the P3 force just like the P1 force is caused by the pitch motion of the bogie. This pitch motion is caused by the presence of the settlement and also affected by the stiffness of suspensions. Also, from this figure, it can be seen that the P3 force is acting on the rail above Sleeper-1, the nearest one to the bridge. The settlement affected zone in the embankment-bridge transition can be estimated by the first increase of the wheel force in this area that is P2 (see Figure 2.13). This force is also due to the pitch motion of the bogie and its location (Sleeper-3 – Sleeper-4 in Figure 2.14) is also defined by the length of the bogie. The settlement affected zone in the embankment-bridge zone (Sleeper-4 –Sleeper-1) defined by the P2-P3 forces correlates well with the field observations [69].

Finally, from these results, it can be concluded that the increase of the wheel forces observed in the simulations can be used to explain the high degradation rate of the track in transition zones observed in the field. Also, the simulation results have shown that the location of these forces (and therefore) is defined by the vehicle dynamics and in particular by the geometrical properties of the bogie. It should be noted that the maximal wheel forces of the first wheel set and their locations are similar to the second wheelset and therefore not shown here.

4.2 Ballast stress

The stresses in the ballast layer caused by the passing trains are discussed in this section. It should be noted that the response of unbound granular materials like ballast is non-linear, which affects the calculated distribution of stresses inside the ballast. However, for the short-term behaviour analysis in this study, the linear model is used as a first attempt, which is a typical approach e.g. in [20, 37] due to the limitation of the computational power. Moreover, the ballast bed in this model is assumed to be well compacted (after the rapid compaction). At the moment the sleeper contacting the top of the ballast, the ballast elements on the top can be simplified as linear materials.

In order to compare the ballast responses at the different locations, the ballast elements under one sleeper are considered as a group (unit), which are 128 elements (32*4=128, there are 4 elements on the wide side and 32 elements on the long side, see Figure 2.15). The maximal vertical stress in all ballast elements during the train passage is collected first. Then the average

values of these stresses within each group (under a sleeper) have been obtained. These stresses obtained in the simulations with and without settlement are shown in Figure 2.15.

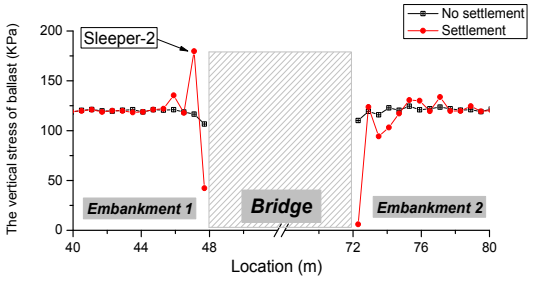

Figure 2.15. Average vertical stress in ballast, simulations with and without the settlement.

PII-II

From Figure 2.15 it can be seen that the stress of the ballast at the relatively distant location from the bridge (e.g. 40-46m and 78-80m) is stable, which is around 125kPa. Considering the sleeper area, which is 0.576m^2 (2.4m*0.24m), the static pressure is: 186KN (wheel load)*40 % (Transfer ratio) /0.576m^2 $\approx$ 125kPa. Moreover, it is also reasonable comparing to the measurement results provided in [28], wherein the ballast stress is within 160-230Kpa. The reason why the calculation results are smaller can be explained by the smaller axle loads. Moreover, the stress of 125kPa is an average of the ballast beneath one sleeper, while the in measurement [28], only the ballast underneath the rail was tested, which is higher than the average.

It also can be seen from Figure 2.15 that, in general, the ballast stresses in case of the differential settlement and stiffness is much higher than the stresses caused by the differential stiffness alone. Therefore, the differential settlement must be considered when studying the degradation of transition zones.

Also, it can be seen that the ballast stresses (see Figure 2.15) and the wheel forces (see Figure 2.13) mostly correlate well. However, in some locations near the bridge, the ballast stresses in the presence of the settlement are lower than that without the settlement (Figure 2.15), even though the wheel loads are increased (see Figure 2.13). The significantly lower stresses under the sleepers closest to the bridge (Sleeper-1 and Sleeper+1) can be explained by their hanging due to the settlement (see Figure 2.6). The danger of this situation is that the stresses in the rails in these locations are extremely higher since the rails over there are not supported (the stresses in rails will be discussed in Section 4.3). These high stresses can result in rail damage due to crack initiation in the rail foot, which is usually observed in the field. It should also be noted that, in the simulation of the transition zone with the settlement, the ballast stresses under Sleeper+1, +3 and +4 are reduced. The slight reduction of the ballast stresses under Sleeper+3 and Sleeper+4 can be explained by the inertia ('flying') effects due to the vehicle velocity, which is in agreement with the theoretical analysis in [17].

Another observation from the stresses results (see Figure 2.15) is that the ballast-stress-affected zones in the two transition zones are different. In the embankment-bridge transition, the ballast stresses are increased within a much shorter zone (2.1m) as compared to the bridge-embankment transition (5.1m). However, the amplification of the stresses in the bridge-embankment transition is smaller than that in the embankment-bridge transition. It agrees well with the increase of the wheel loads in Figure 2.13. These results explain the length of the affected

zones in both transitions and can be used, for instance, when selecting and planning the ballast maintenance activities.

Detailed analysis of the ballast stresses is given in Figure 2.16, wherein the stress distribution under Sleeper-2 is shown. Sleeper-2 is selected since it is the highest in Figure 2.15. The stress distribution is at the moment that the wheel was exactly above the ballast (sleeper), and 4 moments are corresponding to 4 wheels are collected. Moreover, the stresses are due to each passing wheelset (when the wheelset is on this sleeper) with and without settlement are shown in Figure 2.16. The maximum values of these stresses are also collected in Table 2.6. The grey surface in Figure 2.16 corresponds to the limit of the ballast plastic deformation. The value of this limit (165KPa) was obtained experimentally in [71].

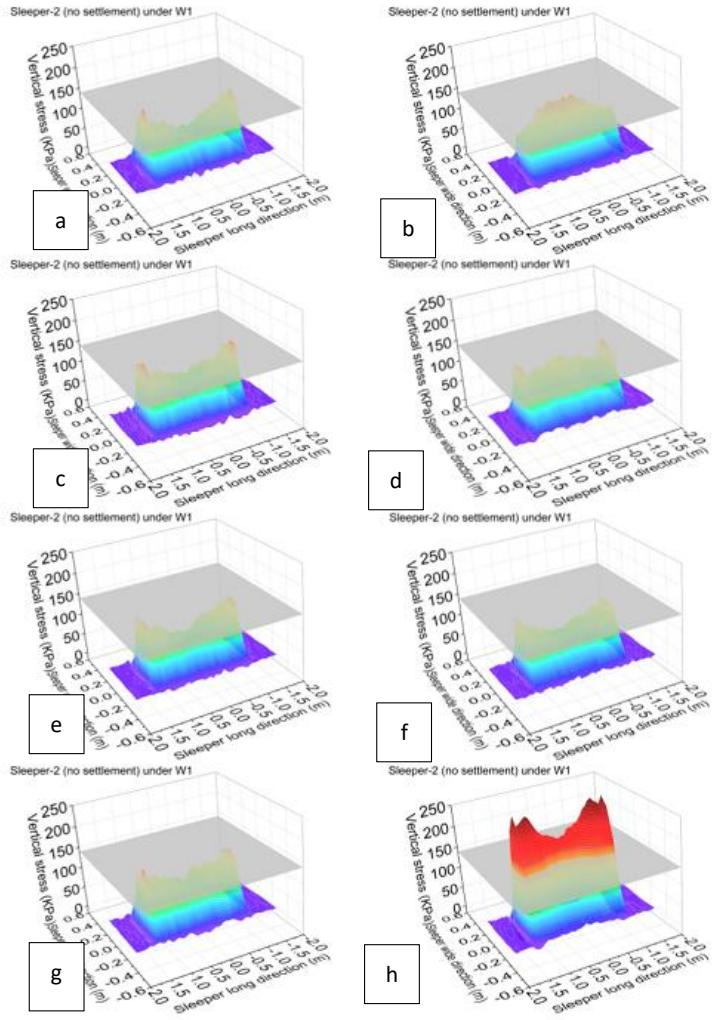

Figure 2.16. Ballast stress distribution under Sleeper-2 due to passing wheelsets: a, c, e, g - without the settlement; b, d, f, h - with the settlement.

Table 2.6. Maximum stress in ballast under Sleeper-2 under four wheelsets

Wheelset No.	1	2	3	4
Max stress, No settlement (KPa)	151.1	147.2	138.9	151.9
Max stress, Settlement (KPa)	143.2	140.2	130.3	259.4

From Figure 2.16a-d, it can be seen that in the no settlement case the ballast stress distribution due to each wheelset is similar, where the stresses are higher at the sleeper ends. However, when the ballast settlement is introduced (see Figure 2.16e-h), the effect of the sleeper motion (due to its bending mode) can be seen in Figure 2.16e, wherein the high stresses in ballast observed in the middle of the sleeper. Also, the ballast stresses due to the 4th wheelset exceed their plastic limit. This will result in permanent deformation of ballast and further contributes to ballast settlement.

These results correlate well with the field observations described in [69] that the large settlement was found at Sleeper-2. Also, these results demonstrate the necessity of the ballast stress analysis when analysing the transition zone behaviour.

4.3 Rail stresses and train accelerations

The rail stress in the transition zones and the acceleration of carbody in both cases with and without settlement are analysed in this section.

As mentioned before, the rail is simulated by beam elements with the length of 75mm (8 elements in a sleeper space). The maximum normal stress of each rail element is obtained and shown in Figure 2.17, where the two cases are also compared. It should be noted that normal stress is mean value of the left and the right rails.

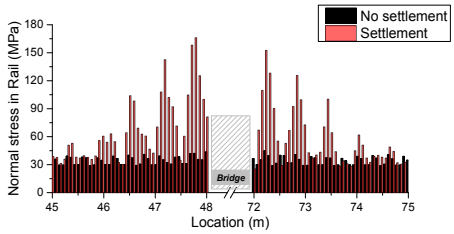

Figure 2.17. Normal stresses in rail, simulations with and without the settlement.

These results confirm the discussion of the ballast stress results from the previous section. The stresses in the rails are extremely higher in the case of settlement, especially near the bridge (i.e. Sleeper-1 and Sleeper+1), where the sleepers are not supported by ballast due to the settlement (see Figure 2.15). When no settlement is introduced, the stresses in the rails are only slightly higher near the bridge.

To analyse the effect of the differential settlement to the passenger's comfort, the vertical accelerations of carbody in the cases with and without settlement are compared and shown in Figure 2.18. A node on the carbody above the front bogie is picked in both cases.

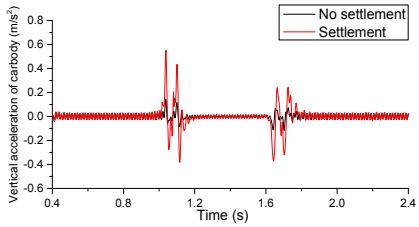

Figure 2.18. Vertical acceleration of the train body, simulations with and without the settlement.

Figure 2.18 shows that the vertical accelerations in both cases are increased in the transition zones. The acceleration in the settlement case is 3 times higher than that in the case without the settlement. Also, the acceleration in the embankment-bridge transition is much higher than that in the bridge-embankment transition. The maximum acceleration ($0.55m/s^2$) in the presence of settlement has already exceeded the maximum permissible acceleration of $0.49m/s^2$ [20]. The increase of the accelerations highly depends on the vehicle velocity and it can be crucial in case of high-speed trains leading to deterioration of the passenger's comfort [72]. The rail stresses and the vehicle acceleration results again have proved the necessity of taking differential settlement into account when analysing the transition zone behaviour.

5 Conclusion

A 3D explicit dynamic finite element model of the track transition zone with differential settlement has been developed. The model uses the contact elements for modelling the connection between sleepers and the ballast, bilinear springs for modelling fastening system and Hertzian spring for modelling wheel-rail contact. It is capable of modelling the transition zones with the differential settlement, a realistic settlement curve of rail and the hanging sleepers. Dynamic responses such as dynamic wheel forces, the hanging distance of sleepers as well as ballast stresses can be obtained. The numerical results obtained by the model are compared with the field measurement results, and a reasonable correlation between them was found, which means that the numerical model is capable of describing the major behaviour of transition zones. Using the model, the transition zones with and without settlement are calculated. Through the analysis of the dynamic behaviour of track components under the train passage, the following conclusions can be drawn.

The results of the simulations have well shown that both differential stiffness and differential settlement result in the increase of the dynamic responses (i.e. wheel force, ballast stress, rail stress and train acceleration), while the increase caused by the settlement is much higher than that generated by the differential stiffness alone. Considering the differential settlement is inevitable after a few months of operation, the differential settlement should be taken into account when analysing and improving the transition zone performance.

The dynamic responses of the embankment-bridge and the bridge-embankment transitions are different. The affected zone in the bridge-embankment transition is longer and the value of the dynamic responses is increased to a smaller extent. On the contrary, the embankment-bridge transition only increases the dynamic responses in a short zone in the embankment close to the bridge but with higher values. As a result, the countermeasures of the two transitions should be considered differently.

When the bogie is half on the bridge and half on the embankment, the wheel force is increased mostly due to the pitch motion of the bogie. The location where the increase occurs is defined by the vehicle dynamics and in particular by the geometrical properties of the bogie.

In the transition zones with the settlement, the ballast closest to the bridge has lower stresses while the stresses in rails above are increased. Also, ballast stress distribution is not only defined by the increased wheel force due to the pitch movement of the vehicle, but also by the spatial movement of the hanging sleepers. Thus, it is necessary to consider both the vehicle movement and sleeper movement in future studies of transition zone degradation.

Reference

1. Li D, Otter D and Carr G. Railway bridge approaches under heavy axle load traffic: problems, causes, and remedies. Proceedings of the Institution of Mechanical Engineers, Part F: Journal of Rail and Rapid Transit. 2010; 224: 383-90.

2. Zuada Coelho B. Dynamics of railway transition zones in soft soils (Doctoral dissertation). 2011.

3. Varandas JN, Hölscher P and Silva MAG. Dynamic behaviour of railway tracks on transitions zones. Computers & Structures. 2011; 89: 1468-79.

4. Hölscher P and Meijers P. Literature study of knowledge and experience of transition zones. Delft: report. 2007.

5. Sasaoka C and Davis D. Long term performance of track transition solutions in revenue service. Technology Digest TD-05-036, Transportation Technology Center. Inc, Association of American Railroads. 2005.

6. Hyslip JP, Li D and McDaniel C. Railway bridge transition case study. Bearing Capacity of Roads, Railways and Airfields 8th International Conference (BCR2A'09). 2009.

7. Gallage C, Dareeju B and Dhanasekar M. State-of-the-art : track degradation at bridge transitions. Proceedings of the 4th International Conference on Structural Engineering and Construction Management 2013. 2013.

8. Paixao A, Fortunato E and Calcada R. Design and construction of backfills for railway track transition zones. Proceedings of the Institution of Mechanical Engineers, Part F: Journal of Rail and Rapid Transit. 2013; 229: 58-70.

9. Stark TD and Wilk ST. Root cause of differential movement at bridge transition zones. Proceedings of the Institution of Mechanical Engineers, Part F: Journal of Rail and Rapid Transit. 2015.

10. Alves Ribeiro C, Paixão A, Fortunato E and Calçada R. Under sleeper pads in transition zones at railway underpasses: numerical modelling and experimental validation. Structure and Infrastructure Engineering. 2014; 11: 1432-49.

11. Coelho B, Hölscher P, Priest J, Powrie W and Barends F. An assessment of transition zone performance. Proceedings of the Institution of Mechanical Engineers, Part F: Journal of Rail and Rapid Transit. 2011; 225: 129-39.

12. Lei X and Zhang B. Influence of track stiffness distribution on vehicle and track interactions in track transition. Proceedings of the Institution of Mechanical Engineers, Part F: Journal of Rail and Rapid Transit. 2010; 224: 592-604.

13. Nicks JE. The bump at the end of the railway bridge (Doctoral dissertation). Texas A&M University, 2009.

14. Read D and Li D. Design of track transitions. TCRP Research Results Digest 79. 2006.

15. Li D and Davis D. Transition of railroad bridge approaches. Journal of Geotechnical and Geoenvironmental Engineering. 2005.

16. Thompson DR and Woodward PK. Track stiffness management using the XiTRACK GeoComposite. Permanent Way Institution Journal and Report of Proceedings. 2004, p. 135-8.

17. Kerr AD and Moroney BE. Track transition problems and remedies. PROC of the American railway engineering association. 1993; 94: 25.

18. (ERRI) ERRI. Bridge ends. Embankment Structure Transition. State of the Art Report. 1999.

19. Selig ET and Waters JM. Track geotechnology and substructure management. Thomas Telford, 1994.

20. Banimahd M, Kennedy J, Medero GM and Woodward PK. Behaviour of train–track interaction in stiffness transitions. Proceedings of the Institution of Civil Engineers-Transport. 2012; 165: 205-14.

21. Dahlberg T. Railway Track Stiffness Variations-Consequences and Countermeasures. International Journal of Civil Engineering. 2010; 8.

22. Hunt H. Settlement of railway track near bridge abutments. Proceedings of the Institution of Civil Engineers-Transport. Thomas Telford-ICE Virtual Library, 1997, p. 68-73.

23. Frohling RD, Scheffel H and EbersÖHn W. The Vertical Dynamic Response of a Rail Vehicle caused by Track Stiffness Variations along the Track. Vehicle System Dynamics. 1996; 25: 175-87.

24. Li Z and Wu T. Vehicle/track impact due to passing the transition between a floating slab and ballasted track. Noise and Vibration Mitigation for Rail Transportation Systems. Springer, 2008, p. 94-100.

25. Namura A and Suzuki T. Evaluation fo countermeasures against differential settlement at track transitions. QR of RTRI. 2007; 48.

26. Lundqvist A, Larsson R and Dahlberg T. Influence of railway track stiffness variations on wheel/rail contact force. Track for High-Speed Railways, Porto, Portugal. 2006.

27. Sato Y. Japanese Studies on Deterioration of Ballasted Track. Vehicle System Dynamics. 1995; 24: 197-208.

28. Indraratna B, Nimbalkar S, Christie D, Rujikiatkamjorn C and Vinod J. Field assessment of the performance of a ballasted rail track with and without geosynthetics. Journal of Geotechnical and Geoenvironmental Engineering. 2010; 136: 907-17.

29. Dahlberg T. Some railroad settlement models—a critical review. Proceedings of the Institution of Mechanical Engineers, Part F: Journal of Rail and Rapid Transit. 2001; 215: 289-300.

30. Gerber U and Fengler W. Setzungsverhalten des Schotters. ETR Eisenbahntechnische Rundschau. 2010; 59: 170-5.

31. Varandas JN, Hölscher P and Silva MAG. A Settlement Model for Ballast at Transition Zones. Proceedings of the Tenth International Conference on Computational Structures Technology. 2010.

32. Lei X and Mao L. Dynamic response analyses of vehicle and track coupled system on track transition of conventional high speed railway. Journal of Sound and Vibration. 2004; 271: 1133-46.

33. Zhai WM and True H. Vehicle-track dynamics on a ramp and on the bridge: simulation and measurement. Vehicle System Dynamics. 1999; 33: 11.

34. Lundqvist A and Dahlberg T. Load impact on railway track due to unsupported sleepers. Proceedings of the Institution of Mechanical Engineers, Part F: Journal of Rail and Rapid Transit. 2005; 219: 67-77.

35. Banimahd M and Woodward PK. 3-Dimensional Finite Element Modelling of Railway Transitions. 9th International Conference on Railway Engineering. 2007.

36. Shahraki M, Warnakulasooriya C and Witt KJ. Numerical study of transition zone between ballasted and ballastless railway track. Transportation Geotechnics. 2015; 3: 58-67.

37. Shi J, Burrow MPN, Chan AH and Wang YJ. Measurements and simulation of the dynamic responses of a bridge-embankment transition zone below a heavy haul railway line. Proceedings of the Institution of Mechanical Engineers, Part F: Journal of Rail and Rapid Transit. 2012; 227: 254-68.

38. Shan Y, Albers B and Savidis SA. Influence of different transition zones on the dynamic response of track–subgrade systems. Computers and Geotechnics. 2012; 48: 21-8.

39. Ribeiro CA. Embankment-structure transitions on high speed railway lines: experimental and numerical analysis. PhD thesis. 2012.

40. Seara I and Correia AG. Performance assesment solutions for transition zones embankment-bridge railways trough numerical simulation 3D. Semana de Engenharia 2010. 2010.

41. Galvín P, Romero A and Domínguez J. Fully three-dimensional analysis of high-speed train–track–soil-structure dynamic interaction. Journal of Sound and Vibration. 2010; 329: 5147-63.

42. Gallego Giner I and López Pita A. Numerical simulation of embankment–structure transition design. Proceedings of the Institution of Mechanical Engineers, Part F: Journal of Rail and Rapid Transit. 2009; 223: 331-43.

43. Cai C, Zhai W, Zhao T, Tian L and Wang Z. Research on dynamic interaction of train and track on roaded-bridge transition section. Journal of Traffic and Transportation Engineering. 2001; 1: 17-9.

44. Sañudo R, Markine V and Dell'Olio L. Optimizing track transitions on high speed lines. IAVSD2011. 2011.

45. Wang H, Markine V and Shevtsov I. Conference presentation in the of The Analysis of Degradation Mechanism in Track Transition Zones using 3D Finite Element Model. Proceedings of the Second International Conference on Railway Technology: Research, Development and Maintenance, J Pombo,(Editor), Civil-Comp Press, Stirlingshire, United Kingdom, paper 227, 2014 doi: 104203/ccp. 2014.

46. H. Wang, V. L. Markine, Shevtsov IY and Dollevoet R. Analysis of the Dynamic Behaviour of a Railway Track in Transition Zones With Differential Settlement. 2015 Joint Rail Conference, San Jose, California, USA, March 2015. 2015, p. 7.

47. Wang H, Markine VL, Dollevoet R and Shevtsov IY. Improvement of train-track interaction in transition zones via reduction of ballast damage. The Dynamics of Vehicles on Roads and Tracks. CRC Press, 2016, p. 1173-84.

48. Hallquist JO. LS-DYNA theory manual. Livermore software Technology corporation. 2006; 3: 25-31.

49. Rezaei E and Dahlberg T. Dynamic behaviour of an in situ partially supported concrete railway sleeper. Proceedings of the Institution of Mechanical Engineers, Part F: Journal of Rail and Rapid Transit. 2011; 225: 501-8.

50. Zhai WM, Wang KY and Lin JH. Modelling and experiment of railway ballast vibrations. Journal of Sound and Vibration. 2004; 270: 673-83.

51. Varandas JN, Holscher P and Silva MA. Settlement of ballasted track under traffic loading: Application to transition zones. Proceedings of the Institution of Mechanical Engineers, Part F: Journal of Rail and Rapid Transit. 2013; 228: 242-59.

52. Iwnick S. Manchester Benchmarks for Rail Vehicle Simulation. Vehicle System Dynamics. 1998; 30: 295-313.

53. Wan C, Markine VL and Shevtsov IY. Improvement of vehicle–turnout interaction by optimising the shape of crossing nose. Vehicle System Dynamics. 2014; 52: 1517-40.

54. Hallquist JO. LS-DYNA Keyword User's Manual. LSTC Co., Livermore, CA, 2007.

55. Esveld C. Modern railway track. MRT-productions Zaltbommel, The Netherlands, 2001.

56. Paixão A, Fortunato E and Calçada R. Transition zones to railway bridges: Track measurements and numerical modelling. Engineering Structures. 2014; 80: 435-43.
57. Grassie S and Cox S. The dynamic response of railway track with unsupported sleepers. Proceedings of the Institution of Mechanical Engineers, Part D: Journal of Automobile Engineering. 1985; 199: 123-36.
58. Olsson E and Zackrisson P. Long-term measurement results, Final report. Banverket, Technical Report, 2002.
59. Augustin S, Gudehus G, Huber G and Schünemann A. Numerical model and laboratory tests on settlement of ballast track. System dynamics and long-term behaviour of railway vehicles, track and subgrade. Springer, 2003, p. 317-36.
60. Kumaran G, Menon D and Krishnan Nair K. Dynamic studies of railtrack sleepers in a track structure system. Journal of Sound and Vibration. 2003; 268: 485-501.
61. ISHIDA M, MOTO T, KONO A and JIN Y. Influence of Loose Sleeper on Track Dynamics and Bending Fatigue of Rail Welds. Quarterly report of RTRI. 1999; 40: 80-5.
62. Nielsen JC and Igeland A. Vertical dynamic interaction between train and track influence of wheel and track imperfections. Journal of Sound and Vibration. 1995; 187: 825-39.
63. Plenge M and Lammering R. The dynamics of railway track and subgrade with respect to deteriorated sleeper support. System dynamics and long-term behaviour of railway vehicles, track and subgrade. Springer, 2003, p. 295-314.
64. Gustavson R and Gylltoft K. Infuence of cracked sleepers on the global track response: Coupling of a linear track model and nonlinear finite element analyses. Proceedings of the Institution of Mechanical Engineers, Part F: Journal of Rail and Rapid Transit. 2002; 216: 41-51.
65. Coelho Z. Dynamics of railway transition zones in soft soils. 2011.
66. Stark TD, Wilk ST and Sussmann TR. Evaluation of tie support at transition zones. Transportation Research Record: Journal of the Transportation Research Board. 2015: 53-8.
67. Grabe PJ, Clayton CRI and Shaw FJ. Deformation measurement on a heavy haul track formation. In: Janeiro Rd, (ed.). Proc, of the 8th Int Heavy Haul Conf. Brazil: International Heavy Haul Association, 2005, p. 287–95.
68. Yang LA, Powrie W and Priest J. Dynamic Stress Analysis of a Ballasted Railway Track Bed during Train Passage. J Geotech Geoenviron Eng. 2009; 135: 680.
69. Markine V, Wang H and Shevtsov I. Experimental Analysis of the Dynamic Behaviour of a Railway Track in Transition Zones. Proceedings of the Ninth International Conference on Engineering Computational Technology, P Iványi and BHV Topping, (Editors), Civil-Comp Press, Stirlingshire, United Kingdom, paper 3, 2014. 2014.
70. Wang H, Markine V and Shevtsov I. The Analysis of Degradation Mechanism in Track Transition Zones using 3D Finite Element Model. Proceedings of the Second International Conference on Railway Technology: Research, Development and Maintenance, J Pombo,(Editor), Civil-Comp Press, Stirlingshire, United Kingdom, paper 227, 2014 doi: 104203/ccp. 2014.
71. Sato Y. Optimization of track maintenance work on ballasted track. Proceedings of the World Congress on Railway Research. 1997, p. 405-11.
72. Li MXD and Berggren EG. A study of the effect of global track stiffness and its variations on track performance: simulation and measurement. Proceedings of the Institution of Mechanical Engineers, Part F: Journal of Rail and Rapid Transit. 2010; 224: 375-82.

Paper III

Modelling of the long-term behaviour of transition zones: Prediction of track settlement

Haoyu Wang, Valeri Markine[1]

[1]Delft University of Technology, Delft, the Netherlands

Published by Engineering Structures, 156, (2018), pp.294-304.

Abstract

Transition zones in railway tracks are the locations with considerable changes in the vertical support structures. Typically, they are located near engineering structures, such as bridges, culverts, tunnels and level crossings. In such locations, the variation of the vertical stiffness and the differential settlement of the track (when the foundation settles unevenly) result in amplification of the dynamic forces acting on the track. This amplification contributes to the degradation process of ballast and subgrade, ultimately resulting in the deterioration of vertical track geometry (settlement).

To analyse and predict the accumulated settlement of the track in transition zones, a methodology using the iterative procedure is proposed. The methodology includes the finite element simulations of the vehicle-track and sleeper-ballast interaction during a train passing a transition zone; and iterative calculations of accumulated track settlement, based on an empirical model for ballast settlement.

The simulations are performed using a 3-D dynamic finite element model (explicit integration) of a track transition zone, which accounts for the differential stiffness and the differential settlement of the track. Also, nonlinear contact elements between sleepers and ballast are used. As a result, the model can perform the detailed analysis of the stresses in ballast and accounts for the effects of vehicle dynamics. The model was validated against field measurements. The empirical settlement model describes the two-stage settlement of ballast and the nonlinear relationship between ballast stresses and permanent settlement.

The proposed methodology is demonstrated by calculating the track settlement in the transition zone for 60,000 loading cycles (3.5 MGT). The dynamic responses such as ballast stresses are analysed to study the effect of the settlement. The parametric study of the iteration step used in the accumulated settlement procedure has been performed, based on which the optimal step is suggested.

Keywords

Railway track modelling, Transition zone, Empirical settlement model, Settlement prediction.

1 Introduction

Transition zones in railway tracks are locations with considerable changes of the vertical support structures. Typically, they are located near engineering structures, such as bridges, culverts, tunnels, and level crossings. In such locations, the variation of the vertical stiffness and the differential settlement of the track (when the foundation settles unevenly) result in amplification of the dynamic forces acting on the track. This amplification contributes to the degradation process of ballast and subgrade, ultimately resulting in the deterioration of the vertical track geometry (settlement), which typically manifests itself in a 'dip' in the vertical geometry profile of the track. An example of a track deflection profile obtained by the measurement train in a transition zone is shown in Figure 3.1. Figure 3.1 shows the signature of the track deformation under the passage of Eurailscout UFM120 [1]. This deformation signature was derived from the measured acceleration signature using a double integration method. Figure 3.1 identifies the embankment and bridge lengths.

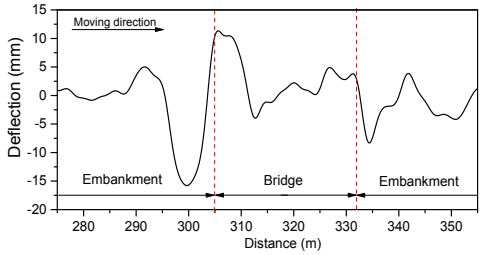

Figure 3.1: Measured track deflection profile in a track transition zone in the Netherlands by EurailScout.

The track profile in Figure 3.1 shows that two significant deflections appear before and after the bridge, indicating that the track suffers from extra settlements. Such dips are often reported in the literature [2-6]. According to a survey of nine railway companies in the US, approximately half of all railway bridges were affected by dips [7]. Such a significant irregularity in the track geometry may trigger considerable wheel-rail interaction forces, which may result in extensive damage to track components, affect passenger's comfort, and lead to even larger permanent settlements. Ultimately, it may raise the need for additional maintenance and hence increase the life cycle costs of tracks. For example, the maintenance activities on the track in transition zones are performed 4-8 times more often than that on the open tracks in the Netherlands [8, 9].

The dynamic behaviour of transition zones including level crossings has already been studied, in [2, 6, 10-32]. In these studies, the short-term behaviour (i.e. behaviour due to a single passage of a train) of track in transition zones was analysed. However, in an exhaustive review of transition zones [32], Sañudo et al. indicated that the studies on the long-term behaviour of the track in transition zones are somewhat lacking. Except in [10, 33], the settlement in transitions was predicted using 2D beam-spring track models combining with empirical models.

This paper presents a methodology to predict the accumulated settlement of the track in transition zones. The methodology combines a 3D FE (finite element) model of the transition zone and an empirical model for ballast settlement. The FE model has several novel features to thoroughly consider the nonlinearity of the sleeper-ballast contact (surface to surface contact [34], further explained in Section 3.1) as compared to the existing models. In addition, an iterative

procedure is used to predict the settlement in transition zones, wherein the transition zone model is coupled with the ballast settlement model based on the relationship between ballast stress and settlement [35]. In addition, the parametric study of the prediction procedure is performed.

In comparison to the existing methodologies, the proposed methodology can predict more precisely the settlement of transition zones, albeit the process would be computationally more expensive. The highlights of the methodology are as following:

- Behaviour of hanging sleepers in transition zones is more accurately described, since contact elements are used to model the interface between sleepers and ballast;
- More realistic settlement curve of rails and the hanging distance of sleepers can be obtained, using pre-loading step in the explicit FE analysis;
- The stresses in ballast and the effects of vehicle dynamics can be calculated;
- The nonlinear relationship between ballast stresses and settlement is considered in the settlement model.

The methodology provides a basis to study the growth of ballast settlement and the geometry degradation of tracks in transition zones. Also, the dynamic responses due to the ballast degradation can be analysed. The methodology can also be used for the comparative analysis of various transition designs. The methodology was originally presented in [36]. The main parts of the procedure are:

(I) simulation of the vehicle-track and sleeper-ballast interaction during a train passing the transition zone, using the 3-D FE transition zone model, to obtain the stresses in the ballast;

(II) calculation of the track settlement for a given number of loading cycles based on the ballast stresses, using the empirical settlement model;

(III) adjusting the FE transition zone model based on the calculated settlement under each sleeper for the step (I) in the next iteration.

The paper is organised as follows. The studies on track settlement are reviewed in Section 2. The FE transition zone model, the empirical settlement model of ballast track, and the integration of models are described in Section 3. In Section 4, the iteration scheme is demonstrated by calculating the track settlement in the transition zone for 60,000 loading cycles, or 3.5 MGT (Million Gross Tonnes). Also, the dynamic responses such as the ballast stress at 0 and 60,000 cycles (3.5 MGT) are compared to study the effect of settlement. In addition, the parametric study of the iteration step is performed. Finally, conclusions are drawn in Section 5.

2 Theory of settlement in transition zones

In [3], the average track settlements on open tracks, approaching zones and bridges were measured on several transition zones, as shown in Figure 3.2. The settlement is accumulated within one maintenance interval, which was 80 MGT of traffic. This figure shows that the settlement on the open track is higher than that on the bridge, and the settlement on the approaching zone is higher than that on the open track. It should be noted that the tracks on bridges in this study are ballast track; therefore the settlement of tracks on bridges is not zero. These findings in Figure 3.2 are in agreement with the deflection of the track shown in Figure 3.2.

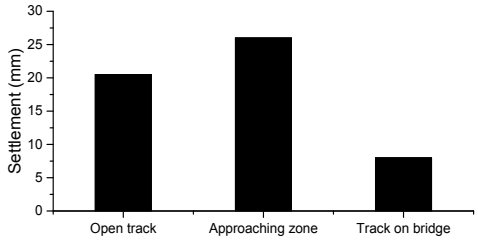

Figure 3.2: Comparison of the settlement in different locations of the transition zones, plotted according to [3].

The high settlement appearing in transition zones usually results from the following three aspects:

(I) the differential settlement between ballast tracks and engineering structures, which can also be considered as the geometrical irregularity, playing a major role in the degradation process of transition zones [4, 18, 19, 37-39];

(II) the significant abrupt change in the vertical stiffness of tracks;

(III) geotechnical, construction and maintenance issues [3, 7].

PII-III

Note that both factor (I) and (II) lead to the increase of wheel loads, which in turn increases track settlement [2, 10]. The higher settlement of ballast tracks as compared to that of engineering structures is mainly due to the breakage and pulverisation of ballast, compaction of ballast and soil layer, and soil-water response [40]. After construction or tamping of open tracks, the permanent settlement of ballast can be divided into two stages, according to the deformation mechanism of ballast [41-44], as schematically shown (the solid line) in Figure 3.3. Stage 1 is the rapid compaction and abrasion process that happens within 3 to 6 months [41, 42] In this stage, the main deformation mechanism is the volumetric compaction of particles. Stage 2 is the normal settlement process happening until the end of a maintenance interval, wherein the main deformation mechanism is the frictional sliding of particles [41, 45-48]. The settlement growth for open tracks is nonlinear in stage 1, while that is almost linear in Stage 2 [41, 43].

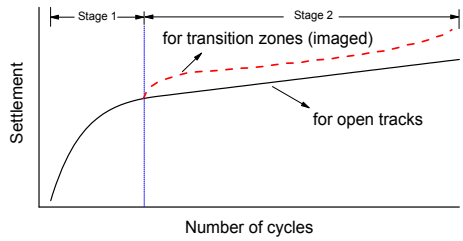

Figure 3.3: Schematic settlement curve of ballast as a function of loading cycles. Solid line: settlement in open tracks; dash line: the imaged settlement in transition zones.

Since the tracks on engineering structures are settled much less as compared to (open) ballast tracks, differential settlement can be generated. According to the numerical simulations presented in [37, 39], the dynamic responses such as wheel-rail interaction forces, sleeper accelerations, ballast stresses, and rail stresses are increased due to the presence of differential settlement. For example, the introduction of 2mm differential settlement triggers 100% growth of the interaction

force as compared to the perfect geometry [39]. Due to the differential settlements, the ballast in transition zones degrades at a higher rate, as the schematic curve (the dashed line) shown in Figure 3.3. The track degradation eventually generates dips. It should be noted that the settlement curve of the ballast in transition zones is the purpose of this study.

The degradation process of track transition zones is schematically shown in Figure 3.4. The effect of the stiffness variation between the embankment and the engineering structure is ignored in this figure, since its contribution is relatively small [37, 39]

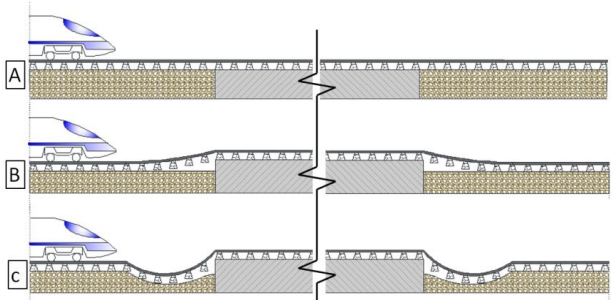

Figure 3.4: The process of degradation of transition zones.

Figure 3.4a shows the track with the perfect geometry before operation (right after construction). After few months of operation, the ballast track settles with a uniform value, which creates the void under sleepers near the bridge (hanging sleepers), shown in Figure 3.4b. Here assuming the settlement of the engineering structure is negligible. Dips appear on both transition zones (approaching and exiting regions of the bridge) and it is remarkable that the geometries of the dips on two sides differ due to the difference in the track–vehicle dynamic interaction in these local zones.

To predict the settlement of tracks in the long term, it is common to combine the numerical vehicle-track interaction models and the empirical settlement models [49]. The dynamic responses calculated by numerical models are used as input to empirical settlement models to predict the settlement after a number of loading cycles. The empirical settlement models are mainly obtained using measurements, considering various factors including number of cycles, tonnage, ballast property, soil contamination, sleeper pressure, ballast acceleration, sleeper type, load history, the velocity of load, the variation of load (i.e. if they do not have the same amplitude), and the frequency of load [33, 50, 51]. An exhaustive review of the empirical settlement models for open tracks can be found in [43]. The empirical settlement model of ballast proposed by Sato [35] is commonly used, e.g. in [48, 49].

By using the models for calculation of the settlement separately under each sleeper, the track settlement of special structures can be predicted. In [49], Li et al. used the combination of the software GENSYS, NASTRAN (an FE software) and an empirical settlement model to predict the settlement in turnout zones. In [52], Fröhling combined a dynamic vehicle-track model with an empirical settlement model to predict the settlement due to vertical irregularities and variation of track stiffness in a section of ballast track. In [53], Suzuki et al. used the combination of a dynamic vehicle-track model (beam, mass and spring system) and an empirical settlement model to predict the settlement at rail joints. In [48], Iwnicki et al. used a combination of the simulation software MEDYNA and ADAMS/Rail (a multibody software) and empirical settlement models to predict the

settlement of open tracks. In [54], Holtzendorff and Gerstberger employed a similar method to predict the settlement of the open tracks with the quasi-periodic void pattern.

In this study, the developed FE model of transition zones using LS-Dyna and the empirical settlement model are combined to predict the long-term track behaviour in transition zones. The transition zone consists of two ballast tracks and a short bridge, which is widely used in the Netherlands. Because the initial settlement stage of rapid compaction (Stage 1 in Figure 3.3) of ballast track is relatively short and mainly determined by the compaction of the ballast bed, it is considered as a given value. The methodology predicts the settlement in the second stage (Stage 2 in Figure 3.3). It should be noted that only the settlement of ballast is considered since ballast contributes the most to the settlement of tracks [6, 42] and the computation power is limited at the current stage.

3 Methodology for settlement prediction

In this section, the methodology for the prediction of the track settlement in transition zones is presented. The methodology combines the FE model of transition zones and a settlement model of ballast. The transition zone model is briefly described below.

3.1 Finite element model of transition zones

The FE model of transition zones consists of two ballast tracks and one track on the bridge in the middle, which is modelled according to a widely used transition zone in the Netherlands, as shown in Figure 3.5. The railway vehicle moves from one ballast track to the other, passing the bridge. Thus, using this model, it is possible to compare the two travel directions of trains, which are named as embankment-bridge and bridge-embankment in the paper.

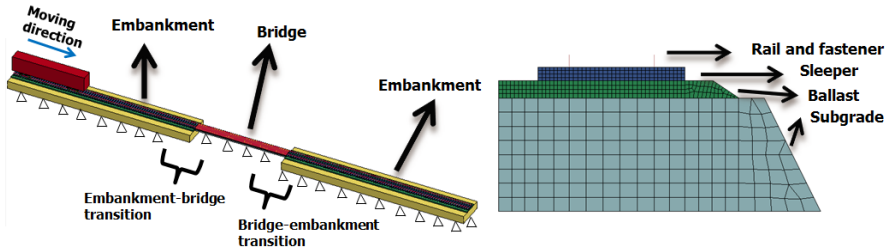

Figure 3.5: FE model of track transition zones.

The length of ballast track is 48m (on both sides of the bridge), and the bridge is 24m. Therefore the total length of the model is 120m (48+24+48=120). The components of the ballast tracks are rails, fasteners, sleepers, ballast and subgrade. The rails are modelled by Hughes-Liu beam elements with 2*2 Gauss quadrature integration [34], whereas the cross-sectional and mass properties of the UIC54 rail are used. The spring and damper elements between rails and sleepers are used to model fasteners. In the vertical direction, these springs have bilinear properties. Thereby, in compression they have the stiffness of rail pads; and in tension the stiffness is much higher to simulate the clamping effect of the fasteners. The tension stiffness is assumed as 1000 times of the compression stiffness. Ballast, sleepers and subgrade are modelled using the fully integrated solid elements with elastic material properties. The thickness of ballast and subgrade is 0.3m and 2m, respectively. The material properties of the elements used in the model are collected in Table 3.1 and Table 3.2.

Table 3.1: Material properties of solid elements.

	Elastic Modulus (MPa)	Poisson ratio
Sleeper	3650	0.167
ballast	120	0.250
Subgrade	180	0.250
Concrete bridge slab	3500	0.167

Table 3.2: Material properties of fasteners.

	Horizontal	Vertical	Longitudinal
Stiffness (KN/mm)	1.5	120 (compression) 120 000 (tension)	1.5
Damping (N·s/m)	5000	5000	5000

The vehicle is a passenger train, which is idealized as a multibody system. It consists of a car body, two bogies and four wheelsets connected by the primary and secondary suspensions, which are modelled using rigid bodies and spring-damper elements. The velocity of the train is 200km/h. The configurations and the parameters of the train are shown in Table 3.3.

Table 3.3: Vehicle parameters.

Parameter	Value	Parameter	Value
Axle load (kN)	142	Primary suspension stiffness (N/m)	8.80e5
Distance between wheels (m)	2.2	Primary suspension damping (N*s/m)	6.00e4
Distance between axles (m)	12.6	Secondary suspension stiffness (N/m)	3.00e5
Length of train body (m)	19.0	Secondary suspension damping (N*s/m)	6.00e4
		Secondary suspension Bending stiffness (Nm/rad)	1.7e3

PII-III

Due to the large size of the model, the wheel-rail contact is simplified as the contact between a node and beam, wherein the linear the Hertzian spring is applied.

The contact stiffness is calculated as Equation (1) [1].

$$k_H = \sqrt[3]{\frac{3E^2Q\sqrt{R_{wheel}R_{railprof}}}{2(1-v^2)^2}}, \quad (1)$$

where: E is the modulus of elasticity of the wheel and rail; v is the Poisson's ratio; Q is the static vertical wheel load; $\mathrm{R_{wheel}}$ is the radius of the wheel; $\mathrm{R_{railprof}}$ is the radius of the railhead [1].

The non-reflecting boundaries [55] are applied on both ends of the model to reduce the wave reflection. The bottom of the embankments (subgrade layer) and the bridge (concrete layer) are fixed.

The nonlinear connection between sleepers and ballast is crucial to model the degradation mechanism of ballast [20, 33]. In the real cases, sleepers generate a nonlinear interaction force to ballast under compression, and no force exists when they are hung [33] since sleepers and ballast are separable. Therefore, contact elements are applied between sleepers and ballast. According to the penalty algorithm employed in the contact elements, the search for penetrations between the bottom surface of sleepers and the top surface of ballast is made every time step during the calculation. When the penetration has been detected, a force proportional to the penetration depth is applied to resist and ultimately eliminate the penetration [34]. This method allows simulating the impact on ballast, which is proportional to the downward acceleration of sleepers.

This model inherently assumes that the stage 1 settlement has already completed and hence is mainly concerned with the stage 2 part of the transition zone settlement. It should be noted that the value of the initial settlement is important, but difficult to measure precisely in the real cases. For instance, the void under sleepers measured in [56] had an error of 3mm. The value of the

differential settlement used in the paper is selected from the values which were frequently reported in the field measurements in the transition zones [8, 9], ranged from 2mm to 10mm. The settlement in Stage 1 depends on axle loads and ballast condition. Higher axle loads and worse ballast condition lead to a higher settlement in Stage 1.In this study, 2mm is used since it can model the transition zone in good condition with a low axle load (14.5t). As a result, the predicted settlement is expected to be low. For higher values of the settlement in Stage 1, the prediction results should be higher. It is also remarkable to note that the model should be tuned according to field measurements before practical usage.

For convenience, the sleepers are numbered starting from the one closest to the bridge. They have the positive sign on the bridge-embankment transition and the negative sign on the embankment-bridge transition depending on the moving direction of the passing train. For example, the train passes Sleeper-10 to Sleeper-1 when it approaches the bridge, and later the train passes Sleeper+1 to Sleeper+10 when it leaves the bridge. Since the sleeper space is 0.6m, the distance from the bridge to each sleeper can be easily calculated. Note that there are no sleepers on the bridge.

At the equilibrium state of the model, due to the separable contact between sleepers and ballast, as well as the application of gravity and the resistance of rails, the voids between sleepers and ballast appear in the vicinity of the bridge, as shown in Figure 3.6.

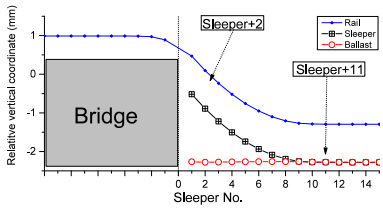

Figure 3.6: Vertical coordinates of rail, sleepers and ballast due to 2 mm settlement of ballast.

As shown in Figure 3.6, the first 10 sleepers close to the bridge are hung as a result of the initial settlement. After the Sleeper+11, the sleepers are fully supported by the ballast. Meanwhile, the hanging distance of Sleeper+1 is the highest, and the hanging distance gradually reduces as the distance from the bridge increases. From this figure, it can clearly be seen that the deflection line of the rail near the bridge is not linear. The hanging values of sleepers are presented as the difference between the vertical coordinates of sleepers and ballast. The same situation is observed on the other side of the bridge (in the embankment-bridge transition).

In the second phase of the simulation, the vehicle moves over the transition zone. Figure 3.7 shows the time history of the vertical coordinates of two sleepers and the corresponding ballast elements, which are located close and far from the bridge (Sleeper+2 and Sleeper+11).

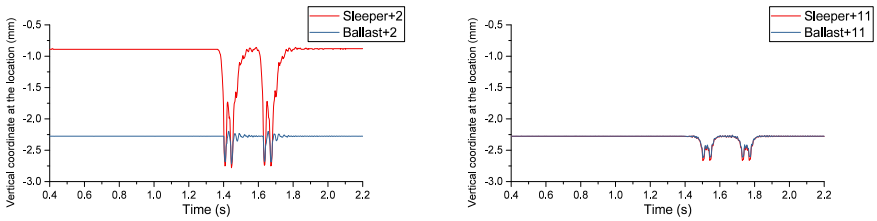

Figure 3.7: Time history of vertical coordinate due to the passing vehicle: sleeper +2 (left) and +11 (right).

As indicated in Figure 3.7, Sleeper+2 are hung before the train comes (1.6s). When the train moves above the sleeper during 1.6s to 2.4s, Sleeper+2 is pushed down and touches ballast, which also generates the displacements of ballast. After 2.4s, Sleeper+2 returns to its original hanging state, while Sleeper+11 is constantly rested on ballast. The significant distinction of the dynamic displacements of sleepers is a result of the differential settlement in the transition zone and may lead to the increase of wheel-rail contact forces and the increase of the stresses in ballast.

When sleepers contact ballast, the penetrations between the bottom surface of sleepers and the top surface of ballast occur. The stress distribution in ballast can be therefore calculated. Because the voids under sleepers are different depending on the locations (Figure 3.6), the stresses in the ballast elements under different sleepers also vary according to their locations (sleeper locations). An example of the stress distribution in ballast under Sleeper+2 corresponding to the four wheelsets is shown in Figure 3.8. The ballast elements under Sleeper+2 are considered as a group (unit), and the vertical stresses of the elements in the top later are collected as shown in Figure 3.8a. The time history of the average stress under Sleeper+2 is shown in Figure 3.8b, wherein the four peaks corresponding to the impacts of the four wheelsets during the train passage can be found. The closer two peaks belong to the two wheelsets of one bogie. The corresponding stress distributions at the four peaks are shown in Figure 3.8c to Figure 3.8f.

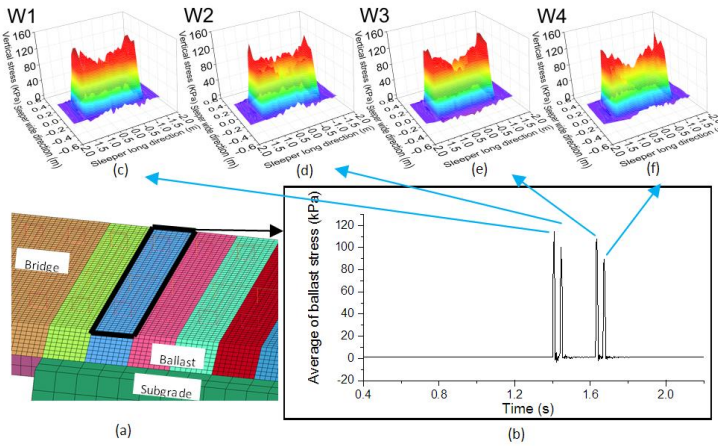

Figure 3.8: Stress distribution in ballast under Sleeper+2 from FE model.

As indicated in Figure 3.8, both the distribution and the average of the ballast stresses are different. The ballast stress generated by the second wheelset is higher than the stresses by other wheelsets. The obtained stresses can be used as the input to the settlement model, which is described in the next section. It should be noted that the FE model described above has been validated against the field measurements presented in [57, 58]. The comparison between the simulated rail displacements and the measured rail displacements in a transition zone is shown in Figure 3.9. The rail displacements were measured at multiple points in the transition zone during trains passing using a DIC-based device. The parameters of the model used in the simulation were adjusted according to the transition zone. More details of the validation can be found in [57, 58].

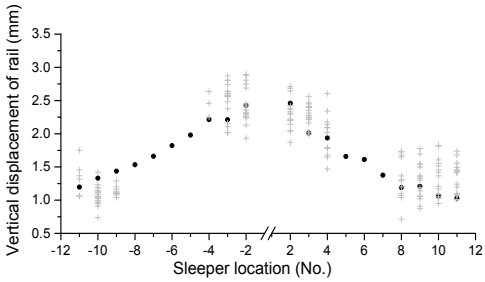

Figure 3.9: Comparison between measurements and simulation: black dots - simulation and cross - measurement results, from [57, 58].

3.2 Empirical settlement model

In this section, the empirical settlement model for ballast used in the methodology is introduced. The total settlement of the ballast at location i can be calculated as:

$$S_i = S_{Ii} + S_{IIi}\,, \tag{2}$$

where S_i is the total settlement of the ballast at location i; S_{Ii} and S_{IIi} are the settlement of the ballast generated at location i in Stage 1 and Stage 2, respectively.

S_I is assumed to be 2mm as mentioned earlier, while S_{IIi} is a linear function of loading cycles, which can be written:

$$S_{IIi} = k_i \times N, \tag{3}$$

where k_i is the settlement rate at location i and N is the number of loading cycles.

The settlement rate k_i can be calculated by the widely used empirical settlement model for (open) ballast tracks, which describes the relationship between the settlement growth and the sleeper-ballast contact pressure. The empirical settlement model was initially proposed in [35] and later developed in [43]. According to this model, the key parameter influencing ballast settlement is the contact pressure between sleepers and ballast, which has been confirmed by the repeated loading experiments on sleepers. Similar conclusion can also be found in [20, 59, 60]. According to the settlement model in [35], the settlement growth is proportional to the sleeper-ballast pressure:

$$k_i = a{p_i}^n, \tag{4}$$

where $\mathrm{p_i}$ is the sleeper-ballast pressure (Pa) at location i; a and n are fitting coefficients.

A non-linear fit according to Equation (4) based on experimental data was first provided in [35], wherein:

$$k_i = 1.839 \times 10^{-13} {P_i}^4, \tag{5}$$

where $\mathrm{P_i}$ is the contact force between the sleeper and the ballast at location i. Later, a better fit was provided in [43], wherein it was found that the power $\mathrm{n} = 5.276$ gives the best fit to the measured data, which reads:

$$k_i = 4.365 \times 10^{-12} \times {P_i}^{5.276}, \tag{6}$$

The two fitting curves are compared with the measurement data provided in [35], as shown in Figure 3.10.

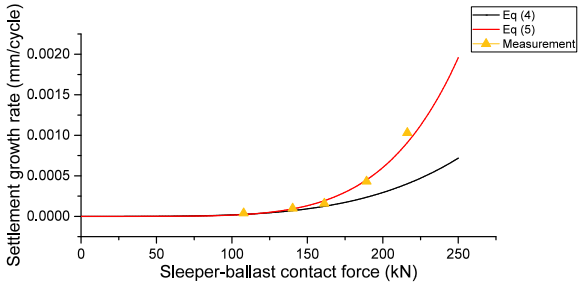

Figure 3.10: Two fitting curves compared from [35] and [43] with measurement data in [35].

As it can be seen from Figure 3.10, the curve provided in [43] fits better to the measurement data and it is therefore adopted in this study. Considering the contact area of the sleeper $\mathrm{A_{sleeper}}$ is 0.68 m2 (the nominal sleeper length 2570mm time the nominal sleeper width 265mm, as used in [49]), Equation (6) can be re-written as:

$$k_i = 4.365 \times 10^{-12} \times (0.68 \times p_i)^{5.276}, \quad (7)$$

The settlement rate $\mathrm{k_i}$ in Equation (7) is shown in Figure 3.10.

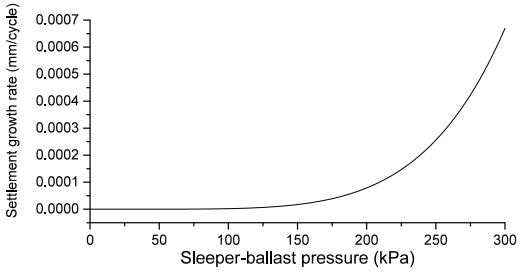

Figure 3.11: Relationship between the settlement growth and the sleeper-ballast pressure.

It can be seen from Equation (7) and Figure 3.11 that the settlement growth increases exponentially as the sleeper-ballast pressure increases. The loading at the lower level corresponds to the elastic behaviour of ballast, and therefore no settlement will occur. The settlement of the ballast grows in an elastic way until the sleeper-ballast pressure reaches around 135kPa. After that, there is a non-linear region where the settlement growth strongly depends on the sleeper–ballast pressure [43].

Using Equation (7) and assuming that the initial settlement $S_{Ii} = 2mm$, Equation (2) can be therefore rewritten as follows:

$$S_i = 2 + 4.365 \times 10^{-12} \times (0.68 \times p_i)^{5.276} \times N, \text{(in mm)} \quad (8)$$

As indicated in Equation (8), the settlement of ballast S_i is a linear function of the loading cycle N, as p_i remains constant; and S_i is an exponential function of the sleeper–ballast pressure p_i, as N remains constant. Because the sleeper-ballast contact pressure varies to a large extent along the track in transition zones, the settlement at the different locations of transition zones will be different.

As mentioned previously, the ballast stresses at the location of each sleeper in transition zones can be calculated using the FE transition model. The sleeper-ballast pressure p_i is obtained from the FE model, which is equal to the average vertical stress in the ballast under the i-th sleeper as

described in Section 3.1. Using the average vertical stress in the ballast as the input to Equation (8) instead of the sleeper–ballast pressure, the settlement after a certain loading cycle N can be obtained.

3.3 Integration of models

In this section, the iterative procedure for the prediction of the ballast settlement in transition zones is presented. The schematic diagram is shown in Figure 3.12. The prediction begins at Stage 2 of the settlement when the ballast track is settled uniformly with $S_{Ii} = 2mm$ (Figure 3.4(b)) after short time of operation due to the rapid compaction of ballast. The ballast stresses under each sleeper can be calculated using the FE model of transition zones, as it was described in Section 3.1. Then, using the ballast stresses as an input to the settlement model, the settlement under each sleeper after N loading cycles can be calculated according to Equation (8). Using these settlement values, the transition zone model can be updated, and the process will be iteratively repeated for the next N loading cycles. It should be noted that the ballast stiffness is assumed unchanged in the settling process.

Since the transition zone model is nonlinear by considering the sleeper-ballast contact, the settlement prediction after several iterations at location i is nonlinear. Therefore the prediction is affected by the iteration step N. The $N = 10{,}000\ cycles$ is adopted (in Section 4.1) to demonstrate the procedure, following [49]. Other values of the iteration step such as 5,000 cycles, 20,000 cycles, 30,000 cycles, and 60,000 cycles are also considered. The effect of the iteration step is discussed in Section 4.3.

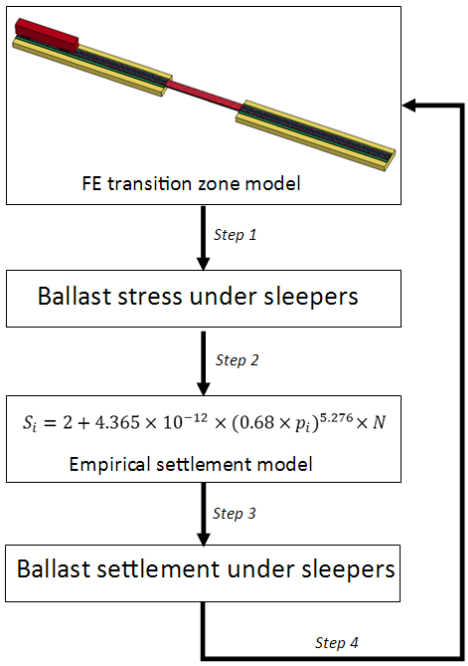

Figure 3.12: Iterative procedure to predict the settlement in track transition zones.

4 Numerical results

In this section, The iteration scheme is demonstrated by calculating the track settlement in the transition zone due to 60,000 loading cycles (3.5 MGT), when the transition zone is exposed to

passenger trains. The dynamic responses such as the ballast stresses at 0 and 60,000 cycles (3.5 MGT) are compared to study the effect of the settlement. The parametric study of the iteration step has been performed as well.

4.1 Numerical example

As mentioned earlier, the vertical stress in ballast at different locations along the track can be calculated using the FE model (see Figure 3.8). Since the permanent settlement of ballast is determined by the maximal stress in ballast [35, 61, 62], the maximum of the average ballast stress in the transition zone are collected, as shown in Figure 3.13.

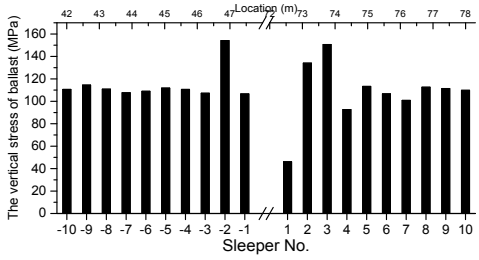

Figure 3.13: Ballast stress in the transition zone.

PII-III

It can be seen from Figure 3.13 that the ballast closer to the bridge (under Sleeper-2, Sleeper +2 and Sleeper +3) suffers from higher stresses than the ballast in other locations. For example, the ballast stress under Sleeper -2 is almost 40% higher than that in other locations. The increase of the ballast stress is caused by the differential stiffness and settlement as well as the pitch motion of the vehicle [39].

Also, from Figure 3.13 it can be seen that the ballast stress in the embankment-bridge transition is different from that in the bridge-embankment transition. In the embankment-bridge transition the stress in ballast is relatively stable except Sleeper-2. In contrast, in the bridge-embankment transition, the stress in ballast fluctuates significantly. The wheels first drop off the bridge and impact on the ballast track (Sleeper+3); then, the wheels bounce over (Sleeper+4) and impact again on the ballast track (Sleeper+5) [39]. This “dropping” phenomenon is consistent with the theoretical analysis in [2].

Using the Equation (8) and the calculated ballast stress, the settlement of the transition zone after the first 10,000 cycles (corresponding to 2,000 train passages, assuming a train consisting of 5 vehicles) can be calculated, as shown in Figure 3.14.

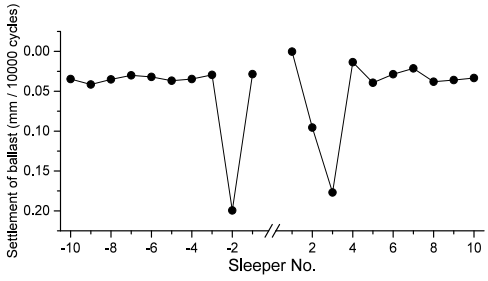

Figure 3.14: Prediction of the ballast settlement using the empirical settlement model.

It can be seen from Figure 3.14 that the settlement appears on both sides of the bridge, which may lead to two large deflections (dips) on each side of the bridge. For example, the ballast settlement under Sleeper-2 is 6 times higher than that in other locations in Figure 3.14, which explains the appearance of the extra settlement close to the bridge observed in [3, 6, 46]. It confirms the theory that the initial differential settlement caused by the rapid compaction of ballast (with different stiffness) leads to a geometry irregularity in transition zones.

By adding the calculated settlement values to the FE transition model, the ballast stresses under the new settlement condition can be calculated. After that, the settlement model can be used again to calculate the additional settlement based on the newly obtained stresses. Using this iterative procedure, the ballast settlement till 60,000 cycles (3.5 MGT) is predicted, as shown in Figure 3.15. Note that the iteration step N is 10,000 cycles and in total 6 iterations are performed.

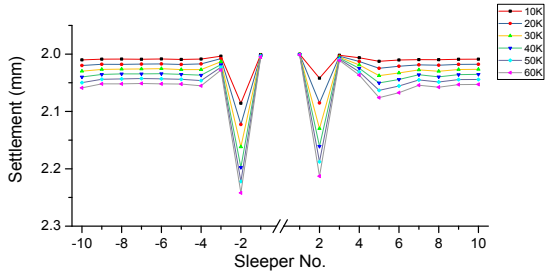

Figure 3.15: Prediction of track settlement in transition zone till 60,000 cycles (3.5 MGT).

Figure 3.15 clearly shows that the two dips continuously grow during the operation, which confirms the observation that once the dips appear, they keep growing instead of being self-healing. Hanging sleepers are expected in such locations.

It can also be found that the settlement in the embankment-bridge transition and the bridge-embankment transition is different. The ballast at Sleeper+5 settles with higher speed. This is also caused by the vibration of the vehicle, as discussed before. If the iterative calculation of the track settlement continues, the settlement at Sleeper+5 may exceed that at Sleeper+2.

It should be noted that the accumulated settlement is 0.24mm in the simulation, which is smaller than the settlement values often observed in the field. The reasons are that a high settlement is most probably caused by freight trains with higher axle loads, various axle loads in mixed traffic lines [63], and poor ballast condition. The model presented in the paper referred to a passenger train and good ballast condition (low settlement value in Stage 1 and “good” material property). In addition, the passage amount 60,000 (3.5 MGT) are relatively low.

The methodology for the settlement prediction in transition zones presented in this study can rather be used:

- for comparative analysis of various transition designs,
- for the qualitative study of the related phenomena (e.g. settlement shape in transition zones with different train moving directions),
- for the study of influential parameters (e.g. iteration step).

For these purposes, 60,000 cycles are sufficient, i.e. the trend can already be seen after that amount of cycles (the results for 100,000 cycles can be seen in Figure. 3.17). In addition, the calculations are very time-consuming since the model is in a large (120m) scale and the model considers the wheel-rail interaction and the sleeper-ballast interaction.

An example of the results using higher axle loads and higher passage amount can be found in [58]. It should be noted that the absolute value obtained using this methodology needs to be verified on the basis of measurement data, which is beyond the scope of this paper. Also, the settlement considered here does not include the subgrade settlement.

To have a better understanding of the trend of settlement and the settlement growth at different locations, the settlement at close locations (Sleeper-2 and Sleeper+2) are compared with the settlement at distant locations (Sleeper-8 and Sleeper+8) in Figure 3.16, as well as their growth.

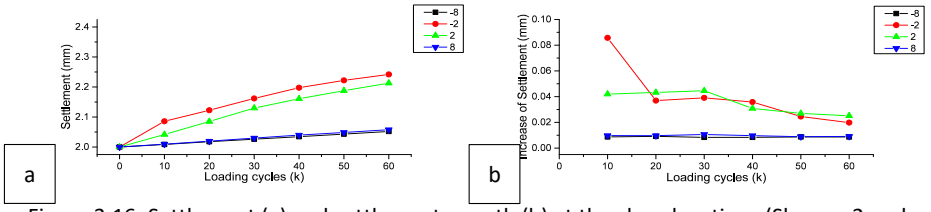

Figure 3.16: Settlement (a) and settlement growth (b) at the close locations (Sleeper-2 and Sleeper+2) and the distant locations (Sleeper-8 and Sleeper+8).

Figure 3.16 shows that the settlement growth of the ballast closer to the bridge (Sleeper-2 and Sleeper+2) is much higher, while the settlement growth of ballast at distant locations (Sleeper-8 and Sleeper+8) remains constant. The constant growth of the Sleeper-8 and Sleeper+8 confirms that the linear growth of the second stage of the settlement in the free ballast track, as in [41] (Stage 2 of the solid line in Figure 3.16). Moreover, the nonlinear settlement growth near the bridge (Sleeper-2 and Sleeper+2) confirms the suggested nonlinear settlement scheme (Stage 2) for transition zones (Stage 2 of the dashed line in Figure 3.16), which differs from the linear settlement scheme (Stage 2) for open tracks. By updating Figure 3.16 with the simulation results, the settlement scheme for transition zones can be obtained

It also proves that it is necessary to consider the non-linear contact between sleepers and ballast. By combining the settlement model for open tracks with the non-linear sleeper-ballast contact model (the FE transition model), the settlement in transition zones can be better predicted.

Furthermore, the settlement growth of ballast closer to the bridge is gradually reducing (Sleeper-2 and Sleeper+2 in Figure 3.16b). It implies that the amplified settlement growth at such locations may eventually decrease to the constant value as the ballast in distant locations. This is because the ballast pressure cannot increase infinitely due to the bending stiffness of rails. With the increase of loading cycles, the pressure will be distributed to neighbouring sleepers resulting in decreasing settlement growth rate [20]. However, since rails are fixed on the bridge side, the stress in rails will increase.

Considering the increasing growth of the settlement at Sleeper+5, it shows that once a dip (at Sleeper+2) is generated, the vertical growth of the dip reduces, while another dip appears at the adjacent location (Sleeper+5). It explains the fact that the ballast profile is very inhomogeneous, which is often observed in transition zones [50]. It also implies that when a track geometry irregularity is formed near the bridge, the geometry irregularity has a trend to spread further, since the differential settlement between bridges and ballast tracks cannot be eliminated.

4.2 Dynamic responses before and after the settlement

In this section, the dynamic responses of the FE model in transition zones before and after 60,000 cycles of passage (3.5 MGT) are compared. The purpose is to study the effects caused by the long-term settlement.

The comparison of the ballast stresses of 0 and 60,000 cycles of train passage (0 and 3.5 MGT) is shown in Figure 3.17. The collection method is the same as previously mentioned in Section 4.1.

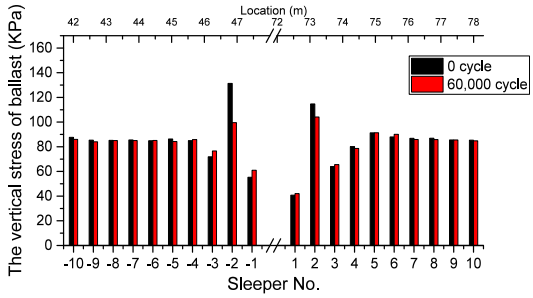

Figure 3.17: Comparison of ballast stress.

Figure 3.17 shows that the ballast stress is changed by the settlement, especially at Sleeper-2 and Sleeper +2. The stress in ballast after 60,000 cycles (3.5 MGT) is more evenly distributed along the track than in the beginning. The ballast stresses at Sleeper-2 and Sleeper +2 are reduced, from 131.3kPa to 99.5kPa and from 114.7kPa to 104.1kPa respectively. On the contrary, the ballast stresses at Sleeper-1 and Sleeper +1 are increased. The difference can be more clearly seen by comparing the variance of the ballast stresses in the embankment-bridge transition and the bridge-embankment transition, which is calculated after each iteration as shown in Figure 3.18.

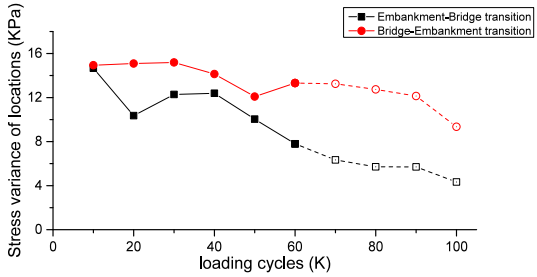

Figure 3.18: Variance of ballast stresses.

As indicated in Figure 3.18, the variance of the ballast stresses reduces gradually, which indicates that the ballast stress becomes evenly distributed as the number of loading cycles increases. This also indicates the growth of the dips will slow down. Note that even though the variance of ballast stresses in the bridge-embankment transition is increased at 60,000 loading cycles, it drops in the further iterations (from 60,000 cycles to 100,000 cycles), as shown in the dash lines in Figure 3.18. Compared with the bridge-embankment transition, the variance of the ballast stress in the embankment-bridge transition is reduced faster.

4.3 Parametric study of iteration steps

To study the influence of iteration steps, five values of the step are used to calculate the settlement of the transition zone till 60,000 cycles (3.5 MGT), or 12,000 train passages assuming 1 train including 5 vehicles. The values of the iteration step and the corresponding number of iterations to reach 60,000 cycles (3.5 MGT) are listed in Table 3.4.

Table 3.4: Iteration steps and number of iterations

Iteration step	Number of iterations
5,000 cycles/ 1,000 train passages	12
10,000 cycles/ 2,000 train passages	6
20,000 cycles/ 4,000 train passages	3
30,000 cycles/ 6,000 train passages	2
60,000 cycles/ 12,000 train passages	1

The settlements at 60,000 cycles (3.5 MGT) calculated by the five cases are shown in Figure 3.19. The settlement from 0 to 60,000 cycles (3.5 MGT) at the locations near the bridge (Sleeper-2 and Sleeper+2) and at distant locations (Sleeper-8 and Sleeper+8) are shown in Figure 3.20. The settlement of Sleeper-2 and Sleeper+2 at 60,000 cycles shown in Figure 3.20a and Figure 3. 20b are listed and analysed in Table 3.4.

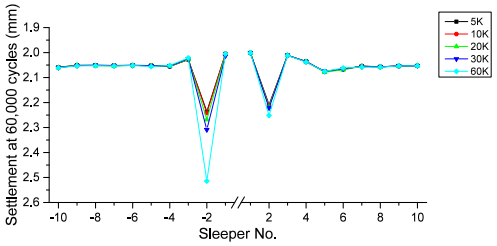

Figure 3.19: Settlement at 60,000 cycles (3.5 MGT) calculated different iteration step.

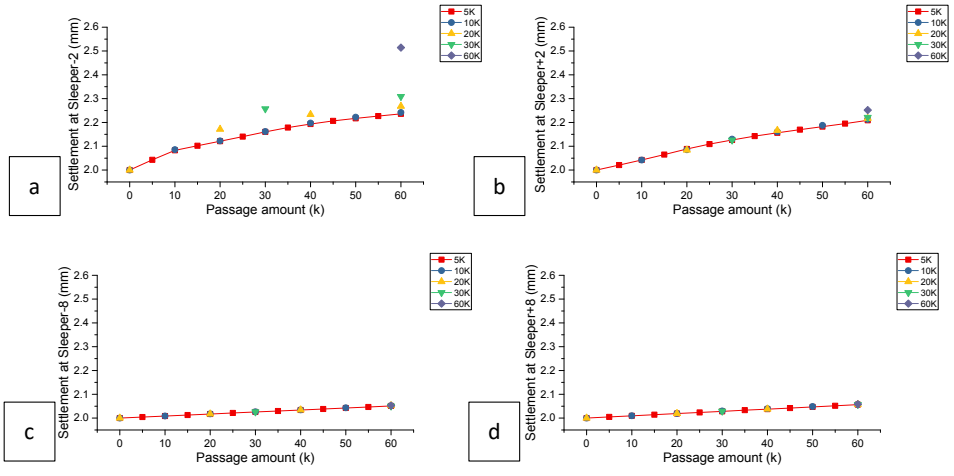

Figure 3.20: Settlement from 0 to 60,000 cycles (0 and 3.5 MGT) calculated different iteration step at close locations (Sleeper-2 and Sleeper+2) and distant locations (Sleeper-8 and Sleeper+8).

Table 3.5: Net settlement after 60,000 cycles (3.5 MGT) calculated by different steps

	Sleeper-2		Sleeper+2	
Iteration step	Value (mm)	Increase percentage (%)	Value (mm)	Increase percentage (%)
5,000	0.236	-	0.209	-
10,000	0.242	2.5	0.213	1.9
20,000	0.268	13.6	0.217	3.9
30,000	0.309	30.8	0.221	5.9
60,000	0.514	117.8	0.252	20.6

As seen from Figure 3.19, Figure 3.20 and Table 3.5, the settlement prediction is affected by iteration steps, especially at dips, comparing the settlement at Sleeper-2 calculated by 60,000 cycles to 5,000 cycles, which is increased by 117.8%. On the contrary, the settlements at distant locations are almost unaffected.

Comparing the settlement at Sleeper-2 and Sleeper+2 calculated by different iteration steps, it can be found that the calculated results are increased as iteration steps increasing. To balance the calculation expense and error, the iteration step of 10,000 cycles is recommended.

5 Conclusions

To predict the permanent settlement of track transition zones, a methodology based on the FE model and the empirical settlement model has been presented. The FE model is a 3-D dynamic model (explicit integration) of a track transition zone modelled according to a widely used transition zone in the Netherlands. The transition model includes the nonlinear contact between sleepers and ballast as well as the vehicle dynamics. The empirical settlement model considers two stages of ballast settlement. The settlement in Stage 1 is expressed as a given value since it appears fast after operation due to the rapid compaction of ballast. The settlement in Stage 2 considers the nonlinear relationship between ballast stress and settlement. The iterative procedure includes the following steps. Firstly, the ballast stress due to passing trains under each sleeper is calculated using the FE model, after the ballast track is settled evenly after Stage 1. Then, the settlement is calculated using the empirical settlement model based on the ballast stresses obtained from the FE model. After that, by applying the obtained settlement to the FE model and performing the FE simulation again, the ballast stresses for the new settlement condition are calculated. The procedure continues iteratively until the requested number of cycles has been achieved.

To demonstrate the methodology, the ballast settlement in the transition zone after 60,000 loading cycles (3.5 MGT) is predicted. It has been shown that the settlements appear on both sides of the bridge already after the first 10,000 loading cycles. The two dips continuously grow as the number of loading cycles increasing, which confirms the track settlement often observed in transition zones.

The settlement growth varies depending on locations. The settlement growth of the ballast closer to the bridge is relatively high at the beginning (0 cycles) and then gradually reduced (during 60,000 cycles or 3.5 MGT). On the contrary, the settlement growth of ballast at distant locations remains constant. In addition, once a dip is generated, the vertical growth of the dip reduces, while another dip appears at an adjacent location along the track. This implies the track geometry irregularity will spread from bridges to the tracks on embankment.

By comparing the dynamic responses of the transition zone after 0 and 60,000 loading cycles (0 and 3.5 MGT), it has been found that the ballast stress after 60,000 cycles (3.5 MGT) is more evenly distributed. However, the stress in rails close to the bridge will increase.

The parametric study of iteration steps shows that the settlement prediction is strongly affected by iteration steps at the locations close to the bridge, while less affected at the distant locations. Moreover, the settlement predicted in the dip of embankment-bridge is increased as the iteration step increases. As a compromise between the expense and accuracy of calculations, the iteration step of 10,000 cycles is recommended.

Acknowledgement

The authors would like to thank ProRail, the Netherlands for providing the measurement data. The authors are very grateful to all the reviewers for their thorough reading of the manuscript and for their constructive comments.

References

1. Esveld C. Modern railway track. MRT-productions Zaltbommel, The Netherlands, 2001.

2. Kerr AD and Moroney BE. Track transition problems and remedies. PROC OF THE AMERICAN RAILWAY ENGINEERING ASSOCIAT 1993; 94: 25.

3. Li D and Davis D. Transition of Railroad Bridge Approaches. JOURNAL OF GEOTECHNICAL AND GEOENVIRONMENTAL ENGINEERING 2005. DOI: 10.1061//asce/1090-0241/2005/131:11/1392.

4. Plotkin D and Davis D. Bridge approaches and track stiffness. 2008.

5. Zuada Coelho B. Dynamics of railway transition zones in soft soils (Doctoral dissertation). Doctoral dissertation, 2011.

6. Stark TD and Wilk ST. Root cause of differential movement at bridge transition zones. Proceedings of the Institution of Mechanical Engineers, Part F: Journal of Rail and Rapid Transit 2015. DOI: 10.1177/0954409715589620.

7. Nicks JE. The bump at the end of the railway bridge (Doctoral dissertation). Texas A&M University, 2009.

8. Varandas JN, Hölscher P and Silva MAG. Dynamic behaviour of railway tracks on transitions zones. Computers & Structures 2011; 89: 1468-1479. DOI: 10.1016/j.compstruc.2011.02.013.

9. Hölscher P and Meijers P. Literature study of knowledge and experience of transition zones. 2007.

10. Hunt H. Settlement of railway track near bridge abutments. Proceedings of the Institution of Civil Engineers-Transport. Thomas Telford-ICE Virtual Library, 1997, p. 68-73.

11. Li Z and Wu T. Vehicle/track impact due to passing the transition between a floating slab and ballasted track. Noise and Vibration Mitigation for Rail Transportation Systems. Springer, 2008, pp.94-100.

12. Namura A and Suzuki T. Evaluation fo countermeasures against differential settlement at track transitions. QR of RTRI 2007; 48.

13. Lundqvist A, Larsson R and Dahlberg T. Influence of railway track stiffness variations on wheel/rail contact force. Track for High-Speed Railways, Porto, Portugal 2006.

14. Lei X and Zhang B. Influence of track stiffness distribution on vehicle and track interactions in track transition. Proceedings of the Institution of Mechanical Engineers, Part F: Journal of Rail and Rapid Transit 2010; 224: 592-604. DOI: 10.1243/09544097jrrt318.

15. Read D and Li D. Design of track transitions. TCRP Research Results Digest 79 2006. digest.

16. Sañudo R, Markine V and Dell'Olio L. Optimizing track transitions on high speed lines. IAVSD2011 2011.

17. Shahraki M, Warnakulasooriya C and Witt KJ. Numerical study of transition zone between ballasted and ballastless railway track. Transportation Geotechnics 2015; 3: 58-67. DOI: 10.1016/j.trgeo.2015.05.001.

18. Banimahd M and Woodward PK. 3-Dimensional Finite Element Modelling of Railway Transitions. 9th International Conference on Railway Engineering 2007.

19. Banimahd M, Kennedy J, Medero GM, et al. Behaviour of train–track interaction in stiffness transitions. Proceedings of the ICE - Transport 2012; 165: 205-214. DOI: 10.1680/tran.10.00030.

20. Lundqvist A and Dahlberg T. Load impact on railway track due to unsupported sleepers. Proceedings of the Institution of Mechanical Engineers, Part F: Journal of Rail and Rapid Transit 2005; 219: 67-77. DOI: 10.1243/095440905x8790.

21. Gallego Giner I and López Pita A. Numerical simulation of embankment–structure transition design. Proceedings of the Institution of Mechanical Engineers, Part F: Journal of Rail and Rapid Transit 2009; 223: 331-343. DOI: 10.1243/09544097jrrt234.

22. Seara I and Correia AG. Performance assesment solutions for transition zones embankment-bridge railways trough numerical simulation 3D. Semana de Engenharia 2010 2010.

23. Shi J, Burrow MPN, Chan AH, et al. Measurements and simulation of the dynamic responses of a bridge-embankment transition zone below a heavy haul railway line. Proceedings of the Institution of Mechanical Engineers, Part F: Journal of Rail and Rapid Transit 2012; 227: 254-268. DOI: 10.1177/0954409712460979.

24. Paixao A, Fortunato E and Calcada R. Design and construction of backfills for railway track transition zones. Proceedings of the Institution of Mechanical Engineers, Part F: Journal of Rail and Rapid Transit 2013; 229: 58-70. DOI: 10.1177/0954409713499016.

25. Alves Ribeiro C, Paixão A, Fortunato E, et al. Under sleeper pads in transition zones at railway underpasses: numerical modelling and experimental validation. Structure and Infrastructure Engineering 2014; 11: 1432-1449. DOI: 10.1080/15732479.2014.970203.

26. Dahlberg T. Railway Track Stiffness Variations-Consequences and Countermeasures. International Journal of Civil Engineering 2010; 8.

27. Insa R, Salvador P, Inarejos J, et al. Analysis of the influence of under sleeper pads on the railway vehicle/track dynamic interaction in transition zones. Proceedings of the Institution of Mechanical Engineers, Part F: Journal of Rail and Rapid Transit 2011; 226: 409-420. DOI: 10.1177/0954409711430174.

28. Ling L, Dhanasekar M, Thambiratnam DP, et al. Minimising lateral impact derailment potential at level crossings through guard rails. International Journal of Mechanical Sciences 2016; 113: 49-60.

29. Ling L, Dhanasekar M, Thambiratnam DP, et al. Lateral impact derailment mechanisms, simulation and analysis. International Journal of Impact Engineering 2016; 94: 36-49.

30. Ling L, Dhanasekar M and Thambiratnam DP. Frontal collision of trains onto obliquely stuck road trucks at level crossings: Derailment mechanisms and simulation. International Journal of Impact Engineering 2017; 100: 154-165.

31. Ling L, Guan Q, Dhanasekar M, et al. Dynamic simulation of train–truck collision at level crossings. Vehicle System Dynamics 2017; 55: 1-22.

32. Sañudo R, dell'Olio L, Casado JA, et al. Track transitions in railways: A review. Construction and Building Materials 2016; 112: 140-157. DOI: 10.1016/j.conbuildmat.2016.02.084.

33. Varandas JN, Holscher P and Silva MA. Settlement of ballasted track under traffic loading: Application to transition zones. Proceedings of the Institution of Mechanical Engineers, Part F: Journal of Rail and Rapid Transit 2013; 228: 242-259. DOI: 10.1177/0954409712471610.

34. Hallquist JO. LS-DYNA theory manual. Livermore software Technology corporation 2006; 3: 25-31.

35. Sato Y. Optimization of track maintenance work on ballasted track. In: Proceedings of the World Congress on Railway Research (WCRR'97), B 1997, pp.405-411.

36. Wang H and Markine V. Analysis of the Long-Term Behaviour of Track Transition Zones. In: Pombo J, (ed.). The Third International Conference on Railway Technology: Research, Development and Maintenance. Civil-Comp Press, 2016, p. 203.

37. Lei X and Mao L. Dynamic response analyses of vehicle and track coupled system on track transition of conventional high speed railway. Journal of Sound and Vibration 2004; 271: 1133-1146. DOI: 10.1016/s0022-460x(03)00570-4.

38. Zhai WM and True H. Vehicle-track dynamics on a ramp and on the bridge: simulation and measurement. Vehicle System Dynamics 1999; 33: 11.

39. Wang H, Markine VL, Shevtsov IY, et al. Analysis of the Dynamic Behaviour of a Railway Track in Transition Zones With Differential Settlement. 2015 Joint Rail Conference, San Jose, California, USA, March 2015. 2015, p. 7.

40. Gallage C, Dareeju B and Dhanasekar M. State-of-the-art : track degradation at bridge transitions. Proceedings of the 4th International Conference on Structural Engineering and Construction Management 2013 2013.

41. Sato Y. Japanese Studies on Deterioration of Ballasted Track. Vehicle System Dynamics 1995; 24: 197-208. DOI: 10.1080/00423119508969625.

42. Selig ET and Waters JM. Track geotechnology and substructure management. Thomas Telford, 1994.

43. Dahlberg T. Some railroad settlement models—a critical review. Proceedings of the Institution of Mechanical Engineers, Part F: Journal of Rail and Rapid Transit 2001; 215: 289-300. DOI: 10.1243/0954409011531585.

44. Indraratna B, Nimbalkar S, Christie D, et al. Field assessment of the performance of a ballasted rail track with and without geosynthetics. Journal of Geotechnical and Geoenvironmental Engineering 2010; 136: 907-917.

45. Suiker ASJ and de Borst R. A numerical model for the cyclic deterioration of railway tracks. International Journal for Numerical Methods in Engineering 2003; 57: 441-470. DOI: 10.1002/nme.683.

46. Varandas JN, Hölscher P and Silva MAG. A Settlement Model for Ballast at Transition Zones. Proceedings of the Tenth International Conference on Computational Structures Technology 2010.

47. Lichtberger B. Track maintenance strategies for ballasted track – a selection. Rail Engineering International Edition 2001.

48. Iwnicki SD, Grassie S and Kik W. Track Settlement prediction using computer simulation tools. Vehicle System Dynamics 2000; 33: 2-12.

49. Li X, Nielsen JCO and Pålsson BA. Simulation of track settlement in railway turnouts. Vehicle System Dynamics 2014; 52: 19. DOI: 10.1080/00423114.2014.904905.

50. Varandas JN. Long-Term Behaviour of Railway Transitions under Dynamic Loading Application to Soft Soil Sites (Doctoral dissertation). 2013.

51. Indraratna B, Thakur PK and Vinod JS. Experimental and Numerical Study of Railway Ballast Behavior under Cyclic Loading. INTERNATIONAL JOURNAL OF GEOMECHANICS 2010; 10: 136-144. DOI: 10.1061//ASCE/GM.1943-5622.0000055.

52. Fröhling RD. Low Frequency Dynamic Vehicle/Track Interaction: Modelling and Simulation. Vehicle System Dynamics 1998; 29: 30-46. DOI: 10.1080/00423119808969550.

53. Suzuki T, Ishida M, ABE K, et al. Measurement on Dynamic Behaviour of Track near Rail Joints and Prediction of Track Settlement. QR of RTRI 2005; 46: 124-129.

54. Holtzendorff K and Gerstberger U. Predicting Settlements of Ballasted Tracks due to Voided Sleepers. Proceedings of the World Congress on Railway Research. Koeln2001.

55. Hallquist JO. LS-DYNA Keyword User's Manual. LSTC Co., Livermore, CA, 2007.

56. Coelho Z. Dynamics of railway transition zones in soft soils. 2011. thesis.

57. Wang H and Markine V. Finite element analysis of the dynamic behaviour of track transition zones during train passing processes. Submitted to Vehicle System Dynamics 2017.

58. Wang H and Markine V. Analysis and improvement of the dynamic track behaviour in transition zone. In: al. Le, (ed.). Tenth International Conference on the Bearing Capacity of Roads, Railways and Airfields. Athens, Greece: Taylor & Francis Group, London, 2017.

59. Guerin N, Sab K, Moucheront P, et al. Experimental identification of a ballast settlement law. CANADIAN GEOTECHNICAL JOURNAL 1999; 36: 523-532.

60. Ionescu D, Indraratna B and Christie H. Behaviour of railway ballast under dynamic loads. Proceedings of 13th Southeast Asian Geotechnical Conference, Taipei, Taiwan. 1998, p. 69-74.

61. Stewart HE. Permanent strains from cyclic Variable-Amplitude loadings. Journal of Geotechnical Engineering 1986; 112: 646-660.

62. Iwnick S. Manchester Benchmarks for Rail Vehicle Simulation. Vehicle System Dynamics 1998; 30: 295-313. DOI: 10.1080/00423119808969454.

63. Kreiser D, Jia SX, Han JJ, et al. A nonlinear damage accumulation model for shakedown failure. International Journal of Fatigue 2007; 29: 1523-1530.

Paper IV

Corrective countermeasure for track transition zones: adjustable fastener

Haoyu Wang[1], Valeri Markine[1]

[1]Delft University of Technology, Delft, the Netherlands

Published by Engineering Structures, 169, (2018): pp.1-14

Abstract

Transition zones in railway tracks are the locations with considerable variation in the vertical stiffness of supporting structures. Typically, they are located near engineering structures, such as bridges, culverts, tunnels and level crossings. In such locations, the variation of the vertical stiffness and the differential track settlement result in amplification of the dynamic forces acting on the track. This amplification contributes to the degradation process of ballast and subgrade, ultimately resulting in the increase of maintenance costs.

The paper studies a corrective countermeasure that can mitigate the track degradation in transition zones when differential settlement appears. The countermeasure is the adjustable rail fastener and its working principle is to eliminate the gap under hanging sleepers by adjusting the shims (height of the fastener). The adjustable fasteners are first tested on three transition zones, wherein the adjusted heights of fasteners (accumulated voiding) are recorded after the 2-month and 5-month operation. The test results show the adjustable fasteners are effective to mitigate the track degradation in the transition zones. The effect of the adjustable fasteners on the dynamic behaviour of transition zones is analysed using the FE method. The results show that the adjustable fasteners are effective to reduce the amplification of wheel forces, achieve a better stress distribution in ballast, and decrease the normal stresses in rails in transition zones. Parametric studies are also performed to study the applicability of the adjustable fasteners.

Keywords

Adjustable fasteners, Railway track modelling, Transition zone, Corrective Countermeasures, Finite element method.

1 Introduction

Transition zones in railway tracks are locations with considerable variation in the vertical stiffness of supporting structures. Typically, they are located near engineering structures, such as bridges and slab tracks. An example of a typical transition zone is shown in Figure 4.1.

Figure 4.1. Track transition zones

In those locations, the variation of the vertical stiffness together with the differential settlement of tracks (when the foundation settles unevenly) results in amplification of dynamic forces, which contributes to the degradation of ballast and subgrade, ultimately resulting in deterioration of the vertical track geometry or even the damage of track components. To keep track transition zones in operation, more maintenance is required as compared to free tracks [1, 2]. For instance, in the Netherlands, the maintenance activities on the tracks in transition zones are performed up to 4-8 times more often than that on free tracks [3, 4]. Transition zones in the other countries of Europe and the US also require additional maintenance [5, 6].

Even though many countermeasures have been used in transition zones, severe track deterioration in transition zones is still often observed [7, 8]. In [9], three countermeasures including geocell, cement, and hot mix asphalt were applied on three similar transition zones. Compared to a plain transition zone (no countermeasure is applied) as a reference, it has been found that all countermeasures were not sufficient to reduce the settlement in the transition zones. In [10], the countermeasure, which uses an approaching slab linking the ballast track onto a concrete culvert, 'has exacerbated rather than mitigated the (transition) problem'. These findings are in agreement with [11], where the authors indicated that 'the problem of track degradation associated with stiffness variations is far from being solved'.

According to the settlement behaviour of ballast tracks [12-17] , the track settlement process can be divided into two stages (as shown in Figure 4.2). Stage 1 is the rapid settlement process, caused by the volumetric compaction and abrasion of ballast particles. Stage 2 is the standard settlement process (until the end of the maintenance interval) caused by the frictional sliding of particles. The settlement of ballast, subballast, and subgrade in Stage 1 is: (1) fast, which happens only after few months; (2) large, accounts for approximately 50% of the total settlement in a maintenance interval; (3) somewhat inevitable, which happens even though it was compacted. On

the contrary to the large settlement appearing in ballast tracks, the engineering structures barely settle, which creates a considerable geometry irregularity (differential settlement). After the differential settlement appears (corresponding to the beginning point of Stage 2, see Point B in Figure 4.2), one end of the rails is settled together with the ballast track, while the other end is constrained by the engineering structures, creating gaps under sleepers (also known as hanging sleepers or voiding) on the embankment side.

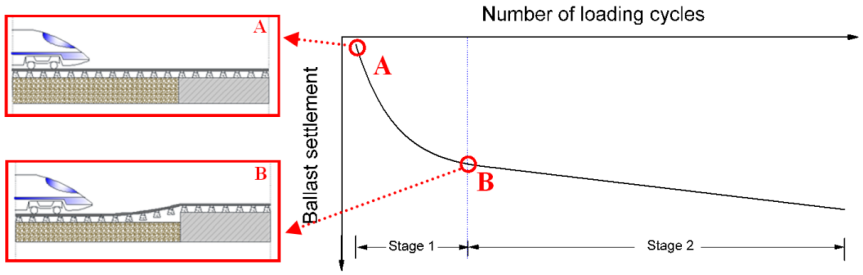

Figure 4.2. Schematic permanent settlement curve of ballast as a function of loading cycles (only for open ballast tracks), from [18].

Due to the existence of the gaps, the dynamic responses in transition zones are significantly increased [19, 20]. For instance, a 1mm gap can increase the sleeper-ballast contact force in adjacent locations by 70% [21]; and the 2mm gap can lead to 85% increase of wheel forces [19]. It should be noted that the settlement curve in Figure 4.2 is only for open ballast tracks. This is because the dynamic responses (e.g. wheel-rail interaction forces and ballast stress) are increased by the differential settlement and alter the settlement curve (mainly in Stage 2). An example of the transition zone with a large differential settlement is shown in Figure 4.3 [18].

Figure 4.3. Transition zone with a large differential settlement.

Therefore, the countermeasures can be categorized according to the settlement behaviour into the preventive countermeasures and corrective countermeasures. The preventive countermeasures are implemented during the construction prior to the track operation, while the corrective ones are used when the track has already settled (the differential settlement is visible). The studies of the transition zones with the perfect geometry, i.e. considering the beginning point of Stage 1 (Point A in Figure 4.2), are more suitable for the preventive countermeasures, such as the studies in [8, 22-27]; while for the analysis of corrective countermeasures, the numerical models have to take the differential settlement into account. The corrective countermeasures that can timely mitigate the transition zone problems caused by differential settlement (at Point B in Figure 4.2) are required further studies.

This study focuses on the corrective countermeasures for transition zones which should satisfy the following requirements:

- The corrective operations should be performed in short track possession windows manually or by using small machines.
- The corrective countermeasures should be able to mitigate the track degradation in transition zones.

The paper presents the experimental and numerical analysis of a corrective countermeasure - the adjustable fastener. The adjustable fastener intents to fill the partial gap between a sleeper and ballast by shims, whereas it prevents a large operation such as tamping. Even though (unloaded) track alignment is not restored, the hanging sleepers in the vicinity of engineering structures are eliminated, which can slow down the track degradation in transition zones.

The paper is organised as follows. The preventive and corrective countermeasures for transition zones are reviewed in Section 2, including the introduction of the adjustable fastener. The measurement results of three transition zones with the adjustable fasteners are discussed in Section 3. In Section 4, the dynamic behaviour of the transition zone (with differential settlement) with the adjustable fasteners is analysed using FE method. Finally, conclusions are given in Section 5.

2 Countermeasures for transition zones

The countermeasures for transition zones can be divided according to their application period, which is either the design stage (preventive measures) or the operation stage (corrective measures).

When designing a transition zone, the primary goal is to construct a zone with smooth changes of the vertical stiffness from the embankment to the engineering structure. A thorough review of the countermeasures for transition zones can be found in [28]. The countermeasures are applied to embankments or/and engineering structure. The intent of the countermeasures on the embankment is to reinforce the ballast track on different levels using various measures such as:

- Subgrade: the geocell, geotextile, cement, hot mix asphalt [9, 29], and transition wedge (special backfill) [30];
- Ballast: the ballast glue [31], under ballast mat [32], pile or steel bar underneath the ballast [8, 33], and ballast containment wall [34];
- Sleepers: sleeper modifications such as increasing its length and reducing the spacing [27, 34] and weight [35, 36].

The countermeasures on engineering structures are intended to decrease the stiffness of the tracks, for instance using rail pads [37], under slab pads [34] and under sleeper pads [24, 25]. In addition, some countermeasures increase the intergrade stiffness of transition zones such as using auxiliary rails [27, 34, 36] and approaching slabs [38]. In some cases, a combination of several countermeasures is used [28].

When the preventive countermeasures do not mitigate the track degradation efficiently, e.g. [9, 10], or no countermeasures are used, e.g. [7, 39], critical differential settlement may appear in a maintenance cycle. The differential settlement may result in the damage of track components and deterioration of the passenger's comfort. To mitigate the existing differential settlement, the corrective countermeasures are necessary. Besides, the hanging sleepers also appear in the vicinity of the engineering structure (0.9m [22] or 1.5m [40] from the engineering structure). However, due to the abutment or the transition structure, it is not always possible for tamping machines to perform track maintenance near engineering structures. In these situations,

corrective countermeasures that can be performed manually or by small packing machines can be applied. The general principle of the corrective countermeasures is to fill the gaps between the sleepers and ballast to eliminate hanging sleepers.

2.1 Existing corrective countermeasures

The most common corrective countermeasure is tamping. During the process, sleepers are lifted to the required level and the ballast around the sleepers is packed into the void below the sleepers, either manually or by mechanical means (when possible). When the mechanised on-track tamping machines are used, vibrating tamping tines are introduced into the ballast on both sides of the sleeper. The vibration frequency is chosen so as to fluidise the ballast, which then is compacted inwards and upwards towards the bottom of the sleeper [41]. In case of some special structures, the tamping machines are difficult to employ. Tamping using manual or mechanised vibrating hammers is therefore necessary. During the process, sleepers are lifted by hydraulic rail jacks (sometimes sleepers are not lifted) and then four vibrating hammers are used, with consolidating heads opposing each other on both sides of the track. It should be noted that the manual tamping is prohibited in some countries (e.g. the Netherlands) due to health and safety rules. Since tamping does not add additional material to the track and make ballast less compacted, hanging sleepers will re-appear at the relatively short time. The principle of tamping and operations using manual vibrating hammers [42] and mechanised vibrating hammers are shown in Figure 4.4.

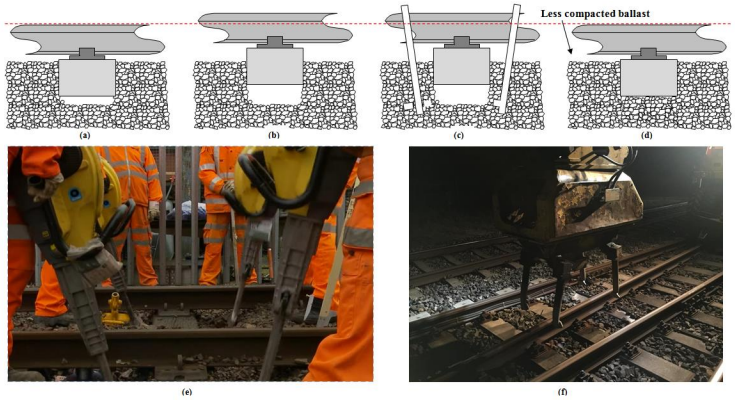

Figure 4.4. Schematic diagram of tamping: (a)-(d) Working principle, (e) Operation using manual vibrating hammers [42], (f) Operation using mechanised vibrating hammers.

One way to fill the gap under hanging sleepers is to use hand-held stoneblower [41, 43] or on-track stoneblower (when possible) [7, 44-46]. The principle is first to lift the sleeper to the required level with minimum disturbances; and then to blow a pre-determined quantity of stones into the void under the sleeper using compressed air. The amount of the added stones is determined by the basis of the sleeper displacement before the stone blowing (using the void meter) [43]. The size of the blown stones is 14-20mm, which is smaller than the ballast particle [41]. The principle of ballast blowing and a hand-held stoneblower are shown in Figure 4.5 [42].

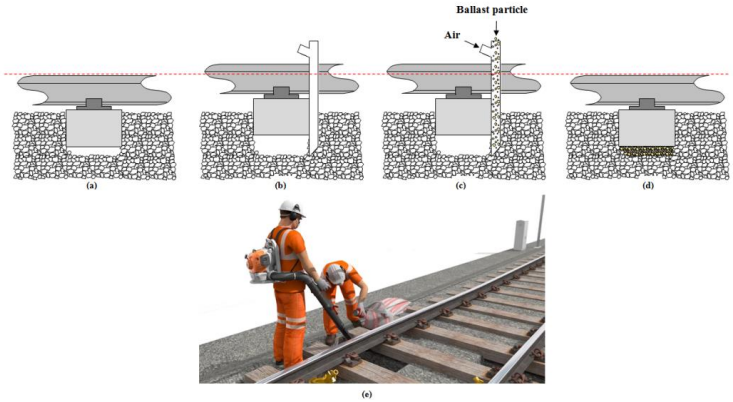

Figure 4.5. Schematic diagram of stone blowing: (a)-(d) Working principle, (e) Demonstration from [42].

Another corrective countermeasure is to use the Automatic irregularity-correcting sleeper [47]. This kind of sleeper consists of a fibre-reinforced polymer sleeper and two automatic subsidence compensating devices under each rail. The automatic subsidence compensating device has two nested boxes (see Figure 4.6a), which allows relative vertical movement. The inner box is connected to the rail through the sleeper, while the outer box is laid on the ballast. The inner box is filled with the (2mm-diameter) granular material. When the differential settlement appears in the track, the outer box sinks together with the ballast. At the moment, the gap between the inner box and the outer box is filled with the granular material as shown in Figure 4.6b. Therefore, the differential settlement is compensated by the granular material as shown in Figure 4.6c.

PII-IV

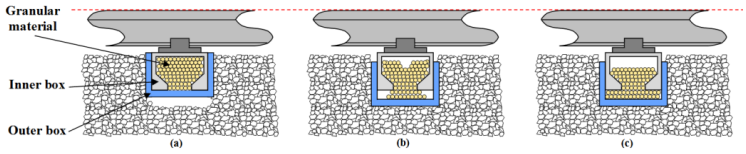

Figure 4.6. Working principle of the Automatic irregularity-correcting sleeper.

2.2 Proposed corrective countermeasure

An innovative way to remove the gap under the hanging sleepers is by using adjustable fasteners which consist of two plastic wedges (shims) inserted between sleepers and rails (Figure 4.7) instead of the rail pad. The height of the adjustable fastener can be changed by adjusting the position of the two wedges (shims) to fill the gap, which is 7mm-37mm (i.e. the net adjustable height is 0mm-30mm). When hanging sleepers appear, the height of the shims can be manually adjusted. As a result, the hanging sleepers can be restored to be fully supported by the ballast under. The principle of using adjustable fasteners is shown in Figure 4.7b and c. An example of the adjustable fastener used in the track is shown in Figure 4.7c. The stiffness of the shims (see Figure 8(c)) has been tested in the laboratory of TU Delft [48] prior to the filed implementation as shown in Figure 4.8, which follows the test procedures of rail fasteners stated in [49]. The load was applied by the hydraulic press machine (see Figure 4.8a) and the displacements were measured by LVDTs (Linear Variable Differential Transformer, see Figure 4.8b). During the test, the height of shims (adjusted height of the fasteners) was set to the maximum (37mm including 30mm adjusted

height). The shims were installed in the fastener attached to an NS90 concrete sleeper and a section of UIC 54E1 rail. The test results show that the vertical stiffness of the shims is 8.02E8 N/m and no heavy visible damage was found after loading.

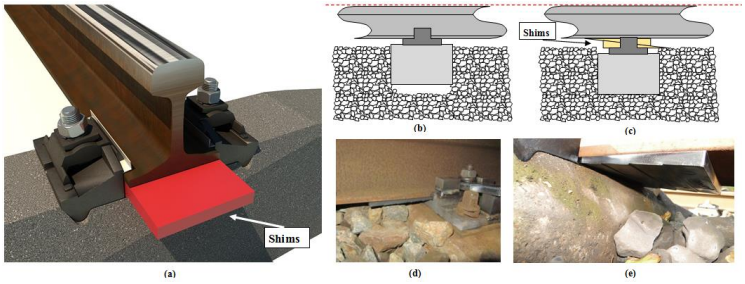

Figure 4.7. Schematic diagram of Adjustable fastener: (a) Adjustable fastener, (b)-(c) Working principle, (d)-(e) Examples of the adjustable fastener used in the track.

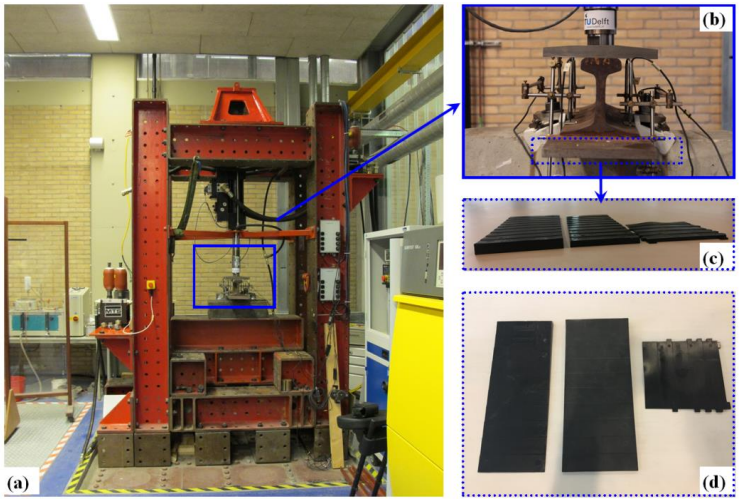

Figure 4.8. Laboratory test of the shims: (a) Hydraulic press machine, (b) Zoom-in photo at the actuator with LVDTs, (c) Side view of the shims, (d) Top view of the shims.

3 Experimental analysis

To study the effectiveness of the adjustable fasteners, they were tested on three transition zones in the track between Utrecht and Houten, the Netherlands. The natural ground in that region mainly consists of soft soil. According to the ground map of the location measured in 2012 [50], the natural ground of the measured lines is mostly clay, as shown in Figure 4.9. A detailed field survey including Cone Penetration Tests and Vertical Seismic penetration Tests at a nearby location can be found in [2] and [37]. The tracks were newly constructed and no transition slabs were employed in the transition zones. Heavy traffic was expected on the tracks, including both passenger trains and freight trains. The change of the traffic amount was negligible during the whole measurement period. Since the fasteners are adjusted to fill the gaps under sleepers, the adjusted height equals the accumulated voiding, which can represent the degradation process of tracks at the moment. Therefore, the adjusted heights of the fasteners are recorded to analyse the track degradation.

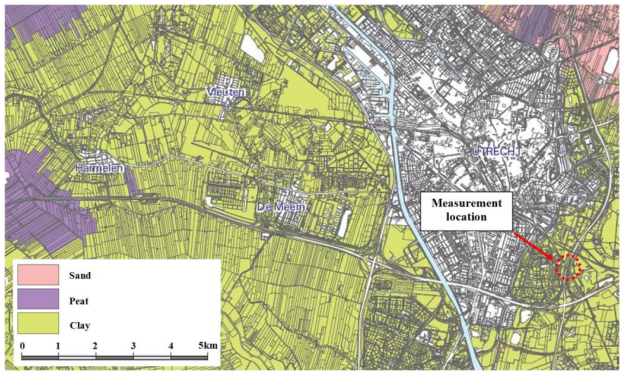

Figure 4.9. Ground map of the measurement location.

3.1 Measurement set-up

The measurements were performed on the transition zones which consist of ballast tracks and slab tracks (the rails are directed fastened on metallic or concrete structures) [51]. The three (Embankment-Slab track-Embankment) transition zones are named Transition Zone A, B, and C, as shown in Figure 4.10.

Figure 4.10. Photographs of the measured transition zones.

The adjustable fasteners had been installed on ten sleepers on both sides of slab tracks when the tracks were constructed. At that moment, the fasteners were set to their lowest position (i.e. adjusted height is 0mm). The new tracks including the transition zones were levelled and aligned by tamping machines before the tracks went into service, as shown in Figure 4.11.

Figure 4.11. Tamping in a transition zone.

The fasteners were adjusted after the 2-month operation and after the 5-month operation. During the adjustments, the fasteners were first unfixed (see Figure 4.12a); then the rails were lifted to the required level by standard rail jacks (see Figure 4.12b) or hydraulic rail jacks. After that, the fasteners were adjusted to the desired height by sliding shims. The schematic diagram of using adjustable fasteners in transition zones are explained in Figure 4.13. Since there was no operation specification for the adjustable fasteners, the adjustment mainly depended on the experience of the working staff. The operation for one side of a slab track (ten sleepers) required approximately fifteen minutes with three or four working staff. The adjusted heights of fasteners after two months and five months were recorded to analyse the development of the settlement in transition zones. It should be noted that due to practical reasons the fasteners on the embankment-slab track side of Transition Zone A were not possible to adjust after five months.

Figure 4.12. Adjustment of the fasteners.

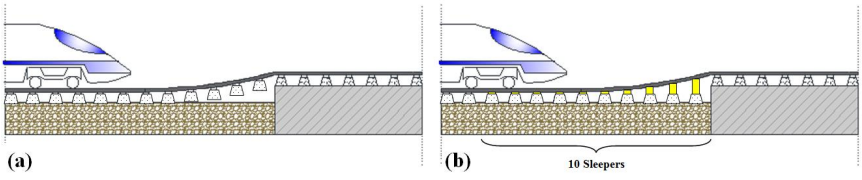

Figure 4.13. Schematic diagram of using adjustable fasteners in transition zones.

3.2 Measurement results

The adjusted heights of fasteners (accumulated voiding) of Transition Zone A, B, and C are shown in Figure 4.14, Figure 4.15, and Figure 4.16, respectively. It should be noted that since the adjusted height of all fasteners is 0mm at 0 month, it is omitted in the figures. For convenience, the sleepers are numbered starting from the one closest to the slab track. The numbers are negative on the left side of the slab track (the embankment-slab track transition) and positive on the right (the slab track-embankment transition). The moving direction of the trains are indicated in the figures.

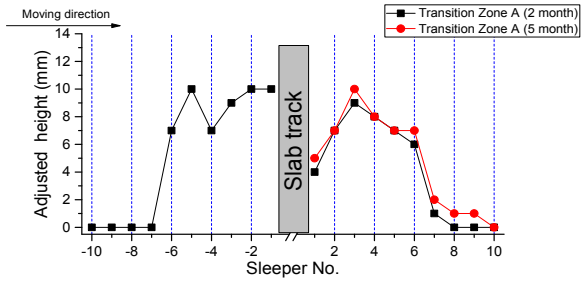

Figure 4.14. Adjusted heights of the fasteners in Transition Zone A.

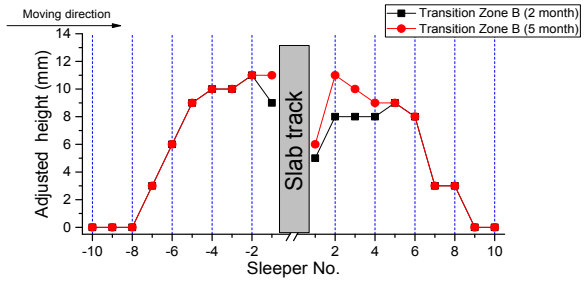

Figure 4.15. Adjusted heights of the fasteners in Transition Zone B.

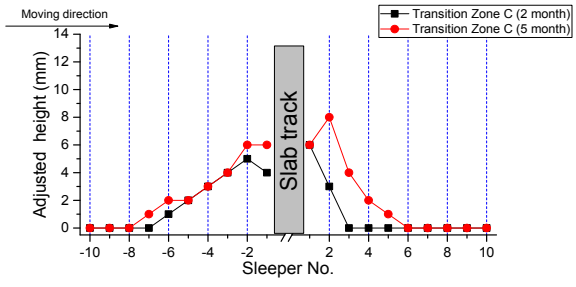

Figure 4.16. Adjusted heights of the fasteners in Transition Zone C.

As it can be seen from Figure 4.14-Figure 4.16, the settlement of ballast tracks appears after the 2-month operation where the maximal settlement values within 5mm (in Transition zone C)-11mm (in Transition zone B) can be found. The settlement is comparable with the measurement results in [2, 10], where more than 10mm settlement were also found after the 2-month operation. This is reasonable since both locations have the soft subsoil. The track settlement close to the slab track is higher in comparison with that farther from slab tracks. The settlement reaches the largest amount at the 2nd or 3rd sleepers from the slab track (Sleeper±2, Sleeper±3); after that, it gradually reduces to 0mm at the 8th or 9th sleepers (Sleeper±8, Sleeper±9). This is mainly because the ballast/subballast layer was not full stabilised before the operation, i.e. the rapid compaction process (Stage 1 in Figure 4.2) happened. This confirms the theory of the appearance of the different settlement in transition zones which is explained in Section 1 that the settlement near engineering structures is much higher than that farther from engineering structures. It is also consistent with the measurement results in [52].

It should be noted that the settlement at the 1st sleeper is less than that at the 2nd or 3rd sleepers. It is because the rail is constrained by the slab track. As a result, the 1st sleeper has less movement under train loads and generate smaller impact to the ballast. In addition, the wheel

forces are increased when the bogie is half on the slab track and half on the embankment, the distance of which corresponds to the 2nd or 3rd sleepers [18].

At the 2-month operation, the ballast tracks were compacted while the slab tracks were almost unchanged, which caused a differential settlement in the transition zones. If no corrective countermeasure was implemented, the tracks in the transition zones would continue degrading due to the amplified dynamic wheel loads and ballast stress [20, 53-57]. However, after filling the voiding using adjustable fasteners at the 2nd month, the growth rate of the settlement in ballast tracks was significantly reduced, which can be seen by comparing the accumulated settlement in the 0-2nd month and that in the 2nd-5th month in Figure 4.14-Figure 4.16. Also, the measurement results of Transition Zone A-C (averaged settlement measured at the locations of the 1st to 4th sleepers to the slab track) are compared with the transition zone without adjustable fasteners (the settlement at 4m from a culvert) from [10] in Figure 4.17. As shown in Figure 4.17, large settlements are found both in the transition zones with and without adjustable fasteners after the 2-month operation, which is mostly caused by the rapid compaction of ballast/subballast. However, there is also a relatively large settlement generated in the 2nd-5th month in the transition zone without adjustable fasteners, which accounts for 40% of the settlement in the 0-2nd month. On the contrary, the proportion is only within 7% (Transition Zone A)-19% (Transition Zone C) in the cases of the using the adjustable fasteners. It indicates that the adjustable fasteners reduce the growth rate of the settlement (i.e. degradation rate) in the transition zones.

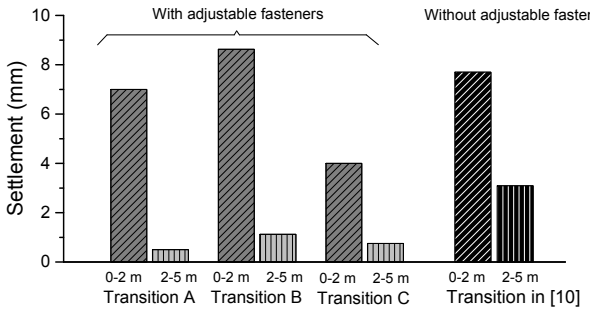

Figure 4.17. Comparison between the settlement transition zones with and without adjustable fasteners.

4 Numerical analysis

Since the adjustable fasteners are proved to be effective in the field measurement, its effect on the dynamic behaviour of transition zones is analysed using FE method.

4.1 Introduction of FE model

The FE model used in the paper is based on the model proposed in [58] and further developed in [18, 57]. In this study, it is tuned according to the measured transition zones. The model is pre-processed in ANSYS and solved in LS-DYNA. The modelling method and the parameters are briefly described here. The model consists of two ballast tracks and a slab track (in between), as shown in Figure 4.18. When the railway vehicle moves from one ballast track to the other (from left to right), it is possible to analyse both the embankment-slab track and the slab track-embankment transition with a single calculation. In the model, the 'slab track' is symbolical and not analysed to reduce calculation costs, because the purpose of the paper is to study the ballast track

degradation in the transition zone rather than the slab track itself. The effect of the mortar layer [59] and the temperature [60] is not considered.

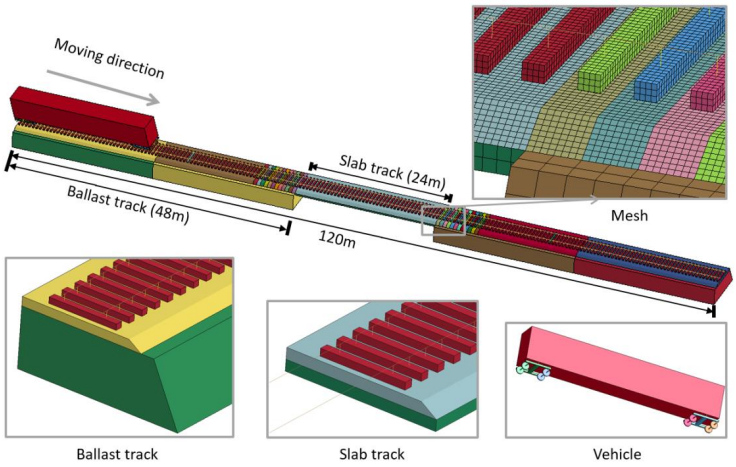

Figure 4.18. FE model of track transition zones.

As the length of the ballast track is 48m and the slab is 24m, thereby, the total length of the transition zone is 120m. The components of ballast tracks are rails, fasteners, sleepers, ballast, and subgrade. The rails are modelled by the beam elements with the cross-section and mass properties of the UIC54 rails. The adjustable fasteners are modelled by spring-damper elements which have bilinear material property. In compression, the elements can model elastic rail pads; and in tension, the elements can model the clamping effect of fasteners. In this way, hanging sleepers can be attached to rails, leaving gaps underneath.

PII-IV

Ballast, sleepers, and subgrade are modelled using the selective reduced integrated solid elements (element type 2 in LS-DYNA) with elastic material properties. This solid element assumes that the pressure is constant throughout the element to avoid pressure locking during nearly incompressible flow. The depth of ballast and subgrade layer is 0.3m and 2m, respectively.

The railway vehicle is a passenger vehicle, which is idealized as a multibody system consisting of one carbody, two bogies, and four wheelsets. The parameters of the vehicle are based on [61] and adapted to a Dutch passenger train [2, 62]. The velocity of the vehicle is 144km/h (standard operation velocity). The contact between the wheels and rails is modelled using the Hertzian spring [43]. The stiffness is calculated according to Equation 1.

$$k_H = \sqrt[3]{\frac{3E^2Q\sqrt{R_{wheel}R_{railprof}}}{2(1-\nu^2)^2}}, \quad (1)$$

where: E is the modulus of elasticity of the wheel and rail; v is the Poisson's ratio; Q is the static vertical wheel load; R_wheel is the radius of the wheel; R_railprof is the radius of the railhead [43, 63].

The connection between sleepers and ballast is modelled by the Penalty-based contact [64] in order to accurately present the spatial movement of sleepers and consequent ballast stresses. The Penalty-based contact employs the penalty method, which places normal interface springs between all penetrating nodes and the contact surface, as shown in Figure 4.19.

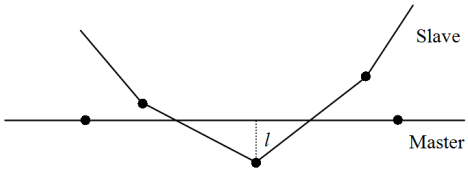

Figure 4.19. Schematic diagram of the penalty contact method.

According to the method, the search for penetrations between the bottom surface of sleepers and the top surface of ballast is made for every time step during the calculation. In the case that the penetration happens, no force is added. When the penetration between contact surfaces has been found, a force proportional to the penetration depth is applied to resist and ultimately eliminate the penetration [65]. If slave node n_s has penetrated through master segment s_i, the interface force vector f_s can be expressed as:

$$f_s = -lk_i n_i, \qquad if\ l < 0, \tag{2}$$

where l is the penetration; k_i is the stiffness factor for master segment s_i; n_i is normal to the master segment at the contact point. The stiffness factor k_i is:

$$k_i = \frac{f_{si} K_i A_i^2}{V_i}, \tag{3}$$

where f_{si} is a scale factor for the interface stiffness; K_i is the bulk modulus; A_i is the face area of the element that contains s_i; V_i is volume [65].

On the contrary, the Constraint-based contact [64] (tied contact) is used between the ballast and subgrade, and between the slab and the support layer. In the tied contact, the slave nodes are constrained to move with the master surface. The non-reflection boundaries [65] are applied to both ends of the model in order to reduce the wave reflection effect. The translation and rotation freedom of the nodes on the bottom of the subgrade and slab track are fixed. The material properties of the track components and the vehicle used in the model are suggested by [24, 30, 34, 66-69] and tuned according to the field measurements described in [18]. The main parameters used in the model are collected in Table 4.1.

PII-IV

Table 4.1: Material properties of the track components.

Parameter	Value
Sleeper Elastic Modulus (Pa)	3.65E+10
Sleeper Poisson ratio	0.17
Sleeper Density (kg/m3)	2.50E+3
Ballast Elastic Modulus (Pa)	1.20E+08
Ballast Poisson ratio	0.25
Ballast Density (kg/m3)	1.80E+3
Subgrade Elastic Modulus (Pa)	1.80E+08
Subgrade Poisson ratio	0.250
Subgrade Density (kg/m3)	2.30E+3
Concrete slab Elastic Modulus (Pa)	3.50E+10
Concrete slab Poisson ratio	0.17
Concrete slab Density (kg/m3)	2.50E+3
Support layer Elastic Modulus (Pa)	3.30E+10
Support layer Poisson ratio	0.17
Support layer Density (kg/m3)	2.50E+3

Fastener Vertical (compression) Stiffness (N/m)	1.20E+8
Fastener Vertical (compression) Damping (N*s/m)	5.00E+4
Fastener Vertical (tension) Stiffness (N/m)	1.20E+11
Fastener Vertical (tension) Damping (N*s/m)	5.00E+4
Primary suspension stiffness (N/m)	4.25E+5
Primary suspension damping (N*s/m)	1.00E+6
Secondary suspension stiffness (N/m)	4.68E+5
Secondary suspension damping (N*s/m)	6.50E+4
Secondary suspension Bending stiffness (Nm/rad)	1.05E+4
Distance between wheels (m)	2.5
Distance between axles (m)	20.0
Length of train body (m)	23.0
Axle load (t)	21.4
Carbody Mass (t)	64.6
Bogie Mass (t)	2.4

The FE model considers the settlement of the ballast track due to the rapid compaction after the operation (settlement in Stage 1 as illustrated in Figure 4.2). Since the exact settlement value is difficult to acquire, it is assumed to be equivalent to the adjusted height of the fasteners after 2 months. The maximal adjusted height varies from 5mm (in Transition zone C) to 11mm (in Transition zone B). As a result, the medium number 8mm is adopted for the differential settlement value in the model. After that, the cases of 4mm and 12mm are also analysed in the parametric study. The rail longitudinal level, sleeper and ballast coordinates in the transition zone model before and after the implementation of the differential settlement are illustrated in Figure 4.20.

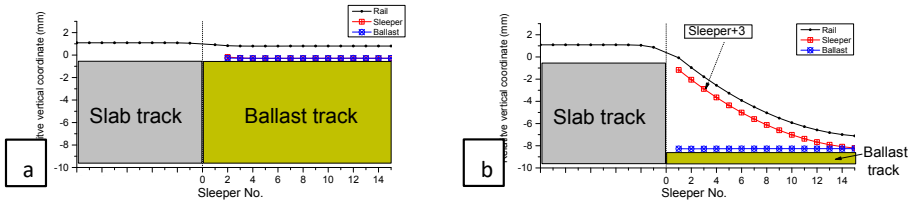

Figure 4.20. Coordinates of track components before and after the implementation of the differential settlement: (a) Before, (b) After.

At the equilibrium state of the model, due to separable contact between the sleepers and ballast, as well as the application of the gravity and the resistance of the rail, the gaps between the sleepers and ballast appear in the vicinity of the slab track, as shown in Figure 4.20b. The hanging distance of Sleeper+1 is the highest and the hanging distance gradually reduces as the distance from the slab track increases. The hanging values of the sleepers are presented as the differences between the sleepers and ballast. The same situation is observed on the other side of the slab track. After the equilibrium state, the vehicle moves over the transition zone. The movement of a hanging sleeper (Sleeper+3) is shown in Figure 4.21.

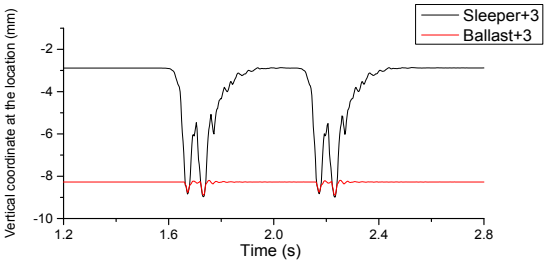

Figure 4.21: Time history of vertical coordinate due to the passing vehicle at Sleeper+3

The gap under the hanging sleeper is eliminated under train loads, where an increase of wheel-rail contact forces can be expected. When the sleepers contact the ballast, the penetrations between the bottom surface of the sleepers and the top surface of the ballast occur. The stress distribution in the ballast can be therefore calculated. Because the voids under sleepers are different depending on the location (see Figure 4.20b), the stresses in the ballast elements under different sleepers also vary according to their locations.

In the transition zone using adjustable fasteners, the spring-damper elements are extended to compensate the gaps between the sleepers and ballast, as shown in Figure 4.22. It should be noted that the stiffness and damping of adjustable fasteners are assumed to be same as normal fasteners (normal rail pads) and constant at various adjusted height. This simplification is made to reduce the computational expenses based on the findings that the effect of the differential settlement on dynamic responses is much larger in comparison with the stiffness variation [20, 54, 55, 57]. The differential settlement is magnified in Figure 4.22. In the actual case, the differential settlement (8mm) is much smaller compared to the size of a sleeper (240mm in height).

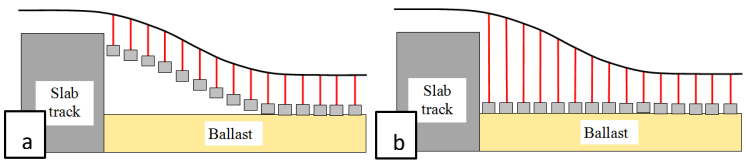

Figure 4.22. Schematic diagram of the simulation of the countermeasure: (a) Reference, (b) Using adjustable fasteners. Fasteners are indicated by the red lines.

The study to find the optimal mesh sizes was performed prior to this study and it is not included due to the limited space. The model contains 675686 nodes, 489,547 solid elements and 3,612 beam elements. The time-step is 1.3E-5s. The calculation takes around 14 hours using a 4-core (I7) workstation with 4 High Parallel Computing (HPC).

4.2 Dynamic responses of transition zones with the adjustable fasteners

Wheel force

The calculated wheel forces of four wheelsets in the reference case and the adjustable fastener case are shown in Figure 4.23. The wheel loads on the slab track are not considered in this study and therefore their responses are covered by the shaded area. The maximal wheel forces acting on ballast tracks are collected in Table 4.2.

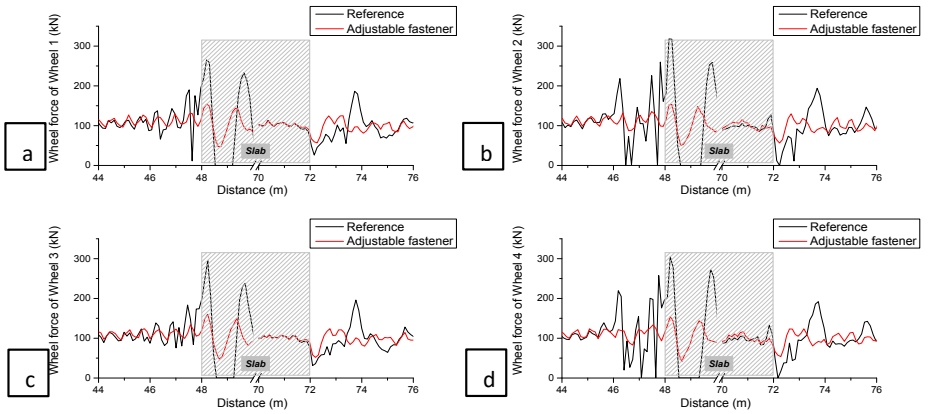

Figure 4.23. Wheel-rail interaction force of four wheelsets: (a) Wheel 1, (b) Wheel 2, (c) Wheel 3, (d) Wheel 4. The wheel loads on the slab track are covered by the shaded area.

Table 4.2. Maximal wheel forces in the ballast track in transition zones from Figure 4.23.

Wheel No.	Embankment-Slab track transition			Slab track-Embankment transition		
	Reference	Adjustable fastener	Reduction	Reference	Adjustable fastener	Reduction
1	190.0	130.8	45%	186.4	124.9	49%
2	259.8	135.4	92%	194.0	129.7	50%
3	183.6	133.9	37%	196.1	124.0	**58%**
4	257.6	133.3	**93%**	192.0	123.7	55%

Figure 4.23 shows that the wheel loads are slightly vibrated around 105kN, which is the static wheel load (210/2=105kN); while they are increased considerably at both the embankment-slab track transition and the slab track-embankment transition in the reference case. This indicates the differential settlement lead to the amplification of wheel loads if no adjustable fastener is implemented, which is consistent with [68]. It can also explain the track degradation in transition zones often reported in [7, 9].

PII-IV

In [68], the dynamic responses of a train passing the transition zone (consisting of a ballast track with backfill and a long bridge) were studied. When the different settlement was 10mm, the wheel load of Wheel 1 was increased on 50% the embankment and 64% on the engineering structure in comparison with the static load. In this study, the increases of the wheel load of Wheel 1 are 81% and 152%, respectively, which is comparable with the study in [68]. The discrepancy is mainly caused by the difference in contact settings and the constrain condition of the engineering structures (the slab track in this study is fixed by all the nodes on the bottom layer; while the bridge in [68] is fixed only at the ends of the bridge deck).

Comparing to the reference case, the wheel loads are reduced significantly when adjustable fasteners are in use (see Figure 4.23 and Table 4.2). The reason is that the hanging sleepers in the transition zone are eliminated by the adjustable fasteners. This moment corresponds to the first adjustment of the fasteners in the measured transition zones after the 2-month operation (Section 3). The decrease of the amplified wheel loads (in Figure 4.23 and Table 4.2) explains the substantial reduction of the track settlement growth rate in the measurement after using the adjustable fasteners.

Ballast stress

Since the ballast settlement depends on the ballast stress, the ballast stress in the transition zone is studied as well. It should be noted that the response of unbound granular materials like ballast is non-linear, which affects the calculated distribution of stresses inside the ballast. However, for the transient behaviour analysis in this study, the linear model is used as a first attempt, which is a typical approach, e.g. in [20, 69], due to the limitation of the computational power. Moreover, the ballast bed in this model is assumed to be well compacted (after the rapid compaction). At the moment the sleeper contacting the top of the ballast, the ballast on the top can be simplified as the linear material. In order to compare the ballast responses at the different locations, the ballast elements under one sleeper are considered as a group (unit), which are 416 elements (52*8=416, there are 8 elements on the wide side and 52 elements on the long side, see Figure 4.24).

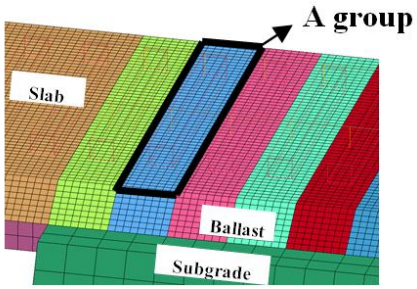

Figure 4.24. Collecting method for ballast stresses. Red lines are sleeper frames.

The vertical stresses in ballast under sleepers are analysed. The average and maximal stresses calculated for the ballast elements in each group along the track are shown in Figure 4.25.

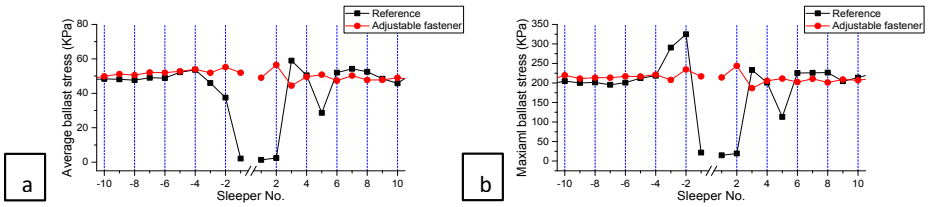

Figure 4.25. Ballast stresses along the track: (a) Average; (b) Maximal

The maximal ballast stress is around 200KPa at the location less affected by the slab track (e.g. Sleeper±10), which is reasonable in comparison with the measurement results in [70]. In [70], the ballast stress was measured during the passage of a coal train with 25t axle load. It is found that the maximal ballast stress was in the range between 160-230kpa (with an outlier at 415kPa due to a wheel-flat).

It also can be seen in Figure 4.25a that, after using the adjustable fasteners, the average of ballast stresses are more evenly distributed along the track. In the reference case, the ballast stress closer to the slab track is lower than that at a greater distance from the bridge. It is because the hanging values of the sleepers are so large that the bending stiffness of rails resists the sleepers to fully contact the ballast. This confirms the finding from the measurement that the settlement at the 1st sleeper is less than that at the 2nd or 3rd sleepers. The stresses in rails at the moment can be expected high which will be discussed later.

Due to the poor support condition, the hanging sleepers can move irregularly, causing the stress concentrations in ballast, which can be proved by Sleeper-2 in Figure 4.25b. The maximal ballast stress reaches 325KPa at Sleeper-2, which is approximately 60% higher comparing to the maximal ballast stress in a well-supported location. The stress distributions in ballast under Sleeper-2 in the two cases are shown in Figure 4.26. The reduction of ballast stresses can be clearly seen from Figure 4.26, where the maximal stress in ballast is reduced from 325KPa to 235KPa. A similar situation can also be found under Sleeper+3, as shown in Figure 4.27, where the maximal stress in ballast is reduced from 233KPa to 187KPa. Since the ballast stress is proportional to the settlement rate of ballast [71, 72], the amplified stress may lead to the permanent settlement in ballast, which indicates the settlement (track degradation) in the transition zone may increase continuously if the adjustable fasteners are not implemented.

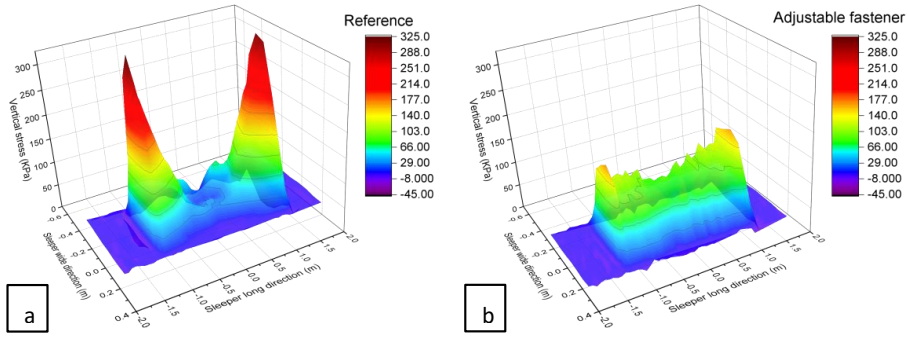

Figure 4.26. Stress distribution in ballast under Sleeper-2: (a) Reference case, (b) Using adjustable fasteners.

PII-IV

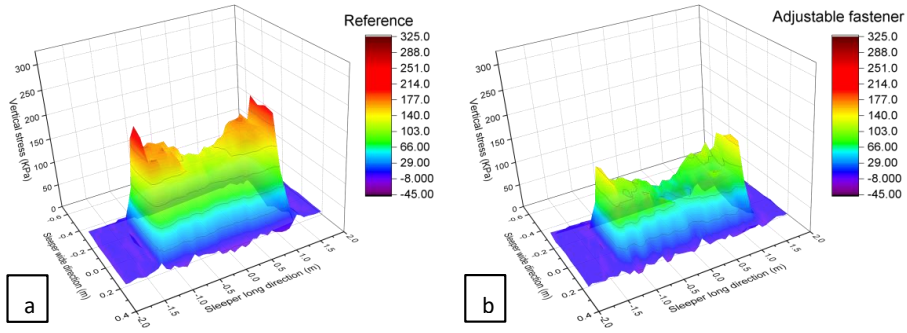

Figure 4.27. Stress distribution in ballast under Sleeper+3: (a) Reference case, (b) Using adjustable fasteners.

Rail stress

The maximal normal stresses in rails in the two cases are shown in Figure 4.28. The rails are simulated by the beam elements with the length of 75mm (eight elements in a sleeper space). As expected, the results show that the normal stresses in rails in the reference case are amplified near the slab track. When the adjustable fasteners are in use, the normal stresses are again decreased significantly. It shows the adjustable fasteners are also beneficial to rails.

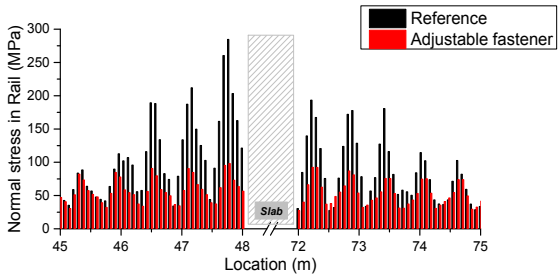

Figure 4.28. Normal stresses in rails in the reference case and the adjustable fastener case.

To conclude, the adjustable fasteners are effective to reduce the amplification of the wheel forces, to achieve a better ballast stress distribution under the hanging sleepers, and to decrease the normal stresses in rails in transition zones.

4.3 Parametric study

Differential settlement value

Since the differential settlement value strongly depends on the material properties of tracks, the construction and operation condition, the differential settlement in transition zones may vary. To study the applicability of the adjustable fasteners, the transition zones with various differential settlements are modelled. Three values of the differential settlement are calculated, including 4mm, 8mm (the reference case in Section 4.2), and 12mm. The wheel forces of Wheel 1 in three cases are compared in Figure4. 29.

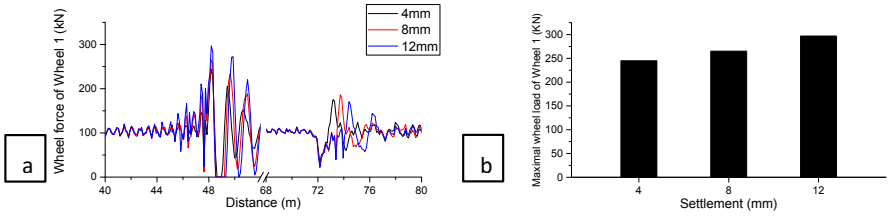

Figure 4.29. Wheel force of Wheel 1 in three cases: (a) Time history; (b) Maximum.

As it can be seen in Figure 4.29, the wheel forces are increased as the differential settlement value grows near the slab track. It indicates that the adjustable fasteners should be used in the early stage of the differential settlement initiation. It should be noted that since the rapid compaction stage (Stage 1 of the settlement in Figure 4.2) is somewhat inevitable, the fasteners should be adjusted as soon as the ballast track is compacted, namely, at the end of Stage 1 or the beginning of Stage 2. Stage 1 of the settlement ends at 0.5MGT according to [16]. Assuming five vehicles in a train, four trains in an operational hour, and fifteen operational hours in a day, it takes approximately twenty days to complete Stage 1 of the settlement.

The transition zones with adjustable fasteners in the cases of 4mm and 12mm are also studied. The wheel forces of Wheel 1 are shown in Figure 4.30. It shows that the adjustable fasteners can significantly reduce the amplification of wheel forces in both cases, which indicates the applicability of the adjustable fasteners is relatively large.

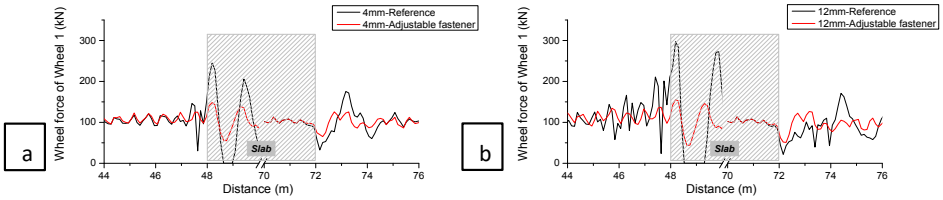

Figure 4.30. Wheel forces of the transition zones using adjustable fasteners: (a) 4mm differential settlement, (b) 12mm differential settlement.

Velocity

The effect of the adjustable fasteners is also studied in the cases of different velocities, including 90km/h, 144km/h (the reference case in Section 4.2) and 198km/h. The wheel forces of Wheel 1 in three cases are shown in Figure 4.31.

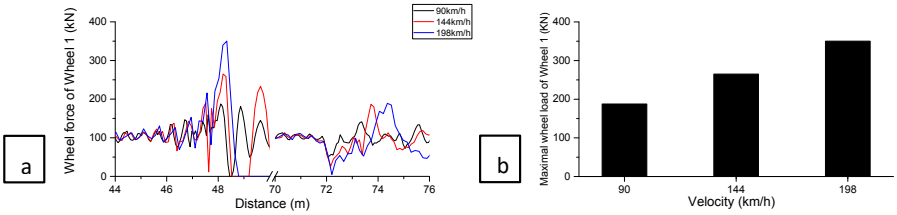

Figure 4.31. Wheel force of Wheel 1 in three cases: (a) Time history; (b) Maximum.

As expected, the wheel forces are amplified significantly near the slab track as the velocity increases, which can be seen in Figure 4.31. The comparison of the wheel forces in the transition zones with and without adjustable fasteners is shown in Figure 4.32.

PII-IV

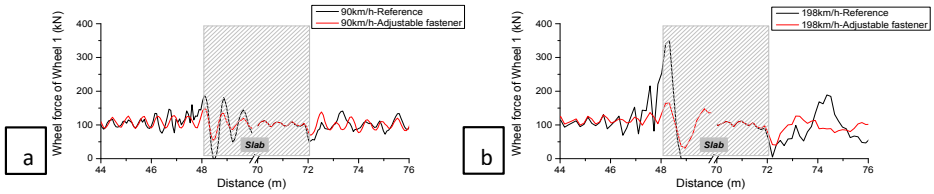

Figure 4.32. Wheel forces of the transition zones using adjustable fasteners: (a) 90km/h, (b) 198km/h.

Figure 4.32 shows the wheel forces are reduced in both cases. A considerable reduction can be found in the case of 198km/h, which is over 50%, from 350kN to 165kN. It indicates that the adjustable fasteners work in both low-velocity and high-velocity range and the benefit is more significant when the velocity is high.

5 Conclusions

The paper presents the experimental and numerical analysis of a corrective countermeasure-the adjustable fastener. Its working principle is to eliminate the gap under the hanging sleepers by adjusting the height of the fastener (relative position of two shims). The following conclusions can be drawn.

(1) Large differential settlements in the three transition zones were found after the 2-month operation, the maximum of which is ranged from 5mm to 11mm. The track settlements near the

engineering structures (slab tracks) were much higher in comparison with that farther from the engineering structures.

(2) The growth rate of the settlement (i.e. degradation rate) of ballast tracks is reduced significantly after the voiding in the track is filled with the adjustable fasteners.

(3) Numerical analysis shows that the adjustable fasteners are effective to reduce the amplification of wheel forces, achieve a better stress distribution in ballast, and decrease the normal stresses in rails in transition zones.

(4) The parametric studies show that the applicability of the adjustable fasteners is relatively wide. The adjustable fastener works effectively at both low-velocity and high-velocity and its benefit is more significant when the velocity is high.

(5) It is recommended that the fasteners should be adjusted once the ballast track is compacted.

Acknowledgement

The authors would like to sincerely thank Jelte Bos (from Movares Nederland B.V) for providing the measurement results, technical details of the adjustable fasteners and comments of the paper. The adjustable fasteners mentioned in the paper is named ShimLift®, developed by Movares Nederland B.V together with BAM Infra Rail BV, and produced by Kampa-International BV. The authors would like to thank Jan Moraal (from TU Delft) for providing the laboratory test report of the adjustable fasteners. The authors would like to thank Network Rail Co. for providing related materials. The authors are very grateful to all reviewers for their thorough reading of the manuscript and their constructive comments.

References

1. Li, D., D. Otter, and G. Carr, Railway bridge approaches under heavy axle load traffic: problems, causes, and remedies. Proceedings of the Institution of Mechanical Engineers, Part F: Journal of Rail and Rapid Transit, 2010. 224(5): p. 383-390.

2. Zuada Coelho, B., Dynamics of railway transition zones in soft soils (Doctoral dissertation). 2011.

3. Varandas, J.N., P. Hölscher, and M.A.G. Silva, Dynamic behaviour of railway tracks on transitions zones. Computers & Structures, 2011. 89(13-14): p. 1468-1479.

4. Hölscher, P. and P. Meijers, Literature study of knowledge and experience of transition zones, in Delft: report. 2007.

5. Sasaoka, C. and D. Davis, Long term performance of track transition solutions in revenue service. Technology Digest TD-05-036, Transportation Technology Center. Inc., Association of American Railroads, 2005.

6. Hyslip, J.P., D. Li, and C. McDaniel. Railway bridge transition case study. in Bearing Capacity of Roads, Railways and Airfields. 8th International Conference (BCR2A'09). 2009.

7. Stark, T.D. and S.T. Wilk, Root cause of differential movement at bridge transition zones. Proceedings of the Institution of Mechanical Engineers, Part F: Journal of Rail and Rapid Transit, 2015.

8. Nicks, J.E., The bump at the end of the railway bridge (Doctoral dissertation). 2009, Texas A&M University.

9. Li, D. and D. Davis, Transition of Railroad Bridge Approaches. JOURNAL OF GEOTECHNICAL AND GEOENVIRONMENTAL ENGINEERING, 2005.

10. Coelho, B., et al., An assessment of transition zone performance. Proceedings of the Institution of Mechanical Engineers, Part F: Journal of Rail and Rapid Transit, 2011. 225(2): p. 129-139.

11. Paixao, A., E. Fortunato, and R. Calcada, Design and construction of backfills for railway track transition zones. Proceedings of the Institution of Mechanical Engineers, Part F: Journal of Rail and Rapid Transit, 2013. 229(1): p. 58-70.

12. Sato, Y., Japanese Studies on Deterioration of Ballasted Track. Vehicle System Dynamics, 1995. 24(sup1): p. 197-208.

13. Shenton, M., Ballast deformation and track deterioration. Track technology, 1985: p. 253-265.

14. Indraratna, B., D. Ionescu, and H.D. Christie, Shear Behaviour of Railway Ballast based on Large Scale Triaxial Testing. JOURNAL OF GEOTECHNICAL AND GEOENVIRONMENTAL ENGINEERING, 1998: p. 439-449.

15. Varandas, J.N., P. Hölscher, and M.A.G. Silva, A Settlement Model for Ballast at Transition Zones. Proceedings of the Tenth International Conference on Computational Structures Technology, 2010.

16. Selig, E.T. and J.M. Waters, Track geotechnology and substructure management. 1994: Thomas Telford.

17. Gerber, U. and W. Fengler, Setzungsverhalten des Schotters (in German). ETR. Eisenbahntechnische Rundschau, 2010. 59(4): p. 170-175.

18. Wang, H. and V. Markine, Analysis and improvement of the dynamic track behaviour in transition zone, in Tenth International Conference on the Bearing Capacity of Roads, Railways and Airfields, L.e. al., Editor. 2017, Taylor & Francis Group, London: Athens, Greece.
19. Wang, H., et al., Analysis of the Dynamic Behaviour of a Railway Track in Transition Zones With Differential Settlement, in 2015 Joint Rail Conference, San Jose, California, USA, March 2015. 2015. p. 7.
20. Banimahd, M., et al., Behaviour of train–track interaction in stiffness transitions. Proceedings of the ICE - Transport, 2012. 165(3): p. 205-214.
21. Lundqvist, A. and T. Dahlberg, Load impact on railway track due to unsupported sleepers. Proceedings of the Institution of Mechanical Engineers, Part F: Journal of Rail and Rapid Transit, 2005. 219(2): p. 67-77.
22. Sañudo, R., V. Markine, and L. Dell'Olio, Optimizing track transitions on high speed lines. IAVSD2011, 2011.
23. Gallego Giner, I. and A. López Pita, Numerical simulation of embankment–structure transition design. Proceedings of the Institution of Mechanical Engineers, Part F: Journal of Rail and Rapid Transit, 2009. 223(4): p. 331-343.
24. Insa, R., et al., Analysis of the influence of under sleeper pads on the railway vehicle/track dynamic interaction in transition zones. Proceedings of the Institution of Mechanical Engineers, Part F: Journal of Rail and Rapid Transit, 2011. 226(4): p. 409-420.
25. Alves Ribeiro, C., et al., Under sleeper pads in transition zones at railway underpasses: numerical modelling and experimental validation. Structure and Infrastructure Engineering, 2014. 11(11): p. 1432-1449.
26. Dahlberg, T., Railway Track Stiffness Variations-Consequences and Countermeasures. International Journal of Civil Engineering, 2010. 8(1).
27. Shahraki, M., C. Warnakulasooriya, and K.J. Witt, Numerical study of transition zone between ballasted and ballastless railway track. Transportation Geotechnics, 2015. 3: p. 58-67.
28. Sañudo, R., et al., Track transitions in railways: A review. Construction and Building Materials, 2016. 112: p. 140-157.
29. Puppala, A.J., et al., Recommendations for design, construction, and maintenance of bridge approach slabs: Synthesis report, in Rep. No. FHWA/TX-09/6022. 2009.
30. Shan, Y., B. Albers, and S.A. Savidis, Influence of different transition zones on the dynamic response of track–subgrade systems. Computers and Geotechnics, 2012. 48: p. 21-28.
31. Kaewunruen, S. Dynamic responses of railway bridge ends: A systems performance improvement by application of ballast glue/bond.
32. Horníček, L., et al., An investigation of the effect of under-ballast reinforcing geogrids in laboratory and operating conditions. Proceedings of the Institution of Mechanical Engineers, Part F: Journal of Rail and Rapid Transit, 2010. 224(4): p. 269-277.
33. Woldringh, R.F. and B.M. New. Embankment design for high speed trains on soft soils.
34. Read, D. and D. Li, Design of track transitions. TCRP Research Results Digest 79, 2006.
35. Sasaoka, C.D. and D.D. Davis, Implementing Track Transition Solutions for Heavy Axle Load Service, in AREMA 2005 Annual Conference. 2005: Chicago.
36. Namura, A. and T. Suzuki, Evaluation fo countermeasures against differential settlement at track transitions. QR of RTRI, 2007. 48(3).

37. Varandas, J.N., Long-Term Behaviour of Railway Transitions under Dynamic Loading Application to Soft Soil Sites (Doctoral dissertation). 2013.
38. Coelho, Z., Dynamics of railway transition zones in soft soils. 2011.
39. Markine, V., H. Wang, and I. Shevtsov. Experimental Analysis of the Dynamic Behaviour of a Railway Track in Transition Zones. in Proceedings of the Ninth International Conference on Engineering Computational Technology, P. Iványi and B.H.V. Topping, (Editors), Civil-Comp Press, Stirlingshire, United Kingdom, paper 3, 2014. 2014.
40. Le Pen, L., et al., The behaviour of railway level crossings: insights through field monitoring. Transportation Geotechnics, 2014. 1(4): p. 201-213.
41. Claisse, P. and C. Calla. Rail ballast: conclusions from a historical perspective. London: Published for the Institution of Civil Engineers by Thomas Telford Services, 1992-.
42. NetworkRail. Pictures from Network Rail. 2016; Available from: https://www.networkrail.co.uk/.
43. Esveld, C., Modern railway track. Vol. 385. 2001: MRT-productions Zaltbommel, The Netherlands.
44. Tutumluer, E., et al. Investigation and mitigation of differential movement at railway transitions for US high speed passenger rail and joint passenger/freight corridors. in 2012 Joint Rail Conference. 2012. American Society of Mechanical Engineers.
45. Stark, T.D., S.T. Wilk, and T.R. Sussmann, Evaluation of tie support at transition zones. Transportation Research Record: Journal of the Transportation Research Board, 2015(2476): p. 53-58.
46. Anderson, W.F. and A.J. Key, Model testing of two-layer railway track ballast. Journal of geotechnical and geoenvironmental engineering, 2000. 126(4): p. 317-323.

47. Muramoto, K., T. Nakamura, and T. Sakurai, A study of the effect of track irregularity prevention methods for the transition zone between different track structures. Quarterly Report of RTRI, 2012. 53(4): p. 211-215.
48. Moraal, J., Dynamische beproeving ShimLift bevestiging op NS90 ligger, in TU Delft Report. 2013, TU Delft.
49. CEN(European-Committee-for-Standardization), Railway applications - Track - Test methods for fastening systems - Part 9: Determination of stiffness. 2009. p. 30.
50. Wageningen, U. and Research, Dutch soil map, part of the Fertilizer Act 2012 - WUR.
51. Bos, J. and J. Jansen, Evaluation of ShimLift pilots Evaluating. 2013.
52. Wang, H., V. Markine, and X. Liu, Experimental analysis of railway track settlement in transition zones. Proceedings of the Institution of Mechanical Engineers, Part F: Journal of Rail and Rapid Transit, 2017: p. 0954409717748789.
53. Lei, X. and L. Mao, Dynamic response analyses of vehicle and track coupled system on track transition of conventional high speed railway. Journal of Sound and Vibration, 2004. 271(3-5): p. 1133-1146.
54. Banimahd, M. and P.K. Woodward, 3-Dimensional Finite Element Modelling of Railway Transitions. 9th International Conference on Railway Engineering, 2007.
55. Zhai, W.M. and H. True, Vehicle-track dynamics on a ramp and on the bridge: simulation and measurement. Vehicle System Dynamics, 1999. 33(Supply): p. 11.
56. Plotkin, D. and D. Davis, Bridge approaches and track stiffness. 2008.

57. H. Wang, et al., Analysis of the Dynamic Behaviour of a Railway Track in Transition Zones With Differential Settlement, in 2015 Joint Rail Conference, San Jose, California, USA, March 2015. 2015. p. 7.

58. Wang, H., V.L. Markine, and I.Y. Shevtsov. The Analysis of Degradation Mechanism in Track Transition Zones using 3D Finite Element Model. in Proceedings of the Second International Conference on Railway Technology: Research, Development and Maintenance, J. Pombo,(Editor), Civil-Comp Press, Stirlingshire, United Kingdom, paper 227, 2014. doi: 10.4203/ccp. 2014.

59. Chen, R., et al., Degradation mechanism of CA mortar in CRTS I slab ballastless railway track in the Southwest acid rain region of China–Materials analysis. Construction and Building Materials, 2017. 149: p. 921-933.

60. Chen, R., et al., The Continuous-Slab-Track Coupling Laws between the Bridge and Track under Temperature Loads. Journal of Railway Engineering Society, 2017. 34(3): p. 15-21.

61. Iwnick, S., Manchester Benchmarks for Rail Vehicle Simulation. Vehicle System Dynamics, 1998. 30(3-4): p. 295-313.

62. Wan, C., V.L. Markine, and I.Y. Shevtsov, Improvement of vehicle–turnout interaction by optimising the shape of crossing nose. Vehicle System Dynamics, 2014. 52(11): p. 1517-1540.

63. Knothe, K. and S. Grassie, Modelling of railway track and vehicle/track interaction at high frequencies. Vehicle system dynamics, 1993. 22(3-4): p. 209-262.

64. Hallquist, J.O., LS-DYNA Keyword User's Manual. 2007: LSTC Co., Livermore, CA.

65. Hallquist, J.O., LS-DYNA theory manual. Livermore software Technology corporation, 2006. 3: p. 25-31.

66. Oregui, M., Z. Li, and R. Dollevoet, An investigation into the modeling of railway fastening. International Journal of Mechanical Sciences, 2015. 92: p. 1-11.

67. K. Nguyen, J.M.G.a.F.G., Dynamic effect of high speed railway traffic loads on the ballast track settlement. Congresso de Métodos Numéricos em Engenharia, 2011.

68. Paixao, A., E. Fortunato, and R. Calcada, A numerical study on the influence of backfill settlements in the train/track interaction at transition zones to railway bridges. Proceedings of the Institution of Mechanical Engineers, Part F: Journal of Rail and Rapid Transit, 2015.

69. Shi, J., et al., Measurements and simulation of the dynamic responses of a bridge-embankment transition zone below a heavy haul railway line. Proceedings of the Institution of Mechanical Engineers, Part F: Journal of Rail and Rapid Transit, 2012. 227(3): p. 254-268.

70. Indraratna, B., et al., Field assessment of the performance of a ballasted rail track with and without geosynthetics. Journal of Geotechnical and Geoenvironmental Engineering, 2010. 136(7): p. 907-917.

71. Sato, Y. Optimization of track maintenance work on ballasted track. in Proceedings of the World Congress on Railway Research (WCRR'97), B. 1997.

72. Dahlberg, T., Some railroad settlement models—a critical review. Proceedings of the Institution of Mechanical Engineers, Part F: Journal of Rail and Rapid Transit, 2001. 215(4): p. 289-300.

PII-IV

Paper V

Analysis of the Dynamic Wheel Loads in Railway Transition Zones Considering the Moisture Condition of the Ballast and Subballast

Haoyu Wang[1, 2,*], Mika Silvast[2], Valeri Markine[1] and Bruce Wiljanen[2]

[1]Delft University of Technology, Delft, the Netherlands;

[2]Roadscanners Oy, Tampere, Finland;

Published by Applied Sciences, 7(12), p.1208.

Abstract

Transition zones in railway tracks are the locations with considerable changes in vertical support structures, e.g. near bridges. Due to possible water flow constrictions in transition zone structures, there is frequently an increased moisture level in the ballast/subballast layers, which is a potential source of track degradation. This paper presents results of the moisture condition measured in three transition zones using ground penetrating radar, where the ballast/subballast are analyzed. The relationship between the moisture condition and track degradation in the transition zones is studied by comparing to the longitudinal track level measured by the track inspection coaches. A strong connection is found between the high moisture condition and track degradation in the transition zones. The dynamic behaviour of the transition zones with high moisture condition is analyzed using the Finite Element method. Differential stiffness and settlement are taken into consideration in the transition zone model, which is also coupled with a vehicle. The ballast/subballast layers are modelled as solid elements. Increased moisture conditions are considered as a reduction of elastic modulus according to laboratory findings. Results show that high moisture leads to an increase of dynamic wheel loads in the transition zone, which explains the connection and confirms that high moisture condition is a source of transition zone problems.

Keywords

Bridge transition zone; Railway; Moisture condition; Ballast; Finite element method; Track degradation

1 Introduction of Transition Zones

Transition zones in railway track network are locations with considerable changes in track support structures. Typically, they are located near concrete structures, such as bridges, culverts and tunnels. An example of a bridge transition zone is shown in Figure 5.1.

Figure 5.1. A typical bridge transition zone.

The track geometry in transition zones degrades at a much faster rate than that of open tracks [1-4], which results in the appearance of a "dip" [5]. This phenomenon has been confirmed by a survey of the performance of track transition zones, which revealed that 51% of the track transition zones had experienced such a settlement [6]. In the field measurement of a bridge transition zone [4], the rail displacements on multiple locations were measured during train passages. Results showed a 5.1mm deep dip in the ballast track. A dip was also found in the transition zone of level crossing in [7], which was 5.3mm in depth.

Such large geometry irregularity leads to an increase of dynamic wheel loads [8] and the redistribution of dynamic wheel loads [3]. The increased dynamic wheel loads may damage track components, for example [1-3, 6, 9-17]:

- rail surface defects and cracks in the rail foot,
- broken fasteners, cracks in concrete sleepers,
- breakage of ballast particles and voids between sleepers and ballast, also known as hanging sleepers.

It also initiates further deterioration of track geometry, causing a self-perpetuating system [15, 17-21]. Increased dynamic wheel loads can result in worsening of the passenger's comfort [18], and can even create a potential for train derailment.

As a result, transition zones require more maintenance, like tamping and adding ballast, as compared to open tracks [11, 22]. For instance, in the Netherlands, maintenance activities on the track in transition zones are performed up to 4-8 times more often than on open tracks [14, 23]. In the US, $200 million is spent annually on maintenance of the track in transition zones, while in Europe, about €97 million is spent on similar maintenance activities [24, 25].

The major factors causing transition zone problems can be divided into three categories [1, 6, 22]:

- Significant abrupt changes in the vertical stiffness of the track;
- Differential settlement or uneven profile of the ballast track, which inherently settles more than a concrete structure;
- Geotechnical issues, such as poor drainage conditions and poor quality of materials.

Many studies have been conducted to analyse the former two factors in transition zones, such as in [6, 8, 11, 17]. A thorough review can be found in [26]. The geotechnical factor has been studied less, which is mainly due to the limitations of measurement methods. For instance, the inspection of the ballast quality was typically conducted by excavating samples from ballast layers, which is costly, destructive, and needs track possession time.

Moisture condition of the ballast may play an important role in the rapid degradation of tracks and consequently geometry irregularities. Excess water in substructures significantly reduces (around 50%) the resilience of tracks [27, 28] and increases (around 40%) track settlement

[29-31]. The loss in resilient modulus and the increase of settlement have significant implications for transient vertical displacements and track performance.

This paper presents an experimental analysis of the moisture condition to explore the relationship between moisture and track condition in transition zones. In total, three transition zones of various conditions are analysed. The moisture condition in the transition zones is measured by the use of ground penetrating radar (GPR) [32, 33], which is compared to the track geometry measured by inspection coaches. The relationship between moisture condition and geometry irregularity is analysed.

Transition zones in high moisture condition are numerically studied using the Finite Element (FE) method. The transition zone model accounts for differential stiffness and settlement at the same time, which is developed in [8, 34] and validated in [35]. Ballast and subballast layers are modelled as solid elements and high moisture conditions are considered as a reduction of elastic modulus. The wheel loads of the transition zone in the high moisture case are compared with a reference case to analyse the effect of moisture conditions.

The paper is organised as follows. Research for the moisture condition in ballast is reviewed in Section 2. The experimental study of the moisture condition in transition zones is presented in Section 3. In Section 4, the transition zone in high moisture condition is analysed using the FE method. Finally, conclusions are given in section 5.

2 Review of the Mechanism of Saturated Ballast

Drainage, as one of the most important functions of track structure, can intercept subsurface water entering the area of the track substructure, intercept surface water approaching the track structure from sides, and remove water draining out of the ballast and subballast [36].

There are three sources of water entering the track substructure: precipitation falling onto the tracks, water flowing down along adjacent slopes, and water seeping upward from the subgrade [36]. The track structure is designed to provide an adequate drainage function. However, due to the special structure in transition zones, e.g. abutment, the water may not be drained efficiently. The excess water in the substructure significantly reduces the resilience [27, 28] and increases the settlement [29-31, 36] of tracks. The problem becomes particularly severe when the substructure reaches a saturated state, leading to considerable increases in track maintenance costs [27, 36].

The resilient modulus of most untreated granular materials has a notable dependence on moisture content, where the modulus decreases with the growth of saturation level [27]. For instance, in [37], a 50% decrease in resilient modulus in the gravel was observed as the degree of saturation increased from 70% to 97%. A field measurement using seismic surface waves in [28] found a 50% decrease of (fouled) ballast modulus when the ballast is saturated. The reason is due to the excess pore-water pressure developed by the saturated granular materials under repeated loading. As the pore-water pressure develops, the effective stress in ballast decreases with a subsequent reduction in both strength and stiffness of ballast bed [27].

3 Experiment Analysis of Transition Zones

Although poor drainage condition is considered as one reason for the track degradation in transition zones, it has not been experimentally analysed in detail in the field. This section presents the measurement of moisture condition in transition zones using GPR. The relationship between moisture condition and track geometry is also studied.

3.1 Introduction of GPR

GPR uses a radio wave source to transmit a pulse of electromagnetic energy into the inspected medium [33]. Its principle in railway measurements is shown in Figure 5.2. GPR is an effective and non-invasive tool for mapping railway structures and analysing subsurface conditions. The reflected energy, originating from the interfaces between materials of different dielectric properties, is received and recorded for analysis. GPR data consists of changes in reflection amplitude, changes in the arrival time of specific reflections, and signal attenuation [32, 38]. The method provides a continuous profile of the thickness and properties of railway

structures, which can be used to analyse the quality of track substructures, such as the moisture susceptibility of ballast and subballast, fouling of ballast, layer deformation and mud pumping [39-41].

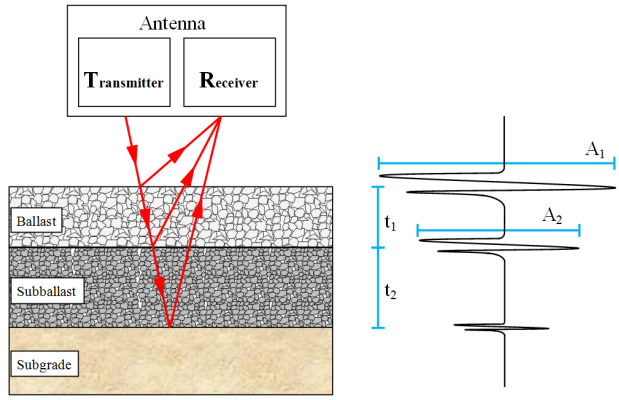

Figure 5.2. Measuring principle of GPR. A_1 stands for the amplitude of the reflection between the sleeper and ballast; A_2 stands for the amplitude of the reflection between the ballast and subballast; t_1 stands for the travel time in ballast; t_2 stands for the travel time in subballast.

GPR measurements for this case study were performed using a GSSI SIR-30 GPR system, manufactured by Geophysical Survey Systems Inc, including a 400 MHz antenna attached to a VR-Track Ltd Tka-8 maintenance engine, as illustrated in Figure 5.3.

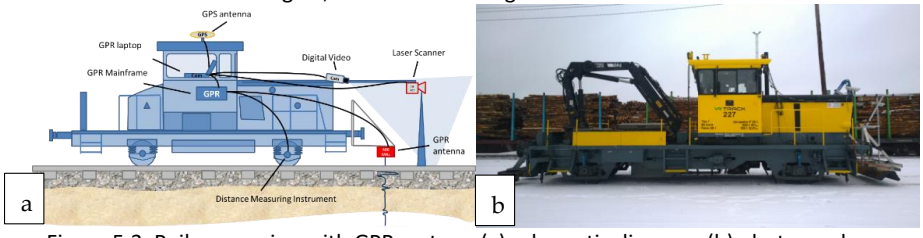

Figure 5.3. Railway engine with GPR system: (a) schematic diagram; (b) photograph.

The GPR antenna can be lifted to 0.3m above the sleeper level and the maximum survey speed is up to 160km/h, depending on data collection settings. Data collection rate was controlled by a distance measurement instrument. During the survey, GPS coordinates and digital video were recorded using Rail Doctor™ Camlink software. The processing, visualization, interpretation and analysis of the GPR data are performed using the Rail Doctor software (version 3.2). The measurement system has been calibrated against sample analysis [38] and pit tests [39]. A screenshot from the recorded video is shown in Figure 5.4a, wherein a transition zone consisting of embankment and a bridge can be found. A measurement result from GPR at the corresponding location is shown in Figure 5.4b. The right axis of Figure 5.4b indicates the depth, in meters, beneath the top of sleepers (or below rails). The ballast layer is located from 0m to 0.6m below rails, where the ballast at 0m-0.25m is between sleepers and 0.25m-0.6m is below sleepers. The subballast is located from 0.6m to 1.2m, and below 1.2m is embankment and subgrade. It should be noted that sleepers are filtered during the data processing to obtain a better visualization of the data. The lateral axis of Figure 5.4b is the distance or location, which is in the form of "km+m". The two sides of the bridge in a transition zone are named as the embankment-bridge side and the bridge-embankment side in the paper depending on the train moving direction. The moving directions of the results presented in this paper are all from left to right. Therefore, the embankment-bridge side is always on the left side of bridges (before the bridges) and the bridge-embankment side on the right side (after the bridges).

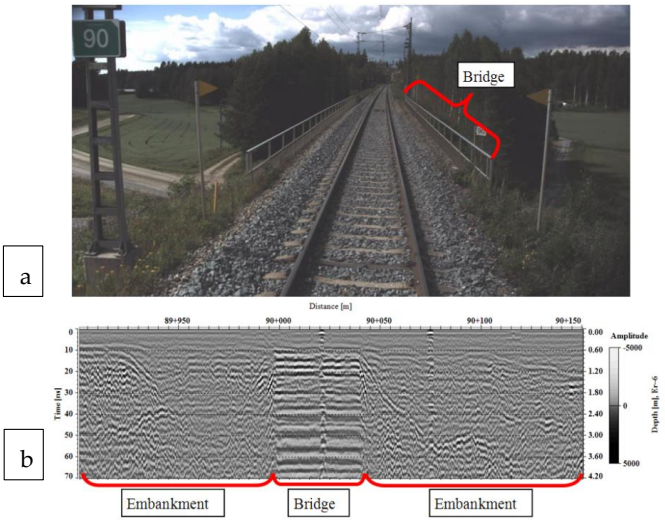

Figure 5.4. Measurement results: (a) the digital video; (b) the GPR data.

Dielectric properties decide the amplitude, arrival time, and signal attenuation of reflections and they are different with a higher content of fines and water [42]. The dielectric constant and the velocity of the signal in various materials are shown in Table 5.1 [43]. This difference can be detected by analysing the GPR signal [38, 43, 44]. As a result, the distribution of the relative moisture susceptibility in ballast and subballast can be obtained.

Table 5.1. Dielectric constant and the velocity of the signal in various material from [43].

Material	Dielectric constant	Velocity (m/s)
Air	1.0	3E8
Dry spent ballast	4.3	1.45E8
Wet spent ballast (5% water)	7.8	1.07E8
Saturated spent ballast	38.5	0.58E8
Water	81.0	0.33E8

In the post-process stage, measurement results are transformed into frequency-domain data and parameterized by means of a sliding calculation window in depth and longitudinal directions using the windowed Fourier transform (WFT) [39]. Results are then visualised as a colour-coded image, wherein the strong reflections (blue) indicate high moisture susceptibility and weak reflections (red) low. This method has been calibrated and utilized in [39, 45, 46]. A comparison of two moisture profiles is shown in Figure 5.5.

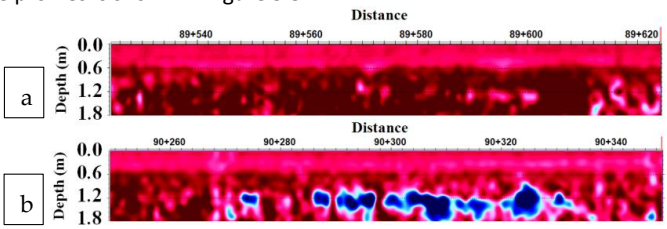

Figure 5.5. Moisture profiles: (a) low moisture; (b) high moisture.

3.2 Measurement Results

The moisture condition of three bridge transition zones on a Finnish railway line was measured using GPR. To study the effect of the moisture condition, the longitudinal level (rail height) measured by track inspection coaches in a similar time period using a 5m-chord method was also collected.

Measurement results of an open track section are shown in Figure 5.6 as a reference case. A photo of the track is shown in Figure 5.6a, the moisture profile in Figure 5.6b and longitudinal level (rail height) in Figure 5.6c. The vertical axis of the moisture profile (Figure 5.6b) indicates the depth under rails in meters. Although the subballast layer ideally ends 1.2m, it often settles deeper, especially in transition zones. As a result, the measurement results are collected down to 1.8m. The ballast, subballast and subgrade are dry, as indicated by the red colour of the moisture profile. The irregularity of the longitudinal track level is less than 2mm, which is relatively small.

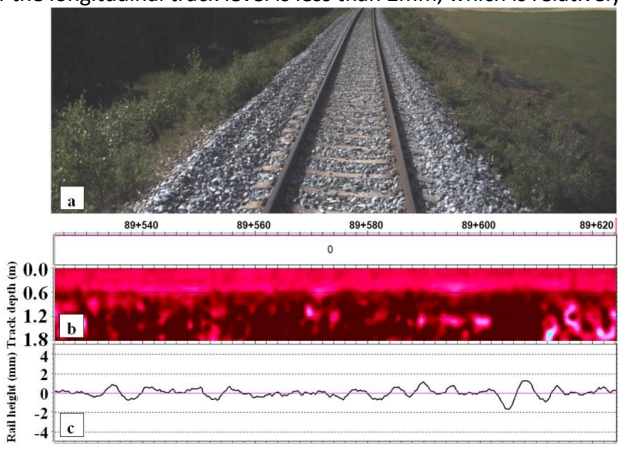

Figure 5.6. Measurement results of open track: (a) photograph of the track; (b) the moisture profile; (c) the longitudinal track level.

Measurement results from Transition Zone A are shown in Figure 5.7. This transition zone is composed of embankment and a 41m long concrete bridge. The photo of the bridge taken by the on-board video camera (Figure 5.3) during the GPR measurements is shown in Figure 5.7a. The ballast is laid on the bridge, the depth of which is around 0.6m beneath rails. GPR data from the concrete bridge is out of the focus of this study and therefore blocked out. Approach slabs are employed at both ends of the bridge. The slabs are made of concrete and laid diagonally from the ballast layer to the subballast layer.

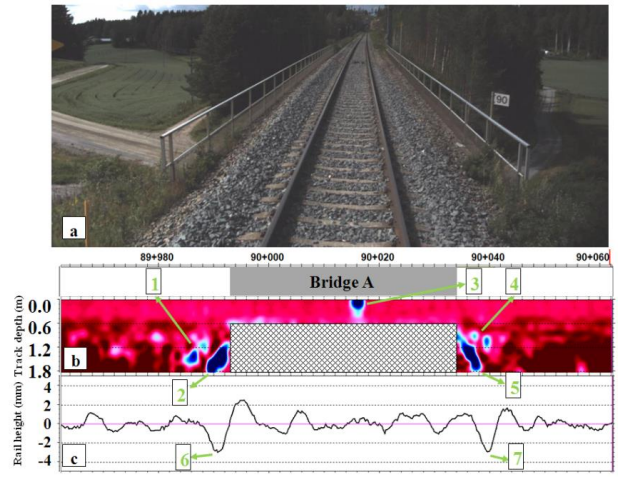

Figure 5.7. Measurement results of Transition Zone A.

Moisture susceptibility increases before and after the bridge, as can be seen from Figure 5.7 (see the blue zones indicated by No. 1 and No. 4). The blue zones of No. 2 and No. 5 are caused by approach slabs, since the concrete has a similar expression as highly susceptible moisture areas

after post-processing. Likewise, the blue zone from No. 3 is caused by a section of rail, as shown in Figure 5.8.

Figure 5.8. Section of rail in Transition Zone A.

Figure 5.7c shows that the irregularity of the track increases significantly before and after the bridge (indicated by No. 6 and No. 7), which reached 3.0mm and 2.9mm, respectively. These two irregularities indicate the appearance of differential track settlement, which agrees with dips found in other transition zones, such as in [4, 6, 7]. Transition Zone A has both increased moisture susceptibility and track irregularity based on the moisture profile and the longitudinal track level data on both ends of the bridge.

Measurement results of two more transition zones (named as Transition Zone B and Transition Zone C) are shown in Figure 5.9 and Figure 5.10. Their structures are similar to that of Transition Zone A.

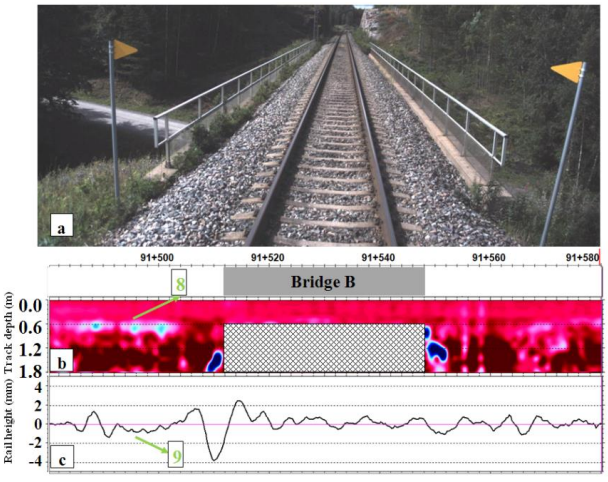

Figure 5.9. Measurement results of Transition Zone B.

Moisture susceptibility increases before the bridge in Transition Zone B. The blue area No. 8 (Figure 5.9) appears at the interface between the ballast layer and the subballast layer, which implies that the water is held at the bottom of the ballast and the drainage system is in poor condition. This is most likely one of the reasons for the track irregularity in the corresponding location (No. 9). However, no significant increase of the moisture can be found above the approaching slab yet a large dip appears in the corresponding location. This irregularity could be caused by other reasons, such as rail defect.

In the bridge-embankment side of Transition Zone B, the moisture in the ballast and the subballast layer is relatively low. As expected, the track geometry at the corresponding location is much smoother, as shown in Figure 5. 9c.

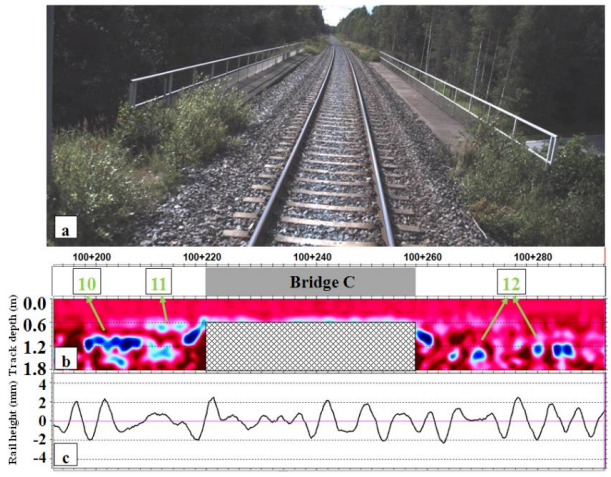

Figure 5.10. Measurement results of Transition Zone C.

Transition Zone C is in worse condition than Transition Zones A and B. The moisture susceptibility of the ballast and the subballast is significantly increased both at the bottom of ballast (No. 11) and bottom of subballast (No. 10 and No. 12) as seen in Figure 5.10b. Severe track irregularity also appears through the entire transition zone, as shown in Figure 5.10c.

In summary, high moisture areas appear mostly before and after the bridges in all transition zones. They can be detected sometimes at the bottom of the ballast layer, bottom of subballast layer, and above the abutments. Track irregularities can also be found at corresponding locations, which implies a connection between high moisture condition and track degradation. When the moisture is high, the track irregularities are higher (see the embankment-bridge side of Transition Zone C, in Figure 5.10); when the moisture is low, the track irregularities are also low (see the bridge-embankment side of Transition Zone B, Figure 5.9).

Since the theoretical findings in Section 2 suggest that high moisture in ballast leads to a reduction of stiffness, the high moisture in the structure can be considered as one of the sources for the extra degradation in transition zones. It should be noted that the high moisture is not the only source leading to the extra degradation, for instance, the large track irregularity above the approaching slab in the embankment-bridge side in Transition Zone B (Figure 5.9) is not caused by the moisture condition.

PII-V

4 Finite Element Analysis of Transition Zones with High Moisture

Since a strong connection between the high moisture condition and track degradation is found from field measurement data, this section aspires to explain the connection using the FE method. The dynamic behaviour of transition zones with high moisture condition is analysed.

4.1 Introduction of the Finite Element Model

The FE model considering both the differential stiffness and settlement in transition zones is introduced in the section. The model used in this paper is based on the model proposed in [47] and further developed in [8, 34]. The model consists of two ballast tracks and one track on the bridge in the middle, as shown in Figure 5.11. It is possible to analyse both the embankment-bridge and the bridge-embankment sides of the transition zone with a single calculation. In this model the “bridge” is symbolical, which is simplified to reduce the calculation costs.

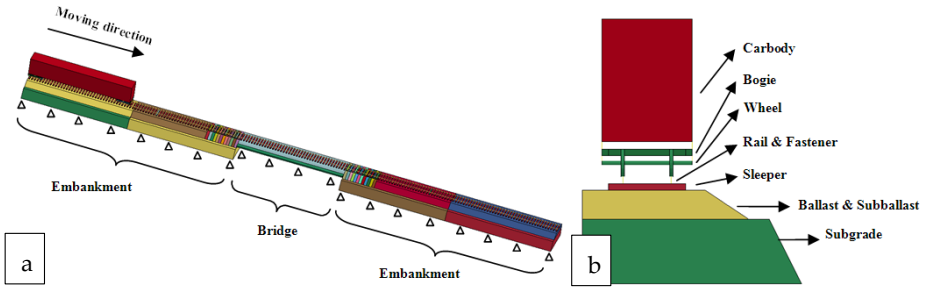

Figure 5.11. FE model of the track transition zone: (a) full view; (b) cross-section of ballast track.

The length of ballast track is 48 m (one on each side) and the bridge is 24 m. Components of the ballast track are rails, fasteners, sleepers, ballast, and subgrade. The rails are modelled as beam elements with the cross-sectional and mass properties of UIC54 rails. Spring and damper elements between the rails and sleepers are used to model fasteners. The springs have bilinear properties in the vertical direction so that they have the stiffness of rail pads in compression, while the stiffness is much higher to simulate the clamping effect of fasteners in tension. Ballast, sleepers, and subgrade are modelled using fully integrated solid elements with elastic material properties. The ballast and subballast are considered as one layer, which is 0.9 m deep. There is no ballast between sleepers since its effect on settlement is negligible. It should be noted that the ballast, subballast and subgrade are simplified in the model. Despite the fact that the responses of unbound granular materials such as ballast, subballast, and subgrade can be more accurately modelled using nonlinear constitutive models, simplifications have to be adopted in the large-scale study (e.g., transition zones) to reduce the computational expense. Many studies (e.g., [10, 48-53]) have proved that some behaviour of ballast and hanging sleepers can be modelled accurately using simplified methods (e.g., solid elements with elastic material properties). Following [10, 48-53], the ballast and subgrade in this model are also modelled by solid elements with elastic material properties. The element length of 75 mm is used for the sleepers and the ballast (there are eight elements within one sleeper space). The thickness of the subgrade is 2 m.

The vehicle model is idealized as a multibody system consisting of one body, two bogies, and four wheelsets. The wheelsets are named Wheel 1 to 4 from the right to the left. Wheel 1 and 2 belong to the front bogie and the Wheel 3 and 4 belong to the rear bogie. Primary and secondary suspensions are modelled by spring-damper elements. The parameters are suggested by literature (vehicle parameters by [11, 54, 55], track parameter by [10, 49, 54, 56]), and are then tuned according to field measurements [35]. The axle load of the vehicle is 19.0 t and velocity is 144 km/h. Material properties of the track components and vehicle used in the model are collected in Table 5.2.

Table 5.2 Material properties of the track components.

Parameter	Value
Sleeper Elastic Modulus (Pa)	3.65E+10
Sleeper Poisson's ratio	0.167
Ballast Elastic Modulus (Pa)	1.20E+08
Ballast Poisson's ratio	0.250
Subgrade Elastic Modulus (Pa)	1.80E+08
Subgrade Poisson's ratio	0.250
Concrete bridge Elastic Modulus (Pa)	3.50E+10
Concrete bridge Poisson's ratio	0.167
Fastening system horizontal stiffness (N/m)	1.5E6
Fastening system horizontal damping (N*s/m)	5.00E4
Fastening system longitudinal stiffness (N/m)	1.5E6

Fastening system longitudinal damping (N*s/m)	5.00E4
Fastening system vertical (compression) stiffness (N/m)	1.20E8
Fastening system vertical (compression) damping (N*s/m)	5.00E4
Fastening system vertical (tension) stiffness (N/m)	1.20E11
Fastening system vertical (tension) damping (N*s/m)	5.00E4
Distance between wheels (m)	2.5
Distance between axles (m)	20.0
Length of train body (m)	23.0
Primary suspension stiffness (N/m)	4.25E5
Primary suspension damping (N*s/m)	1.00E6
Secondary suspension stiffness (N/m)	4.68E5
Secondary suspension damping (N*s/m)	6.50E4
Secondary suspension Bending stiffness (Nm/rad)	1.05E4

The contact between wheels and rails is modelled using the linear Hertzian spring [56]. Silent boundaries are applied on both ends of the model in order to reduce the wave reflection effect. The nodes at the bottom of the subgrade and bridge are fixed.

The model considers differential settlement between the bridge and ballast track on both sides. After construction or tamping, ballast tracks will be compacted within a short period [36, 57-59]. In this period, the large settlement appears in ballast tracks due to the volumetric compaction of particles. On the contrary, the tracks on bridges are barely settled, which generates a differential settlement in transition zones. It should be noted that the value of the differential settlement is important, but is difficult to measure precisely in reality. For instance, the void under sleepers measured in [11] had an error of 3 mm. The value of the differential settlement that is used in the paper is selected from the range of values that are frequently reported in field measurements of transition zones [14, 23], which is 2–10 mm. A value of 4 mm is used, since it can represent the early period of a transition zone. Dynamic responses are expected to be larger for higher differential settlement values.

The nonlinear connection between sleepers and ballast is important for modelling of the ballast degradation mechanism [48, 53]. In the case of hanging sleepers, the sleepers should generate a nonlinear interaction force to the ballast under compression and separable without loading [53]. Therefore, contact elements are applied between sleepers and ballast. According to the penalty algorithm that is employed in the contact elements, the search for penetrations between the bottom surface of sleepers and the top surface of ballast is made for every time step during the calculation. When penetration has been detected, a force that is proportional to the penetration depth is applied to resist and ultimately eliminate the penetration [60]. This method allows for simulating the impact on ballast, which is proportional to the downward acceleration of sleepers.

The simulation procedure consists of two phases. First, only the gravity forces are applied to the model. When the model reaches the equilibrium state, the velocity is applied to the vehicle, so that the vehicle moves from the left end to the right end of the transition zone passing the bridge. The mass-weighted nodal damping is applied globally to the nodes and the track's random irregularity is not considered in this model. The model is solved using the commercial software LS-DYNA, version R8, developed by Livermore Software Technology Corporation, CA 94551, the US, 2015. The time-step is 1.3 ×10-5 s, and the calculation takes approximately 10 h using an 8-core (I7) workstation with High Parallel Computing (HPC).

The model was validated against field measurements in [35]. The comparison between the simulated rail displacements and the calculated measurement displacements is shown in Figure 5.12. Rails from a close location (above the 2nd sleeper) and a far location (above the 11th sleeper), with respect to the bridge, are both compared. The measurement was performed using a Digital Image Correlation-device [4]. Results are filtered using a low-pass filter with cut-off frequency of 35 Hz. It should be noted that the model is tuned according to the measured

transition zone. As it can be seen from Figure 5.12, the simulation results are in a good correlation with the measurement data both in the time and the frequency domains.

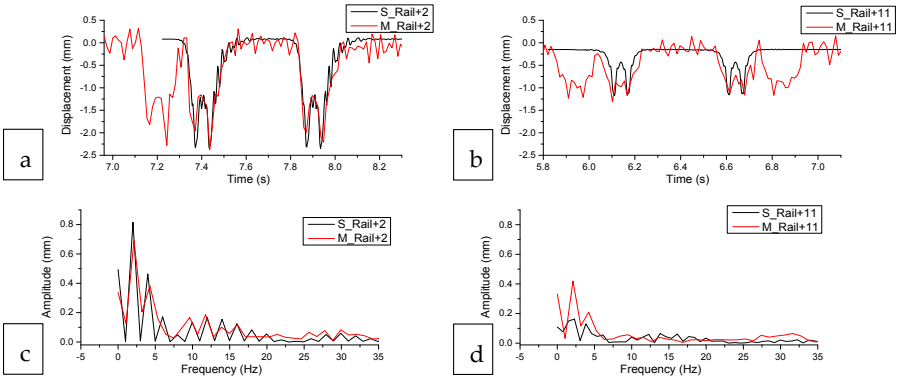

Figure 5.12. Comparisons of measurement and simulation results: (a) the rail close to the bridge in the time domain; (b) the rail far from the bridge in the time domain; (c) the rail far from the bridge in the frequency domain; (d) the rail close to the bridge in the frequency domain

4.2 Simulation of the Transition Zone with High Moisture

Ballast in transition zones often has poor drainage conditions [1, 6, 22]. High moisture in the ballast leads to approximately 50% reduction in stiffness [27, 28]. Therefore, the model considers ballast with high moisture in the transition zone by reducing stiffness by 50%. In this case, ballast areas in the transition zones assumed to be affected by high moisture (50% stiffness reduction) are within an 8-sleeper distance from the bridge and are shown with blue colour in Figure 5.13. The ballast stays unchanged in the reference case.

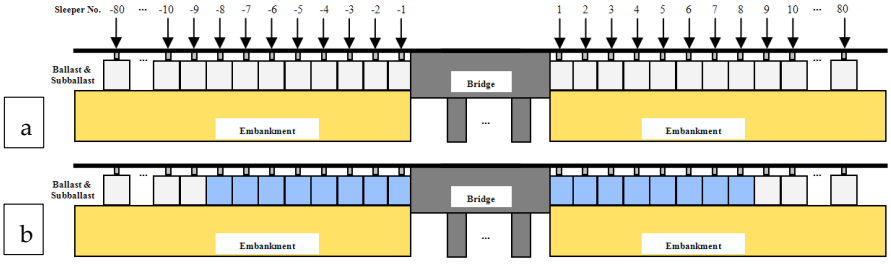

Figure 5.13 Simulation of the transition zone with high moisture: (a) the reference case; (b) the high moisture case.

4.3 Results of the Finite Element Analysis

FE simulation results of the transition zones with and without high moisture are analysed in this section.

The dynamic wheel loads of Wheel 1 are shown in Figure 5.14. The horizontal axis represents the distance along the transition zone model, where the bridge is located between 48m and 72m. Dynamic wheel loads on the bridge are not analyzed here, and therefore their responses are covered by the shaded area. The dynamic wheel loads are zoomed before and after the bridge in Figure 5. 14b and Figure 5. 14c, respectively.

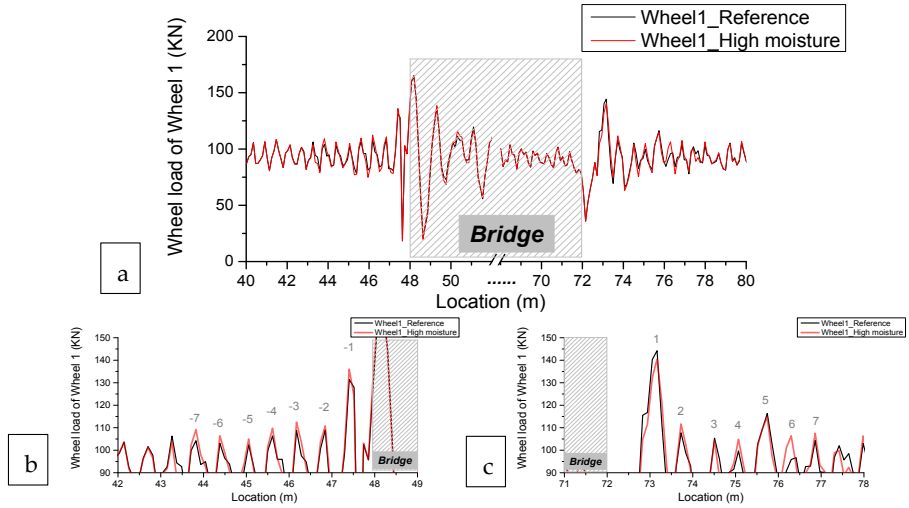

Figure 5.14. Dynamic wheel load of Wheel 1: (a) overview; (b) zoom-in of the embankment-bridge side; (c) zoom-in of the bridge-embankment side [unit: KN].

As shown in Figure 5.14, the dynamic wheel load of Wheel 1 in the reference case is increased near the bridge, which is caused by the differential stiffness and settlement existing in the transition zone. This is one of the sources of degradation in transition zones. In addition, the dynamic wheel loads are different in the embankment-bridge and bridge-embankment sides. In the embankment-bridge side, the dynamic wheel loads are increased at a closer location to the bridge (at 47.4m, 0.6m from the bridge), while in the bridge-embankment side the dynamic wheel loads are increased at a further location (at 73.2m, 1.2m from the bridge). This is caused by the different vehicle dynamics between the elevation and drop-off, which theoretically studied in [17] and numerically studied in [8].

Comparing to the reference case, the dynamic wheel loads of Wheel 1 in the high moisture case are slightly increased at most locations before and after the bridge (43m-48m and 72m-78m), while they remain the same at further locations. This is reasonable since the stiffness of ballast is reduced only at these locations (8-sleeper distances, corresponding to 43.2m-72m and 72m-76.8m). Similarly, the slight increase is also found in the dynamic wheel loads of the other three wheels at most locations before and after the bridge, as shown in Figure 5.15. It should be noted the dynamic wheel loads in the high moisture case are lower than that in the reference case at some individual peaks. This is caused by the dynamic vibration of the vehicle. To study the overall effect of high moisture, the statistics of increased percentage of the peaks close to the bridge (the closest seven peaks to the bridge on both sides, negative towards the bridge and positive away from the bridge, as indicated in Figure 5.14b and c) is performed as shown in Table 5.3. The increase percentages of the dynamic wheel loads in the high moisture case with respect to those at the same location in the reference case are calculated.

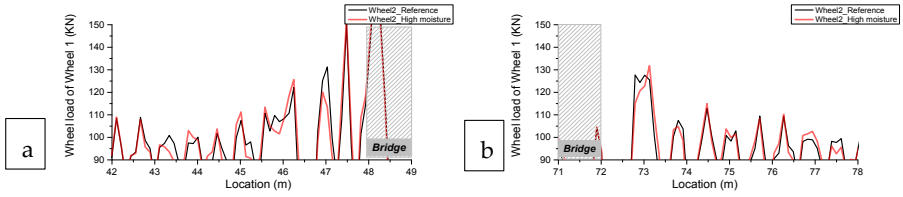

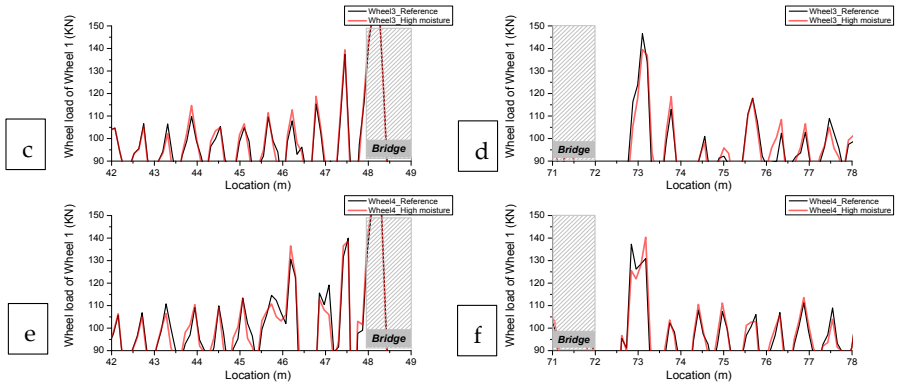

Figure 5.15. Dynamic wheel loads: (a) zoom-in of the embankment-bridge side of Wheel 2; (b) zoom-in of the bridge-embankment side of Wheel 2; (c) zoom-in of the embankment-bridge side of Wheel 3; (d) zoom-in of the bridge-embankment side of Wheel 3; (e) zoom-in of the embankment-bridge side of Wheel 4; (f) zoom-in of the bridge-embankment side of Wheel 4 [unit: KN].

Table 5.3. Increase percentages of the dynamic wheel loads in the high moisture case comparing to the reference case.

Peak	Wheel 1	Wheel 2	Wheel 3	Wheel 4
-7	4.7	2.9	4.4	1.1
-6	3.2	1.9	-0.3	-0.7
-5	2.5	3.5	1.6	-0.1
-4	3.2	2.4	1.7	-3.3
-3	3.4	2.9	4.5	4.5
-2	1.6	-8.5	3.0	-5.4
-1	3.5	1.0	1.4	-1.0
1	-2.6	3.2	-4.8	2.2
2	3.7	-2.5	5.0	1.2
3	-1.0	1.9	-2.7	2.4
4	5.1	0.8	4.0	3.4
5	-1.4	-1.0	0.0	-2.9
6	10.0	0.8	5.9	-1.0
7	3.1	3.5	3.6	2.1
Average	2.6	0.8	1.7	0.2

As shown in Figure 5.15 and Table 5.3, the dynamic wheel loads of all wheels in the high moisture case are increased, where average ranges are from 0.2% (Wheel 4) to 2.6% (Wheel 1). It should be noted that the negative values in Table 5.3 correspond to the peaks in Figure 5.14 and Figure 5.15 where the dynamic wheel loads in the high moisture case are lower than that in the reference case. The increase of the front wheels is higher than that of the rear wheels (Wheel 1 > Wheel 2, Wheel 3> Wheel 4), and the increase of the front bogie is higher than that of the rear bogie (Wheel 1> Wheel 3, Wheel 2> Wheel 4). Because the higher dynamic wheel loads accelerate track degradation, the simulation results confirm that a high moisture condition is one of the sources of fast degradation often reported in transition zones. The increase of dynamic wheel loads also explains the irregularities in longitudinal track level as shown in Section 3.

It should be noted that the vehicle used in the model is a passenger vehicle (19t). In a real situation, freight trains with higher axle loads can bring higher increase to the dynamic wheel loads (e.g. 25t), which exacerbate the track degradation. In addition, various axle loads in mixed traffic lines may also aggravate the degradation [61]. The same situation can be expected if trains travel at a higher velocity (than 144km/h).

5 Discussion

A higher moisture level in the ballast and subballast layers of the measured transition zones was detected with field measurements. According to the experience of others, e.g., [3], wet ballast has often been observed in transition zones. High moisture in the ballast indicates that the drainage system is not fully functional. The intent of a drainage system in railways is to intercept subsurface water entering the area of the track substructure, to intercept surface water approaching the track structure from the sides, and to remove water draining out of the ballast and subballast [36]. When the drainage system does not work properly, it may bring problems that fall [36] into two categories.

1. Changes in physical properties of tracks, such as: pore pressure increases under cyclic load causing increase in plastic strain accumulation, decrease in stiffness.
2. Damage to track components, such as: subgrade attrition and slurry formation from ballast action; ballast degradation from slurry abrasion, chemical action, and freezing of water; sleeper attrition from slurry abrasion.

The first category problems can be observed as the degradation of track alignment, which is shown by the measured longitudinal track level in Section 3 and explained in Section 4. Moreover, track irregularities have also been reported in transition zones, e.g., [1, 3, 4, 6, 7]. An example of a transition zone with large track irregularities is shown in Figure 5.16. The second category problems result in maintenance, such as ballast cleaning (undercutting) by ballast cleaners [36, 56], or ballast adding by track stoneblower [56, 62]. When the problems are not solved timely, frost heave and mud pumping problems may occur. All of the problems cause a significant increase in track maintenance costs and reduction in passenger comfort. A possible solution is to improve the drainage system in transition zones at the design stage, since currently most codes regard the drainage system in transition zones the same as that in free track, e.g., in [63].

Figure 5.16. Transition zone with large track irregularities.

Numerical simulations have demonstrated how increased moisture (represented as reduced ballast stiffness) causes dynamic wheel loads to have a greater impact on transition zone structures (ballast/subballast) during loading (train traffic). This may result in a variation of ballast distribution and consequently accelerate ballast settlement. Since most numerical studies of transition zones only consider the difference of the stiffness and settlement in transition zones, e.g., [6, 8, 11, 64], it is suggested to also consider the effect of ballast moisture in future studies.

In addition to the reduction in stiffness, it is also possible to model the ballast with high moisture as a higher growth rate of settlement. In [29], static one-dimensional tests of ballast were conducted to study the effect of the addition of water on ballast deformation. Specimens with added water had a 40% increase in settlement when compared to dry samples. Similar findings from laboratory tests can also be found in [30], where the additional settlement caused by water for fresh and recycled ballast is 39% and 42%. When the ballast is fouled (e.g., by clay and silt), the extra settlement caused by water is even larger [31].

6 Conclusion

To explore the degradation mechanism in transition zones, this paper studies the moisture condition of the ballast and subballast in transition zones experimentally and numerically.

The paper presents results of moisture condition measured in three transition zones using GPR. It has been found that the high moisture areas appear mostly before and after the bridges in

transition zones. Track irregularities can also be found at the corresponding locations, which imply a strong connection between the high moisture conditions and track degradation. High moisture areas tend to be located at the bottom of the ballast layer, the bottom of the subballast layer, and above the abutments.

To explain the connection, the dynamic behaviour of the transition zone in a high moisture condition is analysed using the FE method (explicit integration). The ballast and subballast are modelled as solid elements and the high moisture conditions are considered as (50%) reduction of the elastic modulus according to laboratory findings. It has been found that the average of dynamic wheel load peaks for all wheels in the transition zone in the high moisture condition is slightly increased (ranging from 0.2% to 2.6%) compared to the reference condition. Since the high dynamic wheel loads will lead to fast track degradation, the simulation results confirm that the high moisture condition is one of the sources of the fast degradation often reported in transition zones.

In a real situation, when higher axle loads or velocities of the trains are in use, faster track degradation can be expected in transition zones in a high moisture condition. To prevent it, more attention should be paid to the drainage system of the ballast track in transition zones. In addition, it is recommended to consider the effect of ballast moisture in the future studies of transition zones.

Acknowledgments:
This project has received funding from the European Union's Horizon 2020 research and innovation programme under the Marie Skłodowska-Curie grant agreement No 691135 "RISEN: Rail Infrastructure Systems Engineering Network".

References

1. Li, D. and D. Davis, Transition of Railroad Bridge Approaches. JOURNAL OF GEOTECHNICAL AND GEOENVIRONMENTAL ENGINEERING, 2005.

2. Coelho, B., et al., An assessment of transition zone performance. Proceedings of the Institution of Mechanical Engineers, Part F: Journal of Rail and Rapid Transit, 2011. 225(2): p. 129-139.

3. Stark, T.D. and S.T. Wilk, Root cause of differential movement at bridge transition zones. Proceedings of the Institution of Mechanical Engineers, Part F: Journal of Rail and Rapid Transit, 2015.

4. Markine, V., H. Wang, and I. Shevtsov. Experimental Analysis of the Dynamic Behaviour of a Railway Track in Transition Zones. in Proceedings of the Ninth International Conference on Engineering Computational Technology, P. Iványi and B.H.V. Topping, (Editors), Civil-Comp Press, Stirlingshire, United Kingdom, paper 3, 2014. 2014.

5. (ERRI), E.R.R.I., Bridge ends. Embankment Structure Transition. State of the Art Report. 1999.

6. Nicks, J.E., The bump at the end of the railway bridge (Doctoral dissertation). 2009, Texas A&M University.

7. Le Pen, L., et al., The behaviour of railway level crossings: insights through field monitoring. Transportation Geotechnics, 2014. 1(4): p. 201-213.

8. H. Wang, et al., Analysis of the Dynamic Behaviour of a Railway Track in Transition Zones With Differential Settlement, in 2015 Joint Rail Conference, San Jose, California, USA, March 2015. 2015. p. 7.

9. Paixao, A., E. Fortunato, and R. Calcada, Design and construction of backfills for railway track transition zones. Proceedings of the Institution of Mechanical Engineers, Part F: Journal of Rail and Rapid Transit, 2013. 229(1): p. 58-70.

10. Alves Ribeiro, C., et al., Under sleeper pads in transition zones at railway underpasses: numerical modelling and experimental validation. Structure and Infrastructure Engineering, 2014. 11(11): p. 1432-1449.

11. Zuada Coelho, B., Dynamics of railway transition zones in soft soils (Doctoral dissertation). 2011.

12. Lei, X. and B. Zhang, Influence of track stiffness distribution on vehicle and track interactions in track transition. Proceedings of the Institution of Mechanical Engineers, Part F: Journal of Rail and Rapid Transit, 2010. 224(6): p. 592-604.

13. Gallage, C., B. Dareeju, and M. Dhanasekar, State-of-the-art : track degradation at bridge transitions. Proceedings of the 4th International Conference on Structural Engineering and Construction Management 2013, 2013.

14. Hölscher, P. and P. Meijers, Literature study of knowledge and experience of transition zones, in Delft: report. 2007.

15. Read, D. and D. Li, Design of track transitions. TCRP Research Results Digest 79, 2006.

16. Thompson, D.R. and P.K. Woodward. Track stiffness management using the XiTRACK GeoComposite. in Permanent Way Institution Journal and Report of Proceedings. 2004.

17. Kerr, A.D. and B.E. Moroney, Track transition problems and remedies. PROC. of the American railway engineering association, 1993. 94: p. 25.

18. Banimahd, M., et al., Behaviour of train–track interaction in stiffness transitions. Proceedings of the Institution of Civil Engineers-Transport, 2012. 165(3): p. 205-214.

19. Dahlberg, T., Railway Track Stiffness Variations-Consequences and Countermeasures. International Journal of Civil Engineering, 2010. 8(1).

20. Hunt, H., Settlement of railway track near bridge abutments, in Proceedings of the Institution of Civil Engineers-Transport. 1997, Thomas Telford-ICE Virtual Library. p. 68-73.

21. Frohling, R.D., H. Scheffel, and W. EbersÖHn, The Vertical Dynamic Response of a Rail Vehicle caused by Track Stiffness Variations along the Track. Vehicle System Dynamics, 1996. 25(sup1): p. 175-187.

22. Li, D., D. Otter, and G. Carr, Railway bridge approaches under heavy axle load traffic: problems, causes, and remedies. Proceedings of the Institution of Mechanical Engineers, Part F: Journal of Rail and Rapid Transit, 2010. 224(5): p. 383-390.

23. Varandas, J.N., P. Hölscher, and M.A.G. Silva, Dynamic behaviour of railway tracks on transitions zones. Computers & Structures, 2011. 89(13-14): p. 1468-1479.

24. Sasaoka, C. and D. Davis, Long term performance of track transition solutions in revenue service. Technology Digest TD-05-036, Transportation Technology Center. Inc., Association of American Railroads, 2005.

25. Hyslip, J.P., D. Li, and C. McDaniel. Railway bridge transition case study. in Bearing Capacity of Roads, Railways and Airfields. 8th International Conference (BCR2A'09). 2009.

26. Sañudo, R., et al., Track transitions in railways: A review. Construction and Building Materials, 2016. 112: p. 140-157.

27. Lekarp, F., U. Isacsson, and A. Dawson, State of the art. I: Resilient response of unbound aggregates. Journal of transportation engineering, 2000. 126(1): p. 66-75.

28. Stark, T.D., et al. Evaluating Fouled Ballast Using Seismic Surface Waves. in 2016 Joint Rail Conference. 2016. American Society of Mechanical Engineers.

29. Indraratna, B., et al., Compression and degradation of railway ballast under one-dimensional loading. Australian Geomechanics, 1997. 32(December): p. 48-61.

30. Indraratna, B., et al., Geotechnical properties of ballast and the role of geosynthetics. Institution of Civil Engineers. Proceedings. Ground... 2006.

31. Han, X. and E.T. Selig. Effects of fouling on ballast settlement.

32. Saarenketo, T., Electrical properties of road materials and subgrade soils and the use of ground penetrating radar in traffic infrastructure surveys. 2006, University of Oulu.

33. Daniels, D.J., Ground penetrating radar. 2005: Wiley Online Library.

34. Wang, H., et al. Improvement of train-track interaction in transition zones via reduction of ballast damage. in The Dynamics of Vehicles on Roads and Tracks. 2016. CRC Press.

35. Wang, H. and V. Markine, Finite element analysis of the dynamic behaviour of track transition zones during train passing processes. Submitted to Vehicle System Dynamics, 2017.

36. Selig, E.T. and J.M. Waters, Track geotechnology and substructure management. 1994: Thomas Telford.

37. Haynes, J.H. and E.J. Yoder, Effects of repeated loading on gravel and crushed stone base course materials used in the AASHO Road Test. Highway Research Record, 1963(39).

38. Silvast, M., et al., An inspection of railway ballast quality using ground penetrating radar in Finland. Proceedings of the Institution of Mechanical Engineers, Part F: Journal of Rail and Rapid Transit, 2010. 224(5): p. 345-351.

39. Silvast, M., et al., Identifying frost-susceptible areas on Finnish railways using the ground penetrating radar technique. Proceedings of the Institution of Mechanical Engineers, Part F: Journal of Rail and Rapid Transit, 2013. 227(1): p. 3-9.

40. Saarenketo, T., M. Silvast, and J. Noukka. Using GPR on railways to identify frost susceptible areas. in Proceedings of the international conference and exhibition railway engineering 2003. 2003. London, UK.

41. Hugenschmidt, J., Railway track inspection using GPR. Journal of Applied Geophysics, 2000. 43(2): p. 147-155.

42. Saarenketo, T., Electrical properties of water in clay and silty soils. Journal of Applied Geophysics, 1998. 40(1): p. 73-88.

43. Clark, M.R., et al., Electromagnetic properties of railway ballast. NDT & E International, 2001. 34(5): p. 305-311.

44. Silvast, M., et al. NDT techniques in railway structure analysis. in Proceedings of the 7th World Congress on Railway Research, Montreal, Canada, June 4-8, 2006. 2006.

45. Vorster, D.J. and P.J. Gräbe, The use of ground-penetrating radar to develop a track substructure characterisation model. Journal of the South African Institution of Civil Engineering, 2013. 55(3): p. 69-78.

46. Saarenketo, T., Experiences of integrated GPR and Laser Scanner analysis, in the 17th Nordic Geotechnical Meeting Challenges in Nordic Geotechnic. 2016: Reykjavik.

47. Wang, H., V. Markine, and I. Shevtsov, Conference presentation in the of The Analysis of Degradation Mechanism in Track Transition Zones using 3D Finite Element Model, in Proceedings of the Second International Conference on Railway Technology: Research, Development and Maintenance, J. Pombo,(Editor), Civil-Comp Press, Stirlingshire, United Kingdom, paper 227, 2014. doi: 10.4203/ccp. 2014.

48. Lundqvist, A. and T. Dahlberg, Load impact on railway track due to unsupported sleepers. Proceedings of the Institution of Mechanical Engineers, Part F: Journal of Rail and Rapid Transit, 2005. 219(2): p. 67-77.

49. Shi, J., et al., Measurements and simulation of the dynamic responses of a bridge-embankment transition zone below a heavy haul railway line. Proceedings of the Institution of Mechanical Engineers, Part F: Journal of Rail and Rapid Transit, 2012. 227(3): p. 254-268.

50. Paixao, A., E. Fortunato, and R. Calcada, A numerical study on the influence of backfill settlements in the train/track interaction at transition zones to railway bridges. Proceedings of the Institution of Mechanical Engineers, Part F: Journal of Rail and Rapid Transit, 2015.

51. Alves Ribeiro, C., R. Calçada, and R. Delgado, Calibration and experimental validation of a dynamic model of the train-track system at a culvert transition zone. Structure and Infrastructure Engineering, 2017: p. 1-15.

52. Banimahd, M., et al., Behaviour of train–track interaction in stiffness transitions. Proceedings of the ICE - Transport, 2012. 165(3): p. 205-214.

53. Zhai, W.M., K.Y. Wang, and J.H. Lin, Modelling and experiment of railway ballast vibrations. Journal of Sound and Vibration, 2004. 270(4-5): p. 673-683.

54. Varandas, J.N., P. Holscher, and M.A. Silva, Settlement of ballasted track under traffic loading: Application to transition zones. Proceedings of the Institution of Mechanical Engineers, Part F: Journal of Rail and Rapid Transit, 2013. 228(3): p. 242-259.

55. Iwnick, S., Manchester Benchmarks for Rail Vehicle Simulation. Vehicle System Dynamics, 1998. 30(3-4): p. 295-313.

56. Wan, C., V.L. Markine, and I.Y. Shevtsov, Improvement of vehicle–turnout interaction by optimising the shape of crossing nose. Vehicle System Dynamics, 2014. 52(11): p. 1517-1540.

57. Esveld, C., Modern railway track. Vol. 385. 2001: MRT-productions Zaltbommel, The Netherlands.

58. Sato, Y., Japanese Studies on Deterioration of Ballasted Track. Vehicle System Dynamics, 1995. 24(Supply): p. 197-208.

59. Dahlberg, T., Some railroad settlement models—a critical review. Proceedings of the Institution of Mechanical Engineers, Part F: Journal of Rail and Rapid Transit, 2001. 215(4): p. 289-300.

60. Indraratna, B., et al., Field assessment of the performance of a ballasted rail track with and without geosynthetics. Journal of Geotechnical and Geoenvironmental Engineering, 2010. 136(7): p. 907-917.

61. Coelho, Z., Dynamics of railway transition zones in soft soils. 2011.

62. Hallquist, J., LS-DYNA theoretical manual, ed. L.S.T. Corporation. 1998, CA: Livermore.

63. Kreiser, D., et al., A nonlinear damage accumulation model for shakedown failure. International Journal of Fatigue, 2007. 29(8): p. 1523-1530.

64. Anderson, W.F. and A.J. Key, Model testing of two-layer railway track ballast. Journal of geotechnical and geoenvironmental engineering, 2000. 126(4): p. 317-323.

65. ProRail, Constructive measures to prevent settlement of the track (in Dutch Constructieve maatregelen ter voorkoming van ontoelaatbare zakkingen van het spoor). 2010.

66. Varandas, J.N., Long-Term Behaviour of Railway Transitions under Dynamic Loading Application to Soft Soil Sites (Doctoral dissertation). 2013.

PII-V

Paper VI

Structural health inspection of railway transition zones using satellite radar data

Haoyu Wang, Ling Chang, Valeri Markine[1]

[1] Delft University of Technology, Delft, the Netherlands

Published by Sensor 2018, 18(2), 413.

Abstract

Transition zones in railway tracks are locations with considerable changes in the rail-supporting structure. Typically, they are located near engineering structures, such as bridges, culverts and tunnels. In such locations, severe differential settlements often occur due to the different material properties and structure behaviour. Without timely maintenance, the differential settlement may lead to the damage of track components and loss of passenger's comfort. To ensure the safety of railway operations and reduce the maintenance costs, it is necessary to consecutively monitor the structural health condition of the transition zones in an economical manner and detect the changes at an early stage. However, using the current in situ monitoring of transition zones is hard to achieve this goal, because most in situ techniques (e.g., track-measuring coaches) are labor-consuming and usually not frequently performed (approximately twice a year in the Netherlands). To tackle the limitations of the in situ techniques, a Satellite Synthetic Aperture Radar (InSAR) system is presented in this paper, which provides a potential solution for a consecutive structural health monitoring of transition zones with bi-/tri-weekly data update and mm-level precision. To demonstrate the feasibility of the InSAR system for monitoring transition zones, a transition zone is tested. The results show that the differential settlement in the transition zone and the settlement rate can be observed and detected by the InSAR measurements. Moreover, the InSAR results are cross-validated against measurements obtained using a measuring coach and a Digital Image Correlation (DIC) device. The results of the three measuring techniques show a good correlation, which proves the applicability of InSAR for the structural health monitoring of transition zones in railway track.

Keywords

Satellite InSAR, transition zones, railway, settlement

1 Introduction

Transition zones in railway track network are locations with considerable changes in the vertical support structures, which are located near engineering structures, such as bridges, culverts and tunnels [1]. A typical embankment-bridge transition zone is shown in Figure 6.1. Due to the difference in the stiffness and the settlement characteristics as well as the geotechnical and construction issues [2-7], the track geometry always degrades faster in transition zones than in open tracks, which causes significant irregularity (dips) in the track geometry. Such geometry irregularities may trigger considerable wheel-rail interaction forces, resulting in damage to track components, affecting the passenger's comfort, and even causing derailment [3, 8-11]. As a result, the maintenance of the track geometry in the transition zones requires substantial efforts. For example, in the Netherlands, the track maintenance in transition zones is performed up to 4–8 times more than on free tracks [12, 13]. In the US $200 million is spent annually to maintain the transition zones, while in Europe about €97 million is spent [14, 15].

Figure 6.1. A typical track transition zone in the Netherlands.

To ensure the safety of railway operations and the reduction of maintenance costs, it is necessary to inspect the structural health condition of transition zones at a high frequency. Structural Health Monitoring (SHM) system would allow the detection of potentially dangerous situations at an early stage to provide an efficient way to extend the operational life of railway structures, while not interfering with train operations [16]. The widely used SHM systems are often impedance-based, which exploit the relationship between the electrical impedance of Piezotransducers (PZT) and the mechanical impedance of the host structure to which the PZTs are bonded or embedded. The results, which are the inverse of the electrical impedance, are functions of the stiffness, mass, damping of the host structure; or length, width, thickness, orientation, and mass of the PZTs. Therefore, the structural damage can be detected from the variation of the monitoring results [17-21]. The current monitoring for transition zones is mainly aimed at observing the rail deflection performed by track-measuring coaches at the frequency of twice a year and rail/sleeper displacements at a higher frequency but only for individual case studies [22-24]. Both these SHM systems perform at a low frequency, which are mainly due to the inspection expense.

PII-VI

Therefore, this paper proposes a contactless SHM system that uses satellite SAR (Synthetic Aperture Radar) measurements to complement the current in situ measurements. The satellite SAR measurements are obtained on a bi-/tri-weekly basis, and with high precision (at millimeter level) [25, 26]. By providing a stack of SAR measurements over a certain period, the settlement behaviour of railway infrastructures can be retrieved using satellite radar interferometric (Synthetic Aperture Radar Interferometry, referred as InSAR) techniques [27-29]. InSAR has been successfully applied to the long-term railway monitoring in [27, 30-32].

To demonstrate the InSAR feasibility and its potential for the structural health monitoring in transition zones, a transition zone is measured and analyzed using the InSAR techniques. Further, the InSAR results are cross-validated using the measurements from a measuring coach and a DIC-device. The paper is organized as follows. The settlement mechanism of the tracks in transition zones is described in Section 2. The measuring principle of the InSAR techniques and the

conventional monitoring systems, including the measuring coach and the Digital Image Correlation (DIC)-based device is illustrated in Section 3. Section 4 introduces the testing site and the data collection using the monitoring systems. The settlement history of the transition zone measured using the InSAR techniques is analyzed in Section 5. To verify the InSAR results, the transition zone is also evaluated by other two validated measuring systems (the measuring coach and the DIC-based device). The relationship between the three measurement systems is discussed in Section 6. The conclusions are eventually drawn in Section 7.

2 Settlement Mechanism in Transition Zones

Since the vertical track stiffness determines the rail deflection due to passing trains, the large abrupt change in the vertical track stiffness in transition zones results in a rapid change in the elevation of wheels [8]. In other words, the wheels "drop down" when trains move from the engineering structure to ballast track, while the wheels are "lifted up" when trains move from the ballast track to engineering structure. In addition to the rail deflection caused by the different track stiffness, the ballast track always settles more as compared to engineering structures. According to the field measurements and laboratory tests [33-39], the ballast track is rapidly compacted immediately after construction or maintenance. Moreover, there are also some geotechnical, construction and maintenance issues, such as inferior quality of used materials, poor drainage conditions, inadequate compaction and consolidation of embankment or backfill [1] (before the construction of the bridge, the embankment is often excavated and refilled afterwards with the backfill). The three factors, including the stiffness variation, the different settlement behaviour, and the geotechnical issues, lead to the differential settlement in transition zones. In [38], the differential track settlement up to 7 mm appeared in the transition zone after half-year operation. In another transition zone [1], the settlement was estimated up to 10 mm after the 10-month operation.

As a result, the wheel-rail interaction forces in transition zones are significantly amplified [6, 8, 40-44]. The analytical results in [40] showed that the wheel-rail interaction forces in the transition zone between the ballast track and slab track were increased up to 54% due to the differential settlement. Similarly, the increase of the wheel-rail interaction forces in the transition between the embankment and the bridge was up to 85% by the differential settlement [41]. The increased wheel-rail interaction forces ultimately lead to the accelerated deterioration of the vertical track geometry, as shown in Figure 6.2.

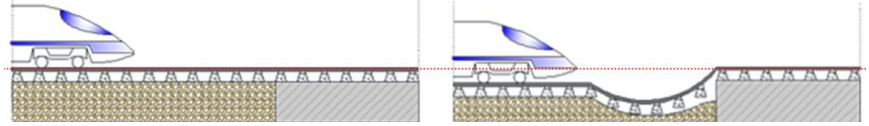

(**a**) (**b**)

Figure 6.2. Schematic diagram of differential settlement in transition zone: (**a**) immediately after construction or maintenance; (**b**) after a few months of operation.

As shown by the "dip" in Figure 6.2b, the extra settlement of the tracks near the engineering structure has been confirmed by [1, 3, 38, 45], which typically appears shortly after the installation/renewal of the track. A survey of the performance of track transition zones [2] reveals that 51% of the track transition zones described in that study have experienced such a settlement.

The affected zones located next to engineering structures often have various lengths, e.g., 4 m in [23, 24], 7 m in [13, 22], and 30 m in [3]. In [46], the following formula for the length of the affected zone L is suggested:

$$L = \sqrt{1.6 \times \Delta h \times V_e^2} \quad (1)$$

where Δh is the height difference of track in the transition zone (m); V_e is the design speed (km/h). Assuming Δh is 0.01 m and V_e is 160 km/h, the length of the affected zone L is approximately 20 m.

3 Condition Monitoring of Transition Zones

The current structural health-monitoring measurements for transition zones are mainly performed by measuring coaches, levelling instruments, and linear variable differential transformers (LVDT). Levelling instruments are the optical instruments used to establish or verify the points in the same horizontal plane, which were used in [3, 22, 47]. LVDTs convert a position or linear displacement from a mechanical reference into a proportional electrical signal containing phase and amplitude information, which was used among others in [38]. A complete introduction to SHM methods used on civil infrastructures can refer to [17]. The most widely used method is the track inspection performed by the measuring coach, which is presented in Section 3.1. Moreover, a detailed measurement method using DIC devices is explained in Section 3.2. The measuring principle of InSAR is provided in Section 3.3. It should be noted that the measuring principles of the three systems are different but related. The relationship between them is discussed in Section 6.

3.1 Measuring Coach

In most countries, track geometry is mainly measured by the inertial measuring system of measuring coaches. For example, in Japan, the condition monitoring has been accomplished using measuring coaches since 1964. The measurement results are compared at a common point of reference. Precise allocation of a test result to a rail is possible via accurate DGPS (Differential Global Positioning System) location reference. For example, the EURAILSCOUT UFM120 measuring coach has been used since 1999 in the Netherlands, as shown in Figure 6.3 [48]. The car is self-propelled by a diesel engine. It operates in both directions with a maximum speed of 120 km/h. The basic technical information of the UFM120 is given in Table 6.1 [5].

Figure 6.3. EURAILSCOUT UFM120 measuring coach [48].

Table 6.1. Technical data of UMF120 measuring coach.

Parameter	Value
Date of construction	1998
Railway gauge	1.435 mm
Vehicle length over the buffer	23.000 mm
Centre casting distance	17.500 mm
Axle base	2.500 mm
Minimum turning radius in movement	90 m
Vehicle weight approximately	70 tons
Maximum drive speed	120 km/h
Maximum measurement speed	120 km/h

The inertial measuring system consists of three high-precision gyro systems and accelerometers for all three spatial directions x, y, z. The position of measuring coaches is determined by means of double integration of the acceleration measurements. The track position is then measured in relation to the resulting coach position by using relative displacement transducers (optical track-measuring system). Assuming that the track settlement on engineering

structures is negligible, the settlement of ballast tracks can be calculated by using the track on engineering structure as a reference.

This geometry measuring system is on the front side of car bodies, positioned between axles. Track geometry is measured at every 0.25 m, stored in onboard computer systems processed and printed immediately during the ride. All the measured data can also be plotted as a graphical representation, as well as be exported to the external data medium [5]. The track geometry signals are produced in three wavebands, which are 3–25 m (D1), 25–70 m (D2) and 70–150 m (D3) and the precision is 0.5 mm [49].

The advantage of measuring coaches is that it can measure multiple parameters at the same time, including track geometry, track videos/photos, and acceleration of bogies/car bodies. However, the cost of performing the measuring coach measurement is high so that its frequency is relatively low, for instance, twice per year in the Netherlands.

3.2 DIC Devices

DIC is an optical method using tracking and image registration techniques for accurate measurements in images. A reference picture is captured before loading, and a series of pictures are taken subsequently during the loading process. The images are analyzed using a numerical matching technique to identify the most similar patterns in the subsequent images, which is based on the assumptions that the pattern is approximately constant between successive images and the local textural information is unique. The matching algorithm compares the image subsets in the reference image with the image subsets in the current image [50]. Matching criteria are available such as in [51, 52]. The method can continuously record of in-plane displacements of targets without any contact, which excludes any interference between the measured surface and the measuring device [53-55].

The DIC devices have been used to monitor the displacement of rails [24], displacement of sleepers [56-58], and strain of rails [59] during train passages. The DIC system can be even mounted on railcars to perform an interrogation of sleepers while moving [16, 60]. A DIC device often consists of high-resolution digital cameras that record the displacement of targets, and post-processors that analyze the changes in images. The DIC device used in this study is shown in Figure 6.4. This device was successfully used in railway applications such as monitoring turnout crossings [61, 62].

Figure 6.4. A DIC-based device: (**a**) a high-speed camera; (**b**) processing system; (**c**) a tripod; (**d**) targets.

DIC devices can measure detailed dynamic responses of the tracks at specific locations in transition zones. However, the cost of performing DIC measurements is also at a high level since it needs the manual operation. Currently, the condition inspection of transition zones using DIC devices is only performed occasionally and locally for the purpose of research.

3.3 Satellite Radar Interferometry

InSAR techniques have been widely applied in monitoring "natural" geophysical processes, and recently, they have been successfully deployed for structural health monitoring of infrastructure, such as railway, buildings and bridges [27, 31, 63, 64].

InSAR uses two or more satellite radar measurements (i.e., SAR images, acquired by SAR satellites) of the same area to extract ground deformation remotely and periodically, with millimeter-level precision. A SAR satellite operates using a side-looking geometry and illuminates a swath parallel to the satellite's nadir track by transmitting a series of radar pulses from a fixed antenna [65], see Figure 6.5a. The ground targets with a strong scattering reflection, e.g., rail bars, can be well observed using SAR satellites. It should be noted that the observability for ground targets may be degraded when the ground targets are temporarily covered by ice, snow, or water. Therefore, the accuracy of railway measurements may be reduced in the extreme weather. However, its effect is not discussed in the paper since such weather is very rare in the Netherlands.

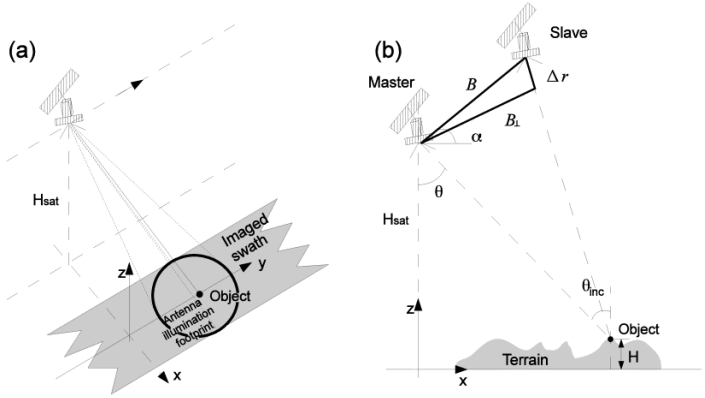

Figure 6.5. (**a**) SAR and (**b**) repeat-pass InSAR imaging geometry, adapted from [29]. (**a**) The satellite at height H_{sat} moves along the azimuth direction for y axis and the direction of the main lobe of microwave pulse is nominated as the range direction for x axis. The area circled by black indicates the footprint of a single pulse. (**b**) Two SAR sensors, master and slave are at a distance by a baseline B. The perpendicular baseline $B_{\perp}$ is defined by the effective distance between master and slave sensors, measured perpendicular to the look direction. The angle between B and horizontal plane is defined as α. The look angle θ is the angle with which the radar looks at the surface. The incidence angle θ_{inc} is defined with regard to the ellipsoid. The height of the object is H with regard to a reference surface.

When two (or more) SAR images, acquired at the same time from a different orbital track or acquired at the separated time but imaging the same area, are available, the temporal evolution of ground targets can be retrieved by the InSAR techniques. For instance, the two SAR images are called the master image and slave image; see Figure 6.5b. The slave image must be co-registered and resampled with regard to the geometry of the master image. The interferometric phase is derived from the pixel-by-pixel multiplication with the conjugate complex of a pixel, in the master and slave image. Such complex multiplication yields a value $\phi^w \in [-\pi, \pi)$ [rad] that referred to as the "wrapped", or relative, interferometric phase. If the "absolute" phase $\phi \in \mathbb{R}$ ($\mathbb{R}$ is the set of real numbers) were observed, it would be directly related to the slant range difference Δr between master and slave (see Figure 6.5b), as in

$$E\{\phi\} = -\frac{4\pi}{\lambda}\Delta r, \tag{2}$$

where $E\{.\}$ expresses the expectation operator. Note that Equation (2) holds for the repeat-pass configuration where the two SAR images are acquired at different times. However, the absolute interferometric phase ϕ cannot straightforwardly be measured, due to the fact that the interferometric observed phase ϕ^w. Instead, a relative phase, modulo 2π radians, expressed as $W\{\varphi\} = \mathrm{mod}\{\varphi + \pi, 2\pi\} - \pi$ is measured, where $W\{.\}$ is the wrapping operator.

The absolute interferometric phase ϕ can be decomposed into four components that are surface topography, temporal displacement, atmospheric delay, and noise,

$$\phi^w = W\{\phi\} = W\{\phi_{topo} + \phi_{defo} + \phi_{atmo} + \phi_{noise}\}, \quad (3)$$

where

$\phi_{\text{topo}} = -\frac{4\pi}{\lambda}\frac{B}{\rho \sin\theta}H$ The topographic phase caused by the surface geometry, ρ is the slant range, H is the height above a reference surface

$\phi_{\text{defo}} = -\frac{4\pi}{\lambda}\Delta r$ The kinematic phase due to surface or object displacement

ϕ_{atmo} The phase contribution from the atmospheric signal delay

ϕ_{noise} Other random additive noise.

It is of importance to properly unwrap the interferometric phase and mitigate the atmospheric and noise influence, in order to generate a high-precision deformation component. Therefore, the persistent scattered interferometric (PSI) method [25, 66], using a stack of SAR images, is further proposed. During PSI processing, the temporal behaviour of the ground targets with strong reflection, high coherence, stable phase values over time, can be observed. It is worthwhile to mention that all the satellite radar measurements are relative with regard to a reference epoch and reference point. By comparing the spatial coordinates of the unloaded tracks to the reference point, the increase of the track settlement at various locations can be obtained. Moreover, the high growth rate of the settlement indicates the fast degradation of the track, which suggests the track condition is poor, and vice versa. For instance, the authors in [20] demonstrates that the settlement behaviour and seasonal deformation of the track can be well measured in the Himalaya region. In [18], the long-term settlement of a railway in the Netherlands measured by InSAR was validated against the measurement data of measuring coaches.

Comparing to the measuring coaches and DIC devices, which will be introduced in Sections 3.2 and 3.3, SAR satellites bring higher frequent measurements, while the precision of the satellite measurements is at millimeter level, which is relatively low, and the spatial resolution/sampling of the satellite measurements is at meter level, which is larger than the measuring coach (0.25 m).

4 Test Site and Data Description

To study the capability of InSAR application on the structural health inspection of transition zones, a transition zone is analyzed. The settlement results for the transition zone derived from SAR data processing are compared with the results of the measuring coach and the DIC device performed on the same transition zone (as introduced in Section 3). The transition zone consists of the tracks on the steel bridge and embankment (located in Moerdijk, The Netherlands) as shown in Figure 6.6. The track on the embankment is the ballast track, while the track on the bridge is the embedded rail system.

Figure 6.6. Photograph of the transition zone.

PII-VI

The track settlement in the transition zone was measured by the SAR satellites. 153 TerraSAR-X satellite images (30 × 50 km) were acquired between April 2009 and October 2015, in descending orbit. The wavelength of the on-board radar sensor is 3.1 cm. The PSI method is used to process the SAR data. The measuring coach is EURAILSCOUT UMF 120 as described in Section 3.1. The track alignment was measured in April 2015. The signal was produced in 3–70 m (D1D2) wavebands. The DIC device shown in Figure 6.4 was employed to measure the vertical displacements of the rails at some locations in the transition zone. The measurement was performed in April 2015, when more than 30 train passages were recorded (sampling frequency 78 Hz). The key parameters of the three systems are summarized in Table 6.2.

Table 6.2. Key parameters of the InSAR, the measuring coach and the DIC device.

Measurement Systems	Measured Object	Sampling Interval Along the Track (m)	Acquisition Dates
InSAR	Settlement	3 [1]	2009-04~2015-10
Measuring coach	Track alignment	0.25	2015-04
DIC device	Displacement	0.6	2015-04

[1] The acquired spatial resolution for the TerraSAR-X is 3 × 3 m. After post-processing, the spatial positioning precision along the track is 0.5 m [67].

5 Measurement Results

In this section, the InSAR measurement results are first discussed. Then the cross-validation is performed using the two in situ measurements from the measuring coach and the DIC devices.

The track settlement measured by the TerraSAR-X satellites in the transition zone is shown in Figure 6.7b, along with the photograph of the transition zone (Figure 6.7a) and track alignment measured by the measuring coach (Figure 6.7c). The sampling resolution is indicated by the yellow square in Figure 6.7a, as well as the satellite flying direction and radar signal direction. Note that since the image resolution of the TerraSAR-X satellite is 3 m, the double tracks are considered as one. The satellite flying direction and radar signal direction are indicated as well. As SAR satellites can only observe the ground targets with a strong scattering reflection (mentioned in Section 3.3), the ground targets with a poor scattering reflection over this railway segment cannot be detected. Therefore, the spatial sampling is not always 3 m, and the distance between the adjacent SAR measurement points shown in Figure 6.7b varies.

As shown in Figure 6.7, the settlement on the embankment and the settlement on the bridge are so different that the bridge can be clearly distinguished from the embankment. The settlement of the track on the bridge is relatively stable with marginal fluctuations. On the contrary, the settlement of the track on the embankment increases over time. The increase of the settlement varies from different locations, i.e., the track settles more at the location close to the bridge and less at the location far from the bridge, which is in agreement with the findings from other field measurements in [3, 24, 38].

To study the track settlement in different regions of the transition zone, the InSAR measurements in three representative points of the transition zone are further analyzed, including one point from the ballast track close to the bridge, one point far from the bridge and one point the on the bridge (indicated by the black arrows in Figure 6.7). The settlement histories of points and their rate are shown in Figure 6.8. Figure 6.8 clearly shows that track close to the bridge settles much faster than that farther from the bridge, while the settlement on the bridge remains stable. This proves that InSAR can measure the settlement rate in transition zones in this case, which can provide insightful information to understand the degradation process of the transition zones. It should be noted that the feasibility and the quality of InSAR-based structural health monitoring over transition zones may differ in other cases, due to e.g., the track orientation of a transition zone, satellite viewing geometry and satellite data availability. In addition, sufficient persistent scatters (PS)s are required in the transition zones in order to measure the condition. It can be insured either by increasing the resolution of the satellite or by installing an object (e.g., a pile) in the transition zones.

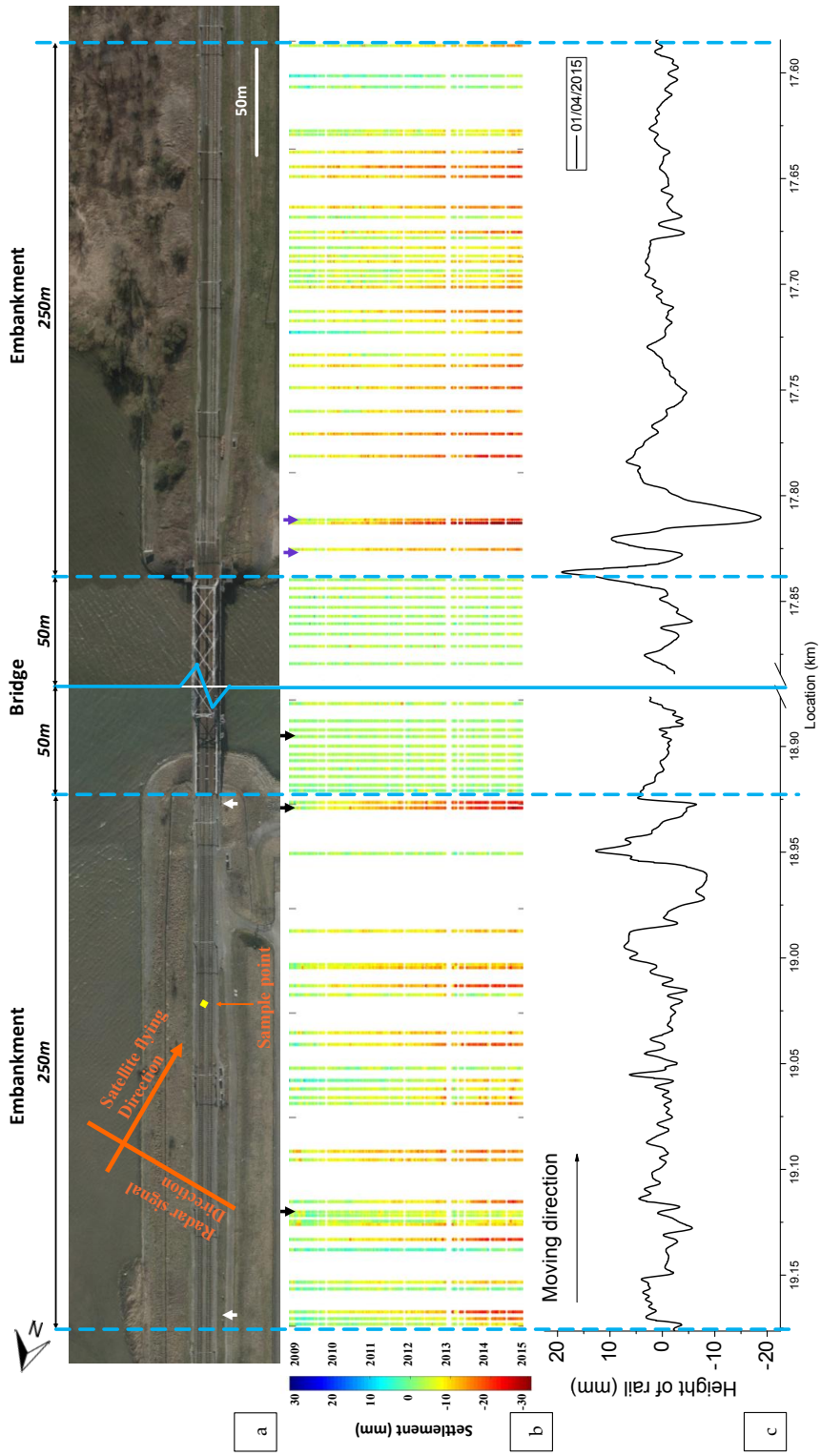
Embankment
250m
Bridge
50m
50m
Embankment
250m
50m
N
Satellite flying Direction
Radar signal Direction
Sample point
a
2009
2010
2011
2012
2013
2014
2015
30
20
10
0
-10
-20
-30
Settlement (mm)
b
Moving direction
01/04/2015
20
10
0
-10
-20
Height of rail (mm)
19.15
19.10
19.05
19.00
18.95
18.90
17.85
17.80
17.75
17.70
17.65
17.60
Location (km)
c

Figure 6.7. Measurement results of the transition zone: (**a**) Top-view photograph; (**b**) Settlement profile measured the satellite system; (**c**) Alignment measured by the measuring coach. The middle parts of the bridge are abbreviated. The yellow square indicates the sampling resolution (3 × 3 m). The satellite flying direction and radar signal direction are indicated. Write arrows are the locations where DIC measurements were performed. Black arrows are the points collected in Figure 6.8. Purple arrows are the locations of the expansion joints shown in Figure 6.11.

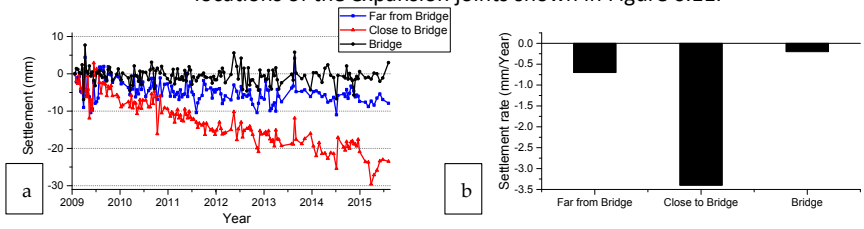

Figure 6.8. Settlement history of the typical points in the transition zones: (**a**) Settlement history curve; (**b**) Settlement rate.

As shown in Figure 6.7, the fluctuation of the track alignment is significantly amplified near the bridge. On the contrary, the track irregularities are much smaller on the bridge and the embankment farther from the bridge. The results of the measuring coach (see Figure 6.7c) correlate very well with the results of the InSAR since the locations with the large fluctuations of track alignment are mostly the locations with the large settlement. It is reasonable because the differential settlement leads to the poor supporting condition of rails and sleepers, which can be observed as track irregularities. It should be noted that the track irregularities are not only caused by the differential settlement, but also by rail defects. This is the reason for the small discrepancies between the settlement and the track alignment.

The dynamic displacements of rail at two typical locations near the bridge were measured by the DIC device. One location is close to the bridge (1.5 m) and the other is far from the bridge (240 m), as indicated by the two white arrows in Figure 6.7a and shown in Figure 6.9. The measurement results are shown in Figure 6.10.

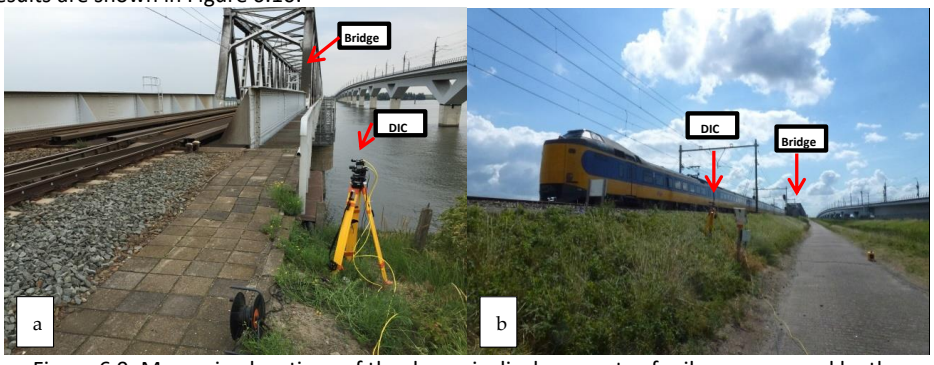

Figure 6.9. Measuring locations of the dynamic displacements of rail are measured by the DIC device: (**a**) the location close to the bridge, (**b**) the location far from the bridge.

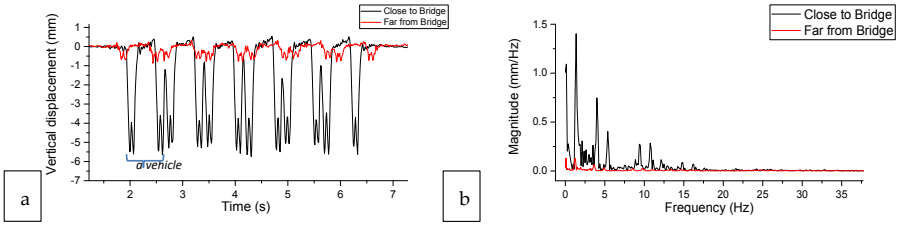

Figure 6.10. Vertical displacements of rail at 1.5 m and 4.5 m of the transition: (**a**) in the time domain, (**b**) in the frequency domain.

Figure 6.10a shows the time curve of the vertical rail displacement. The downward peaks are corresponding to axles (24 wheelsets). The close two peaks belong to one bogie, e.g., the two peaks around 2 s. The relative distant two bogies are from one vehicle, e.g., the bogies at 2 s and 2.6 s (marked by the parentheses in Figure 6.10a). It can be seen in Figure 6.10, the amplitudes of the rail displacements at the two locations are of significant distinction, where the rail close to the bridge reaches 5.65 mm while the rail far from the bridge is only 0.87 mm. The large displacements of the rail close to the bridge imply the appearance of hanging sleepers, which confirms the differential settlement in the transition zone. Therefore, the settlement results measured by the InSAR are again validated by comparison with the measurement results of the DIC measurement.

It is remarkable to note that the transition on the right side (in Figure 6.7) of the bridge is in worse condition than that on the left side. Both the high settlement and track irregularity on the right side of the bridge indicate the track is in poor condition. Especially at 17.81 km, the settlement reaches 31 mm and the dip reaches 18.8 mm. After field observation, it is found that there are two expansion joints at the corresponding location, which probably causes the extra settlement and track irregularity. The expansion joints are shown in Figure 6.11 and their locations are indicated by the purple arrows in Figure 6.7. It shows that the InSAR data is also capable of locating the differential settlement caused by specific track components.

Figure 6.11. Expansion joints on the right side of the bridge.

6 *Discussion*

The satellite, the measuring coach and the DIC measurement unveil the structural health condition of the transition zone. Since the measured objects from these three systems may differ, the relation between the three systems is discussed in this section.

The track deformation is explained in Figure 6.12.

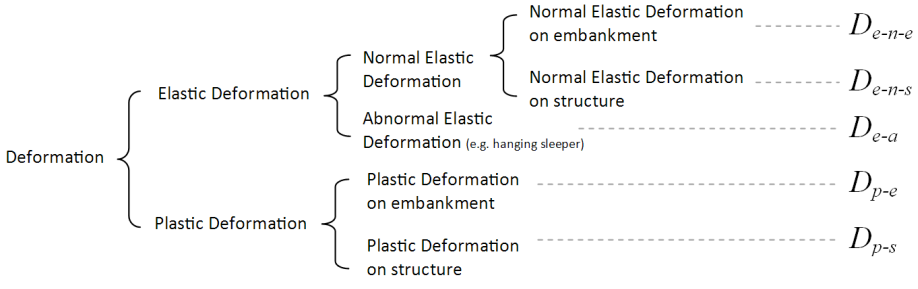

Figure 6.12. Deformation classification.

The normal elastic deformation is determined by the track stiffness, including the stiffness of rail, fastening system, and substructure. It can therefore be different between the track on the embankment and the track on the structure (e.g., embedded rail system on the concrete/steel bridge). The abnormal deformation represents the void under the sleepers (hanging sleepers).

They often exist in transition zones [1, 22, 38], which are hanged by the bending stiffness of the rails and only appears when loaded. The plastic deformation is the track settlement.

As a result, the InSAR techniques can measure the settlement of the unloaded track, which is: D_{p-e}, D_{p-s}. The measuring coach can measure the alignment of loaded track. Considering track on the engineering structures as reference, the relative alignment can be obtained, which is: $(D_{e-n-e} - D_{e-n-s}) + D_{e-a} + (D_{p-e} - D_{p-s})$. The DIC device can measure maximal displacement of track, which is: $D_{e-n-e} + D_{e-a}$, D_{e-n-s}.

In principle, the abnormal elastic deformation (D_{e-a}) is highly correlated with the plastic deformation (D_{p-e}). The local differential plastic deformation may lead to the abnormal elastic deformation, and continuous abnormal elastic deformation in turn causes the plastic deformation. For the transition zone in poor condition, the plastic deformation on embankment is always high as well as the abnormal elastic deformation and vice versa. It is evident in Figure 6.7 that the location where high settlement appears (in red) overlaps with the location where the relative track geometry has high amplification.

For an operated transition zone as shown in Figure 6.2b (with differential settlement), the measurements by SAR satellite, measuring coach and DIC, are shown in Figure 6.13, where the unloaded track geometry after the operation is shown as the black dash line and the loaded track geometry after the operation is shown as the solid black line. The deformation measured by the three systems is indicated as shade in Figure 6.13b–d.

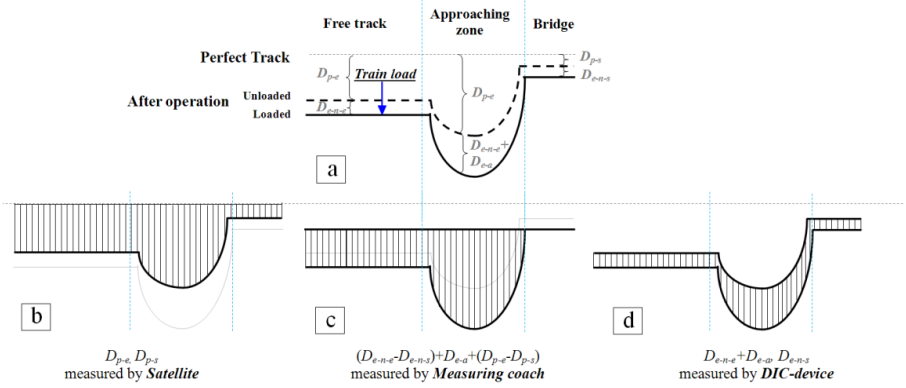

Figure 6.13. Schematic diagram of the measurement of the three systems. In (**a**), the unloaded track geometry after the operation is shown as the black dash line, while the loaded track geometry after the operation is shown as the solid black line. In (**b**–**d**), the deformation can be measured by the three systems is indicated as shade.

Although the measured objects of the three systems are different, their results are inter-related. Therefore, they are capable of showing the health condition of the transition zones. Considering the cost efficiency, the satellite has an advantage in performing long-term health monitoring for transition zones at a high frequency.

PII-VI

7 Conclusions

This study demonstrates the feasibility of InSAR application on the SHM of transition zones in railway track. Measurements using the InSAR technique were performed on transition zones near a steel bridge. The results were cross-validated using the data from a measuring coach and a DIC device.

It has been proved that the settlement on the embankment and bridge are significantly different in the studied transition zone. The embankment and the bridge of the transition zone can be clearly distinguished in the satellite data. The track settles more in the locations close to the bridge and less in the locations far from the bridge. The settlement of the track on the bridge is relatively stable with marginal fluctuation.

The measurement results of the InSAR were compared with the results of two in situ monitoring systems, which are the measuring coach and the DIC-based device. The measuring coach measures the track alignment, and the DIC device measures the transient rail displacements. These measurements have a very good correlation.

The presented results have demonstrated that InSAR can be used in the health condition monitoring of transition zones. The InSAR system can monitor the health condition of the transition zones between the measurement interval of measuring coaches (half-year) and to provide guidance (suspect locations) for the local inspection or maintenance.

The questions needing further research are (1) how to ensure PSs in the measured transition zones and (2) how to guarantee the measurement accuracy in extreme weather.

Acknowledgments: The authors would like to thank ProRail, the Netherlands for providing the measurement data. The authors thank the German Space Agency (DLR) for providing the TerraSAR-X data. The authors would like to thank Eurailscout for sharing the information of UMF120 measuring coach. The authors would like to thank Ivan Shevtsov (from ProRail), Xiangming Liu (from TU Delft) for the assistance during the field measurements. The authors are very grateful to all reviewers for their thorough reading of the manuscript and for their constructive comments.

References

1. Zuada Coelho, B. Dynamics of Railway Transition Zones in Soft Soils. Ph.D. Thesis, Delft University of Technology, Delft, The Netherlands, 2011.
2. Nicks, J.E. The Bump at the End of the Railway Bridge. Ph.D. Thesis, Texas A&M University, College Station, TX, USA, 2009.
3. Li, D.; Davis, D. Transition of Railroad Bridge Approaches. J. Geotech. Geoenviron. Eng. 2005, doi:10.1061/(ASCE)1090-0241131:11.
4. Frohling, R.D.; Scheffel, H.; EbersÖHn, W. The Vertical Dynamic Response of a Rail Vehicle Caused by Track Stiffness Variations along the Track. Veh. Syst. Dyn. 1996, 25 (Suppl. 1), 175–187.
5. Esveld, C. Modern Railway Track; MRT-Productions: Zaltbommel, The Netherlands, 2001.
6. Lundqvist, A.; Larsson, R.; Dahlberg, T. Influence of Railway Track Stiffness Variations on Wheel/Rail Contact Force; Track for High-Speed Railways: Porto, Portugal, 2006.
7. Banimahd, M.; Woodward, P.K.; Kennedy, J.; Medero, G.M. Behaviour of train–track interaction in stiffness transitions. Proc. ICE Transp. 2012, 165, 205–214.
8. Kerr, A.D.; Moroney, B.E. Track Transition Problems and Remedies; American Railway Engineering Association: Landover, MD, USA, 1993; Volume 94, p. 25.
9. Sañudo, R.; dell'Olio, L.; Casado, J.A.; Carrascal, I.A.; Diego, S. Track transitions in railways: A review. Constr. Build. Mater. 2016, 112, 140–157.
10. Banimahd, M.; Woodward, P.K. 3-Dimensional Finite Element Modelling of Railway Transitions. In Proceedings of the 9th International Conference on Railway Engineering, London, UK, 20–21 July 2007.
11. Federal Railroad Administration (FRA). Federal Railroad Administration Office of Safety Analysis; FRA: Washington, DC, USA, 2017. Available online: http://safetydata.fra.dot.gov (accessed on 25 January 2018).
12. Hölscher, P.; Meijers, P. Literature Study of Knowledge and Experience of Transition Zones, Technical Report; GeoDelft: Newtownards, UK, 2007.
13. Varandas, J.N.; Hölscher, P.; Silva, M.A.G. Dynamic behaviour of railway tracks on transitions zones. Comput. Struct. 2011, 89, 1468–1479.
14. Hyslip, J.P.; Li, D.; McDaniel, C. Railway bridge transition case study. in Bearing Capacity of Roads, Railways and Airfields. In Proceedings of the 8th International Conference (BCR2A'09), Champaign, IL, USA, 29 June–2 July 2009.
15. Sasaoka, C.; Davis, D. Long Term Performance of Track Transition Solutions in Revenue Service; Technology Digest TD-05-036; Transportation Technology Center. Inc., Association of American Railroads: Pueblo, CO, USA, 2005.
16. Sabato, A.; Niezrecki, C. Feasibility of digital image correlation for railroad tie inspection and ballast support assessment. Measurement 2017, 103, 93–105.
17. Rizzo, P. Sensing solutions for assessing and monitoring railroad tracks. In Sensor Technologies for Civil Infrastructures; Elsevier: Amsterdam, The Netherlands, 2014, pp. 497–524.
18. Sun, F.P. Automated real-time structure health monitoring via signature pattern recognition. In Smart Structures and Materials 1995: Smart Structures and Integrated Systems; International Society for Optics and Photonics: Washington, DC, USA, 1995.

19. Park, G.; Sohn, H.; Farrar, C.R.; Inman, D.J. Overview of piezoelectric impedance-based health monitoring and path forward. Shock Vib. Dig. 2003, 35, 451–464.
20. Madhav, A.V.G.; Soh, C.K. An electromechanical impedance model of a piezoceramic transducer-structure in the presence of thick adhesive bonding. Smart Mater. Struct. 2007, 16, 673.
21. Madgav, A.V.G.; Soh, C.K. Uniplexing and multiplexing of PZT transducers for structural health monitoring. J. Intell. Mater. Syst. Struct. 2008, 19, 457–467.
22. Coelho, B.; Holscher, P.; Priest, J.; Powrie, W.; Barends, F. An assessment of transition zone performance. Proc. Inst. Mech. Eng. Part F 2011, 225, 129–139.
23. Le Pen, L.; Watson, G.; Powrie, W.; Yeo, G.; Weston, P.; Roberts, C. The behaviour of railway level crossings: Insights through field monitoring. Transp. Geotech. 2014, 1, 201–213.
24. Markine, V.; Wang, H.; Shevtsov, I. Experimental Analysis of the Dynamic Behaviour of a Railway Track in Transition Zones. In Proceedings of the Ninth International Conference on Engineering Computational Technology, Naples, Italy, 2–5 September 2014; Iványi, P., Topping, B.H.V., Eds.; Civil-Comp Press: Stirlingshire, UK, 2014.
25. Ferretti, A.; Prati, C.; Rocca, F. Permanent scatterers in SAR interferometry. IEEE Trans. Geosci. Remote Sens. 2001, 39, 8–20.
26. Ferretti, A.; Savio, G.; Barzaghi, R.; Borghi, A.; Musazzi, S.; Novali, F.; Prati, C.; Rocca, F. Submillimeter accuracy of InSAR time series: Experimental validation. IEEE Trans. Geosci. Remote Sens. 2007, 45, 1142–1153.
27. Chang, L.; Dollevoet, R.; Hanssen, R.F. Railway infrastructure monitoring using satellite radar data. Int. J. Railw. Technol. 2014, 3, 1142–1153.
28. Chang, L. Monitoring Civil Infrastructure Using Satellite Radar Interferometry. Ph.D. Thesis, Delft University of Technology, Delft, The Netherlands, 2015
29. Bamler, R.; Hartl, P. Synthetic aperture radar interferometry. Inverse Probl. 1998, 14, 333–382.
30. Chang, L.; Hanssen, R.F. Detection of permafrost sensitivity of the Qinghai–Tibet railway using satellite radar interferometry. Int. J. Remote Sens. 2015, 36, 691–700.
31. Chen, F.; Lin, H.; Li, Z.; Chen, Q.; Zhou, J. Interaction between permafrost and infrastructure along the Qinghai–Tibet Railway detected via jointly analysis of C-and L-band small baseline SAR interferometry. Remote Sens. Environ. 2012, 123, 532–540.
32. Liu, G.; Jia, H.; Zhang, R.; Zhang, H.; Yu, B.; Sang, M. Exploration of subsidence estimation by persistent scatterer InSAR on time series of high resolution TerraSAR-X images. IEEE J. Sel. Top.Appl. Earth Obs. Remote Sens. 2011, 4, 159–170.
33. Sato, Y. Japanese Studies on Deterioration of Ballasted Track. Veh. Syst. Dyn. 1995, 24 (Suppl. 1), 197–208.
34. Guerin, N. Experimental identification of a ballast settlement law. Can. Geotech. J. 1999, 36, 523–532.
35. Dahlberg, T. Some railroad settlement models—A critical review. Proc. Inst. Mech.Eng. Part F 2001, 215, 289–300.
36. Suiker, A.S.J.; de Borst, R. A numerical model for the cyclic deterioration of railway tracks. Int. J. Numer. Methods Eng. 2003, 57, 441–470.

37. Varandas, J.N.; Hölscher, P.; Silva, M.A.G. A Settlement Model for Ballast at Transition Zones. In Proceedings of the Tenth International Conference on Computational Structures Technology, Valencia, Spain, 14–17 September 2010.
38. Stark, T.D.; Wilk, S.T. Root cause of differential movement at bridge transition zones. Proc. Inst. Mech. Eng. Part F 2015, 230, 1257–1269.
39. Selig, E.T.; Waters, J.M. Track Geotechnology and Substructure Management; Thomas Telford: London, UK, 1994.
40. Namura, A.; Suzuki, T. Evaluation fo countermeasures against differential settlement at track transitions. Q. Rep. RTRI 2007, 48, 176–182
41. Wang, H.; Markine, W.L.; Shevtsov, I.Y.; Dollevoet, R. Analysis of the Dynamic Behaviour of a Railway Track in Transition Zones With Differential Settlement. In Proceedings of the 2015 Joint Rail Conference, San Jose, CA, USA, 23–26 March 2015; p. 7.
42. Hunt, H. Settlement of railway track near bridge abutments. In Proceedings of the Institution of Civil Engineers-Transport; Thomas Telford-ICE Virtual Library: London, UK, 1997; pp. 68–73.
43. Li, Z.; Wu, T. Vehicle/track impact due to passing the transition between a floating slab and ballasted track. In Noise and Vibration Mitigation for Rail Transportation Systems; Springer: Berlin, Germany, 2008, pp. 94–100.
44. Lei, X.; Zhang, B. Influence of track stiffness distribution on vehicle and track interactions in track transition. Proc. Inst. Mech.Eng. Part F 2010, 224, 592–604.
45. Plotkin, D.; Davis, D. Bridge Approaches and Track Stiffness; U.S. Department of Transportation: Washington, DC, USA, 2008.
46. ProRail. Constructive Measures to Prevent Settlement of the Track (in Dutch Constructieve Maatregelen ter Voorkoming van Ontoelaatbare Zakkingen van Het Spoor); ProRail: Utrecht, The Netherlands, 2010.
47. Varandas, J.N. Long-Term Behaviour of Railway Transitions under Dynamic Loading Application to Soft Soil Sites. Ph.D. Thesis, Universidade Nova de Lisboa, Lisbon, Protugal, 2013.
48. Eurailscout. Pictures from Eurailscout. Available online: http://www.eurailscout.com/fleet/ohl--track-geometry/ufm120/ (accessed on 08 November 2017).
49. British Standards Institution. Railway Applications/Track, in Track Geometry Quality; Characterisation of Track Geometry; En, B.S. 13848-1; British Standards Institution: London, UK, 2003.
50. Bhandari, A.R.; Powrie, W.; Harkness, R.M. A digital image-based deformation measurement system for triaxial tests. Geotech. Test. J. 2011, 35, 209–226.
51. Giachetti, A. Matching techniques to compute image motion. Image Vis. Comput. 2000, 18, 247–260.
52. Tong, W. An evaluation of digital image correlation criteria for strain mapping applications. Strain 2005, 41, 167–175.
53. Koltsida, I.; Tomor, A.; Booth, C. The Use of Digital Image Correlation Technique for Monitoring Masonry Arch Bridges. 2013. Available online: http://master.grad.hr/arch/index.html (accessed on 01 October 2017).
54. McCormick, N.; Lord, J. Digital image correlation for structural measurements. Proc. Inst. Civ. Eng. 2012, 165, 185–190.

55. Sutton, M.; Wolters, W.J.; Peters, W.H.; Ranson, W.F.; McNeill, S.R. Determination of displacements using an improved digital correlation method. Image Vis. Comput. 1983, 1, 133–139.
56. Bowness, D.; Lock, A.C.; Powrie, W.; Priest, J.A.; Richards, D.J. Monitoring the dynamic displacements of railway track. Proc. Inst. Mech. Eng. Part F 2007, 221, 13–22.
57. Ribeiro, D.; Calçada, R.; Ferreira, J.; Martins, T. Non-contact measurement of the dynamic displacement of railway bridges using an advanced video-based system. Eng. Struct. 2014, 75, 164–180.
58. Priest, J.; Powrie, W.; Yang, W.; Grabe, P.J.; Clayton, C.R.I. Measurements of transient ground movements below a ballasted railway line. Géotechnique 2010, 60, 667–677.
59. Iryani, L.; Setiawanb, H.; Dirgantarac, T.; Putrad, I.S. Development of a Railway Track Displacement Monitoring by Using Digital Image Correlation Technique. Appl. Mech. Mater. 2014, 548–549, 683–687.
60. Sabato, A.; Beale, C.H.; Niezrecki, C. A novel optical investigation technique for railroad track inspection and assessment. In Nondestructive Characterization and Monitoring of Advanced Materials, Aerospace, and Civil Infrastructure; International Society for Optics and Photonics: Washington, DC, USA, 2017.
61. Liu, X.; Markine, V.; Shevtsov, I. Dynamic experimental tools for condition monitoring of railway turnout crossing. In Proceedings of the Second International Conference on Railway Technology: Research, Development and Maintenance, Corsica, France, 8–11 April 2014.
62. Liu, X.; Markine, V.; Shevtsov, I. Performance study of a double crossover for facing and trailing directions. In Proceedings of the 24th IAVSD 2015 International Symposium on Dynamics of Vehicles on Roads and Tracks, Graz, Austria, 17–21 August 2015; CRC Press: Boca Raton, FL, USA, 2015.
63. Franceschetti, G.; Iodice, A.; Riccio, D. A canonical problem in electromagnetic backscattering from buildings. IEEE Trans. Geosci. Remote Sens. 2002, 40, 1787–1801.
64. Arikan, M.; Hanssen, R.F. Structural Deformation of the High-Speed Line (HSL) Infrastructure in The Netherlands; Observations Using Satellite Radar Interferometry; Delft University of Technology: Delft, The Netherlands, 2008.
65. Elachi, C.; Van Zyl, J.J. Introduction to the Physics and Techniques of Remote Sensing; John Wiley & Sons: Hoboken, NJ, USA, 2006, Volume 28.
66. Kampes, B.M. Displacement Parameter Estimation Using Permanent Scatterer Interferometry. Ph.D. Thesis, Delft University of Technology, Delft, The Netherlands, 2005.
Eineder, M.; Minet, C.; Steigenberger, P. Imaging geodesy—Toward centimeter-level ranging accuracy with TerraSAR-X. IEEE Trans. Geosci. Remote Sens. 2011, 49, 661–671.

Curriculum Vitae

Haoyu Wang

Education

2011-2018	PhD, Delft University of Technology, the Netherlands Research Topic: Measurement, Assessment, Analysis and Improvement of Transition Zones in Railway Track
2010-2012	Master of Science in Railway Engineering, Beijing Jiao Tong University, China GPA 3.5/4.0. Degree project: Optimisation of Track Transitions on the High Speed Lines
2006-2010	Bachelor of Science Civil Engineering, Beijing Jiao Tong University, China GPA 3.8/4.0. Degree project: Mechanical Characteristics of Switches on the Long Slope of High Speed Rail

Work

2018-Now	Railway specialist/Developer - Fugro BV, the Netherlands
2017-2017	Railway specialist/Consultant - Roadscanners OY, Finland
2015-2016	Teaching assistant - Delft University of Technology, the Netherlands

List of Publications

List of Publications

Journal articles

Haoyu Wang and Valeri Markine. Methodology for the Comprehensive Analysis of Railway Transition Zones. *Computers and Geotechnics, 99 (2018), pp.64-79. doi: 10.1016/j.compgeo.2018.03.001.*

Haoyu Wang, Valeri Markine, Xiangming Liu, 2017. Experimental analysis of railway track settlement in transition zones. *Proceedings of the Institution of Mechanical Engineers, Part F: Journal of Rail and Rapid Transit, p.0954409717748789. doi:10.1177/0954409717748789.*

Haoyu Wang and Valeri Markine. Finite element analysis of the dynamic behaviour of track transition zones during train passing processes. *Under review.*

Haoyu Wang and Valeri Markine. Modelling of the long-term behaviour of transition zones: Prediction of track settlement. *Engineering Structures, 156 (2018), pp.294-304. doi:10.1016/j.engstruct.2017.11.038.*

Haoyu Wang, and Valeri Markine. Corrective countermeasure for track transition zones: adjustable fastener. *Engineering Structures 169 (2018): 1-14. doi: 10.1016/j.engstruct.2018.05.004.*

Haoyu Wang, Mika Silvast, Valeri Markine and Bruce Wiljanen. Analysis of the Dynamic Wheel Loads in Railway Transition Zones Considering the Moisture Condition of the Ballast and Subballast. *Applied Sciences, 7(12), p.1208. doi:10.3390/app7121208.*

Haoyu Wang, Ling Chang, Valeri Markine, Structural Health Monitoring of Railway Transition Zones Using Satellite Radar Data. *Sensors 2018, 18(2), 413. doi:10.3390/s18020413.*

Xiangming Liu, Valeri Markine, **Haoyu Wang**, and I. Y. Shevtsov. Experimental tools for railway crossing condition monitoring (crossing condition monitoring tools). Measurement 129 (2018): 424-435.

Conference articles

H. Wang and V.L. Markine, 'Analysis and improvement of the dynamic track behaviour in transition zone', in the Tenth International Conference on the Bearing Capacity of Roads, Railways and Airfields, Loizos et al., Taylor & Francis Group, London, 2017.

H. Wang and V.L. Markine, 'Analysis of the Long-Term Behaviour of Track Transition Zones', in The Third International Conference on Railway Technology: Research, Development and Maintenance, J. Pombo, (Editor), Civil-Comp Press, Stirlingshire, United Kingdom, paper 203, 2016. doi:10.4203/ccp.110.203.

H. Wang, V. L. Markine, R. Dollevoet and I. Y. Shevtsov, 'Improvement of train-track interaction in transition zones via reduction of ballast damage' in Proceedings of 24th International Symposium on Dynamics of Vehicles on Roads and Tracks (IAVSD2015), Graz, Austria, 17-21 August 2015.

H. Wang, V. L. Markine, I. Y. Shevtsov and R. Dollevoet, 'Analysis of the Dynamic Behaviour of a Railway Track in Transition Zones With Differential Settlement', in Proceedings of 2015 Joint Rail Conference, Paper No. JRC2015-5735, pp. V001T01A024; 7 pages, 2015. doi:10.1115/JRC2015-5735.

V.L. Markine, **H. Wang** and I.Y. Shevtsov, 'Experimental Analysis of the Dynamic Behaviour of a Railway Track in Transition Zones', in Proceedings of the Ninth International Conference on Engineering Computational Technology, P. Iványi and B.H.V. Topping, (Editors), Civil-Comp Press, Stirlingshire, United Kingdom, paper 3, 2014. doi:10.4203/ccp.105.3.

H. Wang, V.L. Markine and I. Shevtsov, 'The Analysis of Degradation Mechanism in Track Transition Zones using 3D Finite Element Model', in Proceedings of the Second International Conference on Railway Technology: Research, Development and Maintenance, J. Pombo, (Editor), Civil-Comp Press, Stirlingshire, United Kingdom, paper 227, 2014. doi:10.4203/ccp.104.227.

Acknowledgement

At the end stage of my PhD study, I would like to express my gratitude to everybody who helped me. This thesis would not be made a reality without your help!

In the first place I would like to thank my daily supervisor and co-promotor, Dr. Valeri Markine. Thanks for your patient guidance and inspired advice during our weekly meetings. My logical and academic skills were developed significantly by answering your challenging questions, although sometimes I had to think over them from dark to dawn. You taught me how to be a qualified researcher. Your rigorous attitude, rational thinking, and sharing spirit influenced me greatly in my PhD and will be my lifelong benefit.

I also owe much gratitude to my promotor Prof. Rolf Dollevoet. You broadened my horizons. You guided me to establish cooperation with railway companies, to gain experience from frontline workers, and to validate our thoughts in the field. You always encouraged me to explain my studies in a shorter and more understandable way, which is very important for my further career.

I would like to express my gratitude to my industrial supervisor, Dr. Ivan Shevtsov from *ProRail, the Netherlands*. Thank you for providing all the useful documents and organising field measurements. Without them I would not be confident in my numerical simulations.

I highly appreciated my second industrial supervisor Mika Silvast from *Roadscanners OY, Finland*. Thanks so much for your help both in terms of academic and life. I gained invaluable knowledge of GPR and railway consulting experience during my stay in Roadscanners.

Moreover, I would like to sincerely thank Jelte Bos from *Movares Nederland B.V.* for providing valuable information of the adjustable fasteners, including the measurement results, technical details. Your positive comments encouraged me to conduct more application of my research.

Furthermore essential information of the Dutch railway network was provided by *ProRail*, for which I would like to thank in particular Martijn van Noort. The discussion with you was very helpful.

Also, I wish to acknowledge the valuable information of the transition zones provided by Stefan Bömers from *Strukton Rail Nederland*. They are essential for my thesis.

I very much appreciated the help of Dr. Ling Chang from the *University of Twente*. Thanks so much for sharing me the knowledge of satellites and also for encouraging me, which are crucial for my research.

I am particularly grateful for the assistance given by Frans Podbevsek from *Infinite simulation systems B.V*. Thanks for the numerous questions you answered for me. I learnt priceless knowledge of numerical simulation from you. My numerical model would not exist without your help.

For the assistance of laboratory tests and field measurements, I would like to thank Jan Moraal, Jurjen Hendriks, Evert van Veldhuizen from *TU Delft*, and Greg Lambert, Ruud van Bezooijen from *Rail OK B.V*.

I would also like to express my gratitude to the section secretaries Jacqueline Barnhoorn for the arrangement of administrative issues. I also owe much gratitude to the executive secretary Sandra Ransdorp for valuable encouragement and care. I highly appreciated helpful discussions with Lambert Houben, Prof. Rong Chen, Dr. Yu Zhou, Dr. Zhiwei Qian, Dr. Mauricio Pradena Miquel, Xiangyun Deng, Shaoguang Li, and Chen Shen.

I would like to thank other colleagues and friends. They are Dr. Zilong Wei, Dr. Alfredo Nunez, Bruce Wiljanen, Dr. Zhen Yang, Meysam Naeimi, Dr. Pingrui Zhao, Ali Jamshidi, Dr. Hongqing Liang, Dr. Michaël Steenbergen, Omid Hajizad, Yunlong Guo, Prof. Zili Li, Dr. Xianmai Chen, Martin Hiensch, Dr. Li Wang, Lei Xu, Alf Smolders, Song Liu, Anthonie Boogaard, Dr. Xiubo Liu, Dr. Maria Molodova, Dr. Qian Xiao, Jeroen Wegdam, Tao Lu, Dr. Timo Saarenketo, Dr. Meng Ma, Anssi Hiekkalahti, Tuukka Saikka, Chris Händel, Stephen Verbist, Jos Berker, Sando van der Helm, Wikaas Dihalu, Sanjay Birjmohan, Edward Elson. I am very thankful to my office mate Daan Hoekstra for editing the Dutch summary of my thesis. I am especially grateful to Emma Kärki, Olli Ervelä, Annele Matintupa for your care during my stay in Finland.

I owe much gratitude to Prof. Hong Xiao from *Beijing Jiaotong University*, who guided me during the master study. Thank you for bringing me to the academic world and your constant care.

Also, I am thankful to Dr. Ziquan Yan from the *Chinese Academy of Railway Sciences* who guided me at the beginning of my PhD. I am grateful to Prof. Aijun Gu from *Beijing Jiaotong University* for introducing me to *TU Delft*.

I would like to sincerely express my gratitude to Dr. Yuewei Ma, Xiangming Liu, Dr. Chang Wan. Thank you for sharing me valuable knowledge, assisting me during measurements, and providing comments to my studies.

I am particularly grateful to my Dutch teacher Annet Zwinkels. I have learnt not only language but also culture from you. Your kindness keeps me from suffering homesickness. In addition, I am also thankful to my other Dutch teachers Dr. Jan Gerbrands and Meysam Naeimi.

I would like to sincerely thank Dr. Guoqing Jing. Thank you for the continuous encouragement during my PhD, which is priceless to me.

I am most indebted to my parents, who have been supporting me for so many years. You are the best parents. I am sorry that I did not visit you often during these years.

My deepest gratitude goes to my wife, Xiaoman Xu. Thank you for being always supportive. Thank for proofreading the drafts of my papers, for reminding me of deadlines, for preparing delicious food. Thank you for coming into my life.

Finally, dear readers, thank you for reading.

Haoyu Wang

2018

Delft, the Netherland